USING BRET-BASED G PROTEIN BIOSENSORS TO UNRAVEL THE G PROTEIN MEDIATED PATHWAYS IN INSECTS

Els LISMONT

Supervisor:
Prof. Dr. Jozef Vanden Broeck

Members of the Examination Committee:
Em. Prof. Dr. Roger Huybrechts
Prof. Dr. Lutgarde Arckens
Prof. Dr. Jean-Yves Springael
Prof. Dr. Isabel Beets
Dr. Heleen Verlinden
Dr. Cynthia Lenaerts

Dissertation presented in partial fulfilment of the requirements for the degree of Doctor of Science (PhD): Biology

November 2019

Doctoraatsproefschrift aan de faculteit Wetenschappen van de KU Leuven

Uitgegeven in eigen beheer, ELS LISMONT, 3000 LEUVEN, BELGIUM

Word of thanks

Een paar jaar geleden, of zelfs nog maar een aantal maanden geleden, kon ik mij niet inbeelden dat ik dit stukje tekst ooit zou schrijven. Hoe onwezenlijk het toen ook leek, hier zit ik dan, op een regenachtige zondagochtend, het laatste stukje tekst te schrijven. Ik kan niet ontkennen dat het soms heel zwaar en moeilijk is geweest en het is waarschijnlijk een van de zwaarste dingen die ik ooit heb gedaan, maar ik ben enorm fier dat ik heb kunnen doorzetten en dat het nu eindelijk af is! Ik zou hier vandaag niet geraakt zijn zonder de steun van een heleboel mensen dewelke ik graag uitdrukkelijk wens te bedanken.

Allereerst moet ik natuurlijk mijn promotor **Prof. Jozef Vanden Broeck** bedanken om mij de mogelijkheid te geven om mijn doctoraat aan te vatten. Bedankt voor de steun en voor de verbeteringen van mijn papers en doctoraatsthesis doorheen de jaren.

Ten tweede zou ik ook graag **Prof. Roger Huybrechts** en **Heleen Verlinden** bedanken. **Roger,** bedankt om 6 jaar geleden in mij te geloven en om mij te motiveren om een doctoraat te doen. **Heleen**, ook jij verdient een belangrijke plaats in dit dankwoord. Bedankt om mij te introduceren in het 'Jeffers' labo en voor alles wat ik van jou geleerd heb. Niet alleen binnen het labo, maar ook daarbuiten heb je mij geholpen om mijn grenzen te verleggen en buiten mijn comfort zone te treden, zelfs tot in Zuid-Korea. Bedankt om achter mijn veren te zitten om mijn doctoraat af te maken en om in mij te blijven geloven!

Next, I would like to thank all the remaining members of my examination committee. I will have to start with **Prof. Jean-Yves Springael.** Thank you very much for the opportunity to work in your lab in Brussels. Thank you for all the knowledge you shared with me, our interesting conversations and being so positive and at the same time critical about my research work. I would also like to thank **Prof. Lut Arckens**, **Prof. Isabel Beets** and **Cynthia Lenaerts**. Bedankt om mijn thesis kritisch na te lezen en bedankt voor alle opbouwende commentaren en verbeteringen.

Ook al 'mijn' studenten verdienen oprecht mijn dank voor hun extra paar handen in het labo. **Sander, Nele, Timon, PJ** en **Arnaud**, bedankt voor jullie inzet, ook voor al het werk dat uiteindelijk niet in deze thesis geraakt is! Jullie begeleiden was een plezier en ook voor mij heel leerrijk! Ook bijzondere dank aan **Els W.**, **Maria** en **Marijke** voor de administratieve ondersteuning en **Evelien**, bedankt om zo goed voor de sprinkhanen te zorgen! Uiteraard ook een speciale dank aan **Paulien**,

Evert en vroeger ook **Toon** voor de technische ondersteuning en om het labo in goede banen te leiden! Ook bedankt aan **Sven VB** en **Kurt** voor de hulp met de massaspectrometrie.

Elke dag naar het labo komen zou nooit zo fijn geweest zijn zonder de uitzonderlijk toffe collega's van het Zoölogisch instituut! **Sven Z**., **Pieter, Rut, Senne**, **Rik**, **Niels**, **Jornt**, **Darron**, **Lina M.**, **Lina V.**, **Stijn**, **Marijke**, **Elise**, **Cynthia**, **Katleen C., Joachim en Forkwa**, bedankt voor de toffe sfeer bij de Jeffers! Ook een oprechte dank aan alle andere mensen van het HS(T)V labo voor de toffe sfeer!

Bedankt ook aan de leden van 02.10: **Charline**, **Katleen P**, **Michiel** en vroeger ook **Jornt**! Bedankt om 'onze bureau' zo gezellig te maken en voor alle leuke babbels. Bedankt voor jullie vriendschap en steun de afgelopen jaren!

Ook een bijzondere dank aan al mijn andere vrienden van het labo. **Elisabeth**, bedankt voor al jouw steun op zowel professioneel als persoonlijk vlak. **Lotte**, **Elien**, **Jan W.** en **Lentel,** bedankt dat ik bij jullie altijd terecht kon voor een babbel, voor jullie vriendschap en blijvende steun gedurende de afgelopen jaren! **Dulce**, thank you very much for your continuous support, your friendship and to help me put things in perspective when I was having a hard time.

Ook mijn vriendjes buiten het labo wil ik natuurlijk bedanken voor alle steun en aanmoedigingen! Hierbij nog een speciale dank aan **Arnout,** het was altijd een blijde gebeurtenis om jou tegen te komen in de gang. Bedankt om mij altijd op te vrolijken!

Graag wil ik ook mijn familie en schoonfamilie bedanken voor alle steun die ik de afgelopen jaren heb gekregen. **Riet**, **Miet** en **papa**, bedankt om gedurende deze periode Isaak op te vangen zodat ik kon schrijven! **Opa**, ook aan u een oprechte dank om achter mijn veren te zitten om dit doctoraat af te maken!

Dit boekje zou nooit afgeraakt zijn zonder **Jan**. Voor jou moeten ze aan de stelling 'met uw gat in de boter vallen' een extra dimensie toevoegen. Bedankt dat ik altijd op jou heb kunnen rekenen en dat je altijd in mij bent blijven geloven. Ik ben er mij van bewust dat ook jij veel hebt moeten opofferen zodat ik mijn doctoraat kon afronden. Ik ben jou hiervoor dan ook voor eeuwig dankbaar. Bedankt voor alle steun, jouw geduld, en om zo goed voor Isaak te zorgen als ik wéér aan mijn doctoraat moest werken. Ten slotte, **Isaak**, bedankt om mij altijd te laten lachen, ook al had ik het heel zwaar. Jouw lach heeft geholpen om alles in perspectief te kunnen plaatsen. Jij hebt mij geholpen om in te zien wat werkelijk belangrijk is in het leven.

Table of contents

Summary

G protein-coupled receptors (GPCRs) are membrane-bound receptors which are candidate targets for novel insect pest management strategies. The superfamily of GPCRs is extensively studied in vertebrates since they are pharmacological targets for many important therapeutic compounds. However, in insects, the molecular signaling properties of GPCRs remain poorly understood and studies are usually limited to the detection of fluctuations in the secondary messenger molecules Ca^{2+} and cyclic adenosine monophosphate (cAMP). In this study we tested if bioluminescence resonance energy transfer (BRET)^2-based G protein biosensors, developed to detect a direct activation Gα protein subununits in vertebrates, can also be used to detect Gα protein subununit activation upon insect GPCR activation. We have tested these BRET^2-based G protein biosensors, representing members of all four Gα protein subfamilies (Galés et al., 2006), and have shown that they respond to activation of insect GPCRs for three out of four Gα protein subfamilies, namely $G\alpha_{i/o}$, $G\alpha_s$ and $G\alpha_{q/11}$.

In order to test these BRET^2-based G protein biosensors, we have characterized three insect receptors from two insect species. The first insect species, the buff-tailed bumblebee, *Bombus terrestris*, is a beneficial insect that is regularly used as a pollinator of greenhouse crops. In this insect, we have selected the SIFamide receptor (SIFR) which belongs to the Family A GPCRs since almost nothing is known about the downstream signaling pathways of this receptor. We have demonstrated that stimulation of *Bomte*-SIFR by *Bomte*-SIFa activates the $G\alpha_{i/o}$ and $G\alpha_q$ biosensors. We have also studied the downstream signaling properties of the secondary messenger molecules Ca^{2+} and cAMP, the agonistic properties of a range of related modified peptides and examined the transcript levels of *Bomte*-SIFa and *Bomte*-SIFR in a variety of tissues.

The second insect species, the desert locust *Schistocerca gregaria,* is considered a major pest insect since it can form devastating swarms which have a strong negative impact on agricultural production and human welfare. In this insect we have characterized two receptors from two different GPCR families. The first receptor is the allatotropin receptor (ATR) which belongs to the Family A GPCRs. We have demonstrated that stimulation of *Schgr*-ATR by *Schgr*-AT activates the $G\alpha_{i/o}$ and $G\alpha_{q/11}$ biosensors. We have also studied the downstream signaling properties of the secondary messenger molecules Ca^{2+} and cAMP and found more evidence for the myotropic and allatostimulatory actions of *Schgr*-AT. In addition, we studied the transcript levels of *Schgr*-AT and *Schgr*-ATR in a variety of tissues.

The second receptor we characterized in *S. gregaria* and the third receptor in this study, is the corticotropin-releasing factor (CRF)-related diuretic hormone (DH) receptor (CRF-DHR1) which belongs to the Family B GPCRs. For this neuropeptide receptor system we have identified three putative receptor sequences (*Schgr*-CRF-DHR1, *Schgr*-CRF-DHR2 and *Schgr*-CRF-DHR3) in the (unpublished, in-house) transcriptome database (Verdonck, 2017) and were able to clone the first receptor, namely *Schgr*-CRF-DHR1. We have demonstrated that stimulation of *Schgr*-CRF-DHR1 by *Schgr*-CRF-DH activates the $G\alpha_{i/o}$ and $G\alpha_{s}$ biosensors. We have also studied the downstream signaling properties of the secondary messenger molecules Ca^{2+} and cAMP and studied the transcript levels of two receptors, namely *Schgr*-CRF-DHR1 and *Schgr*-CRF-DHR2. If *Schgr*-CRF-DHR2 and *Schgr*-CRF-DHR3 exist *in vivo* and if they are receptors for *Schgr*-CRF-DH remains a question for future studies.

Although we have shown an activation of biosensors from three Gα protein subfamilies, namely $G\alpha_{i/o}$, $G\alpha_{s}$ and $G\alpha_{q/11}$, we could not show an activation of any biosensors from the $G\alpha_{12/13}$ subfamily. By comparing human Gα sequences with their homologs of *B. terrestris* and *S. gregaria*, we found that the $G\alpha_{12/13}$ subfamily is less conserved than the three other Gα protein subfamilies.

Samenvatting

G-proteïne gekoppelde receptoren (GPCRs) zijn membraangebonden receptoren die een mogelijk doelwit vormen voor nieuwe strategieën van plaagbestrijding van insecten. De superfamilie van GPCRs wordt uitgebreid bestudeerd bij vertebraten omdat ze farmacologische doelwitten zijn voor talrijke therapeutische middelen. Bij insecten daarentegen werden de moleculaire signaleringseigenschappen van deze receptorklasse echter nog maar weinig gedetailleerd bestudeerd en beperken de studies zich tot het detecteren van wijzigingen in de concentraties van secundaire boodschappermoleculen, namelijk Ca^{2+} en cyclisch adenosinemonofosfaat (cAMP).

In deze studie hebben we getest of $BRET^2$-gebaseerde G-proteïne biosensoren, die ontwikkeld zijn om een directe activatie van de Gα subeenheid te detecteren bij vertebraten, ook kunnen gebruikt worden om een directe activatie van de Gα subeenheid te kunnen detecteren na activatie van GPCRs afkomstig van insecten.

We hebben deze $BRET^2$-gebaseerde G-proteïne biosensoren, die alle vier Gα-proteïne subfamilies vertegenwoordigen, getest en hebben bewezen dat de biosensoren van drie van de vier Gα-proteïne subfamilies, namelijk $G\alpha_{i/o,}$ $G\alpha_s$ en $G\alpha_{q/11}$, de activatie van insecten GPCRs kunnen aantonen.

Om deze $BRET^2$-gebaseerde G-proteïne biosensoren te testen, hebben we drie neuropeptidereceptoren van twee insectensoorten gekarakteriseerd. De eerste insectensoort, de aardhommel *Bombus terrestris*, is een nuttig insect dat regelmatig wordt gebruikt als bestuiver in serreteelten. In dit insect hebben we de SIFamide-receptor (SIFR) bestudeerd, dat behoort tot de Familie A GPCRs, omdat er bijna niets over de cellulaire signalering van deze receptor gekend is. We hebben aangetoond dat stimulatie van *Bomte*-SIFR door *Bomte*-SIFa de $G\alpha_{i/o}$ en $G\alpha_q$ biosensoren activeert. We hebben ook onderzocht of er wijzigingen zijn in de concentraties van de secundaire boodschappermoleculen Ca^{2+} en cAMP en hebben de agonistische eigenschappen van een reeks gerelateerde, gemodificeerde peptiden bestudeerd. Bovendien hebben we de transcriptniveaus van *Bomte*-SIFa en *Bomte*-SIFR in verschillende weefsels onderzocht.

De tweede insectensoort, de woestijnsprinkhaan *Schistocerca gregaria*, wordt beschouwd als een plaaginsect omdat het verwoestende zwermen kan vormen die een sterke negatieve impact hebben op de landbouwproductie en het menselijk welzijn. In dit insect hebben we twee receptoren uit twee verschillende GPCR-families gekarakteriseerd. De eerste receptor is de allatotropinereceptor (ATR) die behoort tot de Familie A GPCRs. We hebben aangetoond dat stimulatie van *Schgr*-ATR door *Schgr*-AT de $G\alpha_{i/o}$ en $G\alpha_{q/11}$ biosensoren activeert. We hebben ook onderzocht of er wijzigingen zijn in de concentraties van de secundaire boodschappermoleculen Ca^{2+} en cAMP en hebben meer

bewijs gevonden voor de myotrope en allatostimulerende werking van *Schgr*-AT. Bovendien hebben we de transcriptniveaus van *Schgr*-AT en *Schgr*-ATR in verschillende weefsels bestudeerd.

De tweede receptor die we hebben gekarakteriseerd in *S. gregaria* en de derde receptor in deze studie, is de corticotropin-releasing factor (CRF)-gerelateerde diuretisch hormoon (DH)-receptor (CRF-DHR1), die behoort tot de Familie B GPCRs. Voor dit neuropeptide receptorsysteem hebben we sequenties van drie vermoedelijke receptoren (*Schgr*-CRF-DHR1, *Schgr*-CRF-DHR2 en *Schgr*-CRF-DHR3) geïdentificeerd in de (niet-gepubliceerde, interne) transcriptoomdatabank (Verdonck, 2017). De eerste receptor, *Schgr*-CRF-DHR1 werd succesvol gekloneerd en we hebben aangetoond dat stimulatie van *Schgr*-CRF-DHR1 door *Schgr*-CRF-DH de $G\alpha_{i/o}$ en $G\alpha_s$ biosensoren activeert. We hebben ook onderzocht of er wijzigingen zijn in de concentraties van de secundaire boodschappermoleculen Ca^{2+} en cAMP en hebben de transcriptniveaus bestudeerd van twee receptoren, namelijk *Schgr*-CRF-DHR1 en *Schgr*-CRF-DHR2, in verschillende weefsels. Of *Schgr*-CRF-DHR2 en *Schgr*-CRF-DHR3 werkelijk *in vivo* bestaan, en of deze receptoren ook receptoren zijn voor *Schgr*-CRF-DH blijft een vraag voor toekomstige studies.

Hoewel we een activatie van de biosensoren van drie Gα-proteïne subfamilies hebben aangetoond, namelijk $G\alpha_{i/o}$, $G\alpha_s$ en $G\alpha_{q/11}$, konden we geen activatie van beide biosensoren van de $G\alpha_{12/13}$ subfamilie aantonen. Door de Gα-proteïne sequenties van de mens te vergelijken met deze van *B. terrestris* en *S. gregaria* hebben we aangetoond dat de $G\alpha_{12/13}$ subfamilie minder geconserveerd is dan de andere drie Gα-proteïne subfamilies.

List of abbreviations

7TM regions	7 transmembrane regions
AbG	Abdominal ganglia
AG	Accessory glands
AKAPs	A-kinase anchor proteins
ABLKs	Abdominal neurosecretory cells
AngII	Angiotensin II
AST	Allatostatin
AT	Allatotropin
AT1-R	Angiotensin II type 1 receptor
ATLs	AT-like peptides
ATP	Adenosine triphosphate
ATR	Allatotropin receptor
BLAST	Basic local alignment search tool
Br	Brain
BSA	Bovine serum albumin
CA	Corpora allata
Cae	Caecum
CAMYEL	cAMP sensor using YFP-Epac-*R*luc
AMP	Adenosine monophosphate
cAMP	Cyclic adenosine monophosphate
CBP	CREB binding protein
CC	Corpora cardiaca
cDNA	Complementary DNA
CHO	Chinese hamster ovary
CNS	Central nervous system
CRE	cAMP responsive element
CRH	Corticotropin-releasing hormone
CRHR	Corticotropin-releasing hormone receptor
DAG	Diacyl glycerol
DMEM	Dulbecco's Modified Eagles Medium
DMSO	Dimethylsulphoxide
DNA	Deoxyribonucleic acid
dsDNA	Double stranded DNA
EBI	European Bioinformatics Institute
EDTA	Ethylenediaminetetraacetic acid
EL	Extracellular loop
EF1α	Elongation factor 1 α
EPAC	Exchange factor directly activated by cAMP
Epi	Epidermis
EST	Expressed sequence tag

FA	Farnesoic acid
FB	Fat body
FG	Foregut
$GABA_B$	γ-aminobutyric acid receptor
GADPH	Glyceraldehyde 3-phosphate dehydrogenase
GDP	Guanosine diphosphate
GEF	Guanine-nucleotide exchange factor
GFP	Green fluorescent protein
Gon	Gonads
GPCR	G protein-coupled receptor
GTP	Guanosine triphosphate
HBSS	Hanks' Balanced Salt Solution
HEK	Human embryonic kidney cells
HEPES	4-(2-hydroxyethyl)-1-piperazineethanesulfonic acid
HG	Hindgut
HRP	Horseradish peroxidase
hugin-PK	Hugin pyrokinin
IBMX	3-isobutyl-1-methylxanthine
IL	Intracellular loop
IP_3	Inositol 1,4,5-trisphosphate
JH	Juvenile hormone
LB	Luria-Bertani
LK	Leucokinin
MAPK	Mitogen-activated protein kinase pathway
MG	Midgut
MIP	Myoinhibiting peptide
MOR	Mu opioid receptor
MT	Malpighian tubules
Muscle	Flight muscle
NF	Normalization factor
NKH-477	6-[3-(dimethylamino)propionyl]-forskolin
NPF	Neuropeptide F
NPY	Neuropeptide Y
OL	Optic lobes
OMP	Ovary Maturating Parsin
ORF	Open reading frame
PAM	Peptidyl amidating monooxygenase
PIP_2	Phosphatidylinositol 4,5-bisphosphate
PBS	Phosphate buffered saline
PCR	Polymerase chain reaction
PG	Prothoracic gland
PKA	Protein kinase A
PLC	Phospholipase C

*R*luc	*Renilla* luciferase
qRT-PCR	Real-time quantitative reverse transcriptase PCR
RCA	Radiochemical assay
RhoGEF	RhoGTPase nucleotide exchange factor
RNA	Ribonucleic acid
RNAi	RNA interference
RPL13	Ribosomal protein L13
rpm	Routes per minute
S.E.M.	Standard error of the mean
SG	Salivary gland
SIFa	SIFamide
SIFR	SIFamide receptor
SK	Sulfakinin
sNPF	Short neuropeptide F
SNS	stomatogastric nervous system
SOG	Suboesophageal ganglion
SRET	Sequential resonance energy transfer
Tdt	Terminal deoxynuceotidyl transferase
Tes	Testes
TG1	Prothoracic ganglion
TG2	Mesothoracic ganglion
TG3	Metathoracic ganglion
TM	Transmembrane domains
TR	Truncated
VNC	Ventral nerve cord
YFP	Yellow fluorescent protein

List of mentioned animal species

Binomial name	Abbr.	Subphylum	Class	Order	Common name
Acerentomon sp.	NA	Hexapoda	Protura	Acerentomata	NA
Acromyrmex echinatior	*Acrec*	Hexapoda	Insecta	Hymenoptera	Panamanian leafcutter ant
Acyrthosiphon pisum	*Acypi*	Hexapoda	Insecta	Hemiptera	pea aphid
Aedes aegypti	*Aedae*	Hexapoda	Insecta	Diptera	yellow fever mosquito
Agelastica alni	*Ageal*	Hexapoda	Insecta	Coleoptera	alder leaf beetle
Anopheles gambiae	*Anoga*	Hexapoda	Insecta	Diptera	African malaria mosquito
Aphis gossypii	*Aphgo*	Hexapoda	Insecta	Hemiptera	cotton aphid
Apis mellifera	*Apime*	Hexapoda	Insecta	Hymenoptera	honey bee
Argulus siamensis	*Argsi*	Crustacea	Ichthyostraca	Arguloida	NA
Balanus amphitrite	*Balam*	Crustacea	Hexanauplia	Sessilia	striped barnacle
Bombus terrestris	*Bomte*	Hexapoda	Insecta	Hymenoptera	buff-tailed bumblebee
Bombyx mori	*Bommo*	Hexapoda	Insecta	Lepidoptera	domestic silkworm
Cancer antennarius	*Canan*	Crustacea	Malacostraca	Decapoda	Pacific rock crab
Cancer borealis	*Canbe*	Crustacea	Malacostraca	Decapoda	Jonah crab
Cancer irroratus	*Canir*	Crustacea	Malacostraca	Decapoda	Atlantic rock crab
Cancer magister	*Canme*	Crustacea	Malacostraca	Decapoda	Dungeness crab
Cancer productus	*Canpr*	Crustacea	Malacostraca	Decapoda	red rock crab
Carcinus maenas	*Carma*	Crustacea	Malacostraca	Decapoda	green crab
Cherax quadricarinatus	*Chema*	Crustacea	Malacostraca	Decapoda	Australian red claw crayfish
Clibanarius vittatus	*Clivi*	Crustacea	Malacostraca	Decapoda	thinstripe hermit crab
Crangon septemspinosa	*Crese*	Crustacea	Malacostraca	Decapoda	sand shrimp
Culex pipiens	*Culpi*	Hexapoda	Insecta	Diptera	Northern house mosquito
Culex quinquefasciatus	*Culqu*	Hexapoda	Insecta	Diptera	Southern house mosquito
Danaus plexippus	*Danpl*	Hexapoda	Insecta	Lepidoptera	monarch butterfly
Daphnia pulex	*Dappu*	Crustacea	Branchiopoda	Diplostraca	common water flea
Delia radicum	*Delra*	Hexapoda	Insecta	Diptera	cabbage root fly
Drosophila melanogaster	*Drome*	Hexapoda	Insecta	Diptera	fruit fly
Drosophila pseudoobscura	*Drops*	Hexapoda	Insecta	Diptera	North American fruit fly
Drosophila suzukii	*Drose*	Hexapoda	Insecta	Diptera	spotted wing fruit fly
Echinogammarus veneris	*Echve*	Crustacea	Malacostraca	Amphipoda	NA
Galleria mellonella	*Galme*	Hexapoda	Insecta	Lepidoptera	greater wax moth
Glossina morsitans	*Glomo*	Hexapoda	Insecta	Diptera	tsetse fly
Harpegnathos saltator	*Harse*	Hexapoda	Insecta	Hymenoptera	Jerdon's jumping ant
Helicoverpa armigera	*Helar*	Hexapoda	Insecta	Lepidoptera	cotton bollworm

Hemigrapsus nudus	*Hemnu*	Crustacea	Malacostraca	Decapoda	purple shore crab
Homarus americanus	*Homam*	Crustacea	Malacostraca	Decapoda	American lobster
Homarus gammarus	*Homga*	Crustacea	Malacostraca	Decapoda	European lobster
Homo sapiens	*Homsa*	Craniata	Mammalia	Primates	human
Hyalella azteca	*Hyaaz*	Crustacea	Malacostraca	Amphipoda	NA
Ixodes scapularis	*Ixosc*	Chelicerata	Arachnida	Ixodida	black-legged tick
Jasus edwardsii	*Jased*	Crustacea	Malacostraca	Decapoda	red rock lobster
Latrodectus hesperus	*Lathe*	Chelicerata	Arachnida	Araneae	Western black widow
Leucophaea maderae	*Leuma*	Hexapoda	Insecta	Blattodea	Madeira cockroach
Lithodes maja	*Litma*	Crustacea	Malacostraca	Decapoda	Norway king crab
Litopenaeus vannamei	*Litva*	Crustacea	Malacostraca	Decapoda	king prawn
Locusta migratoria	*Locmi*	Hexapoda	Insecta	Orthoptera	migratory locust
Lophopanopeus bellus	*Lopbu*	Crustacea	Malacostraca	Decapoda	black-clawed crab
Lucilia cuprina	*Luccu*	Hexapoda	Insecta	Diptera	Australian sheep blowfly
Lygus hesperus	*Lyghe*	Hexapoda	Insecta	Hemiptera	Western tarnished plant bug
Macrobrachium rosenbergii	*Macro*	Crustacea	Malacostraca	Decapoda	giant freshwater prawn
Mastotermes darwiniensis	*Masda*	Hexapoda	Insecta	Blattodea	giant Northern termite
Megachile rotundata	*Megro*	Hexapoda	Insecta	Hymenoptera	alfalfa leafcutting bee
Metacarcinus gracilis	*Metgr*	Crustacea	Malacostraca	Decapoda	graceful rock crab
Manduca sexta	*Manse*	Hexapoda	Insecta	Lepidoptera	tobacco hornworm
Mamestra brassicae	*Mambr*	Hexapoda	Insecta	Lepidoptera	Cabbage moth
Mythimna separate	*Mytse*	Hexapoda	Insecta	Lepidoptera	Northern armyworm
Nasonia vitripennis	*Nasvi*	Hexapoda	Insecta	Hymenoptera	jewel wasp
Neotrypaea californiensis	*Neoca*	Crustacea	Malacostraca	Decapoda	bay ghost shrimp
Nephrops norvegicus	*Nepno*	Crustacea	Malacostraca	Decapoda	Norwegian lobster
Neobellieria bullata	*Neobu*	Hexapoda	Insecta	Diptera	grey fleshfly
Nilaparvata lugens	*Nullu*	Hexapoda	Insecta	Hemiptera	brown planthopper
Ovalipes ocellatus	*Ovaoc*	Crustacea	Malacostraca	Decapoda	Atlantic Leopard Crab
Pachycheles rudis	*Pacry*	Crustacea	Malacostraca	Decapoda	thickclaw porcelain crab
Pacifastacus leniusculus	*Pacle*	Crustacea	Malacostraca	Decapoda	signal crayfish
Pagurus acadianus	*Pagac*	Crustacea	Malacostraca	Decapoda	acadian hermit crab
Pagurus granosimanus	*Paggr*	Crustacea	Malacostraca	Decapoda	Grainyhand hermit crab
Pagurus pollicaris	*Pagpo*	Crustacea	Malacostraca	Decapoda	flatclaw hermit crab
Pandalus danae	*Panda*	Crustacea	Malacostraca	Decapoda	dock shrimp
Pandalus platyceros	*Panpl*	Crustacea	Malacostraca	Decapoda	California spot prawn
Panulirus interruptus	*Panin*	Crustacea	Malacostraca	Decapoda	California spiny lobster
Penaeus duorarum	*Pandu*	Crustacea	Malacostraca	Decapoda	pink shrimp
Penaeus monodon	*Penmo*	Crustacea	Malacostraca	Decapoda	black tiger shrimp
Periplatena Americana	*Peram*	Hexapoda	Insecta	Blattodea	American cockroach
Petrolisthes cinctipes	*Petci*	Crustacea	Malacostraca	Decapoda	flat porcelain crab

Petrolisthes eriomerus	*Peter*	Crustacea	Malacostraca	Decapoda	flattop crab
Procambarus clarkia	*Procl*	Crustacea	Malacostraca	Decapoda	red swamp crayfish
Protophormia terraenovae	*Prote*	Hexapoda	Insecta	Diptera	Northern blowfly
Pugettia gracilis	*Puggr*	Crustacea	Malacostraca	Decapoda	graceful kelp crab
Pugettia producta	*Pugpr*	Crustacea	Malacostraca	Decapoda	shield-backed kelp crab
Renilla reniformis	*Renre*	Cnidaria	Anthozoa	Pennatulacea	sea pansy
Rhyparobia maderae	*Rhyma*	Hexapoda	Insecta	Blattodea	Madeira cockroach
Rhodnius prolixus	*Rhopr*	Hexapoda	Insecta	Hemiptera	kissing bug
Schistocerca gregaria	*Schgr*	Hexapoda	Insecta	Orthoptera	desert locust
Scylla olivacea	*Scyol*	Crustacea	Malacostraca	Decapoda	orange mud crab
Scylla paramamosain	*Scypa*	Crustacea	Malacostraca	Decapoda	mud crab
Solenopsis invicta	*Solin*	Hexapoda	Insecta	Hymenoptera	red fire ant
Stegodyphus mimosarum	*Stemi*	Chelicerata	Arachnida	Araneae	velvet spider
Speleonectes lucayensis	*Spelu*	Crustacea	Remipedia	Nectiopoda	Speleonectes
Stenobothrus lineatus	*Steli*	Hexapoda	Insecta	Orthoptera	stripe-winged grasshopper
Symphylella vulgaris	*Symvu*	Myriapoda	Symphyla	NA	garden centipedes
Tenebrio molitor	*Tenmo*	Hexapoda	Insecta	Coleoptera	yellow mealworm
Tetranychus urticae	*Tetur*	Chelicerata	Arachnida	Trombidiformes	two-spotted spider mite
Therea petiveriana	*Thepe*	Hexapoda	Insecta	Blattodea	desert cockroach
Triatoma infestans	*Triin*	Hexapoda	Insecta	Hemiptera	barber bug
Tribolium castaneum	*Trica*	Hexapoda	Insecta	Coleoptera	red flour beetle
Triops newberryi	*Trine*	Crustacea	Branchiopoda	Notostraca	tadpole shrimp

Chapter 1:
General introduction

1.1. Aims and outline of this thesis

Insects are economically valuable organisms occupying almost all ecological niches on Earth. Many insect species are important for our human quality-of-life, since they are pollinators of crops and flowers, and produce economically interesting substances, such as honey, silk and wax. However, several insect species have a negative impact, since they form a threat for agriculture or are important vectors for human diseases, such as malaria, yellow fever and zika virus (Chapman, 2012; World Health Organization, 2017).

Major physiological and behavioral processes in insects are regulated by neuropeptides. Most of these neuropeptides bind to membrane-bound G protein-coupled receptors (GPCRs) which transduce these extracellular signals into cellular physiological responses. They are often referred to as promising candidate targets for the development of more specific pest control agents (Altstein and Nässel, 2010; Bendena, 2010; Vanden Broeck, 2001a; Van Hiel et al., 2010; Verlinden et al., 2014).

The study of the GPCR mediated downstream regulatory pathways in insects is mainly limited to the detection of fluctuations in the secondary messenger molecules. In general, solely the intracellular Ca^{2+} and cyclic adenosine monophosphate (cAMP) concentrations are being monitored upon receptor activation. By monitoring changes in the concentrations of these molecules, we cannot precisely infer which specific Gα protein(s) is (are) activated upon receptor activation.

In contrast, GPCRs and their downstream regulatory pathways are elaborately studied in vertebrates, since these receptors are important pharmacological targets for approximately 30 % of all therapeutic compounds (Hopkins and Groom, 2002). To study the G protein mediated signaling pathways of human receptors in more detail, several bioluminescence resonance energy transfer $(BRET)^2$-based G protein biosensors have been developed, which can detect the direct activation of Gα proteins, not only showing the activation of a given Gα subfamily, but also verifying which member(s) of this subfamily can be activated. Ten human G protein based biosensors have been developed by Galés and co-workers (2006) representing members of all four Gα protein subfamilies ($G\alpha_{i/o}$, $G\alpha_{s}$, $G\alpha_{q/11}$ and $G\alpha_{12/13}$).

The aims of this project is to test whether these $BRET^2$-based G protein biosensors are also reliable biosensors to study the G protein mediated pathways of insect GPCRs. For this purpose, three neuropeptide signaling systems are selected in two insect species. The first species, the buff-tailed bumblebee, *Bombus terrestris*, is chosen as a beneficial insect that is regularly used as a pollinator of greenhouse crops. The second species, the desert locust, *Schistocerca gregaria*, is a major pest species that is able to form devastating swarms. These swarms have been reported since thousands

of years (*e.g.* in the Bible and the Quran) and are known to have a strong negative impact on agricultural production and human welfare.

The first neuropeptide/receptor couple under investigation is *B. terrestris* SIFamide and its receptor (SIFR), which belongs to the Family A GPCRs. This signaling system is selected, since almost nothing is known about its downstream signaling mechanisms. In the other insect species, *S. gregaria*, two receptors are selected, namely the allatotropin receptor (ATR) and the corticotropin-releasing factor (CRF)-related diuretic hormone (DH) receptor (CRF-DHR). Since the former receptor belongs to the Family A GPCRs, and the latter receptor belongs to the Family B GPCRs, members of two distinct GPCR families are represented in this study. These two neuropeptide receptor systems are also selected since they are proposed as candidate targets for insect pest control (Verlinden et al., 2014). For *Schgr*-CRF-DH, three putative receptors are identified in the (unpublished) transcriptome database (Verdonck, 2017).

To get a better understanding of their possible *in vivo* functional roles, a tissue distribution analysis is performed for the different neuropeptide precursor and receptor transcripts [except for *Schgr*-CRF-DH for which this analysis is already performed by Van Wielendaele and co-workers (2012)]. Next, the receptors are molecularly cloned and pharmacologically characterized. I have fully cloned and characterized *Bomte*-SIFR, *Schgr*-CRF-DHR1 and *Schgr*-ATR. The downstream signaling pathways of the cloned receptors are subsequently studied by means of cell-based functional receptor assays, such as the aequorin bioluminescence assay and the cAMP responsive element (CRE)-dependent luciferase reporter assay which can monitor concentration changes of the intracellular secondary messenger molecules Ca^{2+} and cAMP, respectively. For the latter secondary messenger molecule, an alternative biosensor, the cAMP sensor using YFP-Epac-*R*luc (CAMYEL) (ATCC MBA-277; Jiang et al., 2007), is tested which, in contrast to the $CRE_{(6x)}$-based luciferase reporter assay, directly interacts with cAMP.

Finally, the $BRET^2$-based G protein biosensors are tested in order to see if they can also be used to study the G protein mediated pathways of insect GPCRs. In order to interpret the results of the $BRET^2$-based G protein biosensors, the amino acid sequence of the human G protein subunits, which are used to construct the $BRET^2$-based G protein biosensors, are compared to the amino acid sequences of the G protein subunits identified in both *B. terrestris* and *S. gregaria*.

1.2. Insects

Insects are hexapod invertebrates which belong to the Arthropod phylum. They constitute the largest and most diverse group of animals on Earth. Particularly, more than 70 % of the 1.5 million described animal species belong to this class (taxonomic classification indicated in table 1.1) which consists of 24 orders. Four of those orders quantitatively dominate in terms of described species, namely the Coleoptera or beetles, the Lepidoptera or butterflies and moths, the Hymenoptera, to which the sawflies, wasps, bees and ants belong, and the Diptera or flies and mosquitoes (Chapman, 2012).

Table 1.1: Taxonomic classification of insects.

Taxonomic rank	Scientific classification
Superkingdom	Eukaryota
Kingdom	Metazoa
Phylum	Arthropoda
Subphylum	Hexapoda
Class	Insecta

Insects have a large impact on humans and on ecosystems in general. For instance, insects are the principal food source for many animals. They also pollinate most species of flowering plants, produce economically interesting consumables such as honey, silk and wax, and play an important role in nutrient recycling. Insects are also well-known for their negative impact on humans. For instance, insects have a negative impact on human food supply chains, since they are important vectors for plant and livestock diseases. Furthermore, it is estimated that one-sixth of all crops are lost due to herbivorous insects (Chapman, 2012).

Additionally, insects are also important vectors for human diseases such as dengue fever (virus transmitted by *Aedes aegypti*), yellow fever (virus transmitted by mosquitos belonging to the *Aedes* and *Haemogogus* genera), zika virus (virus transmitted by *A. aegypti*), Chagas disease (Trypanosome parasite transmitted by *Triatoma infestans* and *Rhodnius prolixus*), leishmaniasis (Trypanosome parasite transmitted by sandflies) *etc*. (Bendena, 2010; World Health Organization, 2017). Vector-borne diseases account for more than 17 % of all infectious diseases and cause more than 700 000 deaths annually. For instance, in 2017 malaria, which is caused by *Plasmodium* parasites that are transmitted by female *Anopheles* mosquitoes, affected over 219 million people in 90 countries and caused 435 000 people to die (World Health Organization, 2018).

The insect life cycle can be categorized in three strategies, namely ametabolous, hemimetabolous and holometabolous. Ametabolous insects do not undergo metamorphosis and hatch from their eggs in the same form as they will retain throughout their life cycle. Hemimetabolous insects, such

as locusts (order Orthoptera), undergo an incomplete metamorphosis. They hatch from their egg as a small, immature version of the adults lacking both wings and a functional reproduction system. After a series of moults, these nymphs pass via an incomplete metamorphosis to the winged and reproductive adult stage. Finally, holometabolous insects, such as beetles (order Coleoptera), (bumble)bees (order Hymenoptera), butterflies (order Lepidoptera) and flies (order Diptera) undergo complete metamorphosis. After hatching from their egg, the larvae undergo several moults until they enter a non-feeding pupal stage. In this stage, an extreme anatomical makeover (metamorphosis) takes place and the adults appear as winged hexapods (Verlinden et al., 2014).

1.2.1. *Bombus terrestris*: an example of a beneficial insect

The buff-tailed bumblebee *Bombus terrestris* (depicted in Fig. 1.1) is a holometabolous insect which belongs the order of the Hymenoptera. The taxonomic classification of *B. terrestris* is presented in table. 1.2.

Figure 1.1: Female worker of *Bombus terrestris*. (Image credits: Wikipedia, 2019)

Table 1.2: Taxonomic classification of the buff-tailed bumblebee *Bombus terrestris.*

Taxonomic rank	Scientific classification
Class	Insecta
Subclass	Pterygota
Infraclass	Neoptera
Order	Hymenoptera
Suborder	Apocrita
Superfamily	Apoidea
Family	Apidae
Subfamily	Bombinae
Genus	*Bombus*
Species	*terrestris*

Bumblebees are capable of endothermy and are well adapted to relatively cool conditions. The original distribution area of *B. terrestris* comprises Europe and adjacent territories including the north coast of Africa and West and Central Asia (Inoue et al., 2008; Sladen, 1912). Nowadays, they

can be found in almost the entire northern hemisphere. They expanded their distribution area since the late 1980s, when *B. terrestris* became commercially available as a valuable pollinator of flowers and greenhouse crops. After their frequent introduction in foreign territories, it became more apparent that *B. terrestris* is an invasive species with a strong impact on native bumblebee species (Goulson, 2010; Inoue et al., 2008; Velthuis and Doorn, 2006).

Bumblebees are eusocial insects which implies that their nest is sustained by a non-reproductive working caste. They have an annual life cycle founded by a diploid queen that has mated with one or more males. Queens of the *B. terrestris* species emerge from hibernation in late winter and choose an appropriate nesting site. The queen lays her first batch of fertilized and thus diploid eggs that will develop into female workers. The larvae emerge from the eggs after four days and are fed with pollen and nectar. They undergo four moults before they go into the pupal stage in which metamorphosis occurs. New adults emerge after a total development time of four to five weeks, depending on the temperature and food supply. These workers take over the task to sustain the colony, so the queen's only task will be to produce more eggs. The nest growth accelerates and after attaining a sufficient size, the colony switches to rearing haploid males and new diploid queens. The young queen leaves the nest to forage and starts building up fat reserves by consuming large quantities of pollen and nectar. Her most important task is to mate, so she can start a new colony in spring. The males leave the colony after a few days and start searching a mate while feeding on flowers. After mating, young queens start their search for a suitable hibernation site to overcome winter. The original nest rapidly degenerates once the males and queens leave the nest since the remaining workers become lethargic and the original queen is usually worn out (Goulson, 2010).

1.2.2. *Schistocerca gregaria*: an example of a pest insect

The desert locust *Schistocerca gregaria* (depicted in Fig. 1.2) is a hemimetabolous insect, which belongs to the family of Acrididae in the order of Orthoptera. The taxonomic classification of *S. gregaria* is presented in table 1.3.

Figure 1.2: **Crowded-reared desert locust *Schistocerca gregaria*: left** sexually mature female and **right:** sexually mature male. (Image credits: Timon Smeets)

Desert locusts are well-known for their extreme form of density dependent polyphenism, also known as phase polyphenism (Pener, 1991; Pener and Yerushalmi, 1998; Uvarov, 1966). Moreover, they have the ability to change their behavior and physiology in response to changes in density. During quit periods (also known as recession), unharmful solitarious locusts are found in low numbers scattered throughout the desert of North Africa, the Middle east and Southwest Asia covering about 16 million square kilometers (recession area in Fig. 1.3). Under certain environmental conditions, the number of locusts can increase greatly resulting in high density swarms (Symmons and Cressman, 2001). These gregarious locusts show pronounced changes in coloration, morphometry, metabolism, feeding, reproduction, (endocrine) physiology, neurophysiology and immune responses (Verlinden et al., 2009). These swarms consist of up to 80 million locusts per square kilometer and can cover an area of one to several hundred square kilometers. They can travel up to 130 kilometers per day, increasing their distribution area to 29 million square kilometers, covering more than 20 % of the Earth's total land surface (invasion area in Fig. 1.3; Food and Agricultural Organization of the United Nations: Locust watch, 2009; Symmons and Cressman, 2001). These swarm-forming gregarious locusts are a major threat to the people's livelihood, food security, environment and economic development (Food and Agricultural Organization of the United Nations, 2015).

Table 1.3: Taxonomic classification of the dessert locust *Schistocerca gregaria*.

Taxonomic rank	**Scientific classification**
Class	Insecta
Subclass	Pterygota
Infraclass	Neoptera
Order	Orthoptera
Suborder	Caelifera
Superfamily	Acridoidea
Family	Acrididae
Subfamily	Cyrtacanthacridinae
Genus	*Schistocerca*
Species	*gregaria*

The desert locusts pass three stages throughout their life cycle: egg, nymph (hoppers) and adult. Newly hatched locusts appear as small, immature version of the adults lacking both wings and a functional reproduction system. They undergo five (gregarious locusts) to six (solitarious locusts) moults before going into the adult stage. A new adult (also called a fledgling) is initially sexually immature and their wings must dry and harden before they can fly. Once they are mature, they are available for copulation. Females lay their eggs in moist soil, 5 - 10 cm below the surface. Gregarious locusts can lay up to 80 eggs per batch, while solitarious locusts can lay up to 90 – 160 eggs. The

total development time depends on environmental conditions (Symmons and Cressman, 2001). The life cycle of *S. gregaria* is depicted in Fig. 1.4. Due to the devastating impact of locust swarms on agricultural production and human welfare, potential threats are constantly monitored (Food and Agriculture Organization of the United Nations, 2019).

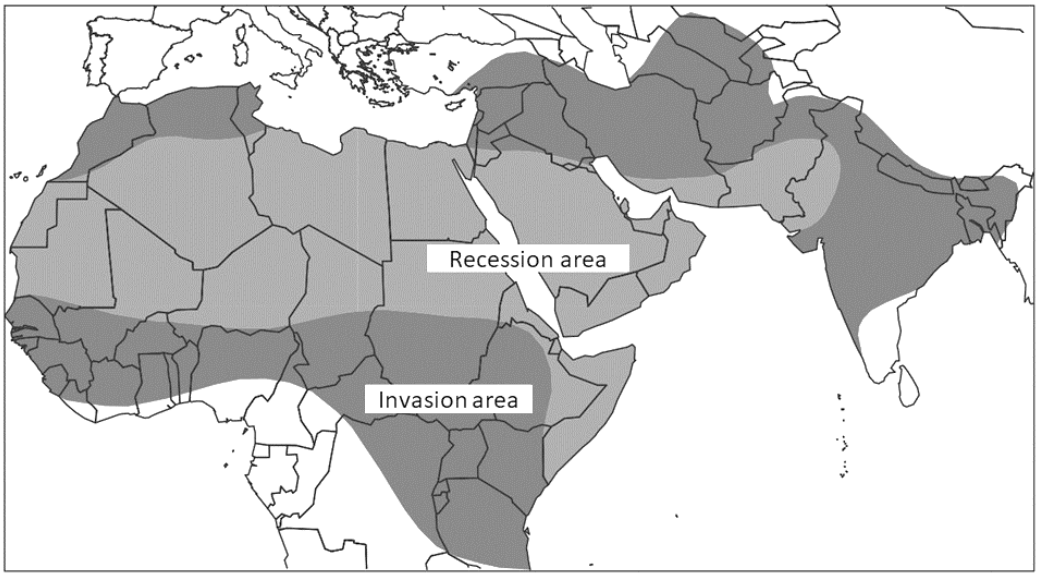

Figure 1.3: Distribution area of *S. gregaria* during the solitarious phase (recession area, light grey) and their possible invasion area during the gregarious phase (invasion area, dark grey). (Image credits: adapted from Lecoq, 2004)

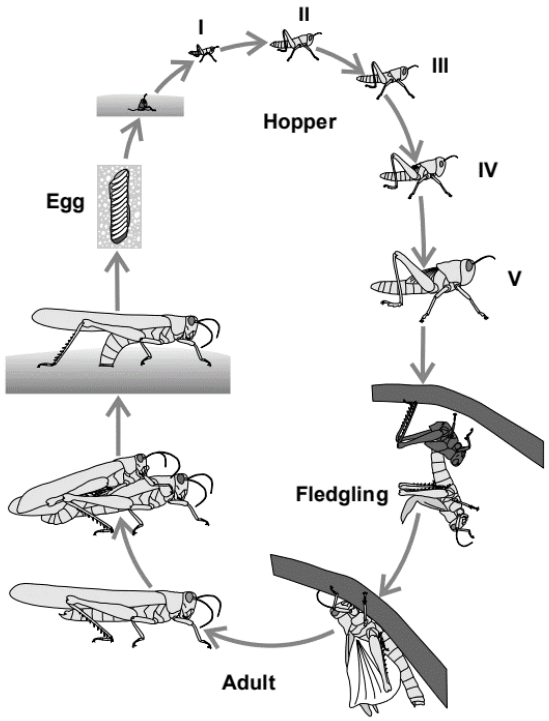

Figure 1.4: The life cycle of *S. gregaria*. (Image credits: Symmons and Cressman, 2001)

1.2.3. Insect pest control

Since estimates by the United Nations (UN) predict that the world population will grow to almost ten billion people by 2050 (United Nations, 2017), food availability and access are becoming increasingly important. An important step in the enhancement of food availability is the reduction of yield losses due to pests, pathogens and weeds. One strategy to reduce these yield losses is crop protection (Verger and Boobis, 2013).

Crop protection is mainly established by the use of insecticides. Despite its widespread use and effectiveness, chemical insecticides are often harmful to humans, ecosystems and animals including beneficial insects (Bendena, 2010). It has been estimated that, in general, 30 % of pesticides marketed in developing countries do not meet the internationally accepted criteria for safe pesticide residues in the food supply (Verger and Boobis, 2013). For example, locust swarms, which mostly take place in developing countries, are primarily fought with acetylcholine esterase inhibitors which have an impact on other animals and the ecosystem as well. Moreover, these chemicals are also harmful for human health (Food and Agricultural Organization of the United Nations: Locust watch, 2009). Earlier efforts to produce more locust-specific biological insecticides have resulted in the production of Green Muscle, a fungus based biopesticide consisting of *Metarhizium anisopliae* var. *acridum*. However, for now, the use of Green Muscle is only recommended for hopper bands and not for adult locusts. Moreover, this insecticide only has its maximum efficacy when the locusts remain in the treated area for at least two days, which might not be the case for fast-moving hopper bands (Enserink, 2004; van der Valk, 2007).

Another problem concerning the use of insecticides is resistance. This problem causes an incessant search for new insecticides with a species-specific mode of action (Van Hiel et al., 2010). In the continuing search for new pest control agents, neuropeptide receptors are regularly mentioned as possible candidate targets. Neuropeptides are produced by the neurosecretory cells of the central nervous system (CNS; box 1.1) and are important regulatory factors in a wide array of key biological processes such as development, growth, metabolism, ecdysis, feeding and reproduction (Altstein and Nässel, 2010; Van Hiel et al., 2010; Verlinden et al., 2014). Neuropeptides usually consist of 5 to 80 amino acid residues (Altstein and Nässel, 2010) and act as neuromodulators or neurohormones (Bendena, 2010). Most neuropeptides exert their function by binding to membrane-bound G protein-coupled receptors (GPCRs). These seven transmembrane receptors (7TM) transduce these extracellular signals into cellular physiological responses (Vanden Broeck, 2001a). One insecticide that is commercially available and targets a GPCR is Amitraz, which targets the biogenic amine octapamine receptor (Casida and Durkin, 2013).

An example of a neuropeptide receptor that could also be an excellent target in the search for new insect pest management strategies is the corticotropin-releasing factor (CRF)-related diuretic hormone (DH) receptor (CRF-DHR) because of its role in regulating feeding behavior, water homeostasis and reproduction (Gäde and Goldsworthy, 2003; Van Wielendaele et al., 2012; Van Wielendaele, 2012). This neuropeptide is synthesized in the neurosecretory cells of the pars intercerebralis and is released into the hemolymph via the corpora cardiaca (Kay et al., 1991a). Another neuropeptide receptor which could be targeted is the allatotropin receptor (ATR). Allatotropin is a pleiotropic neuropeptide, which stimulates the production of juvenile hormone in some insects species, exerts important biological activities in the digestive system, regulates muscle activity and plays a role in the photic entrainment of the circadian clock (Verlinden et al., 2015).

Box 1.1: The central nervous system (CNS) of insects

The central nervous system (CNS) of insects consists of the brain, the ventral nerve cord (VNC) and the ventral ganglia. The pars intercerebralis in the brain contains neurosecretory cells. Neurohormones produced in these cells are transferred via axonal transport to the corpora cardiaca, in which the neurohormones are stored in the neurohemal part and released at the appropriate moment into the hemolymph (neurohemal release sites). The corpora allata are a pair of small endocrine glands which synthesize and release juvenile hormone. The prothoracic gland is also an endocrine gland and is known to synthesize ecdysteroids in larval insects. The suboesophageal ganglion, the frontal and the hypocerebral ganglia are part of the stomatogastric nervous system (Box 5.3: the stomatogastric nervous system; Nation, 2015). The nervous system in a locust's head is depicted in Fig. 1.5 and a dorsal view including the ventral nerve cord and ventral ganglia is depicted in Fig. 1.6. In locusts, the first three (1-3) abdominal ganglia are fused to the metathoracic ganglion and the last four (8-11) are fused to each other and form the terminal abdominal ganglion (Burrows, 1996).

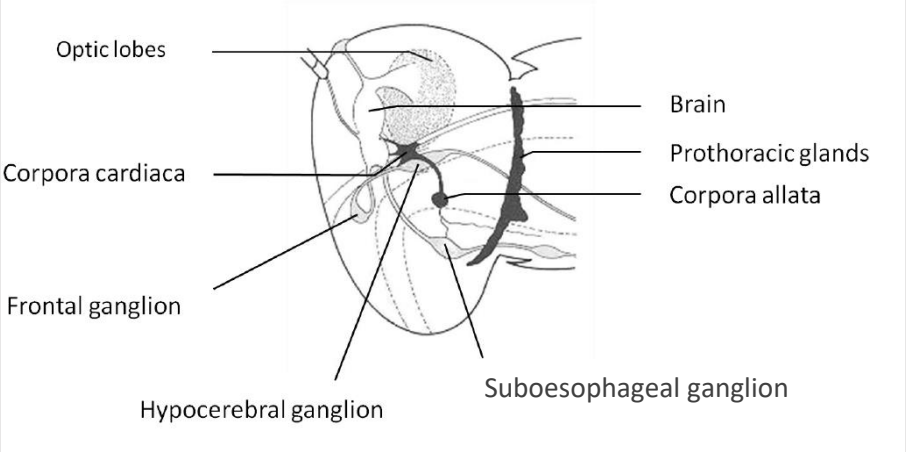

Figure 1.5: The neuroendocrine system in a locust head. (Image credits: CIRAD: French Agricultural Research Centre for International Development, 2007; adapted by Van Wielendaele, 2012)

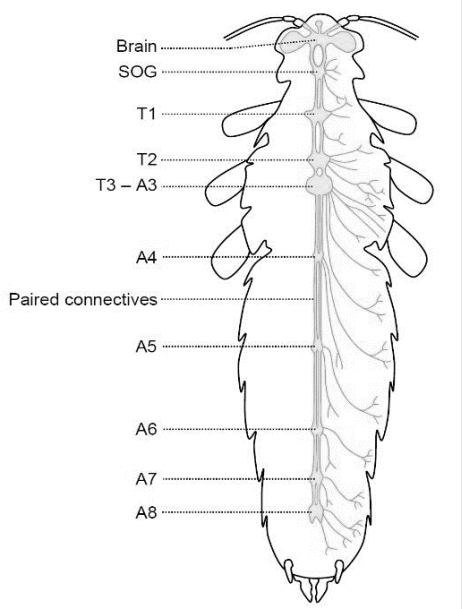

Figure 1.6: Dorsal view of the nervous system of locusts. Abbreviations: SOG = suboesophageal ganglion, T1 = prothoracic ganglion, T2 = mesothoracic ganglion, T3 = metathoracic ganglion, A = abdominal ganglia. (Image credits Cronodon.com, 2018, based on Bharadwaj and Banerjee, 1971)

1.3. G protein-coupled receptors

Guanine nucleotide binding protein (G protein) coupled receptors (GPCRs) are the largest superfamily of cell surface receptor proteins in eukaryotes. They transduce extracellular signals into intracellular cellular responses. These receptors are conserved proteins with an ancient origin that is situated before the divergence of Protostomian and Deuterostomian animals (Vanden Broeck, 1996). GPCRs are expressed in various tissues and are involved in a broad range of physiological processes. Signals activating these receptors range from photons, odorants, ions, small neuromodulatory peptides to large peptide and glycoprotein hormones (Vanden Broeck, 2001a; Wootten et al., 2018).

1.3.1. General structure

The core of GPCRs consists of seven α-helices, each comprising 20 to 30 hydrophobic amino acids, which span the membrane. These transmembrane segments (TM) are interconnected by alternating intracellular (ICL1 - ICL3) and extracellular (ECL1 - ECL3) loops. The amino-terminus (N-terminus) is located extracellularly while the carboxyl terminus (C-terminus) is located intracellularly. The N-terminus and the ECLs are involved in the interaction with the ligand, whereas the C-terminus and the ICLs are involved in the recruitment and activation of intracellular proteins (Kobilka, 1992). In the classical model, GPCRs exert their function through coupling with heterotrimeric G proteins. These G proteins serve as canonical transducer proteins and consist of three subunits: Gα, Gβ and Gγ (Gether, 2000). A schematic representation of the basic GPCR and G protein structure is depicted in Fig. 1.7.

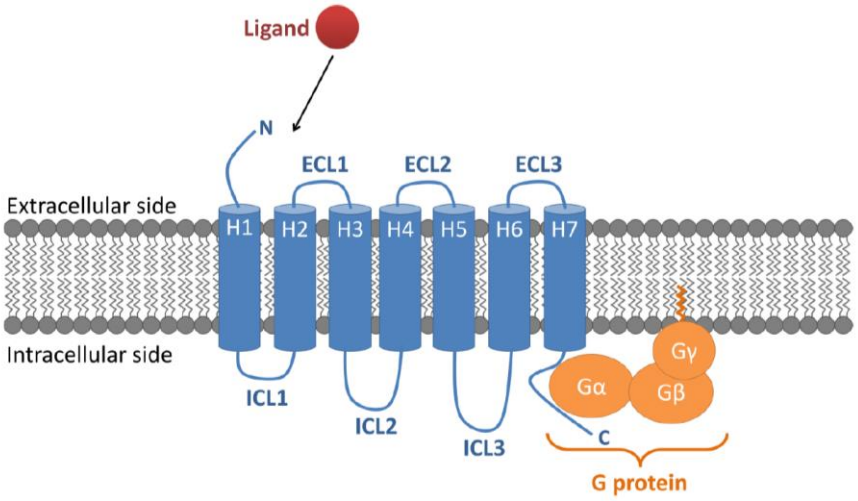

Figure 1.7: Schematic representation of the basic GPCR and G protein structure: A GPCR consists of seven α-helices (H1 - H7) spanning the plasma membrane, an extracellular N-terminus, three extracellular loops (ECL1 - ECL3), three intracellular loops (ICL1 - ICL3) and an intracellular C-terminus. The intracellularly located heterotrimeric G protein consists of three subunits: Gα, Gβ and Gγ. Ligand binding occurs on the extracellular side. (Image credits: Verlinden et al., 2014)

1.3.2. Ligand classification

Before biased agonism (further discussed below) was a well-accepted mechanism, GPCR ligands were classified as follows: agonists are compounds which can induce the maximal response, partial agonists are compounds which can only induce a submaximal response, antagonists are compounds which can competitively inhibit an agonist but do not have intrinsic signaling efficacy, and inverse agonists are compounds that stabilize the inactive receptor state (Luttrell et al., 2015). This classification of GPCR ligands is still widely used to describe different kinds of ligands that can interact with a receptor.

1.3.3. Receptor classification

Based on protein sequence and structure, the GPCR superfamily is typically categorized in five main families. Most GPCRs can be subdivided in the first three major families. The remaining GPCRs are assigned to two additional GPCR families which comprise atypical GPCRs (Bockaert et al., 1999; Fredriksson et al., 2003; Gether, 2000; Horn et al., 2003; Kolakowski, 1994; Schiöth and Lagerström, 2008; Venkatakrishnan et al., 2013; Vroling et al., 2011).

The first major family, (1) the rhodopsin-related receptor family (Family A), is the largest family of GPCRs. Members of this family usually contain a palmitoylated cysteine in their C-terminal causing the formation of a putative fourth intracellular loop (Oldham and Hamm, 2008). (2) Family B, the secretin receptor-related GPCRs, is characterized by a long (~100 amino acids) N-terminus containing a network of disulfide bridges, whereas the third major family, (3) Family C or the metabotropic glutamate receptor-related GPCRs, is characterized by an even longer N-terminus (~600 amino acids). A snake diagram presenting conservative amino acids of the three major GPCR families is depicted in Fig. 1.8. The two remaining GPCR families are (4) the developmental GPCRs activated by Wnt and hedgehog related ligands, therefore named the Frizzled-Smoothened Family, and (5) a Family consisting of a group of atypical GPCRs (Gether, 2000; Verlinden et al., 2014).

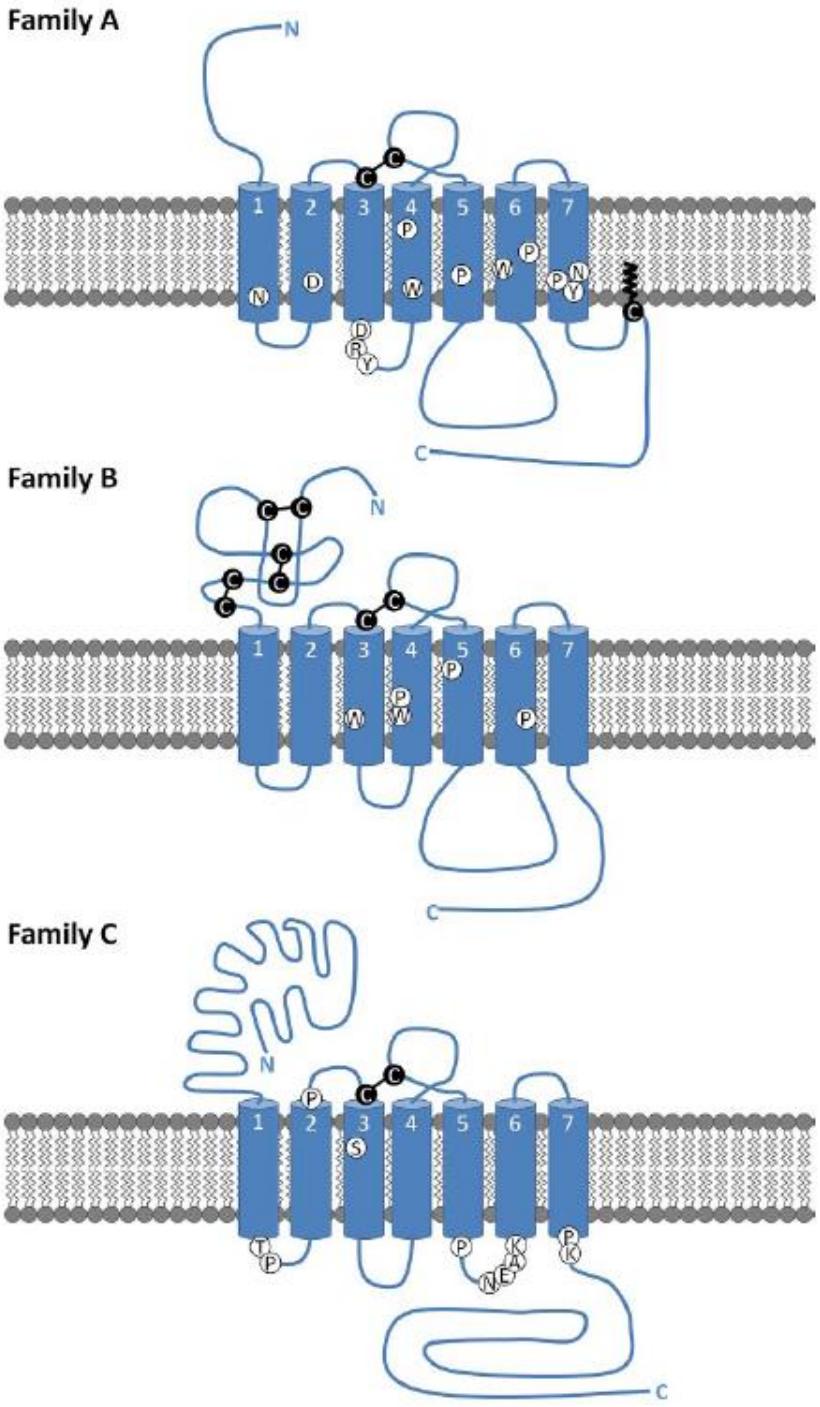

Figure 1.8: Snake diagrams of the three major GPCR families. The most conserved residues are indicated in white circles surrounding the one-letter amino acid nomenclature Conserved cysteine bridges are indicated by connecting black circles. All three families contain a putative disulfide bridge between the first and the second extracellular loop. **Above**: members of the **Family A** GPCRs usually have a palmitoylated cysteine in their C-terminus causing the formation of a putative fourth intracellular loop. **Middle**: members of the **Family B** GPCRs usually have three disulfide bridges in their long N-terminus. **Below**: members of the **Family C** GPCRs usually have an even longer N-terminus and a short conserved third intracellular loop. (Image credits: Verlinden et al., 2014, adapted from Gether, 2000)

1.3.4. Downstream signaling pathways

As indicated by its name, GPCRs transduce their signal via G proteins which can further transduce the signal into a variety of downstream responses. These downstream responses are provoked by a variety of downstream effectors, such as enzymes and ion channels (Shukla et al., 2011). However, in addition to G proteins, GPCRs can also signal through other adaptor proteins that can transduce signals into multiple effector pathways. For instance, GPCR kinases (GRKs) and β-arrestins are now recognized as true adaptor proteins for GPCRs (Rajagopal et al., 2010; Smith et al., 2018). The two best studied GPCR downstream regulatory pathways, the G protein mediated pathways and the β-arrestin mediated pathways, are discussed below.

1.3.4.1. G protein mediated pathways

In the classical GPCR signaling model, GPCR signaling is exerted by coupling with heterotrimeric G proteins consisting of three subunits; namely Gα, Gβ and Gγ. These G proteins act as molecular switches in signal transduction pathways. In humans, 16 Gα, 5 Gβ and 13 Gγ isoforms are identified (Wootten et al., 2018).

Binding of an agonist at the extracellular side of the GPCR activates the receptor inducing a conformational change. This conformational change activates, in turn, the associated heterotrimeric G protein which functions as a guanine-nucleotide exchange factor (GEF) whereby the Gα protein cycles between an inactive guanosine diphosphate (GDP)-bound conformation and an active guanosine triphosphate (GTP)-bound conformation. Upon activation, GDP is released from the Gα subunit and is exchanged for GTP. The activated GTP-bound Gα protein shows a reduced affinity for the Gβγ dimer, leading to the dissociation of the two subunits. Both the activated Gα protein and the Gβγ dimer can modulate the activity of downstream effector proteins. G protein activation is terminated upon hydrolysis of the GTP, restoring the inactivated GDP-bound conformation and reassociation of the Gα subunit to the Gβγ dimer (Bourne et al., 1991; Cabrera-Vera et al., 2003; Gether, 2000; Oldham and Hamm, 2008). A schematic representation of the G protein activation and inactivation cycle is presented in Fig. 1.9.

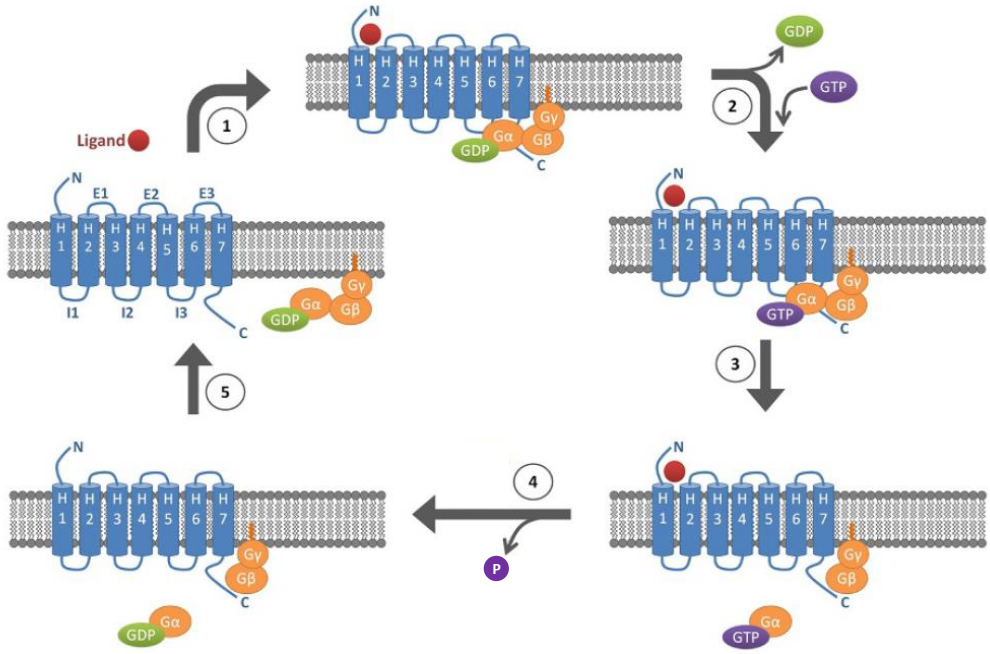

Figure 1.9: Schematic representation of the G protein activation and inactivation cycle. (1) Binding of a ligand to the receptor causes a conformational change of the receptor and subsequent activation of Gα. (2) Gα exchanges guanosine diphosphate (GDP) for a guanosine triphosphate (GTP) and (3) dissociates from the Gβγ dimer. (4) The G protein is inactivated upon hydrolysis of GTP and (5) reassociates with the Gβγ dimer. (Image credits: adapted from Verlinden et al., 2014)

Most of the metazoan Gα proteins can be classified within four major, evolutionally conserved subfamilies: $G\alpha_s$, $G\alpha_{i/o}$, $G\alpha_q$ and $G\alpha_{12/13}$. Each of these G protein subfamilies can regulate several downstream effectors. A schematic illustration of the diversity of G protein mediated signaling pathways is presented in Fig. 1.10. Additionally, a fifth Gα protein ($G\alpha_v$) is identified in zebrafish that also seems to be conserved across the animal kingdom. This $G\alpha_v$ protein appears to be present in vertebrates, arthropods, mollusks, annelids and sponges. Although a decade has passed since its first identification, still nothing is known about the signaling pathways of this protein subfamily (Oka and Korsching, 2009; Oka et al., 2009).

A single GPCR can couple to either one or more Gα proteins simultaneously (Dorsam and Gutkind, 2007). The $G\alpha_s$ and $G\alpha_{i/o}$ subfamilies are well known for their effect on the adenylyl cyclase (AC)/cAMP/ protein kinase A (PKA) pathway while $G\alpha_{q/11}$ pathway is well known for its effect on the phospholipase C (PLC)/Ca^{2+} pathway (Cabrera-Vera et al., 2003). Both pathways are described in more detail below. The $G\alpha_{12/13}$ subfamily is involved in the activation of effectors such as the Rho family of GTPases nucleotide exchange factors (RhoGEFs), a family of small signaling G proteins involved in the activation of small monomeric RhoGTPases (Siehler, 2009), and A-kinase anchor proteins (AKAPs) which can bind to the regulatory subunits of PKA and are involved in cardiac protection (Diviani et al., 2018). Additionally, also the Gβγ dimer can act as a true signal transducing

protein with several effector such as phospholipases, ACs, ion channels, lipid kinases and members of the mitogen-activated protein kinase (MAPK) pathway (Cabrera-Vera et al., 2003; Wootten et al., 2018). The role of the Gβγ dimer is further discussed below.

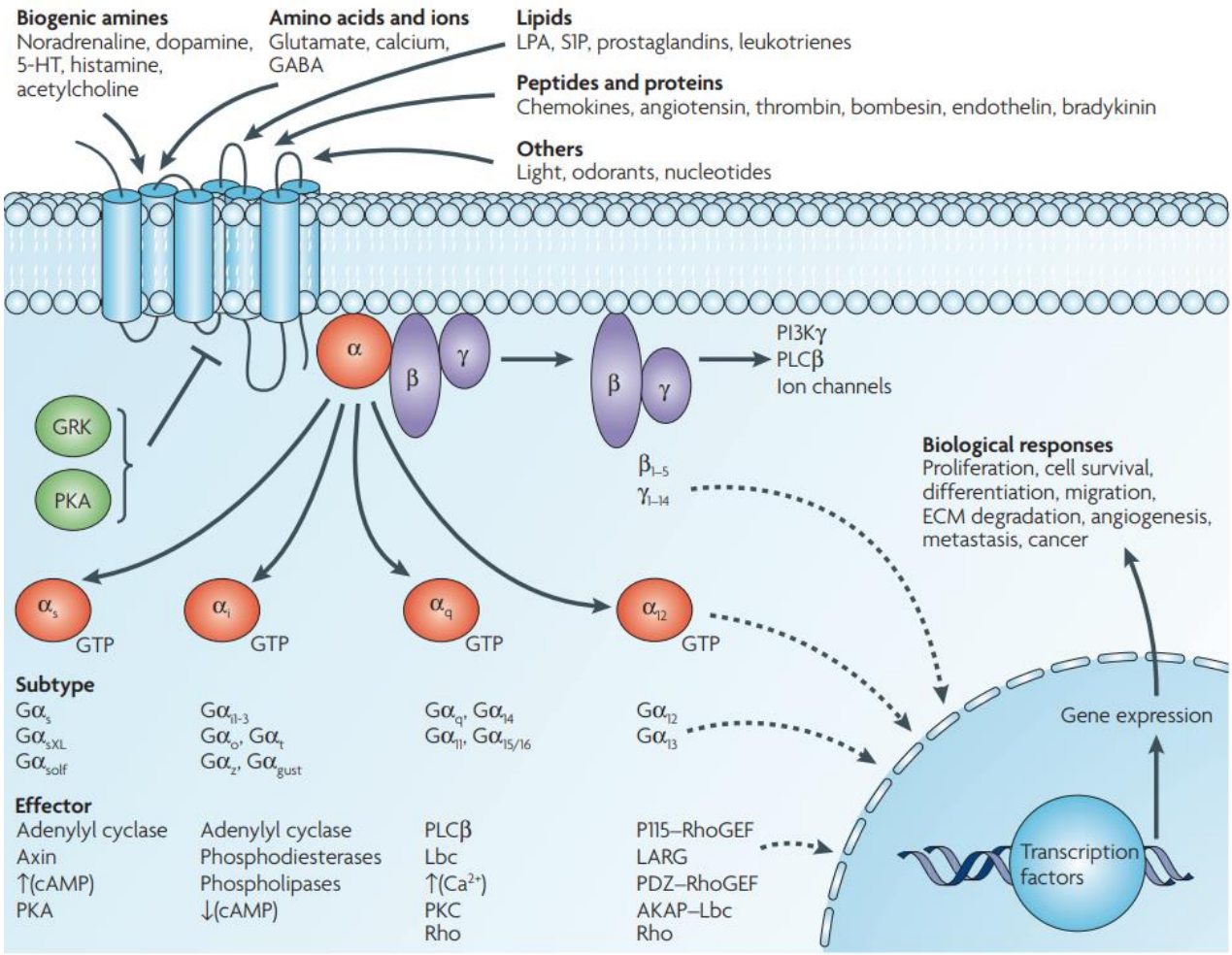

Figure 1.10: Schematic illustration of diverse G protein mediated signaling pathways. GPCRs interact with heterotrimeric G proteins consisting of Gα, Gβ and Gγ subunits. Upon activation of the GPCR by various ligands, the G protein is activated resulting in the dissociation of the Gα protein from the Gβγ dimer. Both the Gα protein and the Gβγ dimer can activate downstream signaling pathways. The Gα proteins are classified in four major subfamilies: $G\alpha_s$, $G\alpha_{i/o}$, $G\alpha_{q/11}$ and $G\alpha_{12/13}$ and each Gα protein subfamily can regulate several downstream effectors. Some of these downstream effectors (indicated by dotted lines) can act as transcription factors modulating gene expression resulting in diverse biological responses. Abbreviations used: PKA = protein kinase A, cAMP = cyclic adenosine monophosphate, PLCβ = phospholipase C, PKC = protein kinase C, RhoGEF = RhoGTPase nucleotide exchange factor; LARG = leukemia-associated RhoGEF, PDZ-RhoGEF = PSD-95/Disc-large/ZO-1 homology (PDZ)-RhoGEF, AKAP-Lbc = A-kinase anchoring protein. (Image credits: Dorsam and Gutkind, 2007)

a) Phospholipase C and Ca^{2+} pathway

The PLC/Ca^{2+} pathway can be regulated by members of the $G\alpha_{q/11}$ subfamily. Binding of an agonist to its GPCR activates this receptor and results in the activation of the $G\alpha_{q/11}$ protein. The activated $G\alpha_{q/11}$ subunit dissociates from the Gβγ dimer and stimulates the plasma membrane associated phospholipase C (PLCβ) which cleaves phosphatidylinositol 4,5-bisphosphate (PIP_2) into diacylglycerol (DAG) and inositol 1,4,5-trisphosphate (IP_3). DAG remains associated with the plasma membrane, while IP_3 diffuses into the cytosol where it can bind to ion channels on intracellular Ca^{2+} storing compartments, triggering the release of Ca^{2+} ions into the cytosol (Cabrera-Vera et al., 2003). A schematic representation of the PLC/Ca^{2+} pathway is presented in Fig. 1.11.

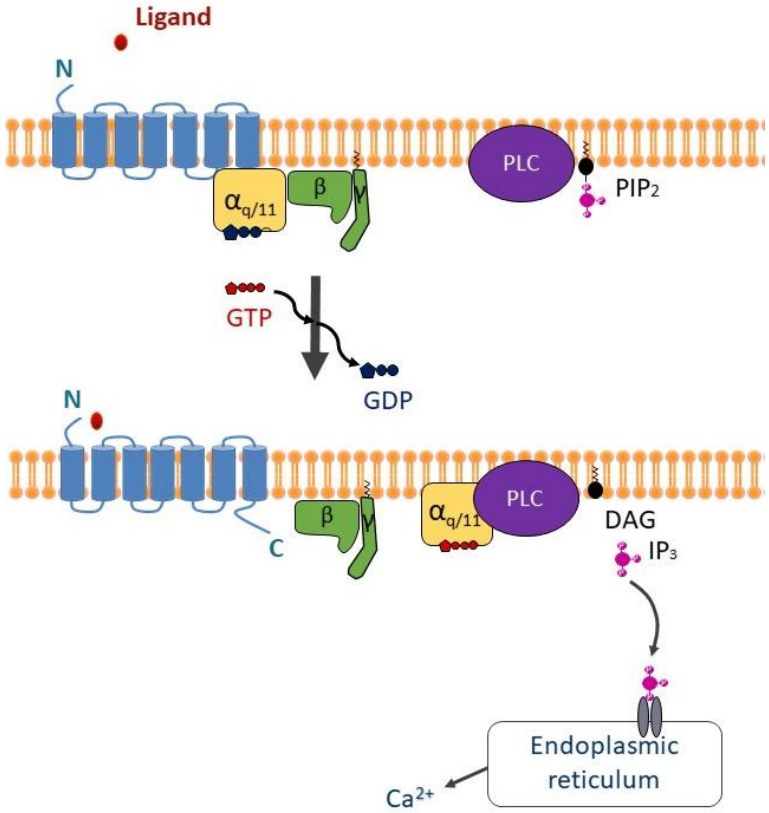

Figure 1.11: Schematic representation of the phospholipase C (PLC)/Ca^{2+} pathway. Agonist binding induces receptor activation, causing a conformational change of the receptor and subsequent activation of $G\alpha_{q/11}$. $G\alpha_{q/11}$ exchanges guanosine diphosphate (GDP) for a guanosine triphosphate (GTP) molecule and dissociates from the Gβγ dimer complex. $G\alpha_{q/11}$ subsequently activates phospholipase C (PLC) which hydrolyses phosphatidylinositol 4,5-bisphosphate (PIP_2) into diacyl glycerol (DAG) and inositol 1,4,5-trisphosphate (IP_3). The former remains associated with the plasma membrane whereas the latter migrates into the cytosol where it can bind to the IP_3-gated-ion channels on the membrane of the endoplasmic reticulum causing the release of Ca^{2+} into the cytosol.

b) The adenylyl cyclase, cAMP and protein kinase A pathway

Both $G\alpha_s$ and $G\alpha_i$ subunits are well known for their possible interaction with AC. Upon activation of the GPCR by stimulation with agonist, the receptor is activated which triggers the activation of the $G\alpha_s$ protein. The activated $G\alpha_s$ subunit dissociates from the Gβγ dimer and activates AC which catalyzes the production of cAMP from adenosine triphosphate (ATP) and thus increases intracellular cAMP levels. In contrast, activation of $G\alpha_i$ inhibits AC which leads to a reduction of intracellular cAMP levels (Cabrera-Vera et al., 2003; Gilman, 1984). A schematic representation of the AC/cAMP/PKA pathway is presented in Fig. 1.12.

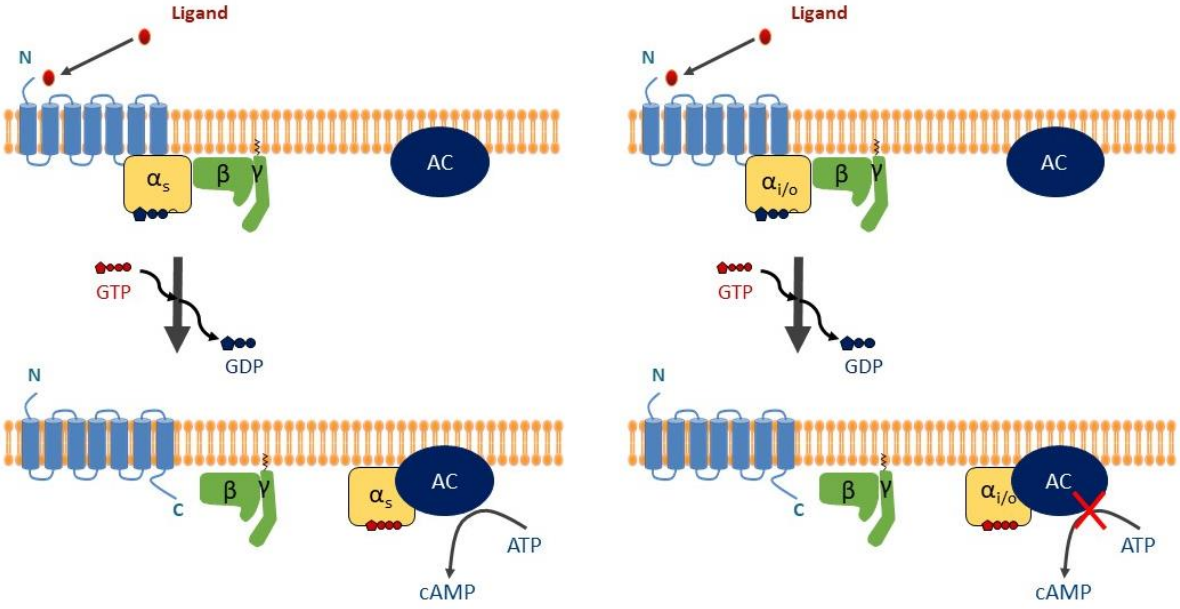

Figure 1.12: Schematic representation of the adenylyl cyclase (AC)/cyclic adenosine monophosphate (cAMP) pathway. Left: Agonist binding induces receptor activation, causing a conformational change of the receptor and subsequent activation $G\alpha_s$. $G\alpha_s$ exchanges guanosine diphosphate (GDP) for a guanosine triphosphate (GTP) molecule and dissociates from the Gβγ dimer complex. $G\alpha_s$ subsequently activates AC which catalyzes the production of cAMP from adenosine triphosphate (ATP) and thus increases intracellular cAMP levels. **Right:** Activation of $G\alpha_{i/o}$ subfamily members can result in an inhibition of AC, which decreases intracellular cAMP levels.

1.3.4.2. β-arrestin mediated pathways

In addition to the canonical G protein mediated pathways, β-arrestins are now recognized as true adaptor proteins that can transduce GPCR mediated signals into multiple effector pathways (Rajagopal et al., 2010).

Four members of the arrestin family exist in vertebrates. Two of those members, arrestin1 and arrestin4, are only expressed in the rods and cones and interact with rhodopsin. Hence, these arrestins are also designated as the “visual arrestins”. The two remaining arrestins; namely arrestin2

and arrestin3 or also named β-arrestin1 and β-arrestin2, respectively, are able to regulate the activity of many non-visual GPCRs (Tobin, 2008; Shukla et al., 2011).

β-arrestins were originally identified in the desensitization mechanism of the receptors, in which an agonist-occupied receptor is phosphorylated followed by the recruitment of β-arrestins. Recruitment of β-arrestins sterically hinders further G protein coupling of the receptor and thus leads to receptor desensitization (Lefkowitz and Shenoy, 2005; Shenoy and Lefkowitz, 2005; Shukla et al., 2011).

β-arrestins are now considered to be multifunctional adaptor proteins that are responsible for many GPCR mediated signaling events, independent of G protein activation. β-arrestins serve as multiprotein scaffolds that interact with many protein partners and bring elements of specific signaling pathways into close proximity. These β-arrestin mediated signaling mechanisms include RhoA-dependent stress fiber formation; inhibition of nuclear factor κB (NF-κB)-targeted gene expression through IκB stabilization; protein phosphatase 2A (PP2A) mediated dephosphorization of protein kinase B (Akt), which leads to the activation of glycogen synthase kinase 3 and dopaminergic behavior; extracellular signal-regulated kinase (ERK) dependent induction of protein translation and anti-apoptotic effects and phosphatidylinositol 3-kinase (PI3K) mediated phospholipase A2 (PLA2; DeWire et al., 2007; Reiter et al., 2011).

1.3.4.3. Other non-canonical signal transducers

Besides G proteins, which serve as canonical transducer proteins, and β-arrestins, other transducers have been identified as well. These transducers include regulatory and scaffolding proteins, such as PDZ-domain-containing scaffolds and non-PDZ scaffolds, such as A kinase anchor proteins (AKAPs) (Wootten et al., 2018). An overview of the canonical and some of the non-canonical signaling pathways is presented in Fig. 1.13.

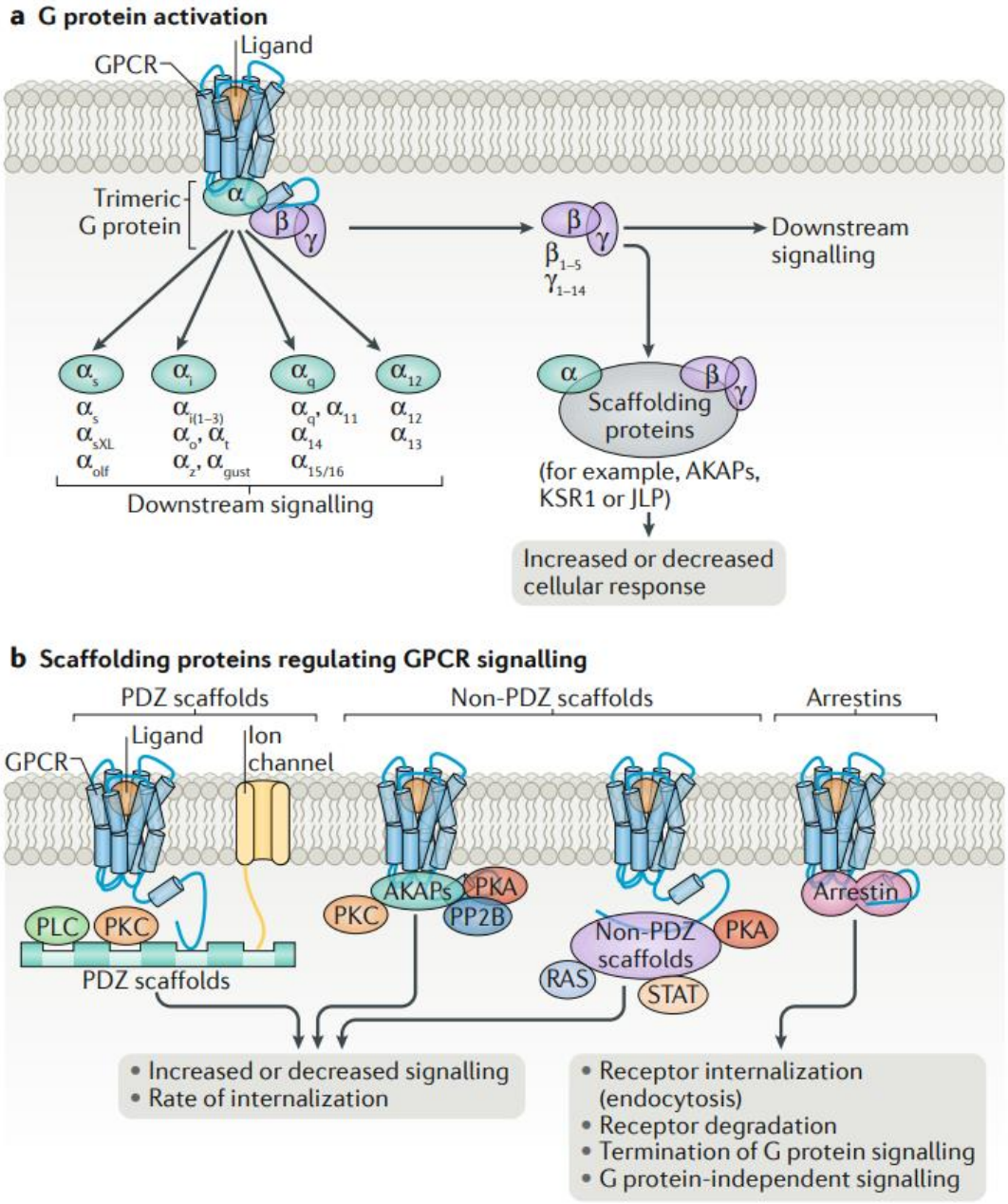

Figure 1.13: Schematic illustration of GPCR signaling: (a) Canonical GPCR signaling whereby signaling is mediated through **G proteins**. Both the Gα protein ($G\alpha_s$, $G\alpha_i$, $G\alpha_{q/11}$ or $G\alpha_{12/13}$) and the Gβγ dimer can activate downstream signaling pathways. Gα and the Gβγ dimer can also bind to scaffolding proteins that regulate their signaling profiles. **(b)** Schematic representation of **non-canonical GPCR transducer proteins** that have key roles in the regulation of GPCR signaling. These transducer proteins are categorized in three broad categories: PDZ-domain-containing scaffolds, non-PDZ scaffolds and Arrestins. Abbreviations used: PLC = phospholipase C, PKC = protein kinase C, AKAPs = A kinase anchor proteins, PKA = protein kinase A, PP2B = serine/threonine-protein phosphatase 2B, and STAT = signal transducer and activator of transcription protein family. (Image credits: Wootten et al., 2018)

1.3.5. Complexity of signaling pathways

GPCR signaling depends on the intracellular milieu and is highly context specific. In this section, I will discuss several concepts which influence GPCR signaling.

1.3.5.1. Posttranslational regulation

Posttranslational modifications are considered the main regulators of all GPCRs which regulate the magnitude and temporospatial aspects of GPCR signaling (Alonso and Friedman, 2013). I will discuss the three main posttranslational modifications, namely phosphorylation, palmitoylation and glycosylation, together with ubiquitination, myristoylation and citrullination.

a) Phosphorylation

Phosphorylation encompasses the covalent addition of a phosphate group to a serine, threonine or a tyrosine residue. This reaction can be catalyzed by GPCR kinases (GRKs), as well as by other protein kinases including protein kinase A and protein kinase C, and is considered one of the most common modes of regulation of protein function. Nearly al GPCRs are phosphorylated in response to agonist occupation. Moreover, agonist occupation results in conformational changes that unmask possible phosphorylation sites at serine and threonine residues in their ICLs and C-terminal tail. Since phosphorylation can occur at the G protein contact sites, this kind of modifications can directly interfere with G protein coupling and thus influence receptor signaling. Phosphorylation results in the recruitment of arrestins, which can result in receptor desensitization and internalization, but can also result in the activation of G protein independent pathways (Butcher et al., 2012; Kristiansen, 2004; Pierce et al., 2002).

b) Palmitoylation

Palmitoylation encompasses the covalent addition of a palmitate, a 16-carbon saturated fatty acid, to the thiol side-chain of cysteine residues through a reversible thioester linkage. This reversible lipid modification is catalyzed by palmitoyl transferases and palmitoyl thioesterases which add or remove the palmitate, respectively (Chini and Parenti, 2009; Linder and Deschenes, 2007; Qanbar and Bouvier, 2003). The process of palmitoylation can be distinguished in two types. The first type, constitutive palmitoylation, refers to the initial protein palmitoylation in the biosynthetic pathway. The second type, dynamic palmitoylation, refers to the regulation of the acylation state once the protein has reached its site of action (Qanbar and Bouvier, 2003).

Most GPCRs are modified with one or more palmitic acid(s) localized in the C-terminus. Insertion of a covalently bound palmitate into the cytoplasmic leaflet of the plasma membrane can create a

fourth intracellular loop (Chini and Parenti, 2009; Moench et al., 1994). Additionally, cysteine residues in the ICLs can also be palmitoylated (Chen et al., 1998; Hawtin et al., 2001).

Palmitoylation has an influence on receptor maturation and receptor signaling. It influences receptor maturation along the biosynthetic route from synthesis to the plasma membrane. A lack of palmitoylation reduces the number of receptors that reach the plasma membrane. In addition, changes in the palmitoylation state of GPCRs influence downstream signaling. Moreover, palmitoylation may direct a GPCR to signal preferentially through a certain pathway. This mechanism, also termed biased agonism, is further discussed below (Chini and Parenti, 2009; Qanbar and Bouvier, 2003).

Furthermore, palmitoylation also influences GPCR desensitization, internalization and protein stability. Receptor desensitization and internalization are influenced, since palmitoylation regulates the accessibility of phosphorylation sites involved in receptor desensitization. The stability of proteins is regulated by palmitoylation through prevention of ubiquitination and thus influences the turnover rate of the protein (Chini and Parenti, 2009; Linder and Deschenes, 2007; Qanbar and Bouvier, 2003).

c) Glycosylation

Glycosylation is an important, highly regulated mechanism which involves the covalent attachment of one or more carbohydrates to a protein. The process of glycosylation takes place within the endoplasmic reticulum and plays an important role in achieving the proper three-dimensional configuration of proteins. Moreover, glycosylation plays a critical role in determining protein structure, function and stability.

Glycosylation can occur on eight different amino acids. N-linked glycosylation comprises the attachment of a glycan to the nitrogen of asparagine or arginine sidechains, whereas O-linked glycosylation comprises the attachment of a glycan to the hydrogen-oxygen sidechains of serine, threonine, tyrosine, hydroxylysine or a hydroxyproline. The mechanism of glycosylation is complex and not fully understood but requires several enzymes. This posttranslational modification can have an impact on receptor signaling since these complexes result in alterations in how they recruit, interact and activate signaling proteins (Arey, 2012; Shental-Bechor and Levy, 2009).

d) Ubiquitination

Ubiquitination is a key molecular mechanism which leads to protein degradation. This enzymatic posttranslational modification process is executed by the action of three enzymes which act

in tandem and ultimately results in the addition of a chain of ubiquitin, a polypeptide of 76 amino acids, to a lysine residue on a protein substrate. This chain of ubiquitin is recognized by proteins with ubiquitin-binding domains which translate the modifications into specific outcomes, such as protein degradation by proteasomes and protein trafficking to lysosomes. Ubiquitination is counteracted by deubiquitinating enzymes that can rescue the substrate from degradation (Alonso and Friedman, 2013).

e) Myristoylation

Myristoylation encompasses the irreversible covalent addition of a myristate, a 14-carbon saturated fatty acid, by an amide bond to the extreme N-terminus of a protein. Myristoylation is catalyzed by N-myristoyltransferase and usually takes place on a glycine residue, although it can occur on other amino acids as well (Escribá et al., 2007). Myristoylation is frequently considered a prerequisite for palmitoylation and membrane association of proteins, since the loss of myristoylation often decreases, but not necessarily abolishes, both palmitoylation and association with membranes (Qanbar and Bouvier, 2003).

f) Citrullination

Citrullination is the smallest posttranslational modification and encompasses the conversion of a peptidylarginine into a peptidylcitrulline. This conversion, specified as deimination, is catalyzed by peptidylarginine deaminases and results in an increased relative molecular mass and the loss of a positive charge. The loss of a positive charge influences the overall charge of the protein, the charge distribution, the isoelectric point, as well as the ionic and hydrogen bond forming abilities of the protein. Hence, citrullination of a receptor may change the three dimensional structure and thus may influence the interaction with other proteins, lipids or glycosaminoglycans and may alter the susceptibility to proteolytic cleavage (György et al., 2006; Mortier et al., 2011). Citrullination receives significant interest in biomedicine since it has been associated with several pathological processes (György et al., 2006). However, to date, citrullination has not been reported in invertebrates (Verlinden et al., 2014).

1.3.5.2. Biased agonism

Biased agonism is defined by DeWire and co-workers (2007) as “the preferential activation of one of a number of possible downstream signaling pathways of a receptor”. While binding of a certain agonist to a GPCR can activate signaling of both G proteins and β-arrestins, binding of another agonist, termed a “biased agonist”, may preferably activate one pathway over the other. Several

biased ligands have been identified that preferentially signal through either G protein signaling pathways or β-arrestin signaling pathways (Rajagopal et al., 2010; Violin and Lefkowitz, 2007).

Early GPCR models propose that GPCRs act as a binary switch in either an "on" or "off" state. However, the fact that several G protein and G protein-independent pathways can be activated upon receptor activation and that ligand structure can affect the efficiency of receptor coupling to different downstream effectors indicates that receptors have more than one active state and that ligand structure can "bias" downstream signaling when compared to the native agonist (Luttrell et al., 2015). Subsequently, awareness is raised that GPCRs do not act as binary switches but should be seen as allosteric microprocessors that generate a multitude of conformations in response to different ligands (Smith et al., 2018). Biased agonism thus describes the ability of ligands to elicit distinct cellular signaling at the same GPCR by stabilizing different active conformational states of the receptor (Wootten et al., 2018).

In addition to orthosteric ligands, which bind to the binding site of the endogenous ligand, a new class of biased ligands, biased allosteric modulators, are identified which bind to non-traditional ligand binding sites topographically distinct from the orthosteric binding site. They modulate agonist affinity and/or efficacy toward a biased receptor conformation without affecting receptor activity on their own (Wisler et al., 2014).

Additionally, also biased antagonism occurs at the receptor. In contrast to an orthosteric antagonist which blocks all downstream signaling pathways by binding to the agonists' endogenous binding site, a biased antagonist binds to an allosteric site and blocks certain, but not all, downstream signaling pathways (Kenakin and Miller, 2010). Ligand classification is thus much more complex than described above, since receptor pharmacology is much more complex and subtle than previously described (Violin and Lefkowitz, 2007).

As reviewed by Smith and co-workers (2018), all three components of the ternary complex, namely the ligand, the receptor, as well as the transducer, can contribute to a biased response. For starters, (1) biased agonism can be evoked through the ligand. Moreover, the ligand induces a unique receptor conformation that results in a biased response relative to a reference agonist, usually the endogenous ligand. (2) Biased agonism can also be provoked by the receptor. For instance, the receptor can be modified in a way that changes its ability to bind to specific ligands or transducers. These modifications can occur through mutation or through differential splicing, both of which can alter coupling to G proteins and β-arrestins. Lastly, (3) the transducer itself can alter the signaling response. This can be caused by the differential expression of transducer elements proximal to the

receptor, such as the receptor itself, β-arrestins or GRKs, as well as expression of amplification cascades distal to the receptor. These three mechanisms are depicted in Fig. 1.14.

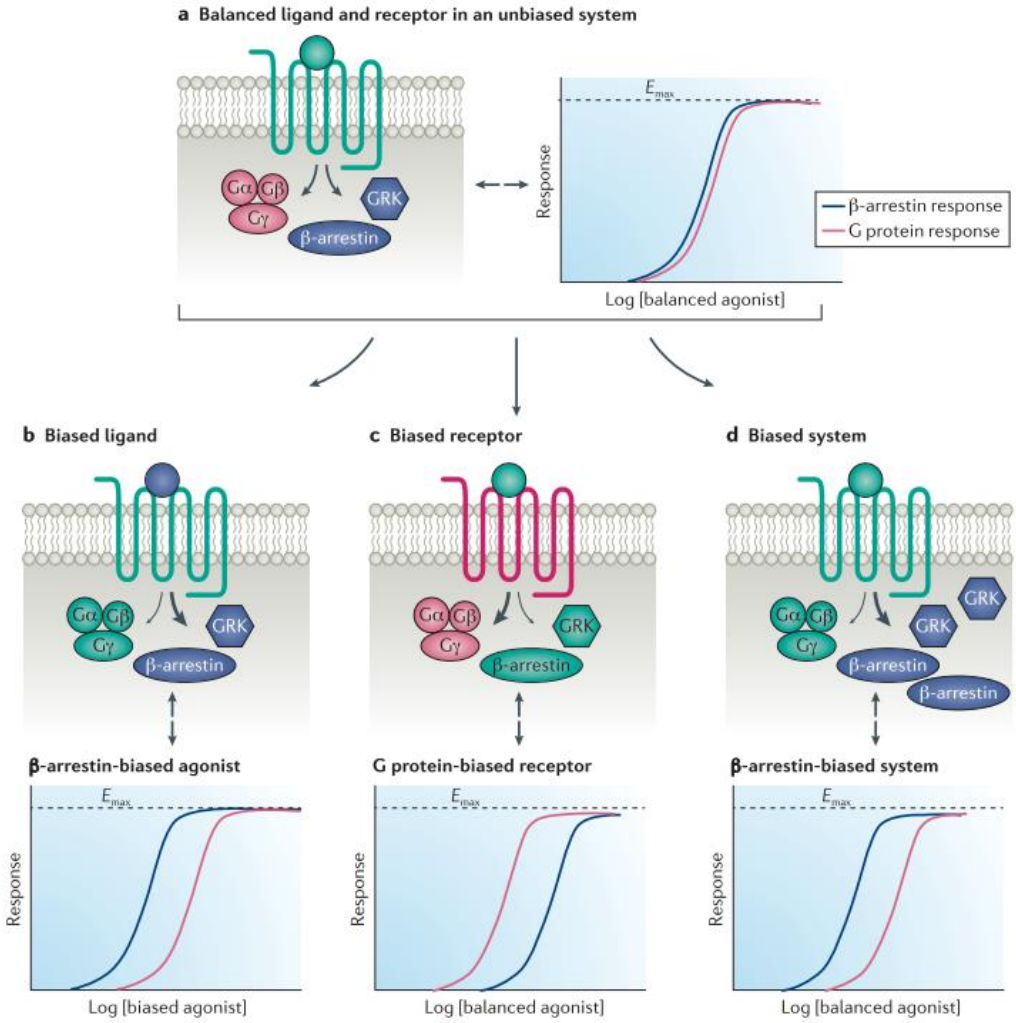

Fig 1.14: The three mechanisms through which biased signaling can be provoked. (a) Binding of a balanced agonist in an unbiased system displays equivalent potencies for the two different pathways such as a G protein and β-arrestin. **(b)** Biased agonism is encoded through the ligand. A ligand–receptor–effector complex generates distinct conformations that preferentially signal through certain pathways, in this case through β-arrestin mediated pathway, relative to the other pathway, in this case the G protein mediated pathway. **(c)** Biased receptors, such as G protein-biased receptors that lack C-terminal phosphorylation sites necessary for β-arrestin recruitment, signal preferentially through one pathway relative to another despite being stimulated by a balanced agonist. **(d)** System bias may be due to differential expression of signaling effectors or other cofactors. In this case a higher expression of certain G protein-coupled receptor kinase (GRK) and/or β-arrestin isoforms can bias signaling towards the β-arrestin pathway. (Image credits: Smith et al., 2018)

Finally, also the rate of GDP to GTP exchange appears to have an effect on the downstream signaling pathway. Moreover, ligands that induce a faster rate of GDP-GTP exchange (and hydrolysis) allow quantitatively more G protein and downstream signaling events per unit of time than ligands that induce a slow rate of exchange (Wootten et al., 2018).

1.3.5.3. The formation of dimers and higher order oligomers

In the classical GPCR model, these receptors function as single monomeric units. However, GPCRs do not always function as single units but they can also form dimers or higher order oligomers with other GPCRs. Oligomerization has a significant impact on receptor signaling, pharmacology, regulation, crosstalk, internalization and trafficking. It is suggested that oligomerization occurs in the endoplasmic reticulum in which these multiple interaction partners are gathered during biosynthesis and that these receptors are delivered to the cellular membranes as pre-assembled functional units. Hence, receptor oligomerization has a major influence on receptor maturation to the plasma membrane (Farran, 2017). For example, the γ-aminobutyric acid receptor ($GABA_B$) is a non-covalently heterodimer composed of $GABA_{B1}$ and $GABA_{B2}$ (both Family C receptors). When expressed individually in a heterologous system, the $GABA_{B1}$ subunit is retained in the endoplasmic reticulum whereas $GABA_{B2}$ is transported to the cell surface. However, the latter is unable to activate downstream pathways on its own since $GABA_{B1}$ harbors the structural elements for ligand binding while $GABA_{B2}$ mediates G protein coupling (Pagano et al., 2001).

All three major GPCR families are able to form homo- and hetero- oligomers. Moreover, di- or oligomerization appears to be an absolute prerequisite for expression and receptor signaling of Family C receptors.

GPCRs in a di- or oligomer can act as an allosteric modulator by several approaches, altering the shape and activity of its partner GPCR. Moreover, heterodimerization can alter the ligand affinities of individual receptors by facilitating crosstalk between the protomers. For instance, the interaction of a ligand with an allosteric site on one protomer of the oligomer can influence binding of the same or another ligand on the other protomer. A negative cooperativity is established by lowering the affinity for its partner GPCR ligand or a positive cooperativity can be established by improving this affinity (Farran, 2017; Møller et al., 2017).

Dimerization may also contribute to the biased signaling profiles of the receptor. Moreover, the activated pathways may even differ depending on whether the receptor is *cis*- or *trans*-activated. For example, it has been shown that the metabotropic glutamate receptor mGlu1 receptor triggers $G\alpha_{q/11}$-coupled signaling through *cis*- and *trans*-activation, while $G\alpha_{i/o}$ and $G\alpha_s$ are exclusively activated through *cis*-activation (Tateyama and Kubo, 2011). Biased agonism is thus an inextricable part of receptor oligomerization (Franco et al., 2016).

1.3.5.4. Receptor desensitization and internalization

GPCR desensitization is essentially a two-step process. In the first step, agonist-occupied receptors are phosphorylated by GRKs, primarily in the carboxyl terminus of the receptors, but also in the intracellular loops. The second step involves the recruitment of multifunctional adaptor proteins, arrestins, which sterically hinder further G protein coupling of the receptor, thereby leading to desensitization (Shukla et al., 2011).

After desensitization, the receptor may be internalized by endocytosis. Three distinct types of endocytic pathways are described, namely the clathrin-dependent pathways, the caveolae-dependent pathways and the clathrin/caveolae-independent pathways (Hanyaloglu and Zastrow, 2008).

Receptors may undergo a transient internalization and enter the recycling pathway, or they can enter the lysosomal pathway in which the receptors are transported to lysosomes which leads to receptor degradation. Endocytic trafficking to lysosomes represents a major mechanism by which GPCRs are downregulated. In contrast, the recycling pathway can promote rapid recovery (or resensitization) of cellular responsiveness. If a receptor undergoes transient internalization or sustained internalization appears to be dependent on the GPCR-arrestin interaction whereby a weak interaction provokes transient internalization whereas a stronger interaction provokes sustained internalization (Hanyaloglu and Zastrow, 2008; Oakley et al., 2000; Pierce et al., 2002; Thomsen et al., 2016). In addition to ubiquitination, also phosphorylation appears to be important for the postendocytic fate of the receptor (Hanyaloglu and Zastrow, 2008; Moore et al., 2006).

Recently, a new signaling paradigm is introduced by Cahill III and co-workers (2017) in which receptor desensitization, internationalization and signaling is mediated by specific GPCR-arrestin conformations. Two types of receptor-arrestin complexes exist. The first type, the tail conformation, involves interaction of arrestin with the phosphorylated cytoplasmic tail of the GPCR whereas the second type, the core interaction, involves interaction of arrestin with the transmembrane core of the GPCR (Kahsai et al., 2018). The tail conformation is shown to be involved in GPCR internalization and some forms of signaling whereas the core conformation is attributed to receptor desensitization (Cahill III et al., 2017; Wootten et al., 2018).

1.3.5.5. Endosomal signaling

Endocytosis of GPCRs was initially recognized as a phenomenon coinciding with rapid desensitization of G protein mediated cellular responses. However, G protein mediated signaling can also take place at the endosomal membrane after receptor internalization for an extended period of time (Irannejad and von Zastrow, 2014; Vilardaga et al., 2014). Recently, Thomsen and co-workers (2016) demonstrated the existence of internalized megaplexes which are composed of a single GPCR which strongly interacts with arrestins through its phosphorylated C-terminal tail and a G protein. The existence of these megaplexes provide a potential physical basis for the newly appreciated sustained G protein mediated signaling from internalized GPCRs.

Additionally, not only G protein mediated signaling but also G protein independent signaling can occur during endocytosis. Eichel and co-workers (2016) have shown that β-arrestin2 remains in its active state and can transduce β-arrestin mediated ERK1/2 signaling from clathrin-coated structures even after dissociation from the β_1-adrenergic receptor (Kahsai et al., 2018). Receptor signaling is thus not always terminated by receptor internalization and the signal can even be maintained without the receptor. Moreover, receptor signaling can also take place from other intracellular structures besides the endosomes such as the endoplasmic reticulum and the Golgi apparatus (Irannejad et al., 2017; Wootten et al., 2018).

1.3.5.6. Role of the Gβγ subunits

GPCR signaling is not only determined by the Gα protein, but also by the Gβγ dimer. In the classical view on G protein mediated effector pathways, the Gβγ dimer only acts as a negative regulator of Gα-dependent signaling necessary for the inactivation of the Gα subunit and allowing the reassociation with the receptor for subsequent rounds of signaling. However, it has become clear that they have regulatory and signaling functions as well and have an effect on the specificity of receptor-effector interactions (Dupré et al., 2009; Wootten et al., 2018).

Besides the important role in the stabilization of the Gα-GDP-Gβγ complex and its requirement in the GDP/GTP exchange, the Gβγ subunit is involved in the regulation of more than twenty downstream effectors including PLCs, ACs, β-adrenergic receptor kinase, PI_3 kinase, components of the MAPK cascade and ion channels (Cabrera-Vera et al., 2003; Dupré et al., 2009; Hildebrandt, 1997; Myung et al., 2006). In addition, many GRKs require interaction with the Gβγ dimer (Wootten et al., 2018) and Gβγ signaling is not only limited to the plasma membrane since the Gβγ can translocate to the cytosolic face of the Golgi apparatus or into the nucleus (Dupré et al., 2009).

Furthermore, receptor signaling is dependent on the composition of the Gβγ dimer (Dupré et al., 2009). In humans, 5 Gβ subunits and 13 Gγ subunits are identified which can result in 65 possible Gβγ combinations (Wootten et al., 2018). Moreover, additional variants exist due to alternative splicing and post-translational processing, leading to up to thousand theoretically possible heterotrimeric combinations (Denis et al., 2012). However, not all Gβγ dimers exist *in vivo*. For example, $G\beta_2$ cannot form a functional dimer with $G\gamma_2$. Additionally, subunit combinations are also dependent on the cell type. Some combinations only exist in one type of cell; for instance, the $G\beta\gamma_1$ dimer is only found in the retinal rod cells, since $G\gamma_1$ expression is limited to this cell type (Cabrera-Vera et al., 2003; Dupré et al., 2009).

Gβγ signaling is not only determined by the specific combination of subunits, but also by Gβ and Gγ separately (Oldham and Hamm, 2008). For instance, McIntire and co-workers (2001) have reported that the Gβ subunit is an important factor in the coupling of $G\alpha_s$ of the β1-adrenergic and A2a adenosine receptors and thus determines the specificity of signaling at these receptors. By pairing five different $G\beta_x\gamma_2$ dimers, it was shown that one pair, $G\beta_4\gamma_2$, demonstrated the strongest coupling ability to both receptors with EC_{50} values 40-200-fold lower than $G\beta_5\gamma_2$ which showed the lowest coupling ability (Dupré et al., 2009). In addition, also the Gγ subunit is an important determinant of receptor signaling. For instance, Hou and co-workers (2000) have shown that $\beta_1\gamma_7$ has increased GTP hydrolysis activity compared to $\beta_1\gamma_5$ when combined with $G\alpha_o$ at the muscarinic receptor, M2 (Myung et al., 2006).

1.3.5.7. Receptor signalosomes

As reviewed by Wootten and co-workers (2018), we can say that GPCRs can assemble into multi-protein complexes and that this can alter observed receptor function and cellular response. These multi-protein complexes are named protein signalosomes, which are defined as spatially restricted groups of transducers and/or regulatory proteins that jointly produce a specific signaling output. These proteins can comprise receptor dimers or oligomers, scaffolding proteins and membrane proteins. The assembly of GPCRs into signalosomes provides the cell with very fine control of signaling events and has been correlated with spatially restricted signaling, very high sensitivity of response and control of specificity of transducer coupling.

1.4. *In cellulo* assays to study GPCR mediated secondary messenger pathways

Numerous *in cellulo* assays have been developed to study the GPCR signaling cascade. Most of these assays focus on fluctuations in downstream intracellular secondary messenger levels, such as Ca^{2+} and cAMP. The aequorin bioluminescence assay is utilized to monitor possible changes in intracellular Ca^{2+} levels whereas the CRE-dependent luciferase reporter assay, which makes use of a $CRE_{(6x)}$-Luc construct, is utilized to monitor possible changes in intracellular cAMP levels. Both assays, which are further discussed below, and the cell lines used in these assays, have proven their value in insect GPCR characterization studies (Bil et al., 2016; Caers et al., 2016a; 2016b; Dillen et al., 2013; Horodyski et al., 2011; Huang et al., 2014; Lenaerts et al., 2017; Lismont et al., 2015; 2018; Marchal et al., 2018; Meeusen et al., 2002; Mertens et al., 2002; Poels et al., 2007; 2009; 2010; Vandersmissen et al., 2013; Verlinden et al., 2013; 2015; Vleugels et al., 2013; Vuerinckx et al., 2011; Zels et al., 2014). Therefore, the aequorin bioluminescence assay and the CRE-dependent luciferase reporter assay are widely utilized as functional cell-based receptor assays. In addition, alternative methods to monitor intracellular cAMP levels have been developed. One of these methods, the cAMP sensor using YFP-Epac-*R*luc (CAMYEL) biosensor (ATCC MBA-277; Jiang et al., 2007) is described below.

1.4.1. Commonly utilized *in cellulo* GPCR mediated activity assays

1.4.1.1. Aequorin bioluminescence assay

The aequorin bioluminescence assay is used to measure intracellular Ca^{2+} levels. In our laboratory, this assay is performed in Chinese hamster ovary (CHO) cells and is used (1) to test whether a specific (neuro)peptide acts as an agonist for the receptor and (2) to test whether activation of the GPCR provokes an increase in intracellular Ca^{2+} levels. Both tests are performed in separate cell lines. The main principle of this assay is explained by Knight and co-workers (2003) and is depicted in Fig. 1.15. The aequorin bioluminescence assay is dependent on the presence of the photoprotein aequorin (Brough and Shah, 2009; Sheu et al., 1993) which consists of two components: apoaequorin and coelenterazine. This photoprotein was cloned for the first time in 1985 from *Aequorea Victoria* (Inouye et al., 1985) and emits light upon binding of two Ca^{2+} ions (Shimomura, 1995). Coelenterazine, the cofactor of aequorin, can easily permeate the cell membrane and is added prior to screening (Knight et al., 1991).

The first test (1) is performed in CHO-WTA11 cells which stably co-express apoaequorin and the promiscuous $G\alpha_{16}$ protein (Blanpain et al., 1999). If a ligand acts as an agonist of the receptor, the $G\alpha_{16}$ protein, which belongs to the $G\alpha_{q/11}$ protein subfamily, couples the activated GPCR to the PLC/Ca^{2+} pathway regardless of the receptors natural signaling cascade (Milligan et al., 1996, Offermanns and Simon, 1995). The subsequent release of Ca^{2+} ions is detected by the emission of a blue light when coelenterazine is decomposed to coelenteramide and CO_2 (Shimomura and Teranishi, 2000).

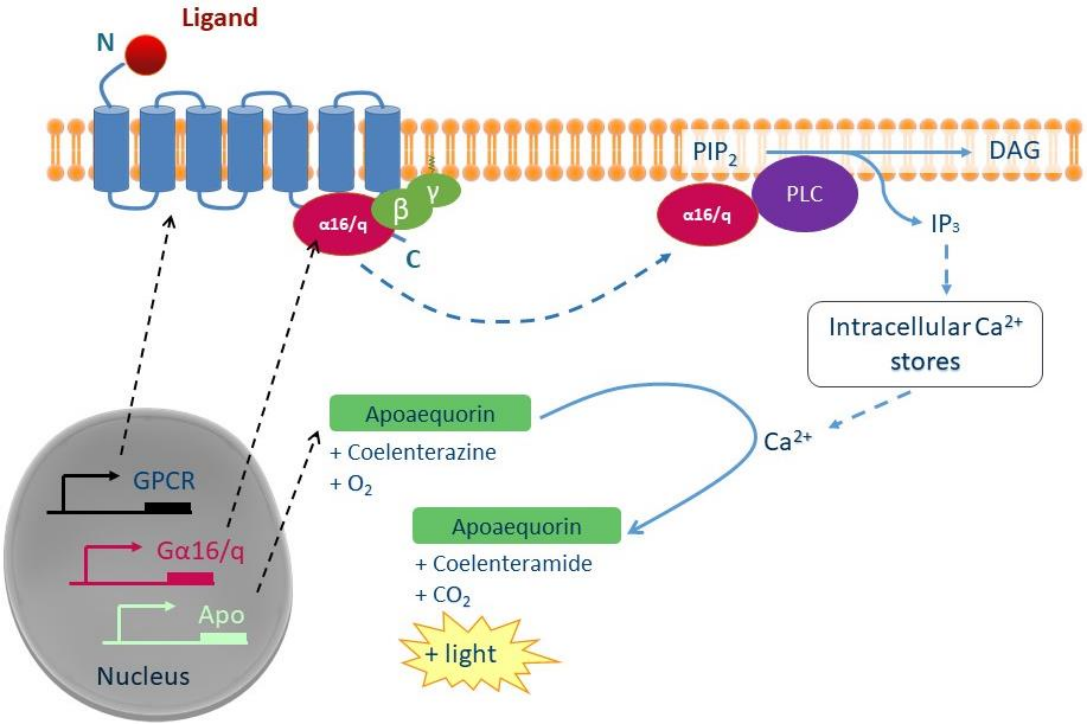

Figure 1.15: Schematic representation of the calcium reporter assay in CHO cells. The receptor of interest is transiently transfected in CHO-WTA11 [stably transfected with $G\alpha_{16}$ and apoaequorin (Apo)] or CHO-PAM28 (stably transfected with apoaequorin) cells. The agonist induced GPCR undergoes a conformational change resulting in the activation of $G\alpha_{16}$ (CHO-WTA11) or other $G\alpha_{q/11}$ proteins (CHO-PAM28). The $G\alpha_{16/q/11}$ protein will, in turn, activate the phospholipase C (PLC) which converts phosphatidylinositol 4,5-bisphosphate (PIP_2) into diacyl glycerol (DAG) and inositol 1,4,5-trisphosphate (IP_3). The IP_3 induces a Ca^{2+} release from the intracellular Ca^{2+} stores resulting in an increase in intracellular Ca^{2+} levels. In the presence of Ca^{2+} in the cytosol, coelenterazine (which forms the holoenzyme aequorin together with apoaequorin) is decomposed into coelenteramide and CO_2 which results in the emission of blue light. Black dashed arrows represent transcribed proteins, blue dashed arrows represent molecule movements and blue full arrows represent catalytic reactions. (Image credits: adapted from Knight et al., 2003)

The second test (2) is performed in CHO-PAM28 cells which are stably transfected with apoaequorin, but not with the promiscuous $G\alpha_{16}$ protein (Wiehart et al., 2002). This cell line does express other $G\alpha_{q/11}$ proteins and can thus be used to test whether the receptor has an effect on the IP_3/Ca^{2+} second messenger system in absence of the promiscuous $G\alpha_{16}$ protein.

1.4.1.2. CRE-dependent luciferase reporter assay

The CRE-dependent luciferase reporter assay is used to detect possible changes in intracellular cAMP levels. In our laboratory, this assay is performed in human embryonic kidney (HEK293) cells and is used to test whether activation of the receptor results in (1) an increase or (2) a decrease in intracellular cAMP levels suggesting $G\alpha_s$ or $G\alpha_{i/o}$ activation, respectively. The general principle of this assay is depicted in Fig. 1.16. To measure decreasing intracellular cAMP levels (2), this assay is performed in the presence of forskolin, which activates AC and thus ensures an increased basal cAMP level which facilitates detection of decreasing cAMP levels that result from agonist-induced GPCR activation.

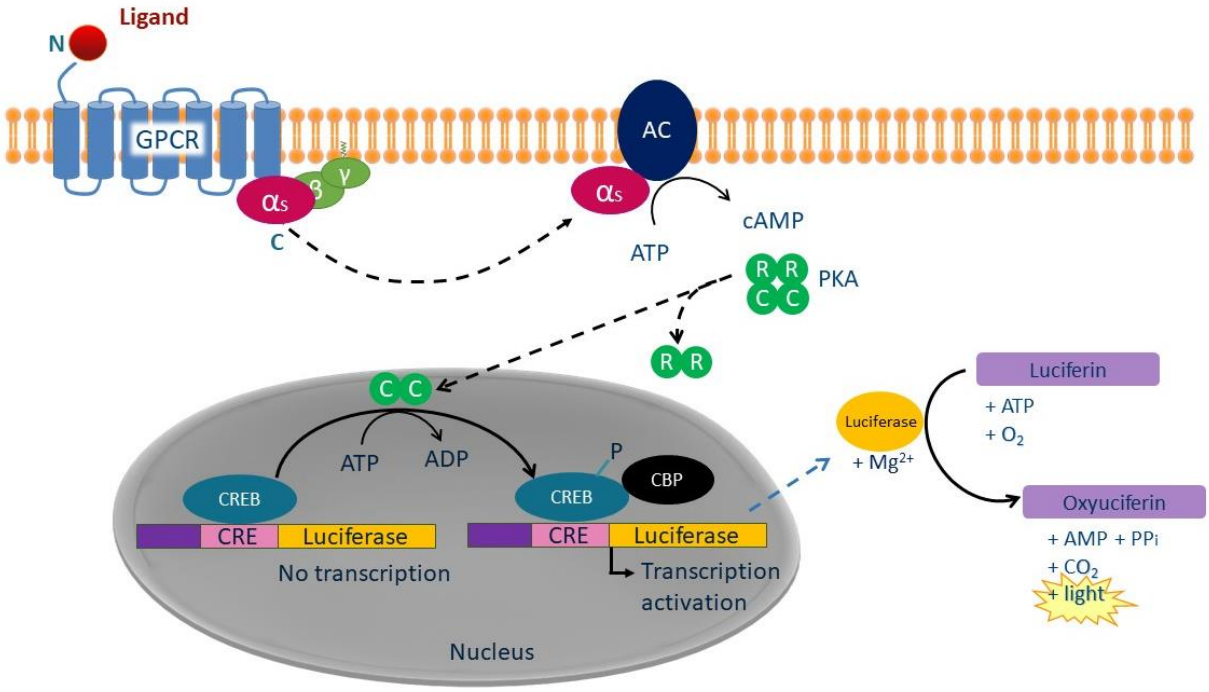

Figure 1.16: Schematic representation of the CRE-dependent luciferase reporter assay. The receptor of interest is transiently co-transfected in HEK293 together with a $CRE_{(6x)}$-Luc construct. This reporter construct contains a minimal promoter (purple), a number of cyclic adenosine monophosphate (cAMP) responsive elements (CRE; pink) and the open reading frame of the *luciferase* reporter gene (orange). The agonist induced GPCR undergoes a conformational change resulting in the activation of $G\alpha_s$. $G\alpha_s$ activates, in turn, adenylyl cyclase (AC) which converts adenosine triphosphate (ATP) into cAMP. The cAMP activates protein kinase A (PKA). The catalytic subunits (C) of PKA dissociate from the cAMP-bound regulatory subunits (R) and translocate to the nucleus where they phosphorylate the CRE binding protein (CREB). Activated CREB results in recruitment of the CREB binding protein (CBP) resulting in the expression of luciferase which, in the presence of Mg^{2+}, oxidizes luciferin to oxyluciferin. This reaction results in the emission of light. The blue dashed arrow represents transcribed protein, full black arrows represent catalytic reactions while black dashed arrows represent protein movements.

HEK293 cells are co-transfected with a reporter plasmid $CRE_{(6x)}$-Luc. This reporter plasmid contains six tandem repeats of a CRE in front of a minimum collate promoter and the open reading frame of *luciferase* ($CRE_{(6x)}$-Luc plasmid). Increasing intracellular cAMP levels lead to the activation of PKA. The catalytic subunits of PKA transfer into the nucleus where they phosphorylate the CRE binding protein (CREB), which eventually leads to the induced transcription of *luciferase*. Luciferase oxidizes luciferin into oxyluciferin, which is accompanied with an emission of light that can be measured using a luminometer (de Wet et al., 1987).

Notably, the measured bioluminescence using the $CRE_{(6x)}$-Luc construct is not directly induced by cAMP but is dependent on the phosphorylation of CREB. However, it has been speculated that CREB can also be phosphorylated by calcium/calmodulin-dependent protein kinase suggesting that bioluminescence may also be caused by increased Ca^{2+} levels (Johannessen et al., 2004).

1.4.2. The CAMYEL biosensor in an alternative assay to study intracellular cAMP levels

The cAMP sensor using YFP-Epac-*R*luc (CAMYEL) biosensor (ATCC MBA-277; Jiang et al., 2007) is an alternative biosensor to measure intracellular cAMP concentrations upon GPCR activation. The core of this bioluminescence resonance energy transfer (BRET)-based biosensor (further discussed below) consists of an exchange factor directly activated by cAMP (EPAC) protein and this core is flanked by a yellow fluorescent protein (YFP) and *R*luc. In proximity, $BRET^1$ between YFP and *R*luc is high. Upon binding of cAMP to EPAC, a conformational change is induced resulting in a larger distance between YFP and *R*luc. Consequently, $BRET^1$ between YFP and *R*luc decreases. Thus, increasing cAMP levels can be detected by a decrease in $BRET^1$ signal. In the presence of forskolin, decreasing levels of cAMP can be measured by an increase in $BRET^1$ signal. A schematic representation of a cAMP reporter assay using the CAMYEL biosensor is presented in Fig. 1.17.

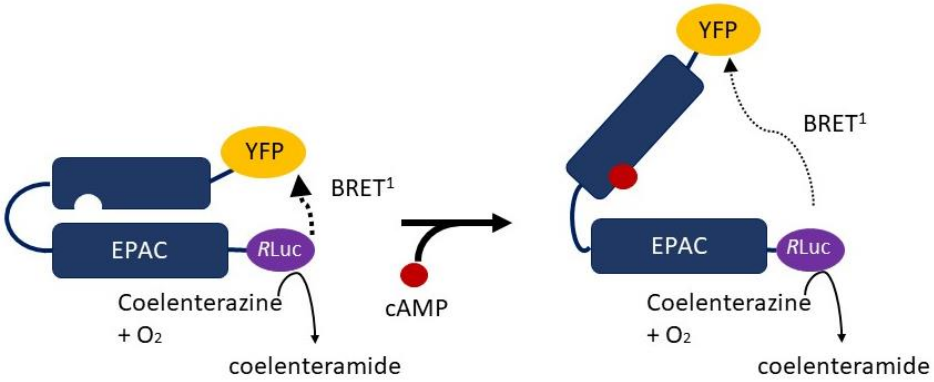

Figure 1.17: Schematic representation of the cAMP reporter assay using the CAMYEL biosensor: The protein exchange factor directly activated by cAMP (EPAC) is flanked by yellow fluorescent protein (YFP) and *R*luc. Upon binding of cAMP to EPAC, a conformational change is induced, which results in a larger distance between YFP and *R*luc. As a consequence, bioluminescence energy transfer $(BRET)^1$ decreases. Coelenterazine acts as a substrate for *R*luc. (Image credits: adopted from Matthiesen and Nielsen, 2011)

1.5. Using BRET^2-based G protein biosensors to study the G protein mediated pathways

1.5.1. Bioluminescence resonance energy transfer (BRET)

Bioluminescence resonance energy transfer (BRET) is a highly sensitive technique, which is very sensitive to distance alterations, and is utilized to study protein-protein interactions at distances up to < 100 Å. This technique consists of a bioluminescent donor molecule and a fluorescent acceptor molecule and involves a non-radiative transfer of energy from a donor enzyme to a suitable acceptor molecule. This transfer of non-radiative, excited-state energy is inversely proportional to the sixth power of distance between the donor and the acceptor allowing the detection of protein-protein interactions. Usually a combination between *Renilla reniformis* luciferase (*R*luc) and a variant of green fluorescent protein (GFP) is used as energy donor and energy acceptor, respectively, whereby coelenterazine is added as a substrate for luciferase. The BRET signal is calculated as the ratio between the acceptor light emission over the donor light emission, measured with appropriate filter settings (De et al., 2014; Lohse et al., 2012; Pfleger and Eidne, 2006).

In summary, upon addition of a substrate, the luminescent protein (donor) is excited and emits light at a characteristic wavelength. In case both the donor and the acceptor are in proximity (up to 10 nm), a resonance energy transfer occurs to the suitable fluorescent acceptor exciting this molecule, which leads to the emission of light at its own characteristic wavelength. Consequently, it is very important to choose the right donor-acceptor combination with an appropriate amount of overlap between the donor emission spectrum and the acceptor excitation spectrum, with the acceptor emission spectrum differing enough from the donor emission spectrum enabling that both emission spectra can be measured separately. The donor emission spectrum is determined by the used coelenterazine while the acceptor emission spectrum is dependent on the fluorescent protein. The original BRET system described by Xu and co-workers (1999) is referred to as BRET^1 and uses *R*luc as a donor with benzyl-coelenterazine (coelenterazine *h*) as a substrate in combination with enhanced yellow fluorescent protein EYFP. An advanced BRET system (BRET)^2 uses different GFP variants in combination with the coelenterazine variant DeepBlueC, also referred to as coelenterazine 400a, which permits the measurement of the acceptor emission spectrum without any overlap of the donor emission spectrum. A schematic representation of the both BRET^1 and BRET^2 systems, including the emission spectra of both donor and acceptor, is depicted in Fig. 1.18. Furthermore, other BRET systems have been developed using different combinations of

donor-acceptor molecules to image protein-protein interactions within deep tissues of living subjects (De et al., 2009; 2014; Dragulescu-Andrasi et al., 2011).

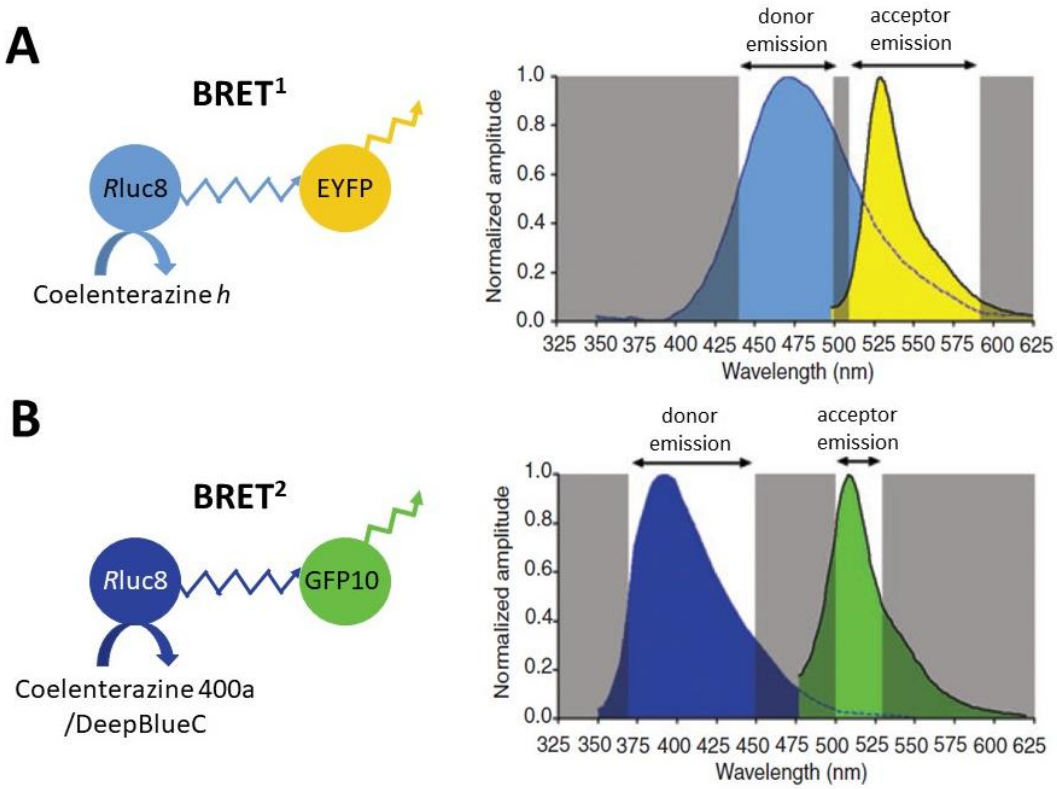

Figure 1.18: Schematic representation of both BRET^1 and BRET^2 systems including the basic elements and illustrating the overlap of normalized *R*luc8 emission spectra with normalized GFP emission spectra, together with typical filter combinations. In the presence of a specific substrate, the donor is excited and emits light at a characteristic wavelength. In case both the donor and the acceptor are in proximity, a non-radiative resonance energy transfer occurs to the suitable fluorescent acceptor. Exciting this molecule leads to the emission of light at its own characteristic wavelength. **A)** Typical filter set for BRET^1 wherein the donor *R*luc8 uses coelenterazine *h* as a substrate together with enhanced yellow florescent protein (EYFP) as a suitable acceptor. **B)** Typical filter set for BRET^2 wherein the donor *R*luc8 uses the coelenterazine analogue 400a/DeepBlueC as a substrate together with green fluorescent protein 10 (GFP10) as a suitable acceptor. (Image credits: adapted from De et al., 2014 and Pfleger and Eidne, 2006)

1.5.2. BRET^2-based G protein biosensors

Several BRET biosensors have been developed to study the biology, pharmacology and signaling of GPCRs. In this thesis, we will use the BRET^1-based CAMYEL biosensor as an alternative method to monitor alterations in intracellular cAMP levels upon GPCR activation and the BRET^2-based G protein biosensors to detect a direct activation of various G proteins representing all four major Gα subfamilies ($G\alpha_{i/o}$, $G\alpha_s$, $G\alpha_{q/11}$ and $G\alpha_{12/13}$).

The latter biosensors are not only used to detect the activation of a certain Gα subfamily, but they are also used for verifying which Gα subunit of a certain Gα subunit family can be activated. Each biosensor consists of three constructs; Gα-*R*luc8, $G\beta_1$ and $G\gamma_2$-GFP10, which form a $\alpha_x\beta_1\gamma_2$ G protein

heterodimer, with α_x representing one of ten different Gα subunit constructs. The ten Gα-*R*luc8 constructs are: $G\alpha_{i1}$, $G\alpha_{i2}$, $G\alpha_{i3}$, $G\alpha_{oa}$, $G\alpha_{ob}$, representing the $G\alpha_{i/o}$ subfamily; $G\alpha_{11}$ and $G\alpha_q$, representing the $G\alpha_{q/11}$ subfamily; $G\alpha_s$ as a representative of the G_s subfamily; and $G\alpha_{12}$ and $G\alpha_{13}$, representing the $G\alpha_{12/13}$ subfamily (Bouvier et al., 2006a; 2006b; Galés et al., 2006).

Each Gα subunit is composed of an intrinsic GTPase domain and a helical domain connected to the GTPase domain. The BRET^2 energy donor, *R*luc8, is genetically inserted after amino acid 91 within the helical domain of Gα, whereas the BRET^2 energy acceptor, GFP10, is N-terminally fused to the Gγ subunit. When the GPCR is not stimulated by the ligand and the receptor is not activated, the energy donor Gα-*R*luc8 and the energy acceptor Gγ-GFP10 are in proximity inducing a high BRET^2 signal. Upon receptor activation, a large interdomain movement within the Gα takes place during GDP/GTP exchange, which results in a major displacement of the helical domain. This major displacement results in an increased distance between the energy donor, *R*luc8, and the energy acceptor, GFP10, and thus results in a subsequent decrease of the BRET^2 signal. These biosensors enable the real-time detection of Gα activation upon receptor stimulation (Denis et al., 2012; Galés et al., 2006). A schematic representation of this assay is depicted in Fig. 1.19.

These BRET^2-based G protein biosensors have been developed by Céline Galés and are patented in the United States (University of Montreal, Bouvier et al., 2006a) and under the International Patent Cooperation Union (University of Montreal, Bouvier et al., 2006b). In particular, they are licensed to Domain Therapeutics for commercial use under the trademark BioSens-All (Domain Therapeutics, 2019a). They have proven their value in the study of the G protein mediated signaling pathways of several vertebrate GPCRs (Audet et al., 2008: Bellot et al., 2015; Bruzzone et al., 2014; Busnelli et al., 2012; Capra et al., 2013; Corbisier et al., 2015; Damian et al., 2015; De Henau et al., 2016; Galandrin et al., 2008; 2016; Galés et al., 2006; Garcia et al., 2018; Hansen et al., 2013; Leduc et al., 2009; Maurice et al., 2010; M'Kadmi et al., 2015; Peverelli et al., 2013; Rives et al., 2012 Onfroy et al., 2017; Saulière et al., 2012; Schmitz et al., 2014; Schrage et al., 2015), but have (so far) never been used to study G protein mediated signaling pathways of insect GPCRs.

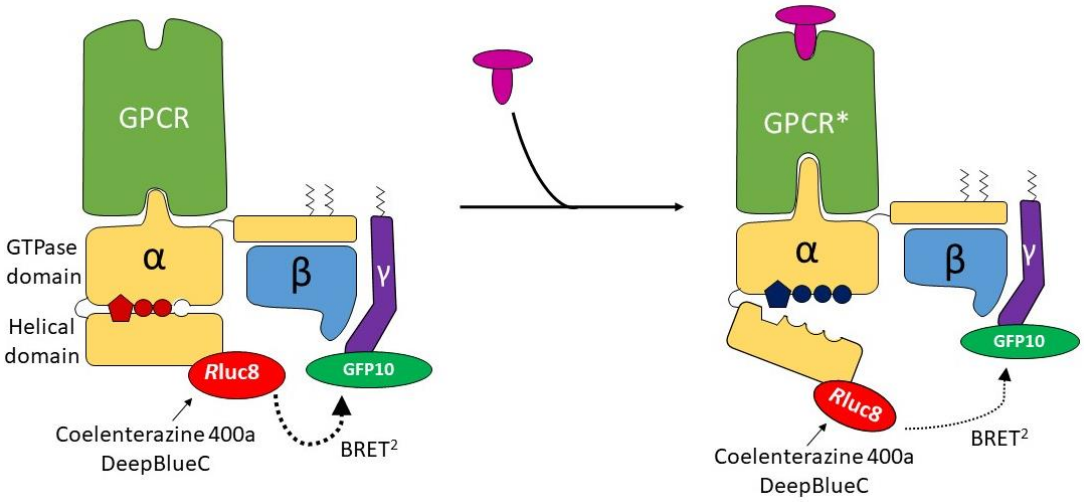

Figure 1.19: Schematic representation of the BRET^2-based G protein biosensors. The energy donor, *R*luc8, is genetically coupled into the helical domain of Gα. GFP10 is N-terminally linked to Gγ. In resting state, when the G protein-coupled receptor (GPCR) is not stimulated by a ligand, the donor *R*luc8 and the acceptor GFP10 are in proximity, inducing a high BRET^2 signal. Upon binding of the ligand to the receptor, this GPCR is activated (GPCR*), inducing the activation of the Gα subunit. When the Gα subunit is activated, GDP is exchanged for GTP and a large interdomain movement in Gα is induced resulting in a larger distance between the donor *R*luc8 and the acceptor GFP10, consequently leading to a lower BRET^2 signal. (Image credits: adapted from Céline Galés)

Chapter 2:
Materials and methods

The materials and methods described in this chapter are partially published in:

Lismont, E., Mortelmans, N., Verlinden, H., Vanden Broeck, J. Molecular cloning and characterization of the SIFamide precursor and receptor in a Hymenopteran insect, *Bombus terrestris* (2018). General and Comparative Endocrinology, 258, 39-52.

Lismont, E., Vleugels, R., Marchal, E., Badisco, L., Van Wielendaele, P., Lenaerts, C., Zels, S., Tobe, S., Vanden Broeck, J., Verlinden, H. (2015). Molecular Cloning and characterization of the allatotropin precursor and receptor in the desert locust, *Schistocerca gregaria*. Frontiers in Neuroscience, 84, 1-14.

In this chapter, the general protocols of several assays are described that are applied in multiple chapters. More details about the specific conditions can be found in each chapter. I was involved in the implementation of the protocol for the rapid amplification of cDNA ends (RACE) and improved the cloning process and the protocol for the CRE-dependent luciferase reporter assay. Furthermore, I was involved in the process of reducing overall costs of real-time quantitative reverse transcriptase PCR (qRT-PCR) by reducing the reaction volume. Additionally, I was also involved in the production of the DH5α cells which are used for cloning instead of the costly TOP10 Chemically Competent Cells (Thermo Fisher). Finally, I was the first person to conduct the $BRET^1$-based CAMYEL biosensor assay and the $BRET^2$-based G protein assay with insect G protein-coupled receptors (GPCRs).

2.1. Rearing of *Schistocerca gregaria*

Gregarious desert locusts are reared under crowded conditions with controlled temperature (30 ± 1 °C), light (14 h photoperiod) and ambient relative humidity (40 - 60 %). The locusts are kept at high density (> 200 locusts/cage) in special wooden cages and fed daily with fresh cabbage leaves supplemented with dry oat flakes. Upon mating, mature females deposit their eggs in pots filled with a slightly moistened sterile sand mixture (7 parts sand, 3 parts peat and 1 part water). These pots are collected once a week and set apart in empty cages resulting in pools of hatched first instar hoppers which differ by no more than seven days in age. Depending on the experimental conditions, the locusts are further synchronized at the time of ecdysis (Badisco et al., 2011b; Marchal et al., 2011).

Breeding of solitarious desert locusts is performed under isolated conditions according to the method described by Hoste and co-workers (2002). Newly hatched hoppers are separated at the day of eclosion and are placed in individual containers. Temperature, light-dark photoperiods and food supply are similar for isolated-reared and crowded-reared locusts. All solitarious animals come from stocks that are reared under isolated conditions for at least three generations. To characterize the phase status of crowded-reared and isolated-reared locusts, morphometric measurements of femur length (F), caput width (C) and elytra (E) are performed (Dirsh, 1953). The F/C ratio increases, whereas the E/F ratio decreases in successive isolated-reared generations, indicating that individuals shift towards the solitarious phase. The color and behavioral characteristics of crowded- and isolated-reared locusts are very typical for the gregarious and solitarious phase, respectively.

2.2. RNA extraction and cDNA synthesis

2.2.1. RNA extraction using the RNeasy Lipid Tissue Mini Kit

Dissected pooled tissues (< 100 mg) are collected in 2.0 ml tubes containing MagNa Lyser green beads (Roche). Semi-automated homogenization of the samples is executed using a MagNA Lyser Instrument (Roche, Mannheim, Germany) for 30 s at 6000g. After homogenization, total RNA is extracted from the tissue homogenate utilizing the RNeasy Lipid Tissue Mini Kit (Qiagen, Germantown, MD) in combination with a DNase treatment (RNase-free DNase set, Qiagen) to eliminate potential genomic DNA contamination. Verification of the RNA quantity and quality is performed by using a Nanodrop spectrophotometer (Thermo Fisher Scientific Inc.). The concentration of the samples is determined by the absorbance at 260 nm whereas the ratio of the sample absorbance measured at 260 nm and 280 nm is used to assess DNA and RNA purity. A ratio of ~1.8 is considered pure DNA while a ratio of ~2 is considered pure RNA.

2.2.2. cDNA synthesis

Reverse transcription of total RNA is performed utilizing the SuperScript III Reverse Transcriptase (Invitrogen Life Technologies, Carlsbad, CA) with random hexamers and oligodT primers, as described in the manufacturer's protocol. For real-time quantitative reverse transcriptase PCR (qRT-PCR) purposes, the resulting cDNA is diluted tenfold.

2.3. Tissue distribution analysis by means of qRT-PCR

By means of qRT-PCR, the relative transcript levels of two insect neuropeptide precursors (*Bomte*-SIFa and *Schgr*-ATR) and several insect neuropeptide receptors (*Bomte*-SIFR, *Schgr*-ATR, *Schgr*-CRF-DHR1 and *Schgr*-CRF-DHR2) are studied in a variety of tissues of the buff-tailed bumblebee*, Bombus terrestris,* or the desert locust, *S. gregaria*. More details about the specific conditions of each target can be found in the corresponding chapter.

2.3.1. qRT-PCR reactions

All qRT-PCR reactions are run on a StepOne Plus System (ABI Prism, Applied Biosystems) using the Fast SYBR Green Master Mix (2x) (Applied Biosystems). This mixture includes the fluorescent dye SYBR Green which binds to the minor groove of double stranded DNA (dsDNA) in a nonspecific matter. Since SYBR Green bound to DNA produces a much stronger (up to 1000-fold; Dragan et al., 2012) fluorescent signal compared to the unbound dye, the amount of fluorescence can be measured in real-time after each cycle in the qRT-PCR. During the early PCR cycles, a horizontal

base-line is observed. If the target gene is present, the fluorescence will be sufficient to exceed the base-line after a few cycles and the amplification signal is visualised. In this exponential phase, the initial quantity can be determined since the amount of fluorescence is proportionally to the number of amplicons generated (Life Technologies Corporation, 2012). Additionally, the Fast SYBR Green Master Mix also includes a ROX™ Passive Reference Dye which provides a stable fluorescent signal which is used to normalize the fluorescent signal of the SYBR green.

In early studies, reactions are performed in 20 µl reactions. For reducing overall costs of the qRT-PCR, the reaction volume is reduced to 15 µl and later to 10 µl. Reduction of the reaction volume has no significant effect on the results of the qRT-PCR and the conclusions that can be drawn from the results. The following thermal cycling profile is used: 95 °C for 10 min, followed by 40 steps of 95 °C for 3 s and 60 °C for 30 s. After 40 cycles, samples are run for the dissociation protocol (*i.e.* melting curve analysis). According to the manufacturer's instructions for Fast SYBR Green Master Mix, a final primer concentration of 500 nM is used.

2.3.2. Primer design

Primers for the target genes are designed using the Primer Express Software v2.0 (Applied Biosystems). The efficiency and sensitivity of the primers are confirmed by means of a standard curve with a serial dilution of cDNA. By means of a post-amplification melting curve analysis (95 °C for 15 s, 60°C for 1 min, and increase in temperature in 0.7 increments from 60°C to 95°C), specificity of the primers is confirmed.

2.3.3. Delta-delta Ct method

To process the raw qRT-PCR data, accurate normalization is required to account for several variables such as differences in the amount of starting material, enzymatic efficiency and differences between tissues in overall transcriptional activity (Vandesompele et al., 2002). For this purpose, the relative transcript levels are calculated using the delta-delta Ct method in which the raw qRT-PCR data for each sample are normalized to the geometric mean of stable reference genes (the normalization factor) and transcript levels are calculated relatively to a calibrator sample.

2.4. Rapid amplification of cDNA ends (RACE)

By means of rapid amplification of cDNA ends (RACE), unknown sequences at the 3'- and 5' ends of a transcript can be sequenced (3' RACE and 5' RACE, respectively). cDNA is synthesized using the Transcriptor High Fidelity cDNA Synthesis Kit (Roche). In the 3' RACE protocol, an oligodT-anchor primer (5'/3' RACE Kit, 2nd Generation, Roche, 5'-GACCACGCGTATCGATGTCGACTTTTTTTTTTTTTTTV-3') is used to start cDNA synthesis while in the 5' RACE protocol a gene-specific reverse primer is used. In both protocols, cDNA synthesis is followed by two PCR rounds performed with the Pwo DNA Polymerase (Roche). In between these two PCR rounds, a PCR clean-up is executed by means of the GenElute PCR Clean-Up Kit (Sigma-Aldrich).

In the 3' RACE protocol, the first PCR round is performed using a gene-specific forward primer and an anchor reverse primer as a starting point for DNA synthesis (5'/3' RACE Kit, 2nd Generation, Roche, 5'-GACCACGCGTATCGATGTCGAC-3') while in the second PCR round a distinct gene-specific forward primer and the same anchor reverse primer are used. In the 5' RACE, cDNA synthesis is followed by a PCR Clean up and the addition of a 5'-poly-A-tail by means of a Terminal deoxynuceotidyl transferase (Tdt, Roche). In the first PCR round the oligodT-anchor primer is used as a forward primer in combination with a second gene-specific reverse primer. In the second PCR round the anchor primer is used as a forward primer in combination with a third gene-specific reverse primer. An overview of both RACE protocols is depicted in Fig. 2.1. Final PCR products are analyzed and cloned for sequencing as described below.

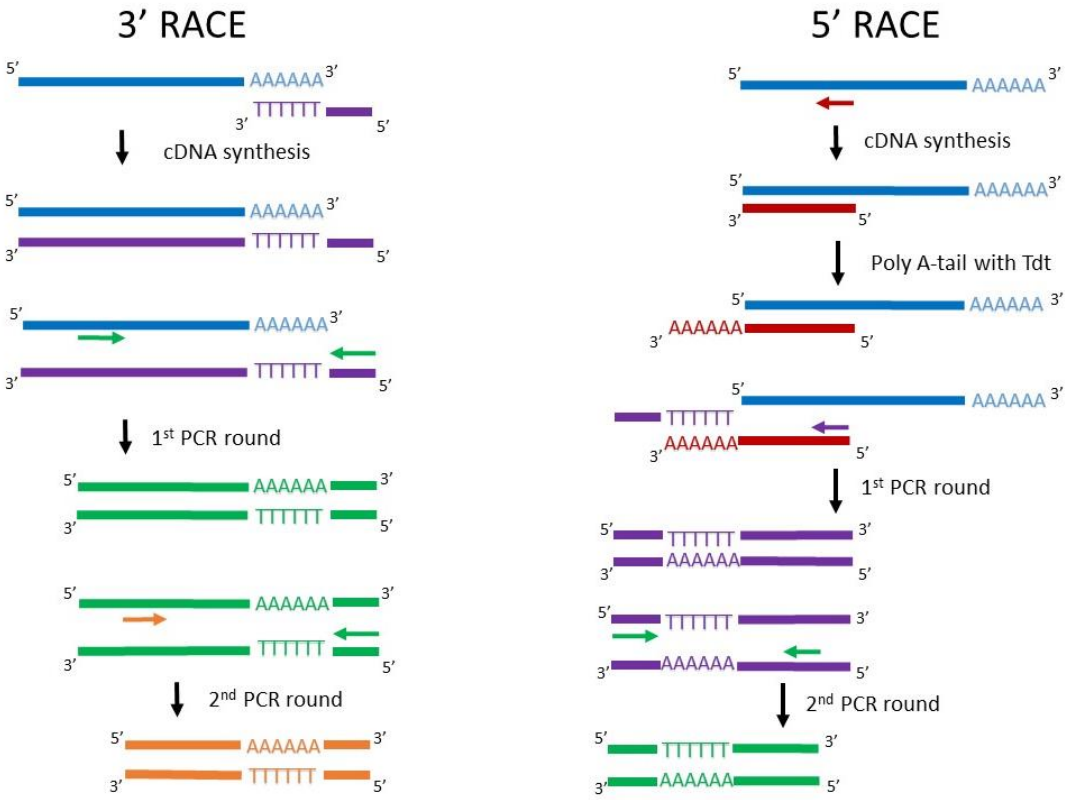

Figure 2.1: Schematic representation of the 3' RACE and the 5' RACE protocol. Left: **3' RACE:** cDNA is synthesized using an oligodT-anchor primer. In the first PCR round a gene-specific forward primer and reverse anchor primer are used. In the second PCR round, a second gene-specific forward primer and the same reverse anchor primer are used. **Right: 5' RACE:** cDNA is synthesized using a gene specific reverse primer followed by addition of a 5' poly-A-tail by means of a Terminal deoxynuceotidyl transferase (Tdt). In the first PCR reaction an oligodT-anchor primer is used as a forward primer in combination with a second gene-specific reverse primer. In the second PCR round, the anchor primer is used as a forward primer in combination with a third gene specific reverse primer.

2.5. Molecular cloning

Several insect receptors (*Bomte*-SIFR, *Schgr*-ATR and *Schgr*-CRF-DHR1) are isolated by means of a PCR reaction on various cDNA samples. More details about the specific PCR conditions of each target can be found in the corresponding chapter. The PCR products are mixed with loading dye (6x Orange DNA Loading Dye, Thermo Fisher) and subsequently run on a 1 % agarose gel together with a DNA ladder to estimate the length of the DNA bands. The DNA can be visualized under UV-light when GelRed Nucleic Acid Gel Stain (Biotum) is added to the agarose gel. Fragments of the expected length are cut out of the gel and the DNA is purified using the GenElute Gel Extraction Kit (Sigma-Aldrich). Next, the purified PCR product is cloned into the pcDNA 3.1/V5-His-TOPO vector (Fig. 2.2, Invitrogen).

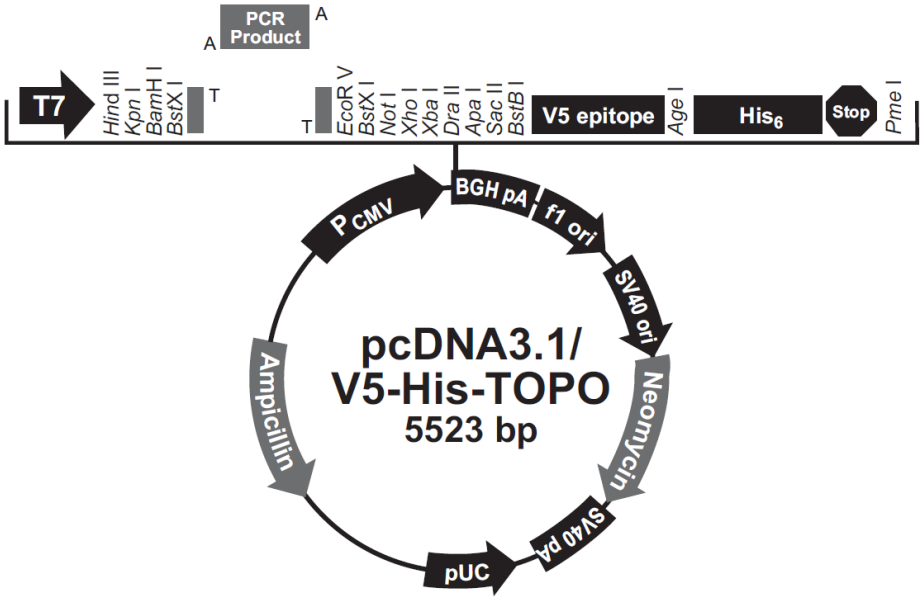

Figure 2.2: pcDNA 3.1/V5-His-TOPO expression vector map. This vector includes a CMV promoter (P_{CMV}), T7 promoter/priming site (T7), a multiple cloning site including cleavage sites for *Hind*III, *Kpn*I, *Bam*HI, *Bst*X, *Eco*R V, *Not*I, *Xho*I, *Xba*I, *Dra*II, *Apa*I, *Sac*II, *BstB*I, *Age*I, and *Pme*I, a TOPO Cloning site, a V5 epitope, a polyhistidine tag (His_6), a stop codon, BGH priming site (BGH pA), an f1 origin of replication (f1 ori) an SV40 promoter and origin of replication (SV40 ori), a Neomycin and an Ampicillin resistance gene, an SV40 polyadenylation signal (SV40 pA) and a pUC origin of replication (pUC). (Image credits: pcDNA 3.1/V5-His-TOPO Expression Kit user Manual, Invitrogen)

Ligation of a purified PCR product in the pcDNA 3.1/V5-His-TOPO vector is performed by means of a TOPO cloning procedure as depicted in Fig. 2.3 (Shuman, 1994). Depending on the used polymerase in the PCR reaction, a 5'-A-overhang is added before ligation by a RedTaq DNA polymerase (Sigma-Aldrich). The ligated vector is transformed to *Escherichia coli* cells [One Shot TOP10 Chemically Competent Cells (Thermo Fisher) or DH5α cells] by means of a heat shock followed by an overnight incubation on Luria-Bertani agar plates (35 g/l; Sigma-Aldrich) with ampicillin (10 mg/ml). Single colonies are picked and grown in Luria-Bertani Broth (Lennox) (25g/l; Sigma-Aldrich) with ampicillin at 37° C overnight. The multiplied vector is isolated by using the GenElute Plasmid Miniprep Kit (Sigma-Aldrich) to check the sequence or by the EndoFree Plasmid Maxi Kit (Qiagen), ensuring an endotoxin-free plasmid DNA purification, when the DNA sample is used to transfect the vertebrate cell lines described below. The inserted DNA sequences are verified on the ABI PRISM 3130 Genetic Analyzer (Applied Biosystems) following the protocol outlined in the BigDye Terminator v1.1 Cycle Sequencing Kit (Applied Biosystems), or purified plasmids are sent to LGC Genomics (Germany) for sequencing. PCR products which merely need to be sequenced (for instance PCR products of the RACE protocol) are cloned into the pCR 4-TOPO vector (Fig. 2.4, Invitrogen) using a similar protocol.

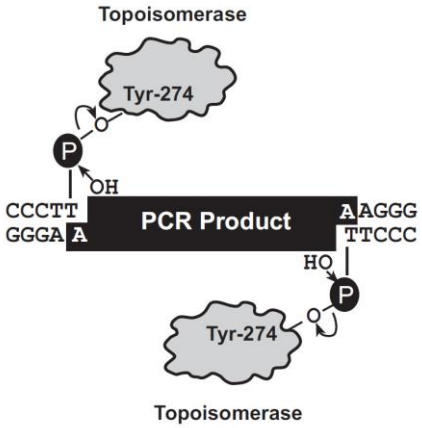

Figure 2.3: Schematic representation of TOPO cloning: The 5' end of the linearized vector is bound by a tyrosyl residue (Tyr-274) of topoisomerase I. Upon hybridization of the 3'-T-overhang of the linearized vector and the 3' A-overhang of the PCR product, the phosphor-tyrosyl bond between the linearized vector and the topoisomerase I is attacked by the 5' hydroxyl from the PCR product resulting in the release of the topoisomerase and subsequent ligation of the PCR product into the vector. (Image credits: pcDNA 3.1/V5-His-TOPO Expression Kit user Manual)

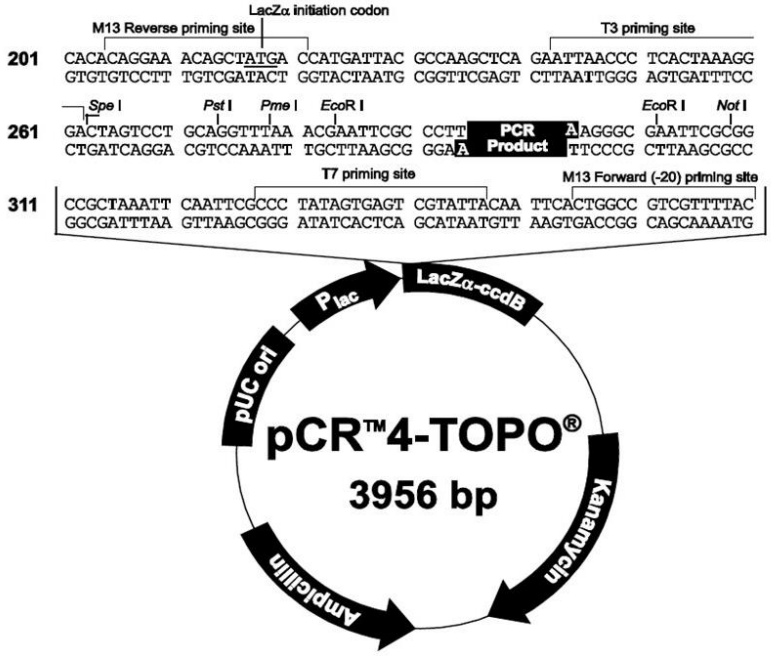

Figure 2.4: pCR 4-TOPO vector map. This vector includes an M13 reverse primer site, a LacZα initiation codon, a T3 priming site, a multiple cloning site including cleavage sites for restriction enzymes *Spe*I, *Pst*I, *Pme*I, *Eco*RI and *Not*I, a TOPO Cloning site, a T7 priming site, an M13 forward (-20) priming site priming site, a LacZα-*ccdB* gene fusion, a Kanamycin resistance gene, an Ampicillin resistance gene, a pUC origin of replication (pUC) and a *Lac* promoter region (P_{lac}). (Image credits: pCR 4-TOPO Kit for sequencing manual, Invitrogen)

2.6. Multiple sequence alignment and percent identity matrix

A multiple sequence alignment is constructed using the EMB-EBI Clustal Omega Multiple Sequence alignment software (http://www.ebi.ac.uk/Tools/msa/clustalo/). Conservation of the amino acids is predicted by the BOXSHADE 3.21 server (http://www.ch.embnet.org/software/BOX_form.html). Putative transmembrane regions of GPCRs (TM1-TM7) are predicted by the TMHMM Server v. 2.0 (http://www.cbs.dtu.dk/services/TMHMM/) and a percent identity matrix is created using the EMB-EBI Clustal Omega Multiple Sequence alignment software. For GPCRs, the percent identity matrix is constructed from TM 1 up to and including TM7.

2.7. Aequorin bioluminescence assay

As described in section 1.4.1.1, Chinese hamster ovary WTA11 cells (CHO-WTA11) and CHO-PAM28 cells are utilized in the aequorin bioluminescence assay to test (1) whether a specific neuropeptide acts as an agonist for the receptor and (2) to test whether activation of the GPCR provokes an increase in intracellular Ca^{2+} levels, respectively. CHO-WTA11 cells stably co-express the photoprotein apoaequorin and the promiscuous $G\alpha_{16}$ subunit (Blanpain et al., 1999) whereas the CHO-PAM28 cells merely stably express the photoprotein apoaequorin, but not the $G\alpha_{16}$ subunit (Wiehart et al., 2002). The CHO cell lines are a kind gift of Prof. Marc Parmentier (University of Brussels) and Dr. Michel Detheux (Euroscreen S.A).Cell culture and transfections of CHO-WTA11 and CHO-PAM28 cells

2.7.1. Cell culture of CHO cells

Both CHO-WTA11 and CHO-PAM28 cell lines are cultured in monolayers in Dulbecco's Modified Eagles Medium nutrient mixture F-12 Ham (DMEM/F-12; Sigma-Aldrich) supplemented with 1 % penicillin/streptomycin (stock solution: 10 000 units/ml penicillin and 10 mg/ml streptomycin; Invitrogen) to prevent bacterial contamination of gram-positive and gram-negative bacteria, respectively. The medium is also supplemented with 10 % fetal bovine serum (Sigma-Aldrich). For CHO-WTA11 cells, 250 mg/ml zeocin (Invitrogen) is added to the medium, whereas for CHO-PAM28 cells, 5 µg/ml puromycin (Sigma-Aldrich) is added to the medium. Puromycin and zeocin are initially used to select for cells stably expressing the apoaequorin (CHO-PAM28; Wiehart et al., 2002), or both apoaequorin and $G\alpha_{16}$ (CHO-WTA11; Blanpain et al., 1999). The cells are subcultured in monolayers in TPP tissue culture flasks T25 (Sigma-Aldrich) twice a week and maintained in an incubator at 37 °C with a constant supply of 5 % CO_2.

Cells are subcultured by detaching the cells with 1 ml trypsin/EDTA [0.25 %; in Hanks' Balanced Salt Solution (HBSS) with phenol red; Sigma-Aldrich]. After removal of the trypsin/EDTA solution, the cells are resuspended in 5 ml fresh culture medium. 0.5 ml of the resuspended cell mix is transferred to 5 ml fresh culture medium in a new TPP tissue culture flasks T25. For transfections, 1 ml of the resuspended cell mix is transferred to 10 ml fresh culture medium in a TPP tissue culture T75 flask (Sigma-Aldrich).

2.7.2. Transfections of CHO cells

CHO cells (CHO-WTA11 and CHO-PAM28) are transiently transfected with either *Bomte*-SIFR, *Schgr*-ATR, *Schgr*-CRF-DHR1, or empty vector construct. Transfections are carried out in TPP tissue culture T75 flasks (Sigma-Aldrich) at 60 - 80 % confluency. Transfections are executed by means of a cationic lipid mediated transfection using the Lipofectamine LTX Kit (Invitrogen). The transfection medium is prepared in 5 ml polystyrene round-bottom tubes containing 2.5 ml serum free DMEM/F-12, 12.5 µl Plus Reagent and 5 µg pcDNA3.1 receptor construct. Thirty µl LTX is added after an incubation period of 5 min at room temperature. After a second incubation period of 30 min at room temperature, the transfection medium is added to the cells in a dropwise manner supplemented with 3 ml fresh culture medium. Finally, the cells are placed in an incubator at 37 °C (5 % CO_2). One day post transfection, 15 ml fresh culture medium is added.

2.7.3. Aequorin bioluminescence assay in CHO cells

Transfected CHO-WTA11 and CHO-PAM28 are detached with PBS complemented with 0.2 % EDTA (pH 8.0; Sigma-Aldrich) and resuspended in DMEM/F-12 (without phenolred, with L-glutamine and 10 mM HEPES; Gibco). After counting the living cells using the NucleoCounter NC-100 (Chemometic) or the TC20 automated Cell Counter (Bio-Rad), the cells are pelleted for 4 min at 800 rpm and resuspended in sterile filtered DMEM/F-12 without phenolred, with L-glutamine and 10 mM HEPES plus 0.1 % bovine serum albumin (BSA/DMEM/F-12) to a density of 5 x 10^6 cells/ml. Coelenterazine *h* (Invitrogen) is added to a concentration of 5 µM and the cells are incubated under dark conditions for 4 hours while gently shaking on a shaker plate at room temperature in order to reconstitute the holoenzyme aequorin. In the meantime, a dilution series of the peptide reconstituted in BSA/DMEM/F-12 is distributed in a 96-well microplate (BD Falcon Clear 96-well Microtest Plate, BD Biosciences) and kept in the dark at room temperature until further screening. BSA/DMEM/F-12 without peptide is pipetted in one well of every row as a blank.

After the 4 hour incubation, the cells are diluted tenfold and incubated for another 30 min under the same conditions. After injection of 50 µl of cell solution (~25000 cell) to the wells of the 96-well

plate containing various concentrations of peptide, the luminescence caused by the calcium response is recorded at 469 nm for 30 s by a Mithras LB940 (Berthold Technologies). This is immediately followed by an injection of 0.2 % Triton X-100 in BSA/DMEM/F-12 to measure the total cellular calcium response for another 9 s in that same well. The total calcium signal (ligand + Triton X-100) is a representative for the total number of cells present in the well. The response of each blank is subtracted from the luminescence obtained for wells within the same row. Calculations are made using the output file from the Microwin2000 software (Mikrotek) in Excel (Microsoft) and further analysis is performed using GraphPad Prism 5 (GraphPad Software Inc.).

2.8. CRE-dependent luciferase reporter assay

HEK293 cells (Invitrogen) are used in the CRE-dependent luciferase reporter assay wherein cAMP levels are measured by means of the $CRE_{(6x)}$-Luc construct as described in section 1.4.1.2.

2.8.1. Cell culture of HEK293 cells

HEK293 cells (Invitrogen) are cultured in monolayers in DMEM (Sigma-Aldrich) supplemented with 10 % fetal bovine serum (Sigma-Aldrich) and 1 % penicillin/streptomycin (stock solution: 10 000 units/ml penicillin and 10 mg/ml streptomycin; Invitrogen) to prevent contamination with gram-positive or gram-negative bacteria. The cells are subcultured in monolayers in TPP tissue culture T75 flasks (Sigma-Aldrich) twice a week and maintained in an incubator at 37 °C with a constant supply of 5 % CO_2.

Cells are subcultured by detaching the cells with 3 ml trypsin-EDTA (0.25 %; in HBSS with phenol red; Sigma-Aldrich). After removal of the trypsin/EDTA solution, the cells are resuspended in 5 ml fresh culture medium. 0.5 ml of the resuspended cell mix is transferred to 10 ml fresh culture medium in a new TPP tissue culture T75 flask for both subculture and transfection purposes.

2.8.2. Transfections of HEK293 cells

HEK293 cells are transiently co-transfected with the pcDNA3.1 receptor construct (*Bomte*-SIFR, *Schgr*-ATR, or empty vector) and the $CRE_{(6x)}$-Luc reported plasmid. Transfections are carried out in TPP tissue culture T75 flasks (Sigma-Aldrich) at ~50 % confluency. Transfections are performed by means of a cationic lipid mediated transfection using the Lipofectamine LTX Kit (Invitrogen). The transfection medium is prepared in 5 ml polystyrene round-bottom tubes containing 2.5 ml serum free DMEM/F-12, 12.5 µl Plus Reagent, 4 µg pcDNA3.1 receptor construct and 2 µg of reporter $CRE_{(6x)}$-Luc plasmid. Sixty µl LTX is added after an incubation period of 5 min at room temperature. After a second incubation period of 30 min at room temperature, the transfection medium is added

to the cells in a dropwise manner supplemented with 3 ml fresh culture medium. Finally, the cells are replaced in an incubator at 37 °C (5 % CO_2).

2.8.3. CRE-dependent luciferase reporter assay

One day post transfection, the co-transfected HEK293 cells are detached using PBS supplemented with 0.2 % EDTA and pelleted for 4 min at 800 rpm. The cells are resuspended in DMEM/F-12 (without phenol red, with L-glutamine and 10 mM HEPES; Gibco) supplemented with 10 % fetal bovine serum (Gibco) and 1 % penicillin/streptomycin (Invitrogen) to a density of 5 x 10^5 cells/ml. A 96-well plate (BD Falcon Clear 96-well Microtest Plate; BD Biosciences) is seeded by adding 100 µl cell solution (~50 000 cells) to each well of the plate and subsequently incubated overnight at 37° C (5 % CO_2).

On the next day, two conditions are tested: (1) in the absence of forskolin to measure increasing levels of cAMP and (2) in the presence of forskolin, ensuring an increased basal cAMP level in the cells, to measure decreasing levels of cAMP. For the first test (1) a dilution series of peptide is made in DMEM/F-12 (without phenolred, with L-glutamine and 10 mM HEPES) supplemented with 200 µM of the phosphodiesterase inhibitor IBMX (Sigma–Aldrich) to prevent cAMP breakdown. To test whether the receptor can reduce cAMP levels upon activation (2), 10 µM NKH-477 (a forskolin-analogue) is added to another series of peptide. After removal of the culture medium from plate, the peptide dilution series (with or without NKH-477) are added to the cells. In the first row of the plate, DMEM/F-12/IBMX (without peptide) is added to the cell as a blank and in the last row of every plate, DMEM/F-12/IBMX/NKH-477 (without peptide) is added as a positive control. Subsequently, the cells are incubated for 4 h at 37 °C (5 % CO_2). By means of a multichannel pipette, 100 µl of Steadylite plus substrate (Perkin Elmer) is added to each well and the plate is incubated for another 10 min under dark conditions at room temperature while gently shaking on a shaker plate. Hereafter, the luciferase enzymatic activity is recorded at 0 s and 5 s on a multimode microplate reader Mithras LB 940 (Mikrotek) at a wavelength of 469 nm. An average of these two measurements is used for further analysis. In the condition without NKH-477 (1), the maximal response is set at the 100 % level. In the condition with NKH-477 (2), the response with DMEM/F-12/IBMX/NKH-477, but no peptide, is set at the 100 % level. In both conditions, the zero level corresponds to the blank condition with DMEM/F-12/IBMX, without peptide. Calculations are made using the output file from the Microwin2000 software (Mikrotek) in Excel (Microsoft) and the results are further analyzed using the GraphPad Prism 5 Software (GraphPad Software Inc.).

2.9. BRET^1-based CAMYEL assay

The bioluminescence resonance energy transfer (BRET)^1-based cAMP biosensor YFP-Epac-*R*luc (CAMYEL; ATCC MBA-277) is used as an alternative biosensor to monitor changes in intracellular cAMP levels upon GPCR activation. The main principle of this assay is described in section 1.4.2. This BRET^1-based assay is performed at the Université Libre de Bruxelles (ULB) at the Institute of Interdisciplinary Research in human and molecular Biology (Institut de Recherche Interdisciplinaire en Biologie Humaine et Moléculaire, IRIBHM) in the lab of Prof. Jean-Yves Springael. Therefore, other protocols for cell culture and transfection of HEK293T cells are applied.

2.9.1. Cell culture of HEK293T cells

HEK293T cells are cultured in monolayers in 10 cm Nunc Cell Culture/Petri Dishes (Thermo Scientific) in DMEM (Gibco) supplemented with 1 % fungizone (Gibco), 10 % fetal bovine serum (FBS; Gibco), 1 % sodium pyruvate (Invitrogen), and 1 % penicillin/streptomycin (stock solution: 10 000 units/ml penicillin and 10 mg/ml streptomycin; Invitrogen) to prevent contamination of gram-positive and gram-negative bacteria, respectively. The cells are subcultured twice a week and maintained in an incubator at 37 °C with a constant supply of 5 % CO_2.

The cells are subcultured by detaching the cells with 3 ml trypsin-EDTA (0.25 %; in HBSS supplemented with $CaCl_2$ and $MgCl_2$ and phenol red). After an incubation period at room temperature, the cells are resuspended in the trypsin/EDTA solution and 0.2 ml is transferred to 10 ml fresh culture medium in a new 10 cm Nunc Cell Culture/Petri Dish. For transfection, the cells are detaching with 3 ml PBS/EDTA. The cells are resuspended in the PBS/EDTA solution and transferred to a conical tube containing 6 ml fresh culture medium. The cells are counted manually using a hemocytometer. Next, the cells are pelleted for 4 min at 800 rpm and resuspended in fresh culture medium to a density of 3 x 10^6 cells/ml. One ml of the cell mixture is transferred to 9 ml fresh culture medium in a new 10 cm Nunc Cell Culture/Petri Dish.

2.9.2. Transfections of HEK293T cells

HEK293T cells are transiently transfected using the calcium phosphate method. Cells are co-transfected with 4 µg CAMYEL vector, 10 µg pcDNA3.1 receptor construct (*Bomte*-SIFR, *Schgr*-ATR or *Schgr*-CRF-DHR1) and 6 µg empty vector. The cell medium is replaced with 10 ml fresh culture medium a half hour prior to transfection and the DNA mixture is prepared in MilliQ water to a final volume of 500 µl.

For transfections using the calcium phosphate method: 50 µl $CaCl_2$ (2.5 M) is added to the DNA mixture. Next, 500 µl HEPES-buffered saline [HBS (2x); 280 mM NaCl, 50 mM HEPES and 1.5 mM

Na_2HPO_4; pH 7.1] is added in a dropwise manner while shaken with a vortex. The solution is mixed a second time by making bubbles using a micropipette (10x) and subsequently added to the cells in a dropwise manner. The transfected cells are maintained in an incubator at 37 °C (5 % CO_2). An additional transfection is performed with 4 µg CAMYEL vector and 16 µg empty vector, but no pcDNA3.1 receptor construct, as a control.

2.9.3. BRET^1-based CAMYEL assay

The BRET^1-based CAMYEL biosensor is used to measure (1) increasing or (2) decreasing intracellular cAMP levels upon activation of a GPCR. Increasing intracellular cAMP levels (1) are measured using several concentrations of peptide in buffer. Decreasing intracellular cAMP levels (2) are measured using several concentrations of peptide in buffer containing forskolin. Blank measurements are added in which only the buffer (1) or buffer with forskolin (2) are added to the cells.

One day post transfection, the co-transfected HEK293T cells are detached using PBS supplemented with 0.2 % EDTA (pH 8.0) and collected in a falcon tube. The cells are pelleted for 4 min at 800 rpm and resuspended to a density of 0.5 x 10^6 cells/ml in DMEM/F-12 without phenolred (Gibco) supplemented with 1 % fungizone (Gibco), 10 % fetal bovine serum (FBS; Gibco), 1 % sodium pyruvate (Invitrogen), and 1 % penicillin/streptomycin. Cells are seeded in white MicroWell 96-Well Optical-Bottom Plates with Polymer Base plates (catalog no. 165306; Thermo Scientific) by adding 100 µl of the cell solution (~50 000 cells) to each well. Subsequently, the cells are incubated overnight at 37 °C (5 % CO_2).

The actual experiment is conducted two days post transfection. Experiments are performed in the presence of IBMX (end concentration 40 µM) to prevent cAMP breakdown and coelenterazine *h* (end concentration 5 µM; Promega) which is used as a substrate for *R*luc.

The HEK293T cells are rinsed with PBS and subsequently resuspended in PBS. Next, cells are incubated for 5 min with the IBMX/coelenterazine *h* mix followed by the addition of peptide (*Bomte*-SIFa, *Schgr*-AT or *Schgr*-CRF-DH) in various concentration (0.10 nM - 1 µM). After another incubation of 10 min, 5 µM of forskolin is added to wells of the experiment wherein decreasing intracellular cAMP levels are measured (2). BRET^1 readings are collected after a third incubation period of 5 min using a Mithras LB940 (Berthold Technologies) and the ratio of emission of YFP (520-570 nm) to *R*luc (370–480 nm) is calculated. Measurements are taken in duplicate per concentration of peptide in two independent transfections for both the experimental condition (with insect receptor) and the control (without insect receptor).

In the first experiment (1) the measurements containing buffer (IBMX/coelenterazine *h*, but no peptide) are used as the baseline. In the second experiment (2) the measurements containing the buffer with forskolin are used as the baseline. Calculations are made using the output file from the Microwin2000 (Mikrotek) in Excel (Microsoft) and further analysis is performed using GraphPad Prism 6 (GraphPad Software Inc.).

2.10. BRET^2-based G protein biosensors

To study if the BRET^2-based G protein biosensors are applicable with insect GPCRs, experiments are performed at the IRIBHM in the lab of Prof. Jean-Yves Springael. The main principle of this assay is described in section 1.5.2.

2.10.1. Cell culture of HEK293T cells

HEK293T cells are cultured as described in section 2.9.1.

2.10.2. Transfections of HEK293T cells

HEK293T cells are transiently transfected using the calcium phosphate method. Cells are co-transfected with either (1) one of the ten Gα-*R*luc8 constructs, $G\gamma_2$-GFP10, $G\beta_1$, an insect pcDNA3.1 receptor construct (*Bomte*-SIFR, *Schgr*-ATR or *Schgr*-CRF-DHR1) and empty vector, constituting the experimental condition, or (2) one of the ten Gα-*R*luc8 constructs, $G\gamma_2$-GFP10, $G\beta_1$ and empty vector, constituting the control condition. The ten Gα-*R*luc8 constructs are: $G\alpha_{i1}$, $G\alpha_{i2}$, $G\alpha_{i3}$, $G\alpha_{oa}$, $G\alpha_{ob}$ representing the $G\alpha_{i/o}$ subfamily, $G\alpha_{11}$ and $G\alpha_{q}$ representing the $G\alpha_{q/11}$ subfamily, $G\alpha_{s}$ as a representative of the G_s subfamily, and $G\alpha_{12}$ and $G\alpha_{13}$ representing the $G\alpha_{12/13}$ subfamily. In all cells, the G protein heterodimer $\alpha_x\ \beta_1\gamma_2$ is expressed with $G\alpha_x$ representing one of the ten Gα constructs.

The cell medium is replaced a half an hour prior to transfection with 10 ml fresh culture medium and the mixtures of DNA constructs are prepared as enlisted in table 2.1 for the experimental condition and in table 2.2 for the control. All mixtures are brought to ~21 µg DNA in 500 µl MilliQ water.

Transfections are performed using the calcium phosphate method as described in section 2.9.2. The transfected cells are maintained in an incubator at 37 °C (5 % CO_2) and on the next day the medium is replaced with fresh culture medium.

Table 2.1: Amount of DNA per construct in DNA mix for transfection of HEK293T cells in the experimental condition. Separate reactions are enlisted per row.

	Gα- *R*luc8 µg	$G\gamma_2$-GFP10 µg	$G\beta_1$ µg	Insect receptor µg	Empty vector µg	Total µg
$G\alpha_{i1}$	0.5	4	4	5	7.5	21
$G\alpha_{i2}$	1	4	4	5	7	21
$G\alpha_{i3}$	2	4	4	5	6	21
$G\alpha_{oa}$	0.5	4	4	5	7.5	21
$G\alpha_{ob}$	0.25	4	4	5	8	21.25
$G\alpha_{11}$	5	4	4	5	3	21
$G\alpha_{q}$	5	4	4	5	3	21
$G\alpha_{s}$	5	4	4	5	3	21
$G\alpha_{12}$	5	4	4	5	3	21
$G\alpha_{13}$	5	4	4	5	3	21

Table 2.2: Amount of DNA per construct in DNA mix for transfection of HEK293T cells in the control. Separate reactions are enlisted per row.

	Gα- *R*luc8 µg	$G\gamma_2$-GFP10 µg	$G\beta_1$ µg	Empty vector µg	Total µg
$G\alpha_{i1}$	0.5	4	4	12.5	21
$G\alpha_{i2}$	1	4	4	12	21
$G\alpha_{i3}$	2	4	4	11	21
$G\alpha_{oa}$	0.5	4	4	12.5	21
$G\alpha_{ob}$	0.25	4	4	13	21.25
$G\alpha_{11}$	5	4	4	8	21
$G\alpha_{q}$	5	4	4	8	21
$G\alpha_{s}$	5	4	4	8	21
$G\alpha_{12}$	5	4	4	8	21
$G\alpha_{13}$	5	4	4	8	21

2.10.3. BRET^2-based G protein assay

To test whether the BRET^2-based G protein biosensors react to the insect GPCRs enabling the detection of the activation of specific G proteins, a first experiment is conducted whereby only one high dose of peptide (1 µM) is applied. This experiment is performed in two separate transfections [for both (1) the experimental condition with insect receptor and (2) the control without insect receptor] per Gα construct ($G\alpha_{i1}$, $G\alpha_{i2}$, $G\alpha_{i3}$, $G\alpha_{oa}$, $G\alpha_{ob}$, $G\alpha_{s}$, $G\alpha_{11}$, $G\alpha_{q}$, $G\alpha_{12}$ or $G\alpha_{13}$). When a significant reaction is obtained, a second experiment is conducted in three separate transfections per Gα construct to examine whether the obtained reaction is dose-dependent by using several concentrations of peptide (0.10 nM – 1 µM).

The experiment is conducted two days post transfection. After removal of the culture medium, the HEK293T cells are detached using PBS supplemented with 0.2 % EDTA (pH 8.0) and collected in a falcon tube. The cells are pelleted for 4 min at 1100 rpm and resuspended to a concentration of

1 µg cells/ml. The concentration of cells per sample is determined using the DC Protein Assay (BIO-RAD) according to the manufacturer's instructions.

In the first experiment, 80 µl cells (1 µg/ml) are added to four wells in a 96-well microplate (Black/White Isoplate-96 Black Frame White Well; PerkinElmer Life Sciences). To the first well, 10 µl PBS (Gibco) is added as a blank. To the remaining three wells, 10 µl of peptide (*Bomte*-SIFa, *Schgr*-AT or *Schgr*-CRF-DH) dissolved in PBS is added to obtain a final concentration of 1 µM. Exactly one minute later, 10 µl of coelenterazine 400a/DeepBlueC (final concentration 5 µM, Gentaur) is added. $BRET^2$ between *R*luc8 (370–450 nm) and GFP10 (510–540 nm) is measured using an Infinite F200 reader (Tecan Group Ltd) one minute after addition of the DeepBlueC. For each well, the $BRET^2$ signal is calculated as the ratio of emission of GFP10 to *R*luc8. The results of the blank (first well) is subtracted from the three other wells (resulting in a $\Delta BRET^2$ value). This experiment is performed in duplicate per transfection (two for each Gα construct) for both experimental and control cells. In order to test the statistical significance between the experimental condition and the control condition, a student's t-test for each biosensor separately is performed using GraphPad Prism 5 (GraphPad Software Inc.).

A significant reduction in $\Delta BRET^2$ signal in the experimental cells (with insect receptor) compared to the control cells (without receptor) may indicate that there is an activation of the Gα protein. The $\Delta BRET^2$ signal of the control cells should remain at the zero level. The magnitude of the $BRET^2$ signal depends on the biosensor used. Therefore, the y-axis of the graphs is set in the same range as observed in earlier studies which use the same $BRET^2$-based G protein biosensors to test receptor signaling of the *Homo sapiens* chemokine receptor (*Homsa*-CCR2; Corbisier et al., 2015) for the $G\alpha_{i/o}$ subfamily, the *H. sapiens* β2-adrenergic receptor (*Homsa*-β2-AR; Saulière et al., 2012) for the $G\alpha_s$ subfamily, the *H. sapiens* angiotensin II type 1 receptor (*Homsa*-AT1R, Saulière et al., 2012) for the $G\alpha_{q/11}$ subfamily and the *H. sapiens* thromboxane TPα receptor (TPα-R; Saulière et al., 2012) for the $G\alpha_{12/13}$ subfamily. The results of these receptors are also shown in the results in order to compare the results using the insect GPCRs.

If the $\Delta BRET^2$ signal is dose-dependent, we can conclude that the biosensor is truly activated. Therefore, HEK293T cells are co-transfected again in triplicate with insect receptor and the G protein biosensor constructs. The protocol of this assay is similar to the procedure described above but instead of adding cells to four wells, cells are added to six wells to test multiple concentrations of peptide (0.10 nM - 1 µM) including the PBS that serves as a blank. The result of the blank (first well) is subtracted from the other wells to calculate $\Delta BRET^2$. This procedure is performed in duplicate per

transfection (in three transfections for each Gα construct) and the data is analyzed using the Excel output file (Microsoft) and GraphPad Prism 5 (GraphPad Software Inc.).

2.11. G protein analysis in *B. terrestris* and *S. gregaria*

All available G protein subunit sequences in *B. terrestris* are identified by means of the Basic Local Alignment Search Tool (BLAST) tool on BeeBase.org (Priyam et al., 2015; Sadd et al., 2015) by using *D. melanogaster* G protein subunit sequences as a query. These sequences are, in turn, used to scan the (unpublished) transcriptome database of *S. gregaria* to identify G protein subunit sequences in this species. All identified G protein subunit sequences are confirmed to be actual G protein subunit sequences by using the online tool GprotPRED (http://aias.biol.uoa.gr/GprotPRED/) which is able to recognize Gα, Gβ and Gγ subunits and is able to assign Gα subunits to one of the four Gα protein subfamilies; namely $G\alpha_{i/o,}$ $G\alpha_{s}$, $G\alpha_{q/11}$ or $G\alpha_{12/13}$ (Kostiou et al., 2016). In case that GprotPRED is unable to assign a Gα protein sequence to a Gα subfamily, the sequence is assigned to a Gα protein subfamily based on sequence identity with other insect Gα subunit sequences by using the BLAST tool on NCBI (https://blast.ncbi.nlm.nih.gov/Blast.cgi).

A multiple sequence alignment is constructed for $G\alpha_{i}$, $G\alpha_{o}$, $G\alpha_{s}$, $G\alpha_{q/11}$, $G\alpha_{12/13}$, Gβ and Gγ using sequences of the G protein subunits of *H. sapiens* used to construct the $BRET^{2}$-based G protein biosensors described in section 1.5.2 and all identified G protein subunit sequences of *B. terrestris* and *S. gregaria*. Since there are construct available for three $G\alpha_{i}$ subtypes and two $G\alpha_{o}$ isoforms, sequences of the $G\alpha_{i}$ and $G\alpha_{o}$ are analyzed separately. These multiple sequence alignments and additional percent identity matrices are constructed as described in section 2.6.

GenBank accession numbers of the *H. sapiens* G protein subunit sequences used to construct the $BRET^{2}$-based G protein biosensors which are studied in the multiple sequence alignment are P63096 for *Homsa*-$G\alpha_{i1}$, P04899 for *Homsa*-$G\alpha_{i2}$, P08754 for *Homsa*-$G\alpha_{i3}$, NP_066268.1 for *Homsa*-$G\alpha_{oa}$, NP_620073.2 for *Homsa*-$G\alpha_{ob}$, P63092 for *Homsa*-$G\alpha_{s}$, P50148 for *Homsa*-$G\alpha_{q}$, P29992 for *Homsa*-$G\alpha_{11}$, Q03113 for *Homsa*-$G\alpha_{12}$, Q14344 for *Homsa*-$G\alpha_{13}$, P62873, for *Homsa*-$G\beta_{1}$, and P59768 for *Homsa*-$G\gamma_{1}$.

Chapter 3:
Characterization of the SIFamide precursor and receptor and its G protein mediated signaling pathways in *Bombus terrestris*

The results described in this chapter are partially published in:

Lismont, E., Mortelmans, N., Verlinden, H., Vanden Broeck, J. Molecular cloning and characterization of the SIFamide precursor and receptor in a Hymenopteran insect, *Bombus terrestris* (2018). General and Comparative Endocrinology, 258, 39-52.

The content of this chapter is updated and additional *in cellulo* BRET assay results and an analysis of the G protein subunit sequences are added. The mass spectrometry analysis is performed by Dr. Kurt Boonen and the dissections were assisted by Em. Prof. Dr. Roger Huybrechts, Dr. Heleen Verlinden, Dr. Magdalena Bil and Dr. Rik Verdonck.

3.1. Introduction

The neuropeptide SIFamide (SIFa) is initially isolated in the grey fleshfly, *Neobellieria bullata,* and is identified as a myotropin, stimulating the contractions of the migratory locust, *Locusta migratoria,* oviduct (Janssen et al., 1996). It is originally described as *Neobu*-LFa but after discovering more family members it is renamed *Neobu*-SIFa (Verleyen et al., 2004a).

SIFa's are widely distributed among insects, crustaceans (Stemmler et al., 2007; Verleyen et al., 2004a; Verleyen et al., 2009) and arachnids (Neupert et al., 2009; Šimo et al., 2009; Veenstra et al., 2012). They are usually dodecapeptides but longer and shorted isoforms of SIFa also exist in arthropods. In the desert locust, *Schistocerca gregaria*, a longer isoform of fifteen amino acids is identified (Gellerer et al., 2015) whereas in both the Western tarnished plant bug, *Lygus hesperus*, (Christie et al., 2017) and the myriapod, *Symphylella vulgaris* (Christie, 2015a), a shorter isoform of eight amino acids is predicted *in silico*.

The SIFa receptor of the fruit fly, *Drosophila melanogaster* (*Drome*-SIFR), is pharmacologically characterized in 2006 (Jørgensen et al., 2006). This rhodopsin-like G protein-coupled receptor (Family A) is activated by *Drome*-SIFa (EC_{50}= 20 nM) but not by any of 32 other tested insect neuropeptides nor by any of eight biogenic amines. In the blacklegged tick, *Ixodes scapularis*, the SIFR is capable of inducing an increase in intracellular Ca^{2+} ion levels upon activation by its agonist (Šimo et al., 2013). Up to date, no further signaling information exists concerning the G protein mediated signaling pathways of these receptors. Based on sequence identity, SIFRs are predicted *in silico* in the genomes of the following insects: the African malaria mosquito *Anopheles gambiae*, the silkworm *Bombyx mori*, the red flour beetle, *Tribolium castaneum*, the honey bee, *Apis mellifera* (Jørgensen et al., 2006) and the pea aphid, *Acyrthosiphon pisum* (Li et al., 2013).

In insects, immunolocalization and *in situ* hybridization studies indicate that SIFa expression is restricted to four medial interneurons in the pars intercerebralis with ramifications throughout the ventral nerve cord and most parts of the brain (Terhzaz et al., 2007; Roller et al., 2008; Carlsson et al., 2010; Inosaki et al., 2010; Galizia et al., 2012; Heuer et al., 2012; Neupert et al., 2012; Zoephel et al., 2012; Siju et al., 2014; Gellerer et al., 2015; Arendt et al., 2016). Furthermore, since SIFa is not identified at the neurohemal release sites, it is suggested that this neuropeptide does not have hormonal functions and is involved in the development and organization of the insect central nervous system (CNS; Gellerer et al., 2015). In contrast to insects, SIFa is widely distributed throughout the CNS in crustaceans (Yasuda et al., 2004; Yasuda-Kamatani and Yasuda, 2006; Christie et al., 2006; *Christie* et al., 2007; Polanska et al., 2007; Kim et al., 2014).

The SIFR is also expressed outside the central nervous system (CNS) and is thus more widely distributed in insects than SIFa. In *D. melanogaster*, SIFR is besides throughout the CNS also expressed in two neurons of the uterus which project to the CNS (Sellami and Veenstra, 2015). In *B. mori*, SIFR is expressed in the brain of fourth instars (Yamanaka et al., 2008).

Over the past decade, several physiological functions of SIFa have been identified in insects and most studies are performed in *D. melanogaster*. Targeted cell ablation of the four medial interneurons in the pars intercerebralis in this insect and RNA interference (RNAi) of the SIFa precursor transcript in the SIFa neurons results in sexually hyper-receptive females and bisexual courtship behavior of males (Terhzaz et al., 2007). The same bisexual behavior is observed when the fruitless neurons that express the *Drome*-SIFR are targeted by cell ablation or RNAi, leading to the conclusion that SIFa acts on fruitless neurons (Sellami and Veenstra, 2015). These neurons express the *fruitless* gene which encodes several splice variants of a transcription factor involved in the development of a variety of neurons necessary for courtship and copulation (Dickson, 2008). Additionally, elimination of SIFa by cell ablation or RNAi in these four cells in the pars intercerebralis results in a reduced sleep-bout length and shortened baseline sleep This short sleep phenotype is also observed when the receptor, *Drome*-SIFR ,is downregulated using RNAi (Park et al., 2014).

Besides sexual and sleeping behavior, SIFa also seems to be involved in feeding behavior of *D. melanogaster*. A recent study by Martelli and co-workers (2017) reports that the four SIFamidergic neurons in the brain are involved in the regulation of appetitive and feeding behavior by promoting taste- and odor-guided appetitive behavior and inducing food uptake upon stimulation of hugin-pyrokinin (hugin-PK). They also report that satiety-mediating myoinhibiting peptide (MIP) inhibits SIFamide production in these neurons (Martelli et al., 2017). However, RNAi of SIFa in *D. melanogaster* does not result in precocious sperm ejection behavior in females (supplementary material of Lee et al., 2015) and does not affect flight duration, but it does result in pupal lethality (Agrawal et al., 2013).

To date, two studies are reported concerning the physiological functions of SIFa in other insects than *D. melanogaster*. An RNAi knockdown of the SIFR in *T. castaneum* results in a significantly reduced number of eggs laid per female per week but has no significant effect on the larval hatching rate (in supplementary material of Bai and Palli, 2016). Additionally, in accordance with the study of Martelli and co-workers (2017), wherein SIFamide is presented as a hunger-induced neuropeptide modulating odor-evoked activity in the olfactory neurons in *D. melanogaster*, Christ and co-workers (2017) observe that SIFamide levels in the paired antennal lobes of the yellow fever mosquito

A. aegypti, the processing centers for olfactory information, do not change 24h and 48h post-blood meal (*i.e.* post-hunger stages).

In ticks, chelicerates which belong to the Arachnida class, other biological activities of SIFa are reported. In *I. scapularis*, SIFa is involved in the stimulation of the hindgut motility (Šimo and Park, 2014). Similarly as shown in *D. melanogaster*, wherein MIP inhibits SIFamide production (Martelli et al., 2017), MIP antagonizes the myostimulatory effect on the hindgut (Kim et al., 2018b). Additionally, the expression patterns of the MIP receptor (*Ixosc*-MIPR) and *Ixosc*-SIFR in the salivary glands also suggest that MIP and SIF act antagonistically whereby the SIFamide system is activated in salivary glands of unfed ticks, whereas the MIP system is activated upon feeding (Šimo et al., 2013). Notably, innervation of the salivary glands in *I. scapularis* takes place by salivary gland neurons producing both MIP and SIFamide (Šimo et al., 2009). Additionally, a recent study has reported that these protocerebral salivary gland neurons also contain elevenin and that the elevenin receptor 1 (*Ixosc*-ElevR1), but not the elevenin receptor 2 (*Ixosc*-ElevR2), is expressed in the salivary glands (Kim et al., 2018a). Kim and co-workers (2018b) also suggest that SIFamide, MIP and elevenin are presumably modulators of dopaminergic autocrine or paracrine control of the salivary glands.

Previous studies indicate that the SIFR system is related to the vertebrate gonadotropin-inhibitory hormone (GnIH) receptor, which also binds NPFF [hence the name neuropeptide FF receptor (NPFFR)]. It is suggested that the GnIH ligand-receptor pair and the SIFa ligand-receptor pair may have diverged from an ancestral signaling system mediated by a member of the Famide group of peptides, which includes FMRFamide, neuropeptide F (NPF), short neuropeptide F (sNPF), sulfakinin (SK), myosuppressin and SIFa, and further co-evolved independently in vertebrates and insects (Ubuka and Tsutsui, 2014). Other studies also suggest that GnIH/SIFamide signaling represents evolutionarily conserved pathways. Hauser and co-workers (2006) suggest an evolutionary link based on phylogenetic tree analysis since SK, neuropeptide Y (NPY), Kinin, NPF and sNPF are presented in the same clade and a recent study by Martelli and co-workers (2017) also suggests a link, since both SIFa and GnIH are involved in inducing feeding behavior and inhibiting reproduction. Additionally, Mirabeau and Joly (2013) suggest a common evolutionary origin based on gene analysis showing the presence of a phase-2 intron at position 65 in both receptor systems. Despite the fact that the SIFR seems to be related to the GnIH/NPFF receptor, no sequence identity is found between SIFa and NPFF/GnIH-type peptides (Mirabeau and Joly, 2013; Elphick and Mirabeau, 2014; Ubuka and Tsutsui, 2014).

The purpose of the current study is to gain more understanding of the SIFa downstream signaling pathways in insects. The sequences of the SIFa precursor and the SIFR are identified in an important

pollinator species, the buff-tailed bumblebee, *Bombus terrestris*, and their transcript levels are studied in a variety of tissues. We enlist all hitherto identified SIFa's in arthropods and construct a WebLogo by aligning the peptide sequence of *Bomte*-SIFa with other insect members of this family to identify the conserved amino acids in this class. Additionally, the *Bomte*-SIFR is cloned and pharmacologically characterized by studying the downstream signaling pathways by means of commonly used *in cellulo* assays such the aequorin bioluminescence assay and the CRE-dependent luciferase reporter assay. We supplement these data with alternative *in cellulo* assays such as the bioluminescence resonance energy transfer (BRET)[1]-based 'cAMP sensor using YFP-Epac-*R*luc' (CAMYEL; ATCC MBA-277) biosensor and BRET[2]-based G protein biosensors (Galés et al., 2006). The latter measure a direct activation of G-proteins and are represented by ten biosensors covering all four major Gα subfamilies ($G\alpha i_{/o}$, $G\alpha_{s}$, $G\alpha_{q/11}$ and $G\alpha_{12/13}$). Additionally, since literature on the G protein subunits in insects is limited, a comparison of the amino acid sequences of the G protein subunits of *B. terrestris* and the amino acid sequences of the human (*Homo sapiens*) G protein subunits used to construct the BRET[2]-based G protein biosensors is performed to interpret the results of the BRET[2]-based G protein assay. Finally, the agonistic signaling properties of *Bomte*-SIFa and related peptides at *Bomte*-SIFR receptor are examined determining the amino acid positions that are important for receptor signaling.

3.2. Material and methods

3.2.1. Sequence analysis of the *Bomte* SIFa precursor and *Bomte* SIFR

Nucleotide sequences of the precursor (*Bomte*-SIFa) and the receptor (*Bomte*-SIFR) are identified using the Basic Local Alignment Search Tool (BLAST) tool on BeeBase.org (Priyam et al., 2015; Sadd et al., 2015). The potential signal peptide sequences in the precursor sequence is predicted by SignalP 4.1 (Petersen et al., 2011) and a WebLogo (Crooks et al., 2004) is created by aligning the peptide sequence of *Bomte*-SIFa with other insect members of this family (enlisted in table 3.1).

A multiple sequence alignment and a percent identity matrix is constructed as described in section 2.6 using the amino acid sequences of the *I. scapularis* SIFR (GenBank accession number KC422392), the *B. terrestris* SIFR (GenBank accession number XP_003401591.1), the *D. melanogaster* SIFR (GenBank accession number NP_650966.2), the human NPFFR1 (*Homsa*-NPFFR1; GenBank accession number. NP_071429.1) and the human NPFFR2 (*Homsa*-NPFFR2; GenBank accession number. NP_004876.2).

Table 3.1: List of SIFamide peptides identified or predicted *in silico* in Arthropods

Organism	Sequence	Reference
Hexapoda		
Class: Insecta		
Order: Diptera		
Aedes aegypti	GYRKPPFNGSIF-NH_2	Siju et al. (2014)
Anopheles gambiae	GYRKPPFNGSIF-NH_2	Riehle et al. (2002)
Delia radicum	AYRKPPFNGSIF-NH_2	Zoephel et al. (2012)
Drosophila melanogaster	AYRKPPFNGSIF-NH_2	Vanden Broeck (2001), Hewes and Taghert (2001), Predel et al. (2004), Baggerman et al. (2005)
Drosophila pseudoobscura	AYRKPPFNGSIF-NH_2	Verleyen et al. (2004a)
Drosophila suzukii	AYRKPPFNGSIF-NH_2	Audsley et al. (2015)
Glossina morsitans	AYRKPPFNGSIF-NH_2	Caers et al. (2015)
Lucilia cuprina	AYRKPPFNGSIF-NH_2	Rahman et al. (2013)
Neobellieria bullata	AYRKPPFNGSIF-NH_2	Janssen et al. (1996), Verleyen et al. (2004a), Verleyen et al. (2004b)
Protophormia terraenovae	AYRKPPFNGSIF-NH_2	Inosaki et al. (2010)
Order: Blattodea		
Periplaneta americana	TYRKPPFNGSIF-NH_2	Neupert et al. (2012), Arendt et al. (2016)
Rhyparobia maderae	TYRKPPFNGSIF-NH_2	Arendt et al. (2016)
Therea petiveriana	TYRKPPFNGSIF-NH_2	Arendt et al. (2016)
Order: Coleoptera		
Agelastica alni	AYRKPPFNGSIF-NH_2	Verleyen et al. (2004a)
Tenebrio molitor	TYRKPPFNGSIF-NH_2	Weaver and Audsley (2008)
Tribolium castaneum	TYRKPPFNGSIF-NH_2	Li et al. (2007)
Order: Hemiptera		
Acyrthosiphon pisum	FRKPPFNGSIF-NH_2	Verleyen et al. (2009)
Aphis gossypii	GFRKPPFNGSIF-NH_2	Christie (2008)
Lygus hesperus	PPFNGSIF-NH_2	Christie et al. (2017)
Nilaparvata lugens	AYKKPPFNGSIF-NH_2	Tanaka et al. (2014)

Rhodnius prolixus	TYKKPPFNGSIF-NH_2	Ons et al. (2009)
Order: Hymenoptera		
Apis mellifera	AYRKPPFNGSIF-NH_2	Verleyen et al. (2004a), Hummon et al. (2006), Audsley and Weaver (2006)
Bombus terrestris	AYRKPPFNGSIF-NH_2	This paper
Nasonia vitripennis	AYRKPPFNGSIF-NH_2	Verleyen et al. (2009), Hauser et al. (2010)
Order: Lepidoptera		
Bombyx mori	TYRKPPFNGSIF-NH_2	Verleyen et al. (2009)
Galleria mellonella	AYRKPPFNGSIF-NH_2	Verleyen et al. (2004a)
Order: Orthoptera		
Locusta migratoria	AAATFRRPPFNGSIF-NH_2	Gellerer et al. (2015)
Schistocerca gregaria	AAATFRRPPFNGSIF-NH_2	Gellerer et al. (2015)
Stenobothrus lineatus	AAATFRRPPFNGSIF-NH_2	Gellerer et al. (2015)
Order: Protura		
Acerentomon sp.	pEGAYRKPPFNGSIF-NH_2	Christie and Chi (2015a), Christie and Chi (2015a)
Order: Blattodea		
Mastotermes darwiniensis	TYRKPPFNGSIF-NH_2	Christie (2015b)
Crustacea		
Class: Malacostraca		
Order: Decapoda		
Cancer antennarius	GYRKPPFNGSIF-NH_2	Stemmler et al. (2007)
Cancer borealis	GYRKPPFNGSIF-NH_2	Huybrechts et al. (2003), Stemmler et al. (2007), Christie et al. (2007)
Cancer irroratus	GYRKPPFNGSIF-NH_2	Stemmler et al. (2007)
Cancer magister	GYRKPPFNGSIF-NH_2	Christie et al. (2007), Stemmler et al. (2007)
Cancer productus	GYRKPPFNGSIF-NH_2	Messinger et al. (2005), Christie et al. (2007), Stemmler et al. (2007)
Carcinus maenas	GYRKPPFNGSIF-NH_2	Stemmler et al. (2007), Ma et al. (2009)
Cherax quadricarinatus	GYRKPPFNGSIF-NH_2	Stemmler et al. (2007), Dickinson et al. (2008)
Clibanarius vittatus	GYRKPPFNGSIF-NH_2	Stemmler et al. (2007)
Crangon septemspinosa	GYRKPPFNGSIF-NH_2	Stemmler et al. (2007)
Hemigrapsus nudus	GYRKPPFNGSIF-NH_2	Stemmler et al. (2007)
Homarus americanus	VYRKPPFNGSIF-NH_2	Christie et al. 2006), Stemmler et al. (2007), Ma et al.(2008), Dickinson et al. (2008)
Homarus gammarus	VYRKPPFNGSIF-NH_2	Stemmler et al. (2007),Dickinson et al. (2008)
Jasus edwardsii	GYRKPPFNGSIF-NH_2	Yasuda et al. (2004)
Lithodes maja	GYRKPPFNGSIF-NH_2	Stemmler et al. (2007)
Litopenaeus vannamei	GYRKPPFNGSIF-NH_2	Christie (2014a)
Lophopanopeus bellus	GYRKPPFNGSIF-NH_2	Stemmler et al. (2007)
Macrobrachium rosenbergii	GYRKPPFNGSIF-NH_2	Vázquez-Acevedo et al. (2009)
Metacarcinus gracilis	GYRKPPFNGSIF-NH_2	Stemmler et al. (2007)
Neotrypaea californiensis	GYRKPPFNGSIF-NH_2	Stemmler et al. (2007)
Nephros norvegicus	GYRKPPFNGSIF-NH_2	Stemmler et al. (2007), Dickinson et al. (2008)
Ovalipes ocellatus	GYRKPPFNGSIF-NH_2	Stemmler et al. (2007)
Pachycheles rudis	GYRKPPFNGSIF-NH_2	Stemmler et al. (2007)
Pacifastacus leniusculus	GYRKPPFNGSIF-NH_2	Stemmler et al. (2007), Dickinson et al. (2008)
Pagurus acadianus	GYRKPPFNGSIF-NH_2	Stemmler et al. (2007)
Pagurus granosimanus	GYRKPPFNGSIF-NH_2	Stemmler et al. (2007)
Pagurus pollicaris	GYRKPPFNGSIF-NH_2	Stemmler et al. (2007)
Pandalus danae	GYRKPPFNGSIF-NH_2	Stemmler et al. (2007)
Panulirus interruptus	GYRKPPFNGSIF-NH_2	Stemmler et al. (2007)
Penaeus duorarum	GYRKPPFNGSIF-NH_2	Stemmler et al. (2007)
Pandalus platyceros	GYRKPPFNGSIF-NH_2	Stemmler et al. (2007)

Penaeus monodon	GYRKPPFNGSIF-NH_2	Sithigorngul et al. (2002)
Petrolisthes cinctipes	GYRKPPFNGSIF-NH_2	Stemmler et al. (2007)
Petrolisthes eriomerus	GYRKPPFNGSIF-NH_2	Stemmler et al. (2007)
Procambarus clarkii	GYRKPPFNGSIF-NH_2	Yasuda et al. (2004), Stemmler et al. (2007), Dickinson et al. (2008)
Pugettia gracilis	GYRKPPFNGSIF-NH_2	Stemmler et al. (2007)
Pugettia producta	GYRKPPFNGSIF-NH_2	Stemmler et al. (2007)
Scylla olivacea	GYRKPPFNGSIF-NH_2	Christie (2016)
Scylla paramamosain	GYRKPPFNGSIF-NH_2	Bao et al. (2015)
Order: Amphipoda		
Echinogammarus veneris	GPYRKPPFNGSIF-NH_2	Christie (2014b)
Hyalella azteca	GYRKPPFNGSIF-NH_2	Christie et al. (2018a)
Class: Remipedia		
Order: Nectiopoda		
Speleonectes lucayensis	GYRKPPFNGSIF-NH_2	Christie (2014c)
Class: Maxillipoda		
Order: Sessilia		
Balanus amphitrite	GYRKPTFNGSIF-NH_2	Yan et al. (2012)
Order: Arguloida		
Argulus siamensis	SYKSKPPFNGSIF-NH_2	Christie (2014d)
Class: Branchiopoda		
Order: Diplostraca		
Daphnia pulex	TRKLPFNGSIF-NH_2	Verleyen et al. (2009), Dircksen et al. (2011)
Order: Notostraca		
Triops newberryi	NRKLPFNGSIF-NH_2	Christie et al. (2018b)
Chelicerata		
Class: Arachnida		
Order: Ixodida		
Ixodes scapularis	AYRKPPFNGSIF-NH_2	Verleyen et al. (2009), Šimo et al. (2013)
Order: Areneae		
Latrodectus hesperus	GRKPPFNGSIF-NH_2	Christie (2015c)
Stegodyphus mimosarum	ARKPPFNGSIF-NH_2	Christie and Chi (2015b)
Order: Trombidiformes		
Tetranychus urticae	RKPPLNGSIF-NH_2	Veenstra et al. (2012)
Myriapoda		
Class: Symphyla		
Order: Symphyla		
Symphylella vulgaris	PPFNGSIF-NH_2	Christie (2015a)

3.2.2. Identification and sequence analysis of the *B. terrestris* G protein subunits

The amino acid sequences of the G protein subunits of *B. terrestris* are identified and analyzed as described in section 2.11.

3.2.3. Tissue collection

A nest of bumblebees and newly emerged drones are obtained at Biobest Group NV (Westerlo, Belgium). They are kept in miniature hives at room temperature under a 12h/12h photoperiod while sugar water is present *ad libitum*. All bumblebees are anaesthetized with CO_2 prior to dissection.

For the tissue distribution and cloning of the receptor, newly emerged drones are collected within a 12-hour time frame. After three days, various tissues (brain, testes, accessory glands, foregut, midgut, hindgut, Malpighian tubules, ventral nerve cord and fat body) are dissected in phosphate buffered saline (PBS) under a binocular microscope and divided over three pools of at least 8 animals (13, 9 and 8 animals respectively, derived from independent colonies). The tissues are collected in 2.0 ml tubes containing MagNa Lyser green beads (Roche) and immediately snap frozen in liquid nitrogen. Until further processing, the samples are stored at -80 °C to protect the tissues from degradation (also see Verlinden et al., 2013).

For the mass spectrometry, a pool of five brains of female bumblebees is dissected in PBS under a binocular microscope. The brains are collected in ice cold extraction solution [methanol:H2O:acetic acid (90:9:1 v/v/v/)] until further processing.

3.2.4. RNA extraction and cDNA synthesis

The RNA extractions and cDNA synthesis are performed as described in section 2.2.

3.2.5. Study of relative transcript levels of *Bomte*-SIFa and *Bomte*-SIFR using qRT-PCR

The relative transcript levels of *Bomte*-SIFa and *Bomte*-SIFR are measured in the different tissues by means of real-time quantitative reverse transcriptase PCR (qRT-PCR). Primers for the target genes *Bomte*-SIFa and *Bomte*-SIFR are designed as described in section 2.3.2. A standard curve is constructed using a serial fivefold dilution of brain cDNA.

In an earlier study, we determined the best combination of reference genes using the qBase+ software v. 2.4 [Biogazelle; based on the proven GeNorm (Vandesompele et al., 2002) and qBase (Hellemans et al., 2007) technology] for this tissue distribution analysis (Verlinden et al., 2013). A combination of six reference genes came out to get to a GeNorm V-value of 0.17. However, by performing multiple analyses with reduced numbers of reference genes, no significant differences are found when only the three most stable reference genes are used compared to the combination of the six reference genes. Therefore, the data in this study are normalized against the three most stable endogenous reference genes, which is the recommended minimum by Vandesompele and co-workers (2002). These three most stable reference genes are: elongation factor 1 α (EF1α), glyceraldehyde 3-phosphate dehydrogenase (GADPH) and ribosomal protein L13 (RPL13). The oligonucleotide sequences of the primers for the target and reference genes are enlisted in table 3.2. The experiments are repeated three times with independent biological pools of at least eight animals each.

Table 3.2: Oligonucleotide sequences of primers for target and reference genes used in the qRT-PCR.

Target gene	**Forward primer**	**Reverse primer**
Bomte-SIFa	5'-GCGATCCAACGCTATCACTGA-3'	5'-TTTCGCAGACCGATGACATG-3'
Bomte-SIFR	5'-TGATCGCGGAGGCTATCAC-3'	5'-GTCCACCCTGCTCCTCCAT-3'
Reference gene	**Forward primer**	**Reverse primer**
Bomte-EF1α	5'-AGAATGGACAAACCCGTGAG-3'	5'-CACAAATGCTACCGCAACAG-3'
Bomte-GADPH	5'-TTTTGAAATCGTTGAGGGTCTT-3'	5'-CCATCACGCCATAACTTTCC-3'
Bomte-RPL13	5'-GGTTTAACCAGCCAGCTAGAAA-3'	5'-CTCCACAGGTCTTGGTGCAA-3'

Abbreviations: *Bomte* = *Bombus terrestris*, SIFa = SIFamide; SIFR = SIFamide receptor, EF1α = elongation factor 1 α, GADPH = glyceraldehyde 3-phosphate dehydrogenase and RPL13 = ribosomal protein L13

All reactions are run in duplicate in 10 µl reactions according to the manufacturer's instructions as described in section 2.3.1. For each sample, the amount of transcripts of the target gene is normalized using the delta-delta Ct method as described in section 2.3.3 in which the brain sample of pool one is used as the calibrator sample. No amplification of the fluorescent signal is detected in any negative control sample, proving that the extraction procedure, including the DNase treatment, effectively removed genomic DNA from all the RNA samples and that there is no contamination.

3.2.6. Mass spectrometry analysis of SIFa in *B. terrestris*

The pool of dissected bumblebee brains is homogenized by sonicating three times for 10 s (Sanyo MSE Soniprep 150). After and in between sonication the sample is immediately put on ice. After a 10 min centrifugation at 9500 rpm at 4°C the supernatant is collected and completely evaporated. The pellet of the sample is resuspended in 25 µl 2 % acetonitrile and 0.1 % trifluoroacetic acid and desalted according to using the manufacturer's instructions (ZipTip C18 Millipore, Billerica, MA). The sample is analyzed in a Q Exactive Orbitrap mass spectrometer (Thermo Scientific, San Jose, CA, USA). Analysis of the MS/MS data is performed with the PEAKS 7 software (Bioinformatics Solutions Inc., Waterloo, ON, Canada) and the MS/MS spectra is matched to the genome database of *B. terrestris* (Priyam et al., 2015; Sadd et al., 2015) according to the procedure described by Caers and co-workers (2015).

3.2.7. Molecular cloning of *Bomte*-SIFR

The open reading frame of *Bomte*-SIFR is amplified by a PCR reaction on a sample of cDNA of brains by means of a Q5 High-Fidelity DNA Polymerase (New England BioLabs Inc.). A specific forward primer (5'-CACCATGGTCGAAACAACGTCG-3'), containing the CACC Kozak sequence at the 5' side to facilitate translation in mammalian cells (Kozak, 1986), and a specific reverse primer (5'-TTAGACGCCGGTGTGGTTGAA-3') are used. According to the manufacturer's protocol the final

concentration of the primers is 500 nM. The following PCR program is used: an initial denaturation of 98 °C followed by 29 cycles of 98 °C for 15 s for denaturation, an annealing step of 30 seconds at 65 °C and an elongation at 72 °C for 100 s. After a final elongation at 72 °C for 2 min the program is paused at 10 °C.

The size of the PCR product is analyzed on a 1 % agarose gel. Fragments of the expected length are cut out of the gel and purified using the GenElute Gel extraction Kit (Sigma-Aldrich). After addition of a 3'-A overhang using the RedTaq DNA polymerase (Sigma-Aldrich) by heating 15 µl RedTaq mixed with 5 µl gel extract at 72°C during 15 min, the sequence is cloned into a pcDNA 3.1/V5-His TOPO vector (Invitrogen) following the manufacturer's instructions as described in section 2.5. The vector is transformed into DH5α cells and grown on LB agar plates (35 g/l; Sigma-Aldrich) with ampicillin (10 mg/ml; Invitrogen). Colonies with an insert are collected and grown in 5 ml LB medium (Sigma-Aldrich) with ampicillin (10 mg/ml). Plasmid purification is performed using the GenElute Plasmid Miniprep Kit (Sigma-Aldrich) and sequencing is performed at LGC Genomics (Germany) using the T7 and BGH primers. Bacterial cells known to contain the correct receptor insert in the right direction are grown at large scale in 100 ml Luria-Bertani Broth medium. The expression vector is subsequently isolated from these cells using the EndoFree Plasmid Purification Kit (Qiagen) and sequenced once again.

3.2.8. Analysis of the downstream signaling properties of the *Bomte*-SIFR using the aequorin bioluminescence assay and the CRE-dependent luciferase reporter assay

Chinese hamster ovary (CHO-WTA and CHO-PAM28) and human embryonic kidney (HEK293) cells are transfected with pcDNA3.1-*Bomte*-SIFR in order to analyze the effect of the receptor on the intracellular Ca^{2+} and cAMP levels after activation with the endogenous peptide *Bomte*-SIFa [(AYRKPPFNGSIF-NH_2; ordered from GL Biochem (Shanghai, China)]. For each cell line, two independent transfections are carried out and the luminescence is measured in triplicate per transfection per concentration of peptide. An additional transfection with empty pcDNA3.1 vector is carried out in each cell line to confirm that the response of the cells is evoked by stimulation of *Bomte*-SIFR and not by any other endogenous receptor.

3.2.8.1. Aequorin bioluminescence assay in CHO cells

Cell culture and transfections of CHO-WTA11 and CHO-PAM28, and how this assay is performed is described in section 2.7. A dilution series (1 fM - 10 µM) of *Bomte*-SIFa is tested.

3.2.8.2. CRE-dependent luciferase reporter assay in HEK293 cells

Cell culture and transfections of HEK293 cells, and how this assay is performed is described in section 2.8. A dilution series (0.01 pM - 10 µM) of *Bomte*-SIFa is tested.

3.2.9. CAMYEL biosensor

Cell culture, transfections and the procedure of this assay are described in section 2.9. Measurements are made in duplicate per concentration of *Bomte*-SIFa (0.10 nM - 1 µM) in two independent transfections for both the experimental condition (with *Bomte*-SIFR) and the control (without *Bomte*-SIFR) in both the presence and absence of forskolin.

3.2.10. BRET^2-based G protein assay to study the G protein mediated pathways of *Bomte*-SIFR

Cell culture, transfections and the procedure of this assay are described in section 2.10. In the first experiment only one concentration of *Bomte*-SIFa (1 µM) is tested whereas in the second experiment multiple concentrations (0.1 nM – 1 µM) of *Bomte*-SIFa are applied.

3.2.11. Agonistic signaling properties of *Bomte*-SIFa and related peptides at *Bomte*-SIFR

To test the pharmacological signaling properties of the *Bomte*-SIFR, three series of peptides are ordered. The first peptide series (1), the alanine series of *Bomte*-SIFa, is ordered from GL Biochem (Shanghai, China) and consists of a series of peptides whereby each amino acid is systematically replaced by an alanine. For instance, Y_2 refers to the peptide wherein the second amino acid is replaced by an alanine (AARKPPFNGSIF-NH_2). The second series (2) consists of truncated (TR) SIFa peptides and the last series of peptides (3) consists of other insect SIFa peptides, namely [G_1]-SIFa as found in *A. aegypti* and [T_1]-SIFa as found in *B. mori*, and other related Hymenopteran neuropeptides. According to Hauser and co-workers (2006), sulfakinin (SK), kinin (K) and short neuropeptide F (sNPF) are related to SIFa. Therefore, *Apime*-SK-I, *Apime*-sNPF and *Bomte*-K-I and *Bomte*-K-II are ordered. The second and third series of peptides are purchased from Synpeptide (Shanghai, China). The sequences of the three peptides series and the abbreviations used in this study are enlisted in table 3.3 in section 3.3.10 on page 82.

The agonistic signaling properties of these peptides are tested in *Bomte*-SIFR-expressing CHO-WTA11 cells. The calcium reporter assay is executed as described in section 2.7, whereby the luminescence is measured in duplicate per concentration per peptide. The endogenous *Bomte*-SIFa is included in each assay as a reference.

3.3. Results

3.3.1. Precursor sequence analysis

The *Bomte*-SIFa precursor sequence contains a 23 amino acid signal peptide (predicted by SignalP 4.1; Petersen et al., 2011) immediately followed by the SIFa sequence (Fig. 3.1.). The SIFa sequence is followed by a G-residue which is a substrate for peptidyl amidating monooxygenase (PAM) resulting in an amidated neuropeptide (Rouillé et al., 1995; Veenstra, 2000). This G-residue is immediately followed by a dibasic (KR) recognition site for proteolytic processing of the pro-peptide.

In contrast to *B. mori* (Roller et al., 2008), no related SIFa paralogue containing an IMFa sequence could be identified using the BLAST tool on BeeBase.org (Priyam et al., 2015; Sadd et al., 2015) in the *Bomte*-SIFa precursor nor in the genome database. The obtained nucleotide sequence of the *Bomte*-SIFa precursor and the sequence of the *Bomte*-SIFR can be found in the European Bioinformatics Institute (EBI) database (*Bomte*-SIFa: GenBank accession no. XP_012170751.1; *Bomte*-SIFR: GenBank accession no. XP_003401591.1).

ATG	ATG	TCC	TCC	CGC	TTC	GTT	GTT	GCC	ATC	GTC	GTT	GCC	CTC	TTC
M	M	S	S	R	F	V	V	A	I	V	V	A	L	F
ATC	CTC	GCC	ATC	GCC	GTG	GAT	GCC	GCC	TAC	AGG	AAG	CCT	CCC	TTC
I	K	A	I	A	V	D	A	A	Y	R	K	P	P	F
AAC	GGA	AGC	ATC	TTC	GGC	AAG	CGA	TCC	AAC	GCT	ATC	ACT	GAT	TAC
N	G	S	I	F	G	K	R	S	N	A	I	T	D	Y
GAA	CTC	ACC	AGC	CGA	GCC	ATG	TCA	TCG	GTC	TGC	GAA	ACC	GTC	AGC
E	L	T	S	R	A	M	S	S	V	C	E	T	V	S
GAA	ACA	TGC	AAC	GCC	TGG	TTG	GCA	CGT	CAG	GAC	TCC	AAC	TAA	
E	T	C	N	A	W	L	A	R	Q	D	S	N	STOP	

Figure 3.1: Precursor sequence of *Bomte*-SIFa. The sequence of SIFamide is highlighted in green. The predicted signal peptide sequence is shown in orange and the recognition sites for proteolytic processing of the pro-peptide are depicted in blue. The G-residue predicted to be transformed into the C-terminal amide by PAM is highlighted in yellow.

3.3.2. SIFa peptide sequence analysis in arthropods

The WebLogo created using all identified and *in silico* predicted insect SIFa amino acid sequences, is depicted in Fig. 3.2. Whereas the sequence of *S. gregaria* contains fifteen amino acids, most SIFa peptides usually consist of twelve amino acids. Therefore, only the fourth amino acid in this WebLogo is the usual first amino acid of most SIFa's. The WebLogo and table 3.1 clearly show that, in contrast to the four N-terminal amino acids, the last eight amino acids are strongly conserved among insects. In general, it appears that three types of SIFa exist among insects; namely [A_1]-SIFa as in *B. terrestris*, [G_1]-SIFa as in *A. aegypti* and [T_1]-SIFa as in *B. mori*.

Figure 3.2: WebLogo of SIFamide peptides in insects. The C-terminal end is amidated in all known insect sequences.

As shown in table 3.1, SIFa generally consists of twelve amino acids in crustaceans and the [G_1]-SIFa isoform is broadly conserved (Stemmler et al., 2007). In contrast to insects, the [A_1]-SIFa nor the [T_1]-SIFa isoforms are found in this subphylum and more variation exists in terms of amino acid length and sequence compared to SIFa in insects. The C-terminal end of all identified SIFa's in arthropod species is amidated.

3.3.3. Sequence analysis of the G protein subunits of B. terrestris.

By means of a BLAST analysis on BeeBase.org scanning the *B. terrestris* genome database (Priyam et al., 2015; Sadd et al., 2015) amino acid sequences of five Gα, two Gβ and two Gγ subunits are identified. All sequences are confirmed to be G protein subunits by the online tool GprotPRED (http://aias.biol.uoa.gr/GprotPRED/). Two of these sequences are a assigned to the $G\alpha_{i/o}$ subfamily; namely *Bomte*-$G\alpha_i$ (Genbank accession number XP_003393073.1) and *Bomte*-$G\alpha_o$ (Genbank accession number XP_003401632.1), one sequence is assigned to the $G\alpha_s$ subfamily; namely *Bomte*-$G\alpha_s$ (Genbank accession number XP_012174114.1), one sequence is assigned to the $G\alpha_{q/11}$ subfamily; namely *Bomte*-$G\alpha_q$ (Genbank accession number XP_012174289.1) and one sequence is assigned to the $G\alpha_{12/13}$ subfamily; namely *Bomte*-$G\alpha_{12/13}$ (Genbank accession number XP_003402502.1). The other identified G protein subunits are *Bomte*-$G\beta_1$ (Genbank accession number XP_003400659.1), *Bomte*-$G\beta_2$ (Genbank accession number XP_012165841.1), *Bomte*-$G\gamma_1$ (Genbank accession number XP_003402137.1) and *Bomte*-$G\gamma_e$ (Genbank accession number XP_003400491.1). A multiple sequence alignment (supplementary Fig. S1-S7) and a percent identity matrix (supplementary tables S1-S7) are constructed comparing the G protein subunit sequences of *B. terrestris* and the sequences of the *H. sapiens* G protein subunits used to construct the $BRET^2$-based G protein biosensors for $G\alpha_i$, $G\alpha_o$, $G\alpha_s$, $G\alpha_{q/11}$, $G\alpha_{12/13}$, Gβ and Gγ. For additional analyses in chapters 4 and 6, the G protein subunit sequences of *S. gregaria*, are added.

Amino acid sequences of the $G\alpha_i$, $G\alpha_o$ $G\alpha_s$ and $G\alpha_{q/11}$ subunits are very similar. *Bomte*-$G\alpha_i$ shows a sequence identity of 81 % with *Homsa*-$G\alpha_{i1}$, 80 % with *Homsa*-$G\alpha_{i2}$, 79 % with *Homsa*-$G\alpha_{i3}$ and 90 %

with *Schgr*-$G\alpha_i$ (supplementary Fig. S1 and supplementary table S1) while *Bomte*-$G\alpha_o$ shows a sequence identity of 82 % with both *Homsa*-$G\alpha_{oa}$ and *Homsa*-$G\alpha_{ob}$ and 96 % with *Schgr*-$G\alpha_o$ (supplementary Fig. S2 and supplementary table S2). *Bomte*-$G\alpha_s$ shows a sequence identity of 74 % with *Homsa*-$G\alpha_s$ and 83 % with *Schgr*-$G\alpha_s$ (supplementary Fig. S3 and supplementary table S3), and *Bomte*-$G\alpha_q$ shows a sequence identity of 79 % with *Homsa*-$G\alpha_q$, 77 % with *Homsa*-$G\alpha_{11}$ and 94 % with *Schgr*-$G\alpha_q$ (supplementary Fig. S4 and supplementary table S4). Compared to the other Gα protein sequences, the sequences of the $G\alpha_{12/13}$ subfamily are much less conserved. *Bomte*-$G\alpha_{12/13}$ shows a sequence identity of nearly 58 % with both *Homsa*-$G\alpha_{12}$ and *Homsa*-$G\alpha_1$ whereas a sequence identity of 80 % is detected with *Schgr*-$G\alpha_{12/13}$ (supplementary Fig. S5 and supplementary table S5).

Additionally, amino acid sequences of both Gβ and Gγ are compared. *Bomte*-$G\beta_1$ shows a sequence identity of 86 % with *Homsa*-$G\beta_1$, 52 % with *Bomte*-$G\beta_2$, 95 % with *Schgr*-$G\beta_1$ and 53 % with *Schgr*-$G\beta_2$, while *Bomte*-$G\beta_2$ shows a sequence identity of 51 % with *Homsa*-$G\beta_1$, 51 % with *Schgr*-$G\beta_1$, and 84 % with *Schgr*-$G\beta_2$ (supplementary Fig. S6 and supplementary table S6). These data suggest that *Bomte*-$G\beta_1$ and *Schgr*-$G\beta_1$ are more related to the *Homsa*-$G\beta_1$ sequence of the $BRET^2$-based biosensor. Finally, the Gγ amino acid sequence is much shorter than the Gα and Gβ subunit sequences. *Bomte*-γ_1 shows a sequence identity of 42 % with *Homsa*-$G\gamma_2$, 28 % with *Bomte*-$G\gamma_e$, 73 % with *Schgr*-$G\gamma_1$ and 26 % *Schgr*-$G\gamma_2$ while *Bomte*-$G\gamma_e$ shows a sequence identity of 34 % with *Homsa*-$G\gamma_2$, 19 % with *Schgr*-$G\gamma_1$ and 92 % with *Schgr*-$G\gamma_2$ (supplementary Fig. S7 and supplementary table S7). These data suggest that *Bomte*-γ_1 and *Schgr*-$G\gamma_1$ on one hand and *Bomte*-$G\gamma_e$ and *Schgr*-$G\gamma_2$ on the other hand are orthologous Gγ subunits, whereas both Gγ orthologues do not show high sequence identity with *Homsa*-$G\gamma_2$ that is incorporated in the $G\gamma_2$-GFP10 $BRET^2$-based biosensor of the $BRET^2$-based G protein assay.

3.3.4. Multiple sequence alignment of the SIFR

In Fig. 3.3 the multiple sequence alignment of the protein sequences *Homsa*-NPFFR1, *Homsa*-NPFFR2, *Ixosc*-SIFR, *Bomte*-SIFR and *Drome*-SIFR is depicted. The sequences consist of seven transmembrane domains (TM), three extracellular loops (EL), three intracellular loops (IL), an extracellular N-terminal and an intracellular C-terminal. Conserved cysteine residues to form disulfide bridges between EL1 and EL2 are indicated. The alignment shows that the sequence is highly conserved, especially in the 7TM regions and the C-terminus. From TM1 to TM7 the *Bomte*-SIFR shows a sequence identity of 34 % with *Homsa*-NPFFR1, 35 % with *Homsa*-NPFFR2, 60 % with *Ixosc*-SIFR and 73 % with *Drome*-SIFR. Amino acid residues that are conserved among rhodopsin-like GPCRs (Family A GPCRs) are also indicated (Gether, 2000; Hauser and Grimmelikhuijzen, 2014; Schiöth and Lagerström, 2008; Venkatakrishnan et al., 2013). The *Drome*-SIFR has extended N- and C-termini compared to the human NPFFRs and other arthropod SIFRs. The TM3 of the SIFR is immediately followed by a DRF motif in insects and a DRC motif in *I. scapularis* instead of the usual DRY motif found in Family A GPCRs, whereby the Arg usually interacts with the C-terminus of the G protein (Gether, 2000; Venkatakrishnan et al., 2013). *Homsa*-NPFFR1 contains an ERF motif in contrast to the *Homsa*-NPFFR2 that contains a DRF motif similarly to the insect SIFRs.

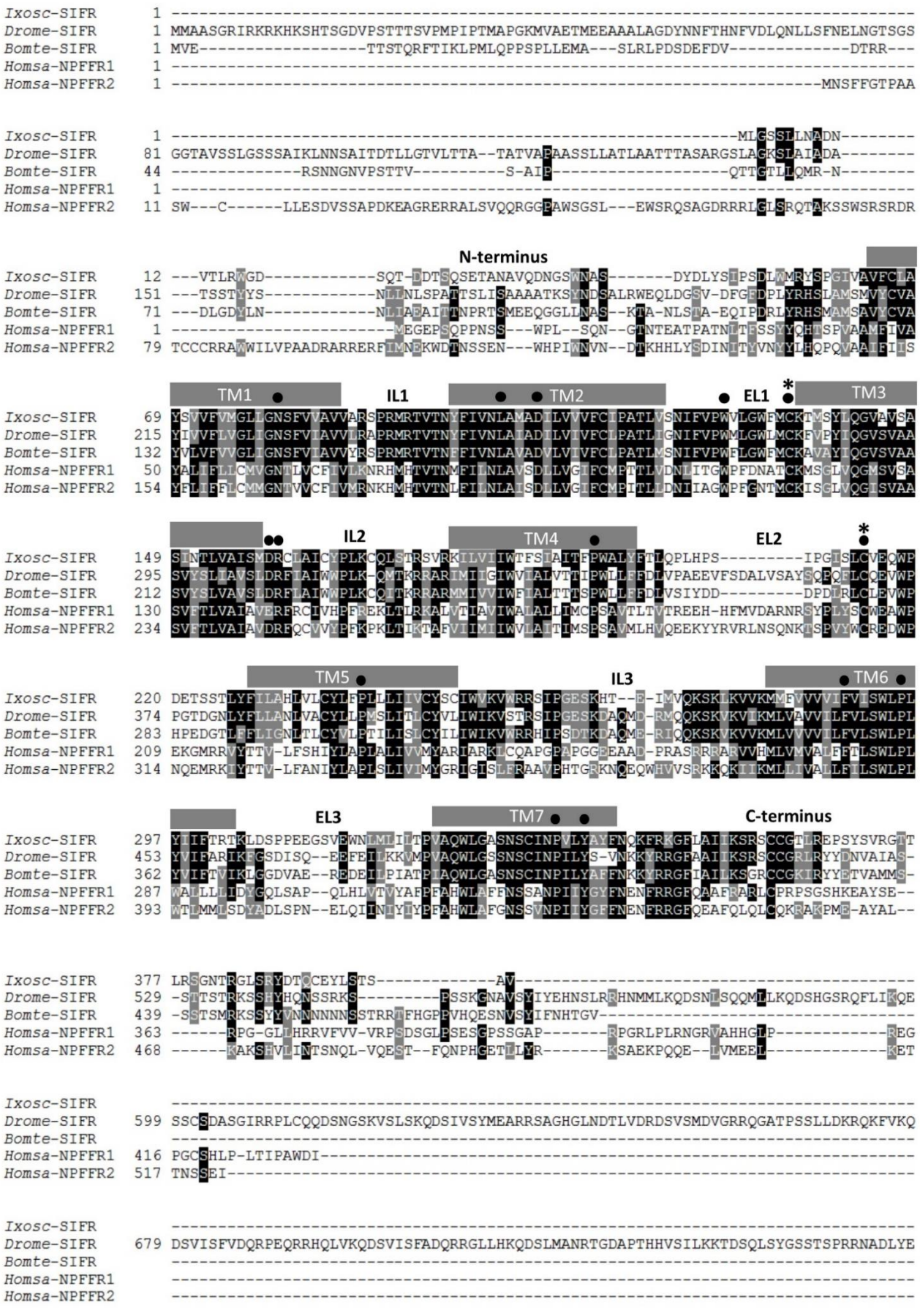
Ixosc-SIFR
Drome-SIFR
Bomte-SIFR
Homsa-NPFFR1
Homsa-NPFFR2
N-terminus
TM1
IL1
TM2
EL1
TM3
IL2
TM4
EL2
TM5
IL3
TM6
EL3
TM7
C-terminus

↑ **Figure 3.3: Multiple sequence alignment** of human NPFFR1 (*Homsa*-NPFFR1; GenBank accession number. NP_071429.1), human NPFFR2 (*Homsa*-NPFFR2; GenBank accession number. NP_004876.2), *Ixodes scapularis* SIFR (*Ixosc*-SIFR; GenBank accession number KC422392), *Bombus terrestris* SIFR (*Bomte*-SIFR; GenBank accession number XP_003401591.1) and *Drosophila melanogaster* SIFR (*Drome*-SIFR; GenBank accession number NP_650966.2). Identical residues between the aligned sequences are highlighted in black, and conservatively substituted residues in grey. Dashes indicate gaps that are introduced to maximize similarities in the alignment. Putative transmembrane regions are indicated by grey bars. Amino acids usually conserved in rhodopsin-like GPCRs are labeled (●) (Gether, 2000; Hauser and Grimmelikhuijzen, 2014; Schiöth and Lagerström, 2008; Venkatakrishnan et al., 2013) and conserved cysteine residues that are predicted to form disulfide bridges in extracellular loop (EL) 1 and EL2 are also indicated (*). The intracellular loops (IL), the N-terminus and the C-terminus of the receptors are indicated as well.

3.3.5. Relative transcript levels of the *Bomte*-SIFa precursor and the *Bomte*-SIFR

The expression of *Bomte*-SIFa is largely restricted to the brain as depicted in (Fig. 3.4A). *Bomte*-SIFR is mainly expressed in the CNS (Br and VNC) and the fat body (FB) (Fig. 3.4B). Lower transcript levels are detected in the testes (Tes), accessory glands (AG) and foregut (FG). Analysis of the dissociation curves of the different amplification products reveal a single melting peak.

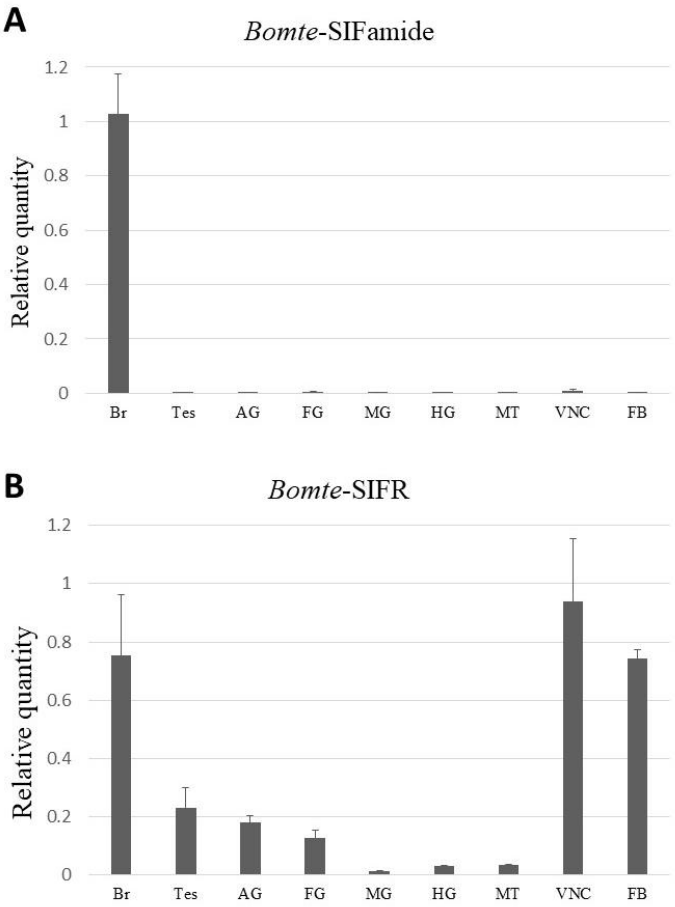

Figure 3.4: Graphic representation of the relative transcript levels of (A) the *Bomte*-SIFa precursor and (B) the *Bomte*-SIFR measured in different tissues dissected from adult male *B. terrestris*. The data represent mean values ± S.E.M. of three independent tissue samples run in duplicate, normalized relative to the reference genes EF1α, GADPH and RPL13. Abbreviations used: Br = brain, Tes = Testes, AG = accessory glands, FG = foregut, MG = midgut, HG = hindgut, MT= Malpighian tubules, VN = ventral nerve cord, FB = Fat body.

3.3.6. Mass spectrometry analysis of SIFa in *B. terrestris*

In Fig. 3.5 the fragmentation table of *Bomte*-SIFa measured by the Q Exactive Orbitrap mass spectrometer is depicted. The full *Bomte*-SIFa (AYRKPPFNGSIF-NH_2) is detected in the sample, but not any shorter form of SIFa.

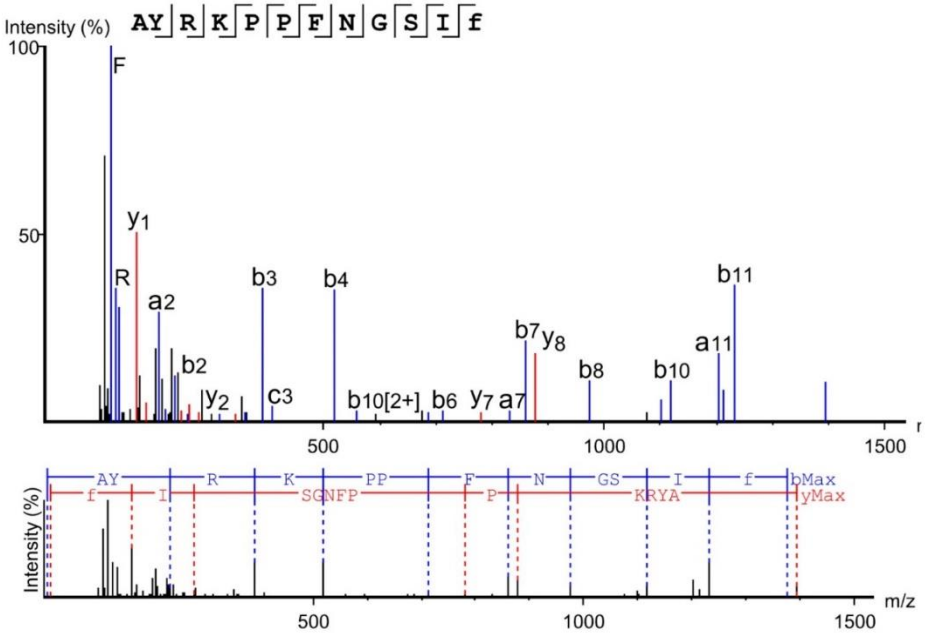

Figure 3.5: Fragmentation table of *Bomte*-SIFa. N-terminal ions are depicted in blue and C-terminal ions are depicted in red.

3.3.7. Downstream signaling properties of the *Bomte*-SIFR using the aequorin bioluminescence assay and the CRE-dependent luciferase reporter assay

*3.3.7.1. Aequorin bioluminescence assay in CHO cells after activation with endogenous Bomte-*SIFa

Stimulation of CHO-WTA11-*Bomte*-SIFR cells by *Bomte*-SIFa results in a sigmoidal dose-dependent response curve with an EC_{50} value in the low nanomolar range (0.15 nM; Fig. 3.6A). Additionally, also in the CHO-PAM28-*Bomte*-SIFR cells a sigmoidal dose-dependent response curve is obtained upon stimulation of *Bomte*-SIFa with an EC_{50} value in the low nanomolar range (0.06 nM; Fig. 3.6B), which indicates that the receptor can induce an increase in Ca^{2+} levels upon receptor activation by natural preference. Both CHO-WTA11 and CHO-PAM28 cells transfected with empty pcDNA3.1 vector did not respond to *Bomte*-SIFa (results not shown).

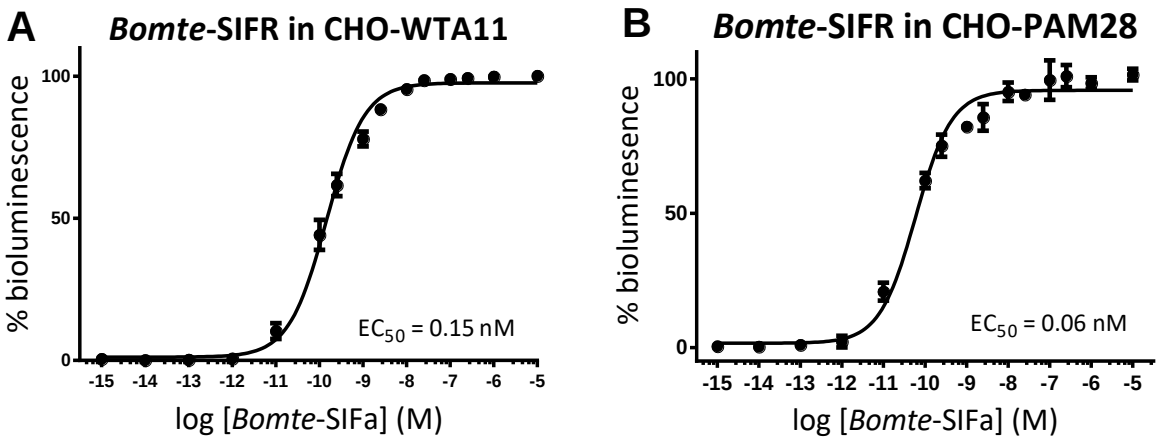

Figure 3.6: Dose-response curve of bioluminescent responses induced in **(A)** CHO-WTA11-*Bomte*-SIFR cells and **(B)** CHO-PAM28-*Bomte*-SIFR cells. The aequorin bioluminescence assay is executed in two independent transfections. The bioluminescence is measured in triplicate per concentration of *Bomte*-SIFa per transfection. Error bars represent the S.E.M. The 100 % level refers to the maximal response level and the zero-response level corresponds to treatment with BSA medium only. In addition, the EC_{50} values are indicated.

3.3.7.2. CRE-dependent luciferase reporter assay in HEK293 cells

Stimulation of co-transfected HEK293-*Bomte*-SIFR cells by *Bomte*-SIFa results in a sigmoidal dose-dependent increase in luciferase reporter activity with an EC_{50} value in the nanomolar range (3.48 nM; Fig.3.7). However, in the experiment wherein bioluminescence is measured upon stimulation of *Bomte*-SIFa in the presence of forskolin, no decrease in luciferase reporter activity can be observed (results not shown). These data suggest that stimulation of *Bomte*-SIFR by *Bomte*-SIFa results in an increase in intracellular cAMP levels.

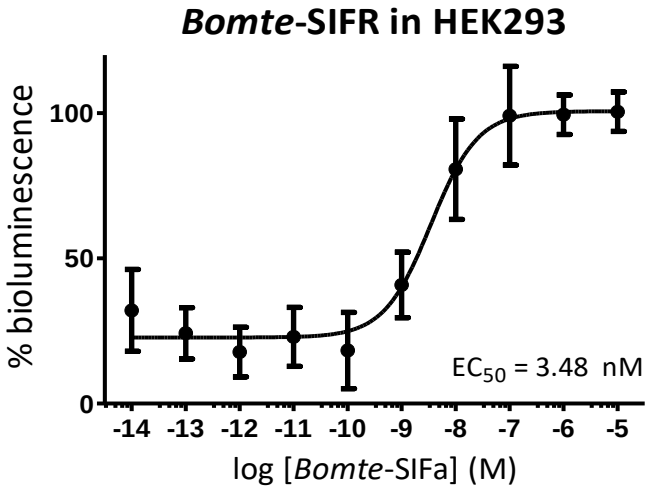

Figure 3.7: Bioluminescent responses induced in HEK293-*Bomte*-SIFR co-transfected with the $CRE_{(6x)}$-Luc construct. This CRE-dependent luciferase reporter assay is performed in two transfections. The bioluminescence is measured in triplicate per concentration of *Bomte*-SIFa per transfection. Error bars represent the S.E.M. The zero level corresponds to treatment with DMEM/F-12/IBMX and the 100 % level refers to the maximal response. The EC_{50} value is indicated.

3.3.8. The CAMYEL biosensor

In the first experiment (Fig. 3.8, left), no decrease in BRET^1 signal is detected when cells are transfected with *Bomte*-SIFR. However, a small decrease in BRET^1 signal is observed in the control cells. In the second experiment (Fig. 3.8, right) no increase in BRET^1 signal is detected. However, since control cells seem to respond to *Bomte*-SIFa, we cannot make conclusions from these results.

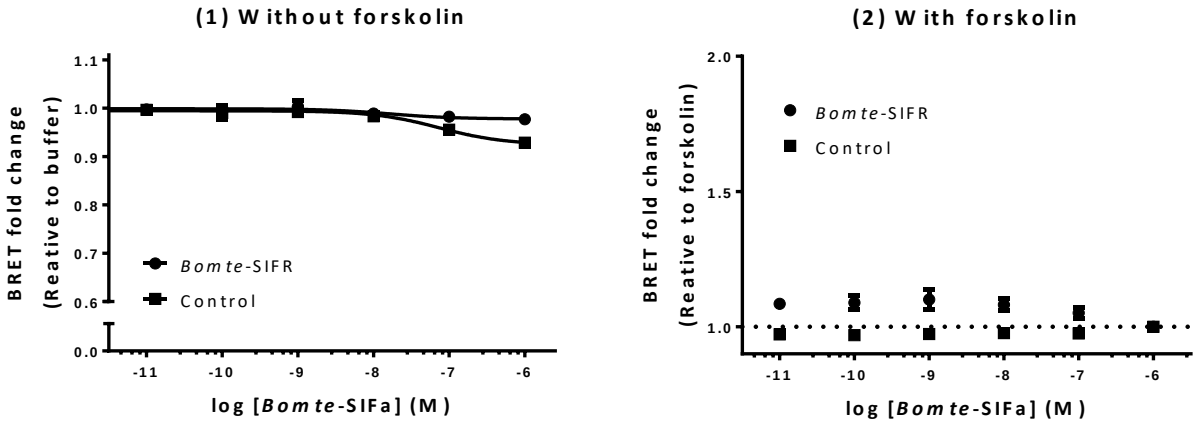

Figure 3.8: Results of CAMYEL biosensor: BRET^1 measured in HEK293T cells transfected with *Bomte*-SIFR (●) or without *Bomte*-SIFR [control (■)] in two independent transfections. Measurements are taken in duplicate for each concentration of *Bomte*-SIFa (10 pM - 1 µM). **Left**: measurements are taken in the absence of forskoline. Data (± S.E.M) are presented relative to the baseline (buffer only). **Right**: measurements are taken in the presence of forskolin. Data (± S.E.M) are presented relative to the baseline (buffer with forskolin). The dotted line represents the baseline.

3.3.9. Measuring a direct activation of various G proteins by using BRET^2-based G protein biosensors

The ΔBRET^2 signal of the HEK293T-*Bomte*-SIFR is significantly lower than the control cells upon addition of 1 µM *Bomte*-SIFa for all five biosensors of the $G\alpha_{i/o}$ subfamily (Fig. 3.9, left). Moreover, the ΔBRET^2 signal of $G\alpha_{i2}$, $G\alpha_{i3}$, $G\alpha_{oa}$ and $G\alpha_{ob}$ are dose-dependent with an EC_{50} value in the high nanomolar range (Fig. 3.10) indicating that these biosensors are activated upon receptor activation. For the $G\alpha_{i1}$ biosensor a dose-dependent trend is observed although the ΔBRET^2 signal is also lower using a concentration of 0.10 nM *Bomte*-SIFa. The magnitude of the ΔBRET^2 signals, except for $G\alpha_{i1}$, are comparable to those detected with the *H. sapiens* chemokine receptor (*Homsa*-CCR2) known to couple to $G\alpha_{i/o}$ proteins (Fig 3.9, right; Corbisier et al., 2015).

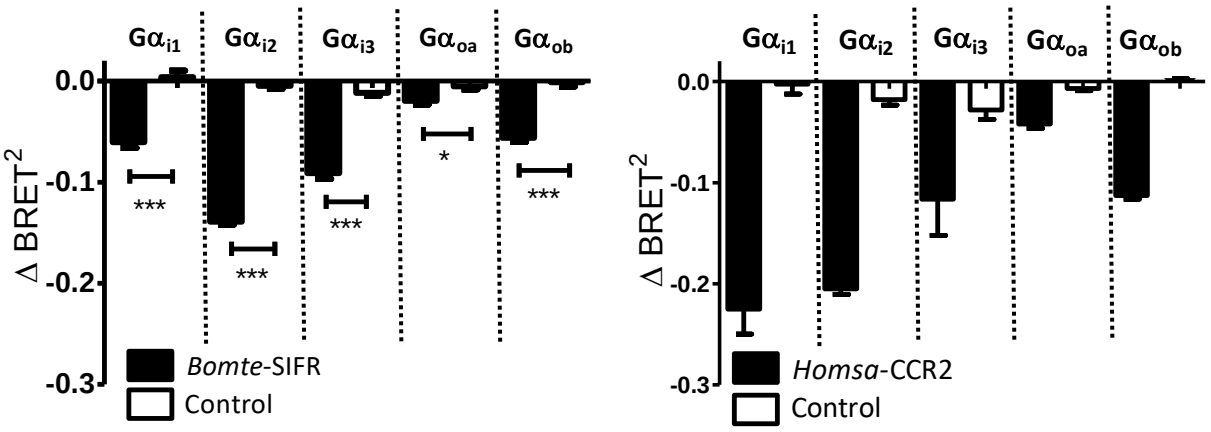

Figure 3.9: Summary of the results of the $G\alpha_{i/o}$ subfamily $BRET^2$-based G protein biosensors. On the **left** the results of HEK293T-*Bomte*-SIFR cells (*Bomte*-SIFR) and HEK293T cells (control) co-transfected with the $G\alpha_{i1}$, $G\alpha_{i2}$, $G\alpha_{i3}$, $G\alpha_{oa}$ or $G\alpha_{ob}$ biosensor upon stimulation of 1 µM *Bomte*-SIFa. The data represent the means ± S.E.M of $\Delta BRET^2$ measured in triplicate in two independent transfections. Significant differences ($p < 0.05$, $p < 0.001$) are indicated by asterisks (* and *** respectively) (student's t-test per $G\alpha_{i/o}$ biosensor). On the **right** the results of the *H. sapiens* chemokine receptor (*Homsa*-CCR2) are depicted (Corbisier et al., 2015). The dotted lines segregate the results per $G\alpha_{i/o}$ biosensor.

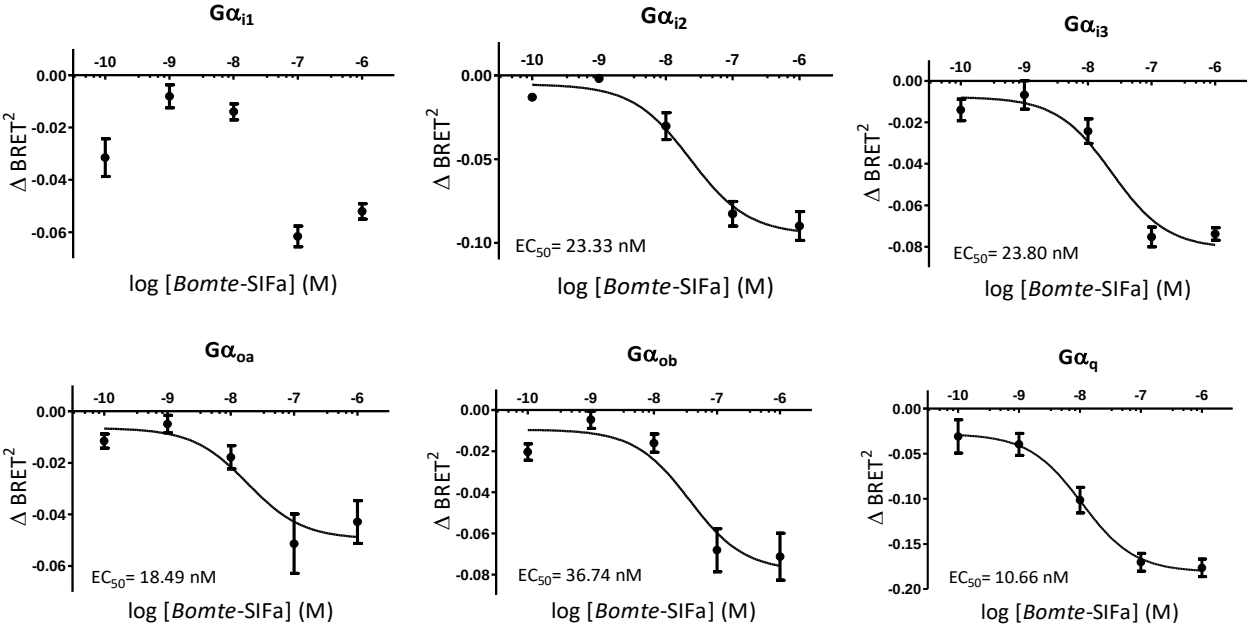

Figure 3.10: Dose-dependent responses in HEK293T-*Bomte*-SIFR cells co-transfected with $BRET^2$-based G protein biosensors consisting of $G\beta_1$, $G\gamma_2$-GFP10 and several Gα subunits upon stimulation of 0.10 nM – 1 µM *Bomte*-SIFa. The data represent the means ± S.E.M of three independent transfections measured in duplicate per concentration. The EC_{50} value is indicated in case a dose-dependent reaction is observed.

For the $G\alpha_s$ biosensor, the only biosensor of the $G\alpha_s$ subfamily that is tested, no activation is observed (Fig. 3.11). When comparing the magnitude of the $\Delta BRET^2$ signal with the magnitude of the $\Delta BRET^2$ signal detected with the *H. sapiens* β2-adrenergic receptor (*Homsa*-β2-AR; Fig. 3.11, right; Saulière et al., 2012), a receptor known to couple to the $G\alpha_s$ protein, no decrease in $\Delta BRET^2$ signal is detected upon stimulation of HEK293T-*Bomte*-SIFR with *Bomte*-SIFa.

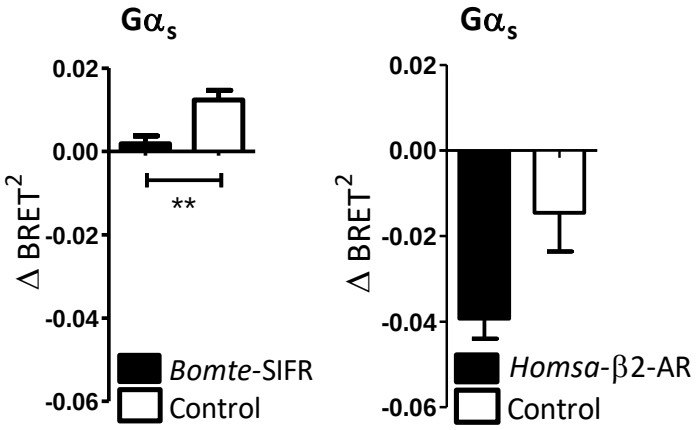

Figure 3.11: Results of the $G\alpha_s$ subfamily $BRET^2$-based G protein biosensors. On the **left** the results of HEK293T-*Bomte*-SIFR and HEK293T cells (control) co-transfected with the $G\alpha_s$ biosensor upon stimulation of 1 µM *Bomte*-SIFa. The data represent the means ± S.E.M of $\Delta BRET^2$ measured in triplicate in two independent transfections. Significant differences ($p < 0.01$) are indicated by asterisks (**) (student's t-test). On the **right** the results of the *H. sapiens* β2-adrenergic receptor (*Homsa*-β2-AR) are depicted (Saulière et al., 2012).

HEK293T-*Bomte*-SIFR cells transfected with G protein biosensors of the $G\alpha_{q/11}$ subfamily only shows a significant reduction in $\Delta BRET^2$ signal compared to the control cells when the cells are transfected with the $G\alpha_q$ biosensor, but not with the $G\alpha_{11}$ biosensor (Fig. 3.12, A). However, the magnitude of the $\Delta BRET^2$ signal is not in the same range as detected with the *H. sapiens* angiotensin II type 1 receptor (*Homsa*-AT1R; Fig. 3.12, B; Saulière et al., 2012) a receptor known to couple to $G\alpha_{q/11}$ proteins. The decrease in $\Delta BRET^2$ signal in cells transfected with the $G\alpha_q$ biosensor is dose-dependent (Fig. 3.10) which infers that this biosensor is activated upon activation of *Bomte*-SIFR.

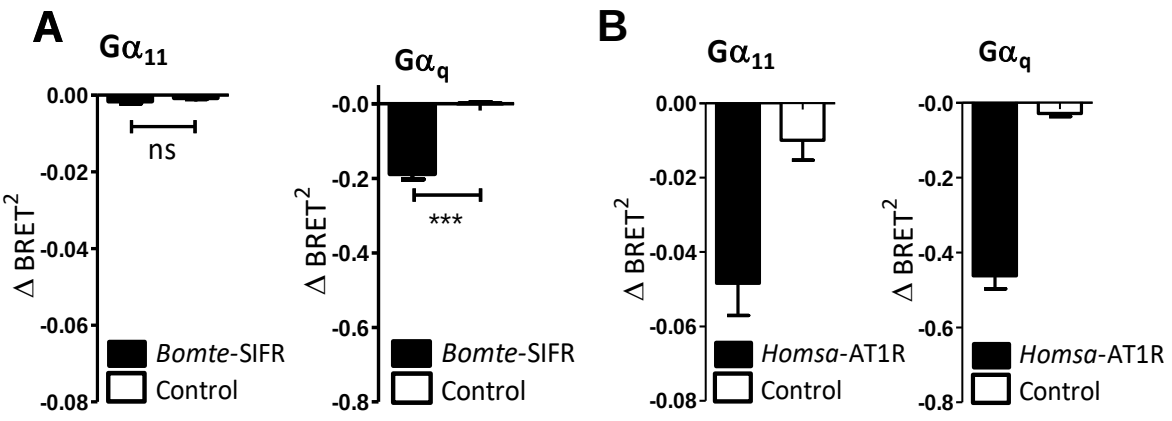

Figure 3.12: Results of the $G\alpha_{q/11}$ subfamily $BRET^2$-based G protein biosensors. (**A)** Results of HEK293T-*Bomte*-SIFR and HEK293T cells (control) co-transfected with the $G\alpha_{11}$ biosensor (left) or the $G\alpha_q$ biosensor (right) upon stimulation of 1 µM *Bomte*-SIFa. The data represent the means ± S.E.M of $\Delta BRET^2$ measured in triplicate in two independent transfections. Significant differences ($p < 0.001$) are indicated by asterisks (***) (student's t-test). **(B)** Results of the *H. sapiens* angiotensin II type 1 receptor (*Homsa*-AT1R) (Saulière et al., 2012).

Finally, neither HEK293T-*Bomte*-SIFR cells transfected with one of the two Gα biosensors of the $G\alpha_{12/13}$ subfamily shows a significant reduction in $\Delta BRET^2$ signal upon addition of *Bomte*-SIFa (Fig. 3.13, A). The results of the $G\alpha_{12/13}$ are compared to the results of the *H. sapiens* thromboxane receptor (*Homsa*-TPα-R; Fig 3.13, B; Saulière et al., 2012), a receptor know to activate $G\alpha_{12/13}$ proteins.

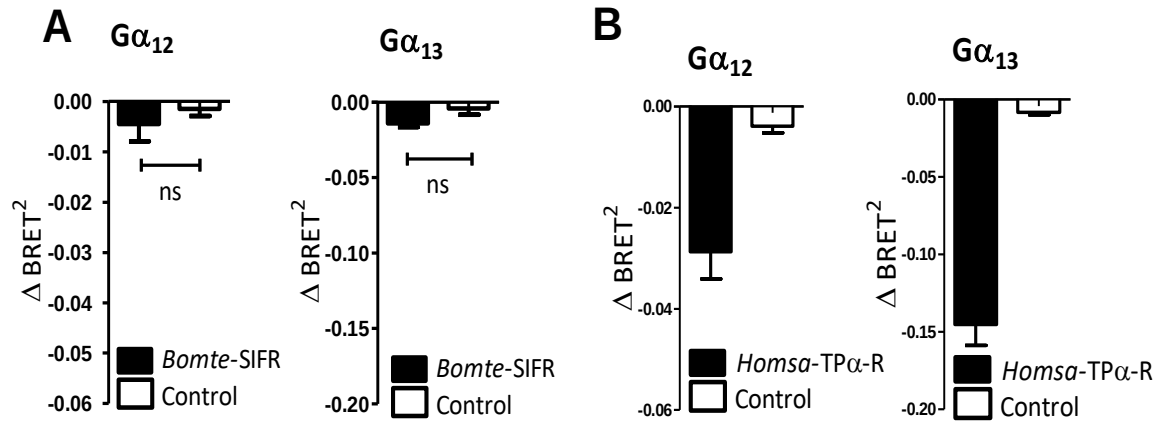

Figure 3.13: Results of the $G\alpha_{12/13}$ subfamily $BRET^2$-based G protein biosensors. (**A)** Results of HEK293T-*Bomte*-SIFR and HEK293T cells (control) co-transfected with the $G\alpha_{12}$ biosensor (left) or the $G\alpha_{13}$ biosensor (right) upon stimulation of 1 µM *Bomte*-SIFa. The data represent the means ± S.E.M of $\Delta BRET^2$ measured in triplicate in two independent transfections. **(B)** Results of the *H. sapiens* thromboxane TPα receptor (*Homsa*-TPα-R) (Saulière et al., 2012).

3.3.10. Agonistic properties of SIFa analogues at *Bomte*-SIFR

Stimulation of CHO-WTA11-*Bomte*-SIFR cells results in a sigmoidal dose-dependent response for most of the peptides from the alanine series (1). The dose-dependent response curves of this peptide series evoked by 0.1 pM – 100 nM peptide are depicted in supplementary Fig. S8. An overview of the full sequence of the peptides, their abbreviation used in this study and the EC_{50} values measured in CHO-WTA11-*Bomte*-SIFR are enlisted in table 3.3. In Fig. 3.14 the bioluminescence evoked by peptide concentrations 1 nM and 100 nM are presented. Replacing the last phenylalanine (F_{12}) with an alanine completely abolished the activation of the receptor. Additionally, also phenylalanine (F_7), asparagine (N_8), glycine (G_9), serine (S_{10}) and especially isoleucine (I_{11}) are crucial for a good activation of the receptor. Replacing the amino acid residues in the N-terminus with an alanine barely affected the receptor response to the ligand. Notably, the N-terminal amino acid alanine is not replaced in this assay since this already is an alanine.

Activation of the CHO-WTA11-*Bomte*-SIFR cells by the truncated (Tr-)SIFa peptide series (2) is measured using several concentrations (0.01 nM - 1 µM) of peptide. The sequence of these peptides and the measured EC_{50} values can be found in table 3.3 and the dose-response curves are depicted in supplementary Fig. S9. In Fig. 3.15 the results of the peptide concentrations 1 µM, 10 nM and 0.1 nM are depicted. Removal of six amino acids at the N-terminus of *Bomte*-SIFa did not result in a drastically reduced receptor activation. Tr-$SIFa_6$, Tr-$SIFa_5$ and Tr-$SIFa_4$ only activate the receptor when 1 µM is added to stimulate the receptor, which is considered a non-physiological concentration. Therefore, the six C-terminal amino acids seem to constitute an active core region in the *Bomte*-SIFa peptide.

Finally, we also tested if the receptor could be activated by [G_1]-SIFa (*Aedae*-SIFa), [T_1]-SIFa (*Bommo*-SIFa) and related Hymenopteran peptides. The sequences of these peptides using several concentrations of peptide (1 µM – 1 pM) and their corresponding EC_{50} values measured in CHO-WTA11-*Bomte*-SIFR cells can be found in table 3.3. The obtained dose-response curves are depicted in supplementary Fig. S10. In Fig. 3.16 the results of the peptide concentrations 1 µM, 10 nM and 0.1 nM are depicted. [G_1]-SIFa and [T_1]-SIFa can equally activate the receptor compared to the endogenous [A_1]-SIFa of *B. terrestris*. *Apime*-sNPF, *Apime*-SK-I and *Bomte* K-I can only activate the receptor when a 1 µM is applied, which is considered not to be a physiologically relevant dose of peptide. No response is measured when *Bomte*-K-II is administered to the cells.

Table 3.3: List of peptide sequences used in this study, their abbreviated name and their corresponding EC_{50} values in CHO-WTA11 cells.

Abbreviation	Peptide sequence	EC_{50} value
Alanine series		
Bomte-SIFa	AYRKPPFNGSIF-NH_2	0.20 nM
A_1	No alanine substitution possible	/
Y_2	AARKPPFNGSIF-NH_2	0.09 nM
R_3	AYAKPPFNGSIF-NH_2	030 nM
K_4	AYRAPPFNGSIF-NH_2	0.16 nM
P_5	AYRKAPFNGSIF-NH_2	0.18 nM
P_6	AYRKPAFNGSIF-NH_2	1.02 nM
F_7	AYRKPPANGSIF-NH_2	1.54 nM
N_8	AYRKPPFAGSIF-NH_2	2.93 nM
G_9	AYRKPPFNASIF-NH_2	10.20 nM
S_{10}	AYRKPPFNGAIF-NH_2	1.14 nM
I_{11}	AYRKPPFNGSAF-NH_2	80.09 nM
F_{12}	AYRKPPFNGSIA-NH_2	/
Truncated peptide series		
Bomte-SIFa	AYRKPPFNGSIF-NH_2	0.31 nM
$SIFa_4$	GSIF-NH_2	0.14 mM
$SIFa_5$	NGSIF-NH_2	6.28 mM
$SIFa_6$	FNGSIF-NH_2	5.43 mM
$SIFa_7$	PFNGSIF-NH_2	0.68 nM
$SIFa_8$	PPFNGSIF-NH_2	0.61 nM
$SIFa_9$	KPPFNGSIF-NH_2	0.13 nM
$SIFa_{10}$	RKPPFNGSIF-NH_2	0.15 nM
$SIFa_{11}$	YRKPPFNGSIF-NH_2	0.14 nM
Insect SIFa peptides		
Bomte-SIFa	AYRKPPFNGSIF-NH_2	0.50 nM
Aedae-SIFa	GYRKPPFNGSIF-NH_2	0.22 nM
Bommo-SIFa	TYRKPPFNGSIF-NH_2	0.23 nM
Related Hymenopteran peptides		
Bomte-SIFa	AYRKPPFNGSIF-NH_2	0.50 nM
Apime-sNPF	SPSLRLRF-NH_2	2.34 mM
Bomte-K-I	TSFDPWSG-NH_2	1.59 mM
Bomte-K-II	ITESVEWTPFNSWG-NH_2	/
Apime-SK-I	pQQFDDYGHLRF-NH_2	0.16 mM

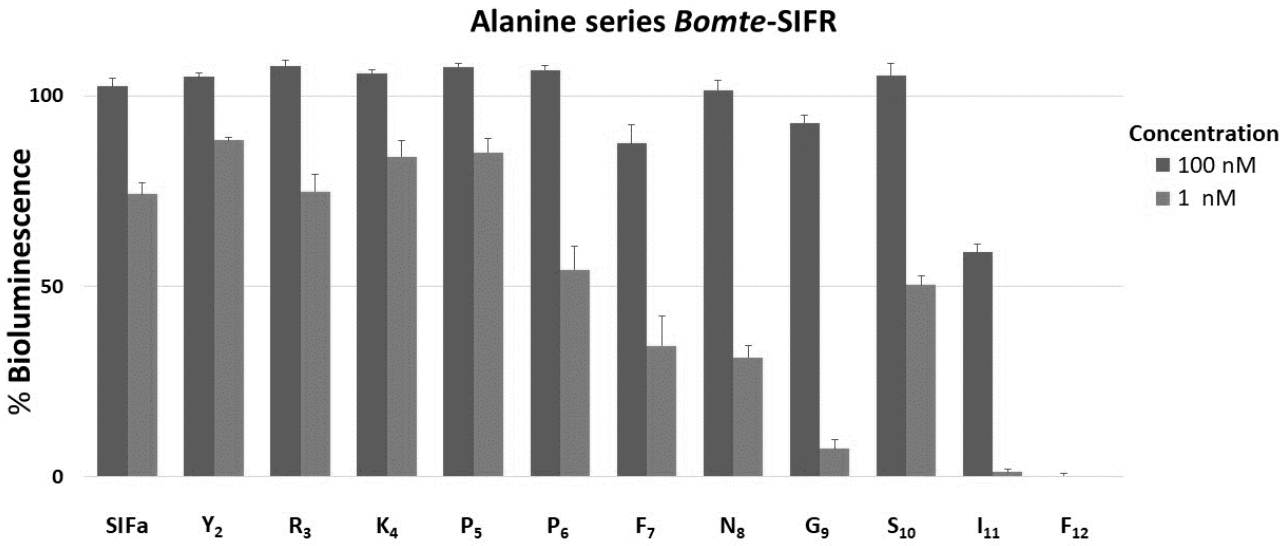

Figure 3.14: Bioluminescent responses induced in CHO-WTA11-*Bomte*-SIFR cells by 100 nM and 1 nM of peptide from the alanine series, whereby every amino acid in the *Bomte*-SIFa sequence is systematically replaced by an alanine. On the left side, the results of the endogenous *Bomte*-SIFa are displayed (SIFa; AYRKPPFNGSIF-NH_2). On the X-axis the different alanine replacement analogues are depicted: Y_2 refers to the peptide where the second amino acid is replaced by alanine (AARKPPFNGSIF-NH_2), *etc*. The bioluminescence is measured in duplicate per concentration of peptide in each of two independent transfections. The data represent mean values ± S.E.M. per analogue per concentration.

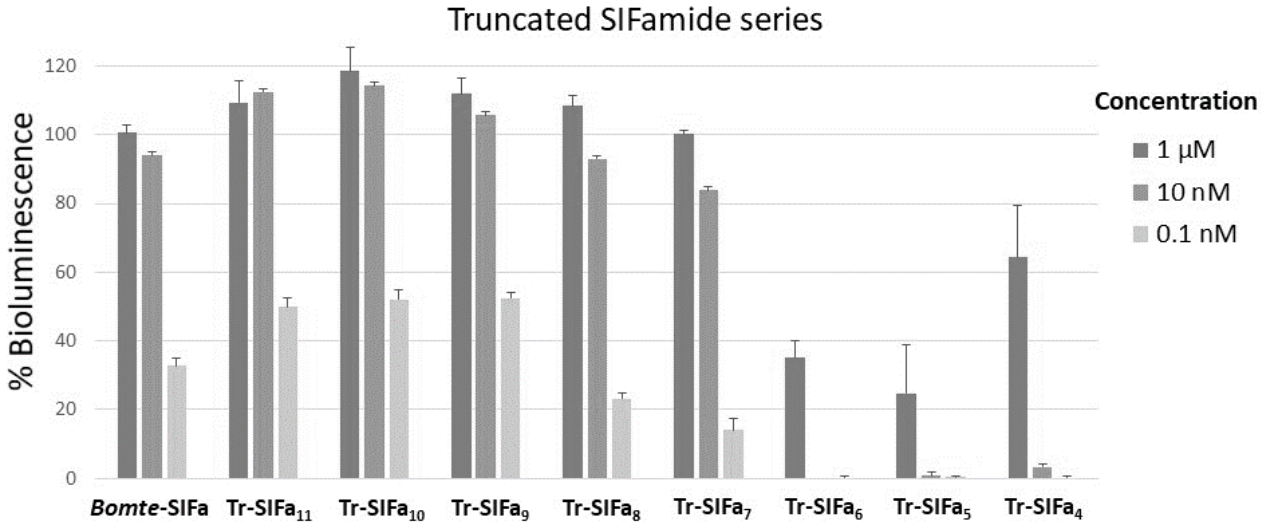

Figure 3.15: Bioluminescent responses induced in CHO-WTA11-*Bomte*-SIFR by 1 µM, 10 nM and 0.1 nM of peptide from the truncated SIFa series. On the left side, the results of the endogenous *Bomte*-SIFa are displayed (SIFa; AYRKPPFNGSIF-NH_2). The bioluminescence is measured in duplicate per concentration of peptide in each of two independent transfections. The data represent mean values ± S.E.M. per analogue per concentration.

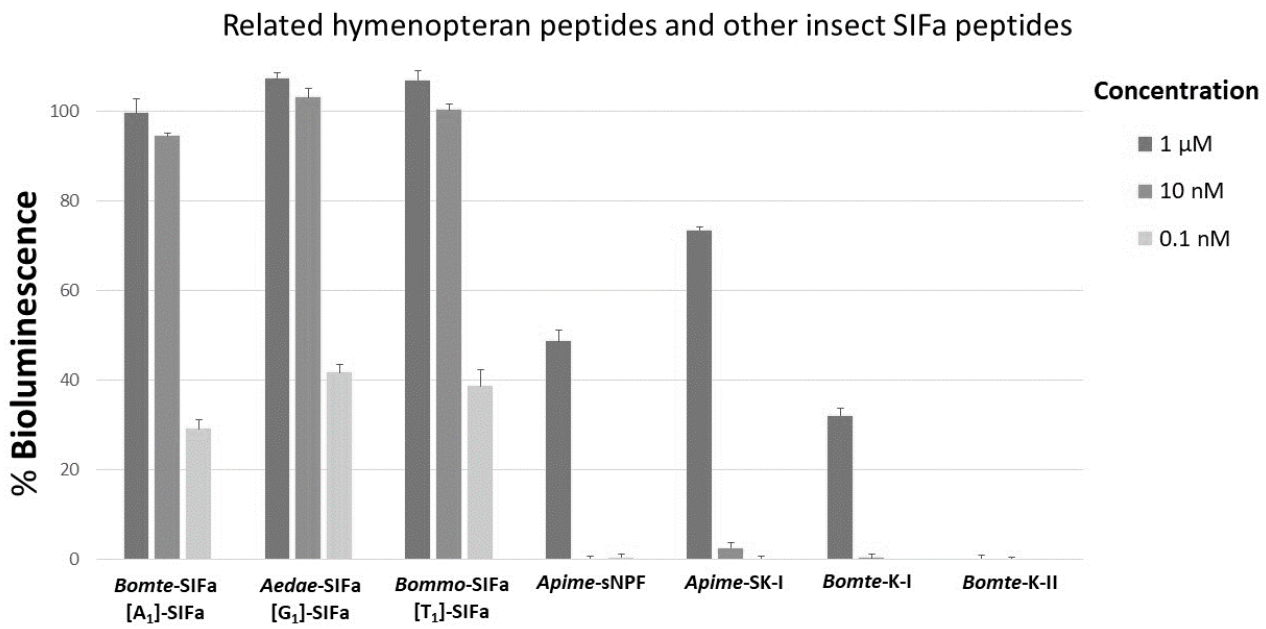

Figure 3.16: Bioluminescent responses induced in CHO-WTA11-*Bomte*-SIFR by 1 µM, 10 nM and 0.1 nM of [G_1]-SIFa (*Aedae*-SIFa), [T_1]-SIFa (*Bommo*-SIFa) and other related Hymenopteran peptides. Additionally, on the left side, the results of the endogenous *Bomte*-SIFa are displayed ([A_1]-SIFa).The bioluminescence is measured in duplicate per concentration of peptide in each of two independent transfections. The data represent mean values ± S.E.M. per analogue per concentration.

3.4. Discussion

3.4.1. Precursor and receptor sequence analysis

In this study, a member of the SIFRs, *Bomte*-SIFR, is identified and subsequently cloned and pharmacologically characterized. As shown in the multiple sequence alignment, the amino acid sequence of *Bomte*-SIFR is well conserved when compared with the two other *in vitro* characterized arthropod SIFRs, from *I. scapularis* and *D. melanogaster*, especially in the 7TM regions and the C-terminus. The sequence also contains amino acid residues which are highly conserved among Family A GPCRs (Gether, 2000; Hauser and Grimmelikhuijzen, 2014; Venkatakrishnan et al., 2013). Furthermore, *Bomte*-SIFR shows a high sequence identity with *Homsa*-NPFFR1 and *Homsa*-NPFFR2, especially in the 7TM regions. These two NPFF/GnIH receptors are considered to be related to SIFR even though no sequence identity is found between SIFa and NPFF/GnIH-type peptides (Mirabeau and Joly, 2013; Elphick and Mirabeau, 2014; Ubuka and Tsutsui, 2014). However, several studies have attempted to prove an evolutionary link between these two peptide systems based on phylogenetic tree analysis (Hauser et al., 2006; Ubuka and Tsutsui, 2014), gene analysis (Mirabeau and Joly, 2013) or overlapping physiological functions (Martelli et al., 2017).

Additionally, the SIFa precursor is identified. In contrast to the study by Roller and co-workers (2008), which reports that the *B. mori* SIFa precursor contains a SIFa paralogue with an IMFa C-terminal, no related IMFa sequence is identified in the SIFa precursor nor in the *B. terrestris* genome database (Priyam et al., 2015; Sadd et al., 2015).

Furthermore, we enlist all hitherto predicted SIFa sequences in arthropods and WebLogo is constructed using all identified and *in silico* predicted insect SIFa sequences. The sequence of the eight C-terminal amino acids is strongly conserved among insects and, in general, three types of SIFa are found in this class; namely [A_1]-SIFa as in *B. terrestris*, [G_1]-SIFa as in *A. aegypti* and [T_1]-SIFa as in *B. mori*. The [G_1]-SIFa isoform is broadly conserved among crustaceans as also shown by Stemmler and co-workers (2007). However, the [A_1]-SIFa nor the [T_1]-SIFa isoforms are predicted in this subphylum. Nevertheless, compared to insects, more variation exists in terms of peptide length and amino acid sequence among crustaceans.

3.4.2. Tissue distribution and mass spectrometry

Expression of the *Bomte*-SIFa precursor is confined to the brain. These data are in agreement with immunostaining and *in situ* hybridization studies performed in other insects, where SIFa expression is shown to be restricted to four medial interneurons in the pars intercerebralis, with a network of ramifications throughout the ventral nerve cord and most parts of the brain (Terhzaz et al., 2007;

Roller et al., 2008; Carlsson et al., 2010; Inosaki et al., 2010; Galizia et al., 2012; Heuer et al., 2012; Neupert et al., 2012; Zoephel et al., 2012; Siju et al., 2014; Gellerer et al., 2015; Arendt et al., 2016). However, our qRT-PCR data shows no detectable expression of *Bomte*-SIFa precursor in the ventral nerve cord.

Additionally, *Bomte*-SIFR transcript levels are high in both the brain and the ventral nerve cord, which is very well in line with the reports mentioned above, the mass spectrometry data in *A. mellifera* (Verleyen et al., 2004; Hummon et al., 2006; Boerjan et al., 2010), as well as with the suggestion that SIFa may be involved in the development and organization of the insect CNS (Gellerer et al., 2015). However, we also detect high SIFR transcript levels in the fat body and other peripheral tissues such as the testes, accessory glands and the foregut. This is in contrast with the hypothesis that SIFa is merely present within the CNS and is not released into the hemolymph and thus has no hormonal role(s), as suggested by Terhzaz and co-workers (2007) and Gellerer and co-workers (2015). Sellami and Veenstra (2015) also reported two neurons in *D. melanogaster* expressing SIFR in the uterus projecting into the CNS. However, it is also possible that these SIFRs in peripheral tissues bind other ligands, besides SIFa. Whether this means that *Bomte*-SIFa indeed occurs in circulating hemolymph remains an interesting question for future studies and could be investigated using mass spectrometry.

By means of a mass spectrometry analysis using a Q Exactive Orbitrap mass spectrometer, the full endogenous AYRKPPFNGSIF-NH_2 is detected in the brain sample of *B. terrestris*. The truncated forms, YRKPPFNGSIF-NH_2 (Tr-$SIFa_{11}$), RKPPFNGSIF-NH_2 (Tr-$SIFa_{10}$), KPPFNGSIF-NH_2 (Tr-$SIFa_9$) and PPFNGSIF-NH_2 (Tr-$SIFa_8$), are not detected in this pool of bumblebee brain extracts.

Already in 2004, the question is raised if truncated isoforms of SIFa exist *in vivo* in insects (Verleyen et al., 2004a). Especially the existence of the shorter isoform PPFNGSIF-NH_2 (Tr-$SIFa_8$), the C-terminal part of SIFa which is very much conserved among insects, has been discussed in literature (Dickinson et al., 2008; Verleyen et al., 2004a; Verleyen et al., 2009). Dickinson and co-workers (2008) point out that the truncated isoform Tr-$SIFa_8$ may exist since Arg_3-Lys_4 is a putative convertase processing site. However, they conclude that the shorter isoform is not the major product of post-translational processing, since it is not detected by MALDI-FTMS. Additionally, according to Veenstra, (2000), Arg_3-Lys_4 is a rare cleavage site in insects. Up till now, this truncated isoform is only detected in *Galleria mellonella* by mass spectrometry (Verleyen et al., 2004a). Nevertheless, the authors mention that it is highly unlikely that this truncated peptide is present the CNS since this mass is found in separate fractions.

On the other hand, the truncated isoforms YRKPPFNGSIF-NH_2 (Tr-$SIFa_{11}$), RKPPFNGSIF-NH_2 (Tr-$SIFa_{10}$) are detected with mass spectrometry in the CNS of *A. mellifera* by both Hummon and co-workers (2006) and Boerjan and co-workers (2010). In the latter study, the authors suggest that these truncated isoforms may not be artefacts. However, they also point out that these truncated isoforms of SIFa are less distributed along the CNS and are less abundantly detected. Additionally, in *R. prolixus*, YRKPPFNGSIF-NH_2 (Tr-$SIFa_{11}$), RKPPFNGSIF-NH_2 (Tr-$SIFa_{10}$) and KPPFNGSIF-NH_2 (Tr-$SIFa_9$) are detected using mass spectrometry (Ons et al., 2009) and truncated peptides of SIFa are also detected in the tsetse fly *Glossina morsitans* (YRKPPFNGSIF-NH_2; Caers et al., 2015), but not in *A. aegypti* (Siju et al., 2014), *A. gambiae* (Riehle et al., 2002), *D. melanogaster* (Baggerman et al., 2005; Predel et al., 2004), the grey fleshfly, *Neobellieria bullata* (Verleyen et al., 2004b), the spotted wing fruit fly, *Drosophila suzukii* (Audsley et al., 2015), the Australian sheep blowfly, *Lucilia cuprina* (Rahman et al., 2013), the Northern blowfly, *Protophormia terraenovae* (Inosaki et al., 2010), the yellow mealworm, *Tenebrio molitor* (Weaver and Audsley, 2008), the American cockroach, *Periplatana Americana* (Neupert et al., 2012), the jewel wasp, *Nasonia vitripennis* (Hauser et al., 2010), nor in the red flour beetle *T. castaneum* (Li et al., 2007).

3.4.3. Pharmacological receptor characterization and G protein mediated signaling pathways

Upon stimulation of CHO-WTA11-*Bomte*-SIFR cells by *Bomte*-SIFa in the aequorin bioluminescence assay, a sigmoidal dose-dependent response with an EC_{50} value in the nanomolar range is obtained indicating that *Bomte*-SIFa is a ligand of *Bomte*-SIFR. Additionally, a sigmoidal dose-dependent response is also observed in CHO-PAM28-*Bomte*-SIFR cells indicating an increase in intracellular calcium ions upon receptor activation with an EC_{50} value in the low nanomolar range. To date, activation of the PLC/Ca^{2+} pathway is only reported in *I. scapularis* (Šimo et al., 2013), a member of the Arachnida class, but not in any member of the insect class.

Additionally, to our knowledge, also the effects on intracellular cAMP levels have hitherto not been reported for SIFRs in insects. In this study, we monitor possible changes in the cAMP levels upon activation of the *Bomte*-SIFR by using two biosensors; the $CRE_{(6x)}$-Luc construct and the CAMYEL biosensor. In the CRE-dependent luciferase reporter assay, a stimulatory dose-dependent effect is observed with an EC_{50} value in the nanomolar range. Notably, the measurement of the bioluminescence in the CRE-dependent luciferase reporter assay is dependent on the presence of cAMP response elements and thus on the phosphorylation of CREB by the cAMP-dependent protein kinase (PKA). However, it is speculated that a change in bioluminescence may also be caused by Ca^{2+}, since CREB can also be phosphorylated by calcium/calmodulin-dependent protein kinase

(Johannessen et al., 2004). This could mean that, since *Bomte*-SIFR has a stimulatory effect on Ca^{2+} levels, the measured bioluminescence using the $CRE_{(6x)}$-Luc construct might also be evoked by the increased Ca^{2+} levels. However, this hypothesis may need further investigation.

No conclusions can be drawn using the CAMYEL biosensor since a decrease in $BRET^1$ signal is detected in the control cells. These results suggest that the control cells or the EPAC protein might respond to *Bomte*-SIFa.

Additionally, we study the downstream G protein mediated signaling pathways in more detail using $BRET^2$-based G protein biosensors which can measure a direct activation of the G protein. To interpret the results obtained in this assay, the *B. terrestris* genome database on BeeBase.org (Priyam et al., 2015; Sadd et al., 2015) is screened by means of a local blast in order to find G protein subunit sequences. Five Gα (*Bomte*-$G\alpha_i$, *Bomte*-$G\alpha_o$, *Bomte*-$G\alpha_s$, *Bomte*-$G\alpha_q$ and *Bomte*-$G\alpha_{12/13}$), two Gβ (*Bomte*-$G\beta_1$ and *Bomte*-$G\beta_2$) and two Gγ (*Bomte* -$G\gamma_1$ and *Bomte* –$G\gamma_e$) subunit sequences are identified. The amino acid sequences of the *B. terrestris* Gα subunit are relatively similar to the human Gα subunit sequences of the $BRET^2$-based G protein biosensors, except for the $G\alpha_{12/13}$ subfamily. *Bomte*-$G\beta_1$ seems to be more related to *Homsa*-$G\beta_1$ than *Bomte*-$G\beta_2$ while neither *Bomte*-$G\gamma_1$ nor *Bomte*–$G\gamma_e$ show high sequence identity with *Homsa*-$G\gamma_2$. Both *Homsa*-$G\beta_1$ and *Homsa*-$G\gamma_2$ are used to construct the two other subunit sequences of the $BRET^2$-based G protein biosensors encompassing a G protein heterodimer consisting of $\alpha_x\beta_1\gamma_2$ with α_x representing one of the ten Gα subunit constructs.

The $G\alpha_q$ biosensor, but not the $G\alpha_{11}$ biosensor, is activated upon stimulation of *Bomte*-SIFR with *Bomte*-SIFa, although the magnitude of the signal is lower compared to *Homsa*-AT1R (Saulière et al., 2012). The results of $G\alpha_q$ biosensor, but not $G\alpha_{11}$ biosensor, are in line with our results in this chapter using the aequorin bioluminescence assay which also indicates an increase in intracellular Ca^{2+} levels upon receptor stimulation.

In addition, four out of five members of the $G\alpha_{i/o}$ subfamily, but not the $G\alpha_s$ biosensor, are activated. The magnitude of the $\Delta BRET^2$ signal for these four biosensors are comparable with the $\Delta BRET^2$ signal detected with *Homsa*-CCR2 (Corbisier et al., 2015). The fact that the $G\alpha_{i/o}$ proteins but not the $G\alpha_s$ protein are activated seems in contradiction with our results of the CRE-dependent luciferase assay in this chapter. However, as mentioned above, the results of this assay should be interpreted with caution. Furthermore, it should be noted that the $G\alpha_{i/o}$ subfamily may also influence other effector proteins such as phospholipases (Dorsam and Gutkind, 2007) and thus may influence other secondary messenger molecules such as Ca^{2+}. Therefore, activation of this subfamily does not necessarily result in a decrease in intracellular cAMP levels. Unfortunately, no reports on cAMP

signaling of the SIFRs in other insects exist. Therefore, these results cannot be compared with other studies.

No response was observed for neither of the $G\alpha_{12/13}$ biosensors. This might be explained by the fact that *Bomte*-$G\alpha_{12/13}$ only shows a much lower sequence identity percentage compared to the other Gα subfamilies.

As mentioned earlier, these $BRET^2$-based G protein biosensors are also used to verify which Gα subunit within a Gα subunit family can be activated. However, since only one $G\alpha_q$ subunit sequence is identified in *B. terrestris*, knowing that the $G\alpha_q$ biosensor, but not the $G\alpha_{11}$ biosensor, is activated may not represent an added value for understanding the *in vivo* situation. This may also apply to the $G\alpha_{i/o}$ biosensors, since only one $G\alpha_i$ and one $G\alpha_o$ are identified in this insect species.

Taking all this together, we can conclude that *Bomte*-SIFa is an agonist of *Bomte*-SIFR and activation of the receptor has a stimulatory effect on the PLC/Ca^{2+} pathway. Concerning the use of the $BRET^2$-based G protein biosensors to detect signaling of this insect GPCR we make four observations: (1) four out of five biosensors of the $G\alpha_{i/o}$ subfamily and the $G\alpha_q$ biosensor respond to the agonist induced insect receptor *Bomte*-SIFR, (2) the results of the $G\alpha_q$ biosensor, but not the $G\alpha_{11}$ biosensor, are in accordance with the data of the aequorin bioluminescence assay (in absence of the promiscuous $G\alpha_{16}$ subunit), (3) no activation of $G\alpha_s$ nor both Gα biosensors of the $G\alpha_{12/13}$ subfamily is detected, and (4) with respect to the second messenger cAMP, the results of $G\alpha_{i/o}$ biosensors nor $G\alpha_s$ are supported by the results of obtained by the CRE-dependent luciferase assay. However, the effect on the AC/cAMP/PKA pathway is still inconclusive since the CRE-dependent luciferase reporter assay does not measure cAMP levels in a direct manner.

3.4.4. Agonistic properties of SIFa analogues on *Bomte*-SIFR

The results of the alanine series of *Bomte*-SIFa and the truncated SIFa peptides correspond well to the WebLogo, which shows that the eight amino acids in the C-terminus are well conserved, indicating that these amino acids are important for receptor activation. Elimination of six or more of the N-terminal amino acids (Tr-$SIFa_6$, Tr-$SIFa_5$ and Tr-$SIFa_4$) results in a drastically reduced receptor activation, since bioluminescence is only measured when 1 µM of peptide is used, which is not considered a physiologically relevant concentration. Additionally, replacement of the C-terminal amino acids by an alanine [phenylalanine (F_7), asparagine (N_8), glycine (G_9), serine (S_{10}), and especially isoleucine (I_{11}) and the C-terminal phenylalanine (F_{12})] also compromises proper signaling. Replacing the C-terminal phenylalanine (F_{12}) even results in the complete abolishment of receptor activation at 1 µM of the peptide agonist. Notably, the amide group attached to this

phenylalanine is not removed from the peptide and is thus attached to the C-terminal alanine of this peptide.

In contrast, the four N-terminal amino acids are less conserved among insects. Both elimination of six (or less) of the N-terminal amino acids (Tr-SIFa$_{11}$, Tr-SIFa$_{10}$, Tr-SIFa$_{9}$, Tr-SIFa$_{8}$ and Tr-SIFa$_{7}$) and replacement of these amino acids by an alanine [tyrosine (Y_2), arginine (R_3), lysine (K_4), and proline (P_5)] does not strongly influence the dose-dependent response at *Bomte*-SIFR, with EC_{50} values remaining in the same (low nanomolar) range as the endogenous *Bomte*-SIFa.

Finally, the *Bomte*-SIFR can also be activated by [G_1]-SIFa and [T_1]-SIFa, but not by *Apime*-sNPF, *Apime*-SK-I and *Bomte* K-I unless a high concentration of 1 µM is applied, which is considered non-physiological. *Bomte* K-II cannot elicit a detectable response at any of the applied concentrations.

Chapter 4:
Characterization of the allatotropin precursor and receptor and its G protein mediated signaling pathways in *Schistocerca gregaria*

The results described in this chapter are partially published in:

Lismont, E., Vleugels, R., Marchal, E., Badisco, L., Van Wielendaele, P., Lenaerts, C., Zels, S., Tobe, S., Vanden Broeck, J., Verlinden, H. (2015). Molecular Cloning and characterization of the allatotropin precursor and receptor in the desert locust, *Schistocerca gregaria*. Frontiers in Neuroscience, 84, 1-14.

The content of this chapter is updated and additional *in cellulo* BRET assay results and an analysis of the G protein subunit sequences are added. The Bioassay is executed by Dr. Heleen Verlinden and the radiochemical assay is performed by Dr. Elisabeth Marchal.

4.1. Introduction

Allatotropin (AT) is originally identified as an amidated tridecapeptide isolated from the nervous system of the tobacco hornworm *Manduca sexta*. It is named after its first known biological function, namely the ability to stimulate juvenile hormone (JH) biosynthesis in the corpora allata (CA) *in vitro* (Kataoka et al., 1989). The minimum sequence for this property in *M. sexta* is found to be the C-terminal octapeptide and this effect is antagonized by the C-terminal tetrapeptide (Kai et al., 2018). Most ATs have a conserved C-terminal pentapeptide that consists of a TARGF-NH_2 motif although the Hymenopteran ATs and the Western tarnished plant bug, *Lygus hesperus,* AT have an exceptional TAYGF-NH_2 C-terminus (Veenstra et al., 2012) and SARGF-NH_2 C-terminus (Christie et al., 2017), respectively. There are also AT-like peptides (ATLs) that contain more variation in their C-terminal motif but can elicit allatotropic activity as well (Lee et al., 2002). ATs have been isolated or deduced *in silico* from numerous arthropod species (Christie, 2015b; Christie and Chi, 2015a; Egekwu et al., 2014; Christie et al., 2017; Christie, 2017; Christie et al., 2018a; Christie et al., 2018b Elekonich and Horodyski, 2003; Veenstra et al., 2012; Weaver and Audsley, 2009) but appear to be lost in decapods (Veenstra, 2016). An overview of all predicted ATs and AT(L)s in insects can be found in the Database for Insect Neuropeptide Research (DINeR; Yeoh et al., 2017). Despite its widespread appearance in numerous insects, neither the AT precursor gene nor the AT receptor gene have been identified in the fruit fly, *Drosophila melanogaster,* or in any other members of this genus (Hewes and Taghert, 2001; Vanden Broeck, 2001). Meiselman and co-workers (2017) have shown in a recent study that ecdysis triggering hormone is responsible for the stimulation of JH synthesis in *D. melanogaster*. This is also observed in the yellow fever mosquito, *Aedes aegypti*, an insect in which AT and ATR are present (Areiza et al., 2014).

Related allatotropin peptides are reported in other phyla beyond Arthropoda. These related peptides are isolated or predicted *in silico* in mollusks (Ahn et al., 2017; Harada et al., 1993; Li et al., 1993; Veenstra, 2010), flatworms (Adami et al., 2011; Koziol et al., 2016), nematodes (Koziol et al., 2016) and annelids (Kerbl et al., 2017; Ukena et al., 1995; Veenstra, 2011), and recent phylogenetic analysis also shows the presence of this peptidergic system in other protostomes (Koziol, 2018) and some deuterostomes (Mirabeau and Joly, 2013).

AT has pleiotropic functions in a variety of insect species. It stimulates visceral muscle activity (Paemen et al., 1991; Duve et al., 1999; Duve et al., 2000), heart activity (Sterkel et al., 2010; Veenstra et al., 1994; Villalobos-Sambucaro et al., 2015), ventral diaphragm oscillation (Koladich et al., 2002), plays a role in the photic entrainment of the circadian clock (Petri et al., 2002), controls the release of digestive enzymes in the midgut (Lwalaba et al., 2010), inhibits active ion transport in

the midgut (Lee et al., 1998) even when only the C-terminal tetrapeptide fragment is applied (Deng et al., 2016), and elicits mosquito immune responses (Hernaândez-Martõânez et al., 2017). Additionally, in the Northern house mosquito, *Culex pipiens*, ovarian development is arrested when non-diapausing females are injected with AT dsRNA immediately after adult eclosion, mimicking the diapausing phenotype (Kang *et al.*, 2014) and in the red flour beetle, *Tribolium castaneum*, injections of AT dsRNA in young pupae results in disrupted adult development and fecundity (Abdel-Latief and Hoffmann, 2014). Notably, in the migratory locust, *Locusta migratoria*, a member of the AT family is named accessory gland myotropin 1, since it is initially isolated from the male accessory glands (the male reproductive system, Box 4.1), and stimulates contractility of the locust oviduct (Paemen et al., 1991; Paemen et al., 1992; the female reproductive system, Box 5.2).

Box 4.1: The male reproductive system

The male reproductive system (Fig. 4.1) comprises the testis, vas deferens, the accessory glands, the seminal vesicle and the ejaculatory duct. Spermatogenesis occurs in the testis which consists of a series of tubes. Mature spermatozoa are guided towards the ejaculatory duct through the vas deferens and are stored in the seminal vesicles. Upon their release, the spermatozoa are enclosed by a spermatophore secreted by the accessory glands (Chapman, 2012; Uvarov, 1966).

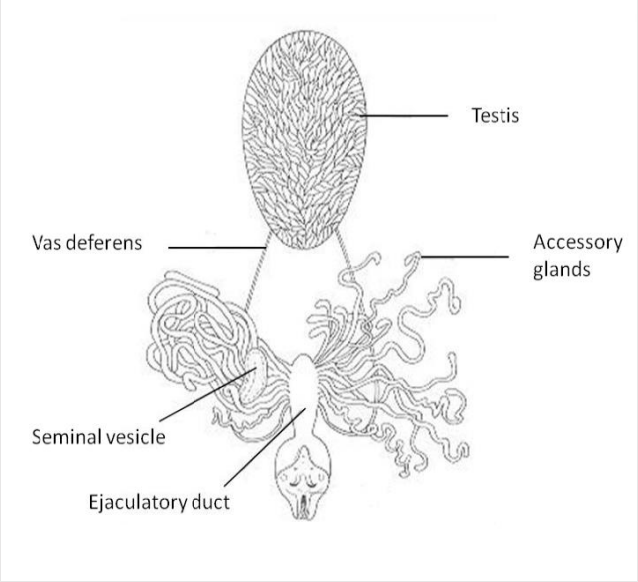

Figure 4.1: The male reproductive system in locusts. (Image credits: CIRAD: French Agricultural Research Centre for International Development, 2007; adapted by Van Wielendaele, 2012)

AT plays a very specific role in the rapid elimination of salts and water subsequent to consumption of a large bloodmeal in the hematophagous insects the kissing bug*, Rhodnius prolixus,* and the barber bug, *Triatoma infestans,* which are both important vectors for Chagas disease. In the latter insect, an AT-like peptide is found to be released from the cells in the Malpighian tubules causing hindgut contractions (Santini and Ronderos, 2007; Sterkel et al., 2010), a quality which is not found

in *R. prolixus* (Masood and Orchard, 2014). Diuresis is also facilitated by increasing hemolymph circulations due to aorta contractions and increased midgut contractions due to the synergistic effect of AT and serotonin in both *R. prolixus* (Villalobos-Sambucaro et al., 2015) and *T. infestans* (Sterkel et al., 2010), a property which is counteracted by allatostatin C in *R. prolixus* (Villalobos-Sambucaro et al., 2016). Finally, it is also found in *R. prolixus* that AT stimulates the secretion of saliva and the contractions of the muscles surrounding the salivary glands which is important for its anti-hemostatic properties allowing a continuous blood flow to the host (Masood and Orchard, 2014).

Even though AT is named after the stimulatory role in JH biosynthesis, it is suggested that this is not the ancestral role of this peptide family. For instance, Elekonich and Horodyski (2003) suggest that the ancestral role is related to its myotropic activity, while the stimulation of JH biosynthesis evolved secondarily in some insect groups. This myotropic activity of AT on the gut is likely important for feeding, since gut contractions are necessary to allow food motility and the flow of digestive enzymes (Audsley and Weaver, 2009; Nagata et al., 2012; Oeh et al., 2001).

ATs exert effects on their cellular targets by binding to receptors with high affinity binding sites that are members of the family of rhodopsin-like G protein-coupled receptors (GPCRs). The AT receptors (ATRs) are orthologous to vertebrate orexin/hypocretin receptors (Mirabeau and Joly, 2013). At the start of this project, five ATRs are characterized; namely the neuropeptide 16 receptor in the silkworm, *Bombyx mori* (Yamanaka et al., 2008) and the AT receptors of *M. sexta* (Horodyski et al., 2011), *T. castaneum* (Vuerinckx et al., 2011), *A. aegypti* (Nouzova et al., 2012) and the buff-tailed bumblebee*, Bombus terrestris* (Verlinden et al., 2013). The first three are dose-dependently activated by *Manse*-AT. The *T. castaneum* receptor is also activated by *Locmi*-AT (which is also named *Lom*-AG-MT1 and is identical to *Schgr*-AT) and by an endogenous AT-like peptide (*Trica*-ATL) predicted from the *T. castaneum* genome (Vuerinckx et al., 2011). The ATR receptor of *B. terrestris* also responds to *Manse*-AT, *Schgr*-AT and *Trica*-ATL, but much higher concentrations are needed for generating these pharmacological effects (Verlinden et al., 2013). By means of the aequorin bioluminescence assay and CRE-dependent luciferase reporter assay, elevated intracellular calcium and cAMP levels are detected upon activation of AT(L) receptors of *M. sexta*, *T. castaneum* and *B. terrestris* (Horodyski et al., 2011; Vuerinckx et al., 2011; Verlinden et al., 2013). An overview of pharmacologically characterized insect ATRs is presented by Verlinden and co-workers (2015).

Recently, a sixth insect ATR is pharmacologically characterized in the cotton bollworm, *Helicoverpa armigera,* whereby *Helar*-ATR is activated by *Helar*-AT and *Helar*-ATL peptides. By means of an aequorin reporter, elevated Ca^{2+} levels are measured upon stimulation of *Helar*-AT(L) peptides

(Zhang et al., 2017). However, in contrast to other insect ATRs, *Helar*-ATR signaling appears to be independent from the AC/cAMP/PKA pathway when cAMP levels are measured by the cAMP-Glo assay from Promega. Additionally, the ATR of *R. prolixus* is cloned and characterized based upon sequence identity (Villalobos-Sambucaro et al., 2015).

ATR-like receptor genes are also be found in the genomes of the African malaria mosquito, *Anopheles gambiae*, the Southern house mosquito*, Culex quinquefasciatus*, the pea aphid, *Acyrthosiphon pisum*, the monarch butterfly, *Danaus plexippus*, the jewel wasp, *Nasonia vitripennis*, the honey bee, *Apis mellifera*, the alfalfa leafcutter bee, *Megachile rotundata*; the ant species *Harpegnathos saltator*, *Acromyrmex echinatior* and *Solenopsis invicta*, and various other insect species (Caers et al., 2012; unpublished BLAST analysis).

The purpose of the current study is to gain more understanding of AT and the ATR in the desert locust, *Schistocerca gregaria*, a member of the Orthoptera well-known for its extreme form of density dependent polyphenism. This insect appears in two phases: an unharmful solitarious phase and a swarm forming gregarious phase (Cullen et al., 2017; Pener and Yerushalmi, 1998; Symmons et al., 2001; Uvarov, 1966; Uvarov, 1977). Earlier studies in this insect have shown the presence of AT in the brain (protocerebrum, antennal lobes and tritocerebrum), the circumoesophageal connectives, the suboesophageal ganglion, the stomatogastric nervous system and all thoracic and abdominal ganglia. No mass peak corresponding to AT is found in the locust corpora cardiaca (CC) or retrocerebral complex (Homberg et al., 2004; Clynen and Schoofs, 2009). In this study, these data are complemented with a quantitative analysis of the AT precursor and receptor transcripts in several tissues of *S. gregaria*.

Additionally, the AT receptor (*Schgr*-ATR) of this insect is pharmacologically characterized and the downstream signaling pathways are studied in more detail by using the aequorin bioluminescence assay and the CRE-dependent luciferase reporter assay. Furthermore, the bioluminescence resonance energy transfer (BRET)^{1}-based cAMP sensor using YFP-Epac-*R*luc (CAMYEL; ATCC MBA-277) biosensor is used as an alternative reporter system for detecting possible changes in intracellular cAMP levels and the BRET^{2}-based G protein biosensors are used to detect a direct activation of specific G proteins (Galés et al., 2006). Additionally, sequences of the human G protein subunits used to construct these BRET^{2}-based G protein biosensors are compared with the G protein sequences of *S. gregaria*. Finally, more evidence is presented for the allatostimulatory and myoactive roles of *Schgr*-AT in this insect.

4.2. Materials and methods

4.2.1. Rearing of animals

Gregarious and solitarious locust of the species *S. gregaria* are reared as described in section 2.1.

4.2.2. Tissue collection

The locust tissues are dissected under a binocular microscope and immediately snap frozen in liquid nitrogen. In a first experiment, three pools of each tissue [brain (Br), optic lobes (OL), corpora cardiaca (CC), corpora allata (CA), prothoracic gland (PG), suboesophageal ganglion (SOG), salivary glands (SG), prothoracic ganglion (TG1), mesothoracic ganglion (TG2), metathoracic ganglion (TG3), gonads (Gon), fat body (FB), flight muscle (FM), foregut (FG), midgut (MG), hindgut (HG), Malpighian tubules (MT) and male accessory glands (AG)] are collected from ten day old gregarious and solitarious males and females. The three pools consist of, respectively, 40, 10 and 10 animals. In a second tissue collection, the abdominal ganglia (AbG) are dissected from ten day old gregarious animals. The first three (1-3) abdominal ganglia are fused to the metathoracic ganglion (TG3) and the last four (8-11; AbG-8) are fused to each other and form the terminal abdominal ganglion (Burrows, 1996). Abdominal ganglia 4-5 (AbG 4-5) and 6-7 (AbG 6-7) are dissected together. The three pools of males and females each consist of 10 animals. All tissue samples are stored at -80 °C until further processing to protect the samples from degradation.

4.2.3. RNA extraction and cDNA synthesis

RNA extractions and cDNA synthesis are performed as described in section 2.2.

4.2.4. Molecular cloning of *Schgr*-ATR

The *Schgr*-AT precursor cDNA and a partial sequence of the putative *Schgr*-ATR cDNA are found by scanning the expressed sequence tag (EST) database of *S. gregaria* (Badisco et al., 2011a). The sequence of the *Schgr*-AT precursor is confirmed by sequencing the plasmid that is used to produce the cDNA library. Additional sequence information of *Schgr*-ATR is obtained by 3’ and 5’ rapid amplification of cDNA-ends (RACE) using the 5'/3' RACE Kit, 2nd Generation (Roche) in combination with *Schgr*-ATR gene specific primers (supplementary table S8) as described in section 2.4.

cDNA covering the entire *Schgr*-ATR is amplified using a three step procedure. In the first step gene specific cDNA is made using the Transcriptor High Fidelity cDNA Synthesis Kit (Roche) and the gene specific primer 5’-TGATAAACATCACTCTGTAT-3’. Next, two PCR rounds are performed using the Pwo DNA Polymerase (Roche). The following cycle program is used twice: 94 °C for 180 s followed by 30 cycles of 94 °C for 45 s, 61 °C for 60 s, 72 °C for 120 s. The program ends at 4 °C after a final

elongation at 72 °C for 10 min. In the first PCR round, the forward primer 5'-TCTGCCCACAGTACATCCAA-3' and the reverse primer 5'-CACTCCACTAGCGACCACAA-3' are used whereas in the second PCR round the forward primer 5'-CACCATGACAGAGAACGAAAC-3' and the reverse primer 5'-GTTGCGGGTAAGGAGGTGT-3' are used. After the first PCR round, a clean-up is performed using the GenElute PCR Clean-Up Kit (Sigma-Aldrich).

The resulting PCR products are purified from a 1 % agarose gel with the GenElute Gel extraction Kit (Sigma-Aldrich). A 3'-A overhang is added using the RedTaq DNA polymerase (Sigma-Aldrich) by heating 15 µl RedTaq mixed with 5 µl gel extract at 72°C during 15 min. Subsequently, the *Schgr*-ATR is cloned into a pcDNA 3.1/V5-His TOPO vector (Invitrogen) following the manufacturer's instructions (described in section 2.5). The vector is transformed into One Shot TOP10 chemical competent *Escherichia coli* cells (Invitrogen) and grown on LB agar plates (35 g/l; Sigma-Aldrich) with ampicillin (10 mg/ml; Invitrogen). Colonies with an insert are collected and grown in 5 ml LB medium (Sigma-Aldrich) with ampicillin (10 mg/ml). The plasmid is purified using the GenElute Plasmid Miniprep Kit (Sigma-Aldrich). DNA sequences are determined using the ABI PRISM 3130 Genetic Analyzer (Applied Biosystems) following the protocol outlined in the BigDye Terminator v1.1 Cycle Sequencing Kit (Applied Biosystems). Bacterial cells known to contain the correct receptor insert in the right direction are grown at large scale in 100 ml Luria-Bertani Broth medium. The expression vector is subsequently isolated using the EndoFree Plasmid Purification Kit (Qiagen) and sequenced once again.

4.2.5. Phylogenetic and structural analysis

The *Schgr*-ATR (GenBank acc. no. JN543509) sequence is compared with other *in cellulo* characterized insect ATRs and ATR-like receptors of *T. castaneum* (*Trica*-ATR, GenBank acc. no. XP_973738), *A. aegypti* (*Aedae*-ATR; GenBank acc. no. AEN03789), *B. terrestris* (*Bomte*-ATR; GenBank acc. no. XP_003402490), *B. mori* (*Bommo*-A16; GenBank acc. no. NP_001127714), *M. sexta* (*Manse*-ATR; GenBank acc. no. ADX66344), and the recently characterized receptor from *H. armigera* (*Helar*-ATR; GenBank acc. no. AXF38049.1). A multiple sequence alignment and a percent identity matrix is constructed as described in section 2.6.

In addition, a phylogenetic tree is constructed with the Neighbor-joining method using the amino acid sequences [from transmembrane region (TM)1 to TM7] from the *Schgr*-ATR and ATR-like receptors of insect organisms: *M. sexta*, *T. castaneum*, *B. terrestris*, *A. aegypti*, *A. mellifera* (*Apime*-ATR; GenBank acc. no. XP_001120335), *M. rotundata* (*Megro*-ATR; GenBank acc. no. XP_003708421), *N. vitripennis* (*Nasvi*-ATR; GenBank acc. no. XP_008217710*), R. prolixus*

(*Rhopr*-ATR; GenBank acc. no. AHE41431), *B. mori* (*Bommo*A5; GenBank acc. no. NP_001127740, and *Bommo*A16) and *D. plexippus* (*Danpl*-ATR; GenBank acc. no. EHJ74388), and the FMRFamide receptor of *D. melanogaster* (*Drome*-FMRFa; GenBank acc. no. AAF47700) to root the tree (constructed by MEGA software version 6; Tamura et al., 2013; with 1000-fold bootstrap resampling).

4.2.6. Identification and sequence analysis of the *S. gregraria* G protein subunits

The amino acid sequences of the G protein subunits of *S. gregaria* are identified and analyzed as described in section 2.11.

4.2.7. Study of relative transcript levels of *Schgr*-AT and *Schgr*-ATR using qRT-PCR

The relative transcript levels of *Schgr*-AT and *Schgr*-ATR are measured in the different tissues by means of real-time quantitative reverse transcriptase PCR (qRT-PCR). Primers for the target genes *Schgr*-AT and *Schgr*-ATR are designed as described in section 2.3.2. A standard curve is constructed using a serial tenfold dilution of brain cDNA.

β-actin and GADPH are selected as the best combination of reference genes for accurate normalization of the raw data by Verlinden and co-workers (2010). Primer sequences of the reference and target genes are enlisted in table 4.1.

Table 4.1: Oligonucleotide sequences of primers of reference and target genes used in the qRT-PCR.

Reference genes	**Forward primer**	**Reverse primer**
Schgr-β-actin	5'-AATTACCATTGGTAACGAGCGATT-3'	5'-TGCTTCCATACCCAGGAATGA-3'
Schgr-GADPH	5’-GTCTGATGACAACAGTGCAT-3’	5’-GTCCATCACGCCACAACTTTC-3’
Target genes	**Forward primer**	**Reverse primer**
Schgr-AT	5'-ATGCAGAACAACCCGGAACT-3’	5'-CTGGTTAGCGTCCACGAACTT-3’
Schgr-ATR	5’-CGTCAACCCAGTCATCTACAACTT-3’	5’-TAGGCGCACGTCCAGAACA-3’

Abbreviations: *Schgr* = *Schistocerca gregaria*, GADPH = glyceraldehyde-3-phosphate dehydrogenase, AT = Allatotropin; ATR = Allatotropin receptor

All reactions are run in duplicate in 20 µl reactions according to the manufacturer’s instructions as described in section 2.3.1. For each sample, the amount of transcripts of the target gene is normalized using the delta-delta Ct method as described in section 2.3.3, in which a mix of all measured tissues of males and females, gregarious and solitarious is used as the calibrator sample. No amplification of the fluorescent signal is detected in any negative control sample, proving that the extraction procedure, including the DNase treatment, effectively removed genomic DNA from all the RNA samples and that there is no contamination. Additionally, PCR products are analyzed via

agarose gel electrophoresis. The resulting single band with expected amplicon size for each transcript is sequenced.

The tissue, phase and sex distribution experiments are repeated three times with independent biological pools of adult *S. gregaria* tissues (40, 10 and 10 animals per pool). Statistical analysis is performed by means of SPSS (v17.0, SPSS Inc., Chicago, Illinois), using the Mann-Whitney U test for comparing two independent groups. A level of $P < 0.05$ is considered significant.

In a second qRT-PCR study, the transcript levels of *Schgr*-AT and *Schgr*-ATR are measured in the abdominal ganglia of male and female gregarious animals. The first three abdominal ganglia are fused to the metathoracic ganglion. Therefore, the same TG3 samples as in the first transcript study are used. Similarly to the first qRT-PCR study, the relative transcript amounts for each sample are normalized to the reference genes coding for *Schgr*-β-actin and *Schgr*-GADPH. The brain sample of the females (a sample from the first qRT-PCR study) is used as the calibrator sample.

4.2.8. *Schgr*-AT bioassay

Schgr-AT is tested on an isolated gut preparation, as described by Schoofs and co-workers (1990). The midgut from a sexually mature male is ligated at both ends with strings by which the gut is suspended between the arm of a transducer and the bottom of a plastic chamber containing 2.5 ml *S. gregaria* saline (1L: 8.766 g NaCl; 0.188 g CaCl2; 0.746 g KCl; 0.407 g MgCl2; 0.336 g NaHCO3; 30.807 g sucrose; 1.892 g trehalose; pH 7.2) at room temperature (supplementary Fig. S11). The transducer monitors the contractions of the gut, which are visualized on a connected recorder (LKB 2210 recorder). When a constant rhythm of contractions is reached, 25 µl of 10 mM *Schgr*-AT (GL Biochem, Shanghai, China) dissolved in saline (to reach a final concentration of one micromolar) or the same volume of saline without peptide is added to the chamber. In between two measurements the chamber is rinsed three times with saline; after this the constant contraction rhythm is restored.

4.2.9. *In vitro* measurement of JH biosynthesis – radiochemical assay (RCA)

Rates of JH release and the JH content are measured by an *in vitro* radiochemical assay (RCA) originally described by Tobe and Pratt (Tobe and Pratt, 1974; Pratt and Tobe, 1974) and further discussed by Feyereisen and Tobe (1981) and Yagi and Tobe (2001). The RCA measures the rate of incorporation of the methyl group from [Methyl-14C] methionine (50 µM, 2.11 GBq/mmol, New England Nuclear Co.) into JH in isolated CA. CA are dissected out of the head of vitellogenic adult females, since it is known that their CA produce a high amount of JH (Tobe and Pratt, 1975). The dissected CA are directly transferred to conical glass vials holding 50 µl of radioactive TC199 medium

[3µCi/ml medium; lacking L-methionine, glucose, acetate and calcium (Gibco, with Hank's sals, HEPES 25 mM)]. The individual CA are shaken at 30°C during the first incubated period of 3h. Next, CA are transferred to fresh radioactive TC199 medium supplemented with 30 µM farnesoic acid (FA) to stimulate JH synthesis. 1 µM *Schgr*-AT is added to the experimental CA. Eight control CA and nine *Schgr*-AT treated CA are tested. Incubation medium is extracted using 300 µl of iso-octane. The samples are vortexed and centrifuged for 10 min at 2000 rpm. The top 200 µl of the iso-octane layer is removed and put into scintillation vials containing 3 ml of scintillant (ICN) and measured in a liquid scintillation counter (Beckman, LS-6500).

The effect of *Schgr*-AT on the JH production of the CA is calculated by dividing the difference between the JH production during the second incubation and the JH production during the first incubation by the JH production during the second incubation. Significance is determined with a student's t-test in GraphPad Prism 5 (GraphPad Software Inc.).

4.2.10. Analysis of the downstream signaling properties of the *Schgr*-ATR using the aequorin bioluminescence assay and the CRE-dependent luciferase reporter assay

Chinese hamster ovary (CHO-WTA11 and CHO-PAM28) and human embryonic kidney (HEK293) cells are transiently transfected with *Schgr*-ATR in order to test the signaling properties of the receptor after activation with the endogenous peptide *Schgr*-AT [(GFKNVALSTARGF-NH_2; ordered from GL Biochem (Shanghai, China)]. For each cell line, two independent transfections are carried out and the luminescence is measured in triplicate per transfection per concentration of peptide.

An additional transfection with empty pcDNA3.1 vector is carried out in each cell line to confirm that the response of the cells is evoked by stimulation of *Schgr*-ATR and not by any other endogenous receptor.

4.2.10.1. Aequorin bioluminescence assay in CHO cells

Cell culture and transfections of CHO-WTA11 and CHO-PAM28, and how this assay is performed is described in section 2.7. A dilution series (1 fM - 10 µM) of *Schgr*-AT is tested.

4.2.10.2. CRE-dependent luciferase reporter assay in HEK293 cells

Cell culture and transfections of HEK293 cells, and how this assay is performed is described in section 2.8. A dilution series (0.1 pM – 10 nM) of *Schgr*-AT is tested. In contrast to the description in that section, the cells are not seeded one day post transfection, but on the day of the assay. HEK293 cells co-transfected with *Schgr*-ATR (or empty vector) and reporter gene plasmid ($CRE_{(6x)}$-Luc construct) are detached with PBS, complemented with 0.2 % EDTA (pH 8.0), and rinsed off the flask

with DMEM/F-12 without phenolred (Gibco). The number of viable and non-viable cells is determined using the NucleoCounter NC-100. The cells are pelleted for 4 min at 800 rpm and finally resuspended to a density of 10^6 cells/ml in DMEM/F-12 without phenolred, but containing 200 µM 3-isobutyl-1-methylxanthine (IBMX, Sigma–Aldrich; 20 µl of 0.1 M IBMX in DMSO in 10 ml DMEM/F-12) to prevent cAMP breakdown.

Into each well of a white 96-well plate, 50 µl of cell suspension (~50000 cells/well) is added to either 50 µl of DMEM/F-12 (with IBMX, but without phenolred) or DMEM/F-12 [with IBMX, without phenolred and containing 10 µM NKH-477 (a forskolin analogue)] containing various concentrations of *Schgr*-AT (0.1 pM - 10 µM; GL Biochem, Shanghai, China). In each row of the plate at least one well with only phenol red-free DMEM/F-12 with IBMX is measured to serve as blank. The cells are then incubated (37 °C, 5 % CO_2) for 4 h.

4.2.11. CAMYEL biosensor

Cell culture, transfections and the procedure of this assay are described in section 2.9. Measurements are performed in duplicate per concentration of *Schgr*-AT (0.10 nM - 1 µM) in two independent transfections for both the experimental condition (with *Schgr*-ATR) and the control (without *Schgr*-ATR), both in the presence or absence of forskolin.

4.2.12. BRET^2-based G protein assay to study the G protein mediated pathways

Cell culture, transfections and the procedure of this assay are described in section 2.10 with *Schgr*-ATR. In the first experiment only one concentration of *Schgr*-AT (1 µM) is tested whereas in the second experiment multiple concentrations (0.1 nM – 1 µM) of *Schgr*-AT are applied.

4.3. Results

4.3.1. Cloning and sequence analysis

As described in the *S. gregaria* EST paper (Badisco et al., 2011a), a partial sequence of an ATR-like receptor and the *Schgr*-AT precursor are represented in the EST database. These sequences are confirmed by PCR, cloning and sequencing. The sequence of the *Schgr*-ATR is further completed by means of RACE. The *Schgr*-ATR amino acid sequence is presented in the multiple sequence alignment in Fig. 4.2 which also compares the *Schgr*-ATR sequence to the other *in cellulo* characterized ATRs and ATR-like receptor of *M. sexta, T. castaneum, A. aegypti*, *B. terrestris*, *B. mori*, *M. sexta* and *H. armigera*. The sequences consist of seven transmembrane domains (TM), three extracellular loops (EL), three intracellular loops (IL), an extracellular N-terminal and an intracellular C-terminal. The alignment shows that the sequence is highly conserved, especially in the 7TM regions and the C-terminus. From TM1 to TM7 the *Schgr*-ATR shows a sequence identity of 68 % with *Bomte*-ATR and *Bommo*-A16, 67 % with *Manse*-ATR and *Helar*-ATR, and 65 % with *Aedae*-ATR and *Trica*-ATR. Amino acid residues that are conserved among rhodopsin-like GPCRs (Family A GPCRs) and conserved cysteine residues to form disulfide bridges between EL1 and EL2 in all GPCRs are indicated (Gether, 2000; Hauser and Grimmelikhuijzen, 2014; Schiöth and Lagerström, 2008; Venkatakrishnan et al., 2013). In contrast to the usual DRY motif present in the second intracellular loop of Family A GPCRs, the third transmembrane region is followed by a DRW motif, as it is the case for other AT receptors. In addition, the conserved W in the sixth TM region is replaced by a Y.

The sequence of the *Schgr*-AT precursor is depicted in Fig. 4.3. The sequence contains a signal peptide predicted by SignalP 4.1 (Petersen et al., 2011) and two recognition motifs for proteolytic processing of the preproallatotropin. The G-residue at the C-terminal can act as a substrate for peptidyl amidating monooxygenase (PAM) resulting in an amidated neuropeptide (Rouillé et al., 1995; Veenstra, 2000). The obtained nucleotide sequence of the *Schgr*-ATR fragment and the sequence of *Schgr*-AT have been submitted to the European Bioinformatics Institute (EBI) database (*Schgr*-ATR: GenBank accession no. JN543509; *Schgr*-AT: GenBank accession no. KP233881).

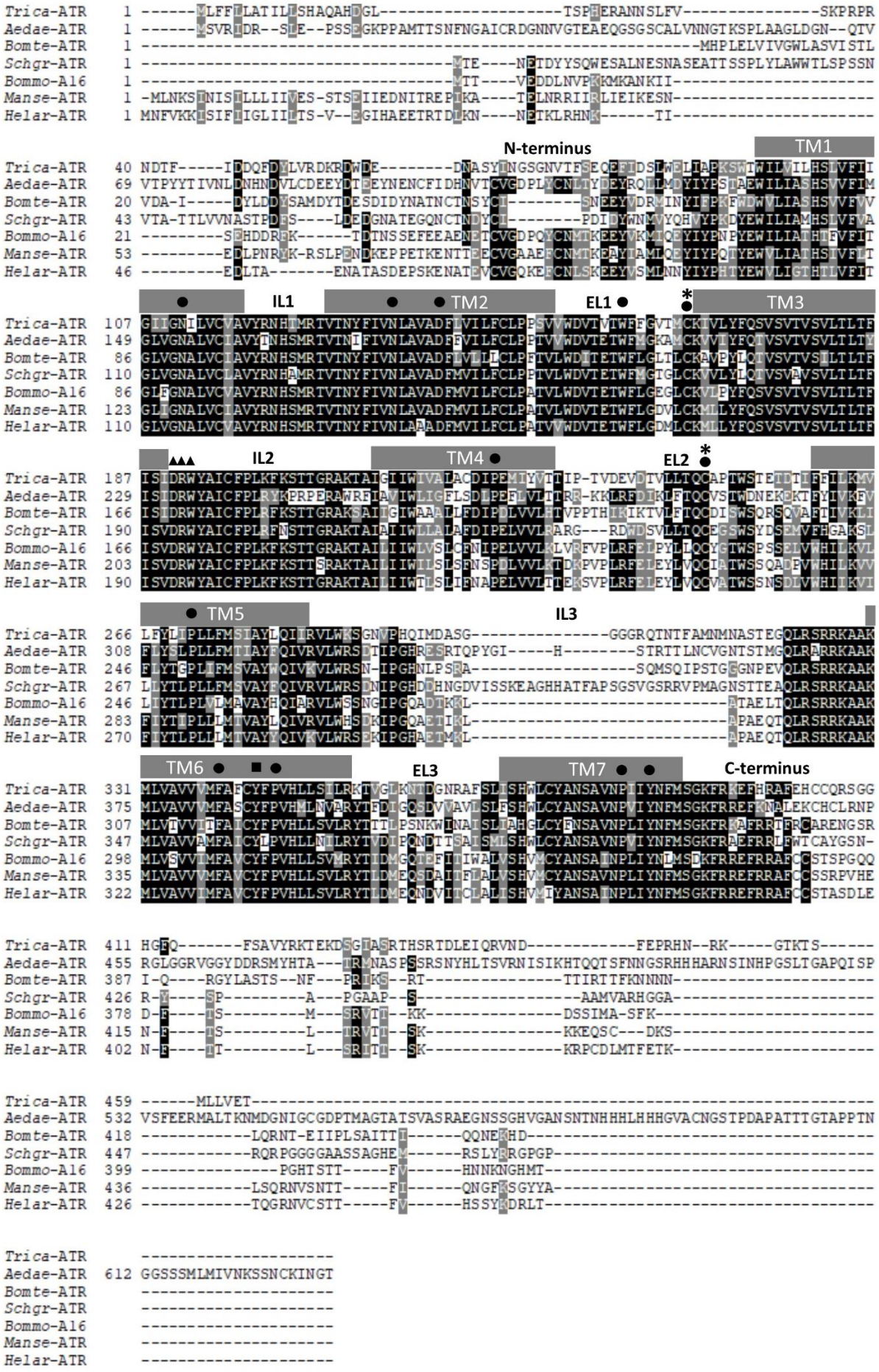
N-terminus
TM1
IL1
TM2
EL1
TM3
IL2
TM4
EL2
TM5
IL3
TM6
EL3
TM7
C-terminus
Trica-ATR
Aedae-ATR
Bomte-ATR
Schgr-ATR
Bommo-A16
Manse-ATR
Helar-ATR

↑ **Figure 4.2**. **Multiple sequence alignment of amino acid sequence of the *Schgr*-ATR** (GenBank acc. no. JN543509) **and homologous receptors** from *T. castaneum* (*Trica*-ATR, GenBank acc. no. XP_973738), *A. aegypti* (*Aedae*-ATR; GenBank acc. no. AEN03789), *B. terrestris* (*Bomte*-ATR; GenBank acc. no. XP_003402490), *B. mori* (*Bommo*-A16; GenBank acc. no. NP_001127714), *M. sexta* (*Manse*-ATR; GenBank acc. no. ADX66344) and *H. armigera* (*Helar*-ATR; GenBank acc. no. AXF38049.1). Amino acid position is indicated at the left. Identical residues between the aligned sequences are highlighted in black, and conservatively substituted residues in grey. Dashes indicate gaps that are introduced to maximize homologies. Putative transmembrane regions (TM1-TM7) are indicated by grey bars. The position of the W (here changed to Y) (■) that is usually conserved in many rhodopsin-like GPCRs and the unusual DRW motif (▲▲▲) are labelled. Amino acids usually conserved in rhodopsin-like GPCRs are labeled (●) (Gether, 2000; Hauser and Grimmelikhuijzen, 2014; Schiöth and Lagerström, 2008; Venkatakrishnan et al., 2013) and conserved cysteine residues that are predicted to form disulfide bridges in extracellular loop (EL) 1 and EL2 are also indicated (*). The intracellular loops (IL), the N-terminus and the C-terminus of the receptors are shown as well.

ATG	CGC	TGC	GCC	GCC	GCC	GCC	CTG	TGC	CTG	CTG	GTC	GCC	CTC	GCC
M	R	C	A	A	A	A	L	C	L	L	V	A	L	A
GCC	CTC	TGC	GCC	GCC	GCC	GCC	GCC	GCC	CCC	GCG	GCT	CAC	TAC	GGC
A	L	C	A	A	A	A	A	A	P	A	A	H	Y	G
CGC	GGC	TCC	CGC	CCC	CGC	ACG	ATA	CGG	GGC	TTC	AAG	AAC	GTG	GCA
R	G	S	R	P	R	T	I	R	G	F	K	N	V	A
CTC	TCC	ACC	GCG	CGG	GGC	TTC	GGC	AAG	CGA	GAC	GGC	AAC	CAG	CTG
L	S	T	A	R	G	F	G	K	R	D	G	N	Q	L
GAG	GCC	GCG	CTC	GCT	GAC	CGC	GAC	ACC	ACC	CTC	CCG	GAC	AGC	TTC
E	A	A	L	A	D	R	D	T	T	L	P	D	S	F
CCT	GTG	GAA	TGG	TTC	GCC	GCC	GAG	ATG	CAG	AAC	AAC	CCG	GAA	CTG
P	V	E	W	F	A	A	E	M	Q	N	N	P	E	L
GCT	CGC	ATG	ATC	GTC	AGC	AAG	TTC	GTG	GAC	GCT	AAC	CAG	GAT	GGA
A	R	M	I	V	S	K	F	V	D	A	N	Q	D	G
GAA	CTG	ACG	GCA	GAG	GAA	CTC	CTC	AGG	CCC	ACT	TAC	TGA		
E	L	T	A	E	E	L	L	R	P	T	Y	STOP		

Figure 4.3: Precursor sequence of *Schgr*-AT. The AT sequence is highlighted in green. The predicted signal peptide sequence is highlighted in orange and the two recognition sites for proteolytic processing of the proneuropeptide are highlighted in blue. The G-residue predicted to be transformed into the C-terminal amide by PAM is highlighted in yellow.

4.3.2. Analysis of phylogenetic relationships

Amino acid sequence comparison between the *Schgr*-ATR and other insect ATR and ATR-like receptors shows high overall amino acid similarity (identical and conservatively substituted residues; Fig. 4.2). The amino acid sequences (TM1-7) of the ATR-like receptors and the FMRFamide receptor from *D. melanogaster*, to root the tree, are aligned with MUSCLE. A Neighbor-joining tree is constructed using MEGA software with 1000-fold bootstrap resampling (Fig. 4.4). The ATRs cluster together as compared to the root of the tree and the lepidopteran and Hymenopteran ATRs cluster within their insect class. The overall insect phylogeny is however not respected in the tree. Bootstrap values already indicate that the power of some nodes is less compared to the lepidopteran and

Hymenopteran cluster. Future characterization projects will hopefully result in more ATR sequences from diverse phylogenetic classes and will hopefully increase the overall power of phylogenetic studies.

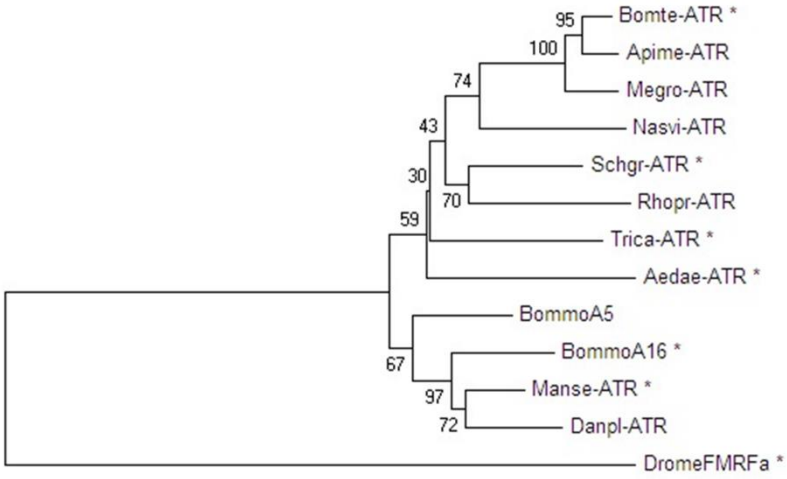

Figure 4.4. **Neighbor-joining tree of insect ATR-like receptors** in dendrogram. Phylogenetic and molecular evolutionary analyses are conducted by using MEGA version 6. The FMRFamide-receptor of *D. melanogaster* (GenBank acc. no. AAF47700) is used as an outgroup to root the tree. Receptors marked with an asterisk are pharmacologically characterized. Bootstrap-support values are based on 1000 replicates and are indicated on the nodes. The other GenBank accession numbers are: *S. gregaria* ATR (*Schgr*-ATR; JN543509), *M. sexta* ATR (*Manse*-ATR; ADX66344), *T. castaneum* ATR (*Trica*-ATR; XP_973738), *B. terrestris* ATR (*Bomte*-ATR; XP_003402490), *A. mellifera* ATR (*Apime*-ATR; XP_001120335), *M. rotundata* ATR (*Megro*-ATR; XP_003708421), *N. vitripennis* ATR (*Nasvi*-ATR; XP_008217710), *R. prolixus* ATR (*Rhopr*-ATR AHE41431), *A. aegypti* ATR (*Aedae*-ATR; AEN03789), *B. mori* neuropeptide A5 and A16 receptor (*Bommo*-A5; NP_001127740, and *Bommo*-A16; NP_001127714, respectively) and *D. plexippus* ATR (*Danpl*-ATR EHJ74388).

4.3.3. Sequence analysis of the G protein subunits of *S. gregaria*

The G protein subunit sequences identified in *B. terrestris* (section 3.3.3) are used to scan the (unpublished) transcriptome database of *S. gregaria* to find G protein subunit sequences in this insect. All sequences are confirmed to be G protein subunits by the online tool GprotPRED (http://aias.biol.uoa.gr/GprotPRED/). Two of these sequences are assigned by GprotPRED or BLAST analysis on NCBI to the $G\alpha_{i/o}$ subfamily; namely *Schgr*-$G\alpha_i$ and *Schgr*-$G\alpha_o$, one sequence is assigned to the $G\alpha_s$ subfamily; namely *Schgr*-$G\alpha_s$, one sequence is assigned to the $G\alpha_{q/11}$ subfamily; namely *Schgr*-$G\alpha_q$, and one sequence is assigned to the $G\alpha_{12/13}$ subfamily; namely *Schgr*-$G\alpha_{12/13}$. The other identified G protein subunits are *Schgr*-$G\beta_1$, *Schgr*-$G\beta_2$, *Schgr*-$G\gamma_1$ and *Schgr*–$G\gamma_2$.

A multiple sequence alignment (supplementary Fig. S1-S7) and a percent identity matrix is constructed (supplementary tables S1-S7) comparing the G protein subunit sequences of *S. gregaria* and the sequences of the *H. sapiens* G protein subunits used to construct the $BRET^2$-based G protein

biosensors for $G\alpha_i$, $G\alpha_o$, $G\alpha_s$, $G\alpha_{q/11}$, $G\alpha_{12/13}$, Gβ and Gγ. For additional analyses in chapters 3 and 6 the G protein subunit sequences of *Bombus terrestris* are added.

Amino acid sequences of the $G\alpha_i$, $G\alpha_o$ $G\alpha_s$ and $G\alpha_{q/11}$ subunits are very similar. *Schgr*-$G\alpha_i$ shows a sequence identity of 83 % with *Homsa*-$G\alpha_{i1}$, 82 % with both *Homsa*-$G\alpha_{i2}$ and *Homsa*-$G\alpha_{i3}$, and 90 % with *Bomte*-$G\alpha_i$ (supplementary Fig. S1 and supplementary table S1) while *Schgr*-$G\alpha_o$ shows a sequence identity of 83 % with both *Homsa*-$G\alpha_{oa}$ and *Homsa*-$G\alpha_{ob}$ and 96 % with *Bomte*-$G\alpha_o$ (supplementary Fig. S2 and supplementary table S2). *Schgr*-$G\alpha_s$ shows a sequence identity of 77 % with *Homsa*-$G\alpha_s$ and 83 % with *Bomte*-$G\alpha_s$ (supplementary Fig. S3 and supplementary table S3), and *Schgr*-$G\alpha_q$ shows a sequence identity of 79 % with both *Homsa*-$G\alpha_q$ and *Homsa*-$G\alpha_{11}$ and 94 % with *Bomte*-$G\alpha_q$ (supplementary Fig. S4 and supplementary table S4). Compared to the other Gα subunit sequences, the sequences of the $G\alpha_{12/13}$ subfamily are much less conserved. *Schgr*-$G\alpha_{12/13}$ shows a sequence identity of 60 % with both *Homsa*-$G\alpha_{12}$ and 59 % with *Homsa*-$G\alpha_{13}$ while, on the contrary, a sequence identity of 80 % is detected with *Bomte*-$G\alpha_{12/13}$ (supplementary Fig. S5 and supplementary table S5).

Additionally, amino acid sequence of both Gβ and Gγ sequences are compared. *Schgr*-$G\beta_1$ shows a sequence identity of 86 % with *Homsa*-$G\beta_1$, 53 % with *Schgr*-$G\beta_2$, 95 % with *Bomte*-$G\beta_1$ and 51 % with *Bomte*-$G\beta_2$, while *Schgr*-$G\beta_2$ shows a sequence identity of 52 % with *Homsa*-$G\beta_1$, 53 % with *Bomte*-$G\beta_1$, and 84 % with *Bomte*-$G\beta_2$ (supplementary Fig. S6 and supplementary table S6). These data suggest that *Schgr*-$G\beta_1$ and *Bomte*-$G\beta_1$, are more related to the *Homsa*-$G\beta_1$ sequence used to construct the BRET biosensor. Finally, the Gγ subunit sequence is much shorter than the Gα and Gβ subunit sequences. *Schgr*-γ_1 shows a sequence identity of 40 % with *Homsa*-$G\gamma_2$, 21 % with *Schgr*-$G\gamma_2$, 73% with *Bomte*-$G\gamma_1$ and with 19% with *Bomte*-$G\gamma_e$ while *Schgr*-$G\gamma_2$ shows a sequence identity of 34 % with *Homsa*-$G\gamma_2$, 26 % with *Bomte*-$G\gamma_1$ and 92 % with *Bomte*-$G\gamma_e$ (supplementary Fig. S7 and supplementary table S7). These data suggest that *Schgr*-$G\gamma_1$ and *Bomte*-γ_1 on one hand and *Schgr*-$G\gamma_2$ and *Bomte*-$G\gamma_e$ on the other hand are orthologue Gγ subunits and neither of both Gγ orthologues show sequence identity with *Homsa*-$G\gamma_2$ protein which is used to construct the $BRET^2$-based G protein biosensors.

4.3.4. Relative transcript levels of the *Schgr*-AT precursor and the *Schgr*-ATR

The expression of the *Schgr*-AT precursor is largely restricted to the central nervous system (CNS; Fig. 4.5). The data of the gregarious and solitarious animals are presented together since no significant differences are observed between these two phases. In general, females show higher *Schgr*-AT precursor transcript levels as compared to males. The effect is significant ($p < 0.05$) in the

central brain parts, the optic lobes and abdominal ganglia 4-5 and 6-7. On the contrary, the transcript levels in the last abdominal ganglion are higher in the males than in the females ($p < 0.05$).

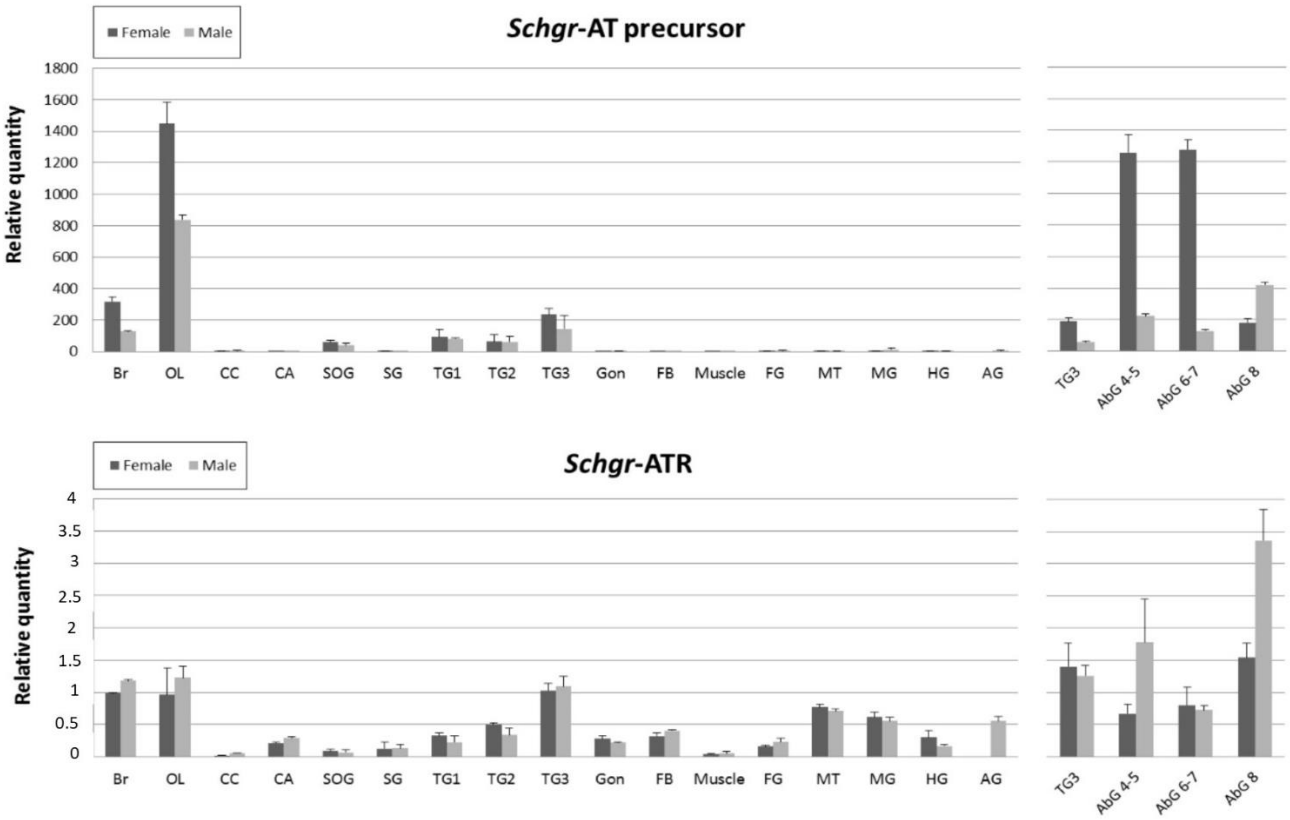

Figure 4.5: Graphic representation of the relative transcript levels of the *Schgr*-AT precursor and the *Schgr*-ATR measured in sexually mature *S. gregaria* in two experiments. The data represent mean values ± S.E.M. of three independent tissue samples run in duplicate, normalized relative to *Schgr*-β-actin and *Schgr*-GADPH transcript levels. Abbreviations used: Br = brain, OL = optic lobes, CC = corpora cardiaca, CA = corpora allata, PG = prothoracic gland, SOG = suboesophageal ganglion, SG = salivary gland, TG1 = prothoracic ganglia, TG2 = mesothoracic ganglion, TG3 = metathoracic ganglion, Gon = gonads, FB = fat body, Muscle = flight muscle, FG = foregut, MT = Malpighian tubules, MG = midgut, HG = hindgut, AG = male accessory glands, AbG = abdominal ganglia. The first three abdominal ganglia (1-3) are fused to the metathoracic ganglion (TG3). On the left the results of the first qRT-PCR study are depicted and on the right the results of the second qRT-PCR study are depicted. The data of the gregarious and solitarious animals are represented together.

The *Schgr*-ATR is also mainly expressed in the CNS. The highest transcript levels can be measured in the brain, the optic lobes, the metathoracic ganglion and the abdominal ganglia (Fig. 4.5). The receptor also shows relatively high transcript levels in the Malpighian tubules, intestines, male accessory glands, mesothoracic ganglion, prothoracic ganglion, fat body, gonads, CA and the salivary glands. No significant differences in transcript levels are observed between sexes, or phases nor between larval and adult CA (results not shown). The *Schgr*-ATR transcript levels are 200 to 1000-fold lower in the central nervous system as compared to the *Schgr*-AT precursor transcript levels. Analysis of the dissociation curves of the different amplification products reveal a single melting

peak and sequencing of the PCR products ultimately confirms the identity of the amplified DNA with their respective target sequences.

4.3.5. Gut motility bio-assay

Schgr-AT is added to the midgut preparation *in vitro* when a constant contraction rhythm is observed. This leads to an immediate tetanus (Fig. 4.6 left). After rinsing, the tetanus disappears and normal contraction rhythm is restored (results not shown). No change in contraction strength or rhythm of the midgut is observed upon addition of saline without the peptide (results not shown). The entire procedure is repeated and yet again only a change in contraction of the midgut is be observed when *Schgr*-AT is added (Fig. 4.6 right).

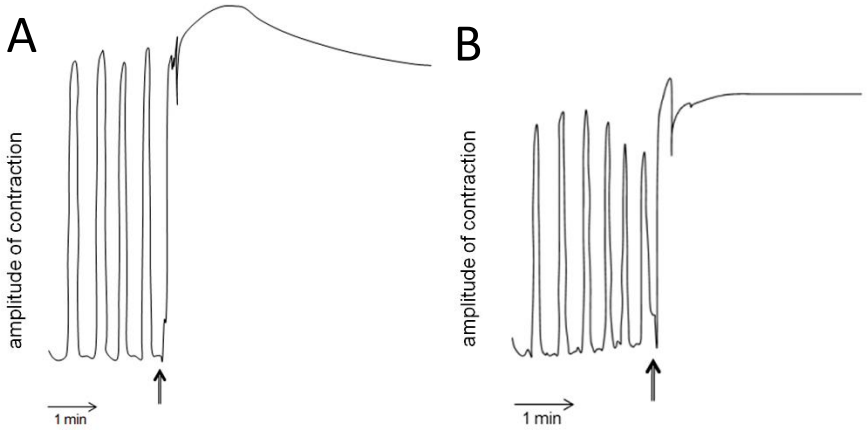

Figure 4.6. Myotropic activity of *Schgr*-AT on the midgut of *Schistocerca gregaria*. Arrows indicate the administration of *Schgr*-AT. A and B represent two independent measurements on the same midgut.

4.3.6. *In vitro* measurement of JH biosynthesis – radiochemical assay (RCA)

In the control CA the JH production is slightly lower during the second incubation period when compared to the first incubation. This is likely the result of the natural decrease in JH biosynthesis by senescence of the CA cells or a decrease in JH precursor pools as in the *in vitro* nature of the experiment. However, if the CA are treated with AT during the second incubation period, the JH production increased significantly ($p < 0.05$; Fig. 4.7).

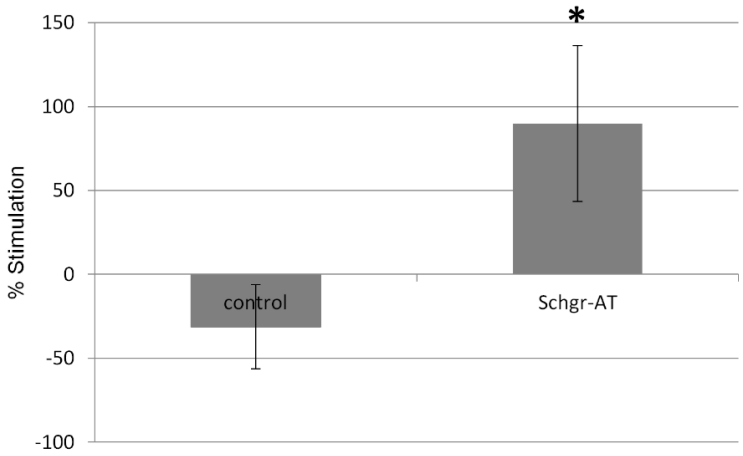

Figure 4.7. The effect of *Schgr*-AT on the rate of JH biosynthesis in the corpora allata (CA) as measured in an *in vitro* radio-chemical assay (RCA). The bars represent averages ± S.E.M. of eight control and nine *Schgr*-AT treated, individual CA dissected from vitellogenic adult females. Significant differences ($p < 0.05$) are indicated by an asterisk (*).

4.3.7. Downstream signaling properties of *Schgr*-ATR using the aequorin bioluminescence assay and the CRE-dependent luciferase reporter assay

Schgr-AT elicits a sigmoidal dose-dependent response with an EC_{50} value in the nanomolar range in both CHO-WTA11-*Schgr*-ATR (4.43 nM; Fig. 4.8A; containing the promiscuous $G\alpha_{16}$ protein) and CHO-PAM28-*Schgr*-ATR cells (5.57 nM; Fig. 4.8B; which do not express $G\alpha_{16}$). The former indicates that *Schgr*-AT is an agonist of *Schgr*-ATR, while the latter indicates that the receptor can also induce an increase in intracellular calcium levels by natural preference. Additionally, increased luciferase reporter activity is observed in HEK293 cells co-transfected with *Schgr*-ATR and the $CRE_{(6x)}$-Luc construct, with an EC_{50} value in the high nanomolar range (81.02 nM; Fig. 4.9) suggesting an increase in intracellular cAMP levels upon stimulation by *Schgr*-AT. However, no response was observed when this assay was performed with a forskolin-analogue (results not shown). Finally, CHO-WTA11, CHO-PAM28 and HEK293 cells transfected with an empty pcDNA 3.1 vector do not show any response to *Schgr*-AT (results not shown).

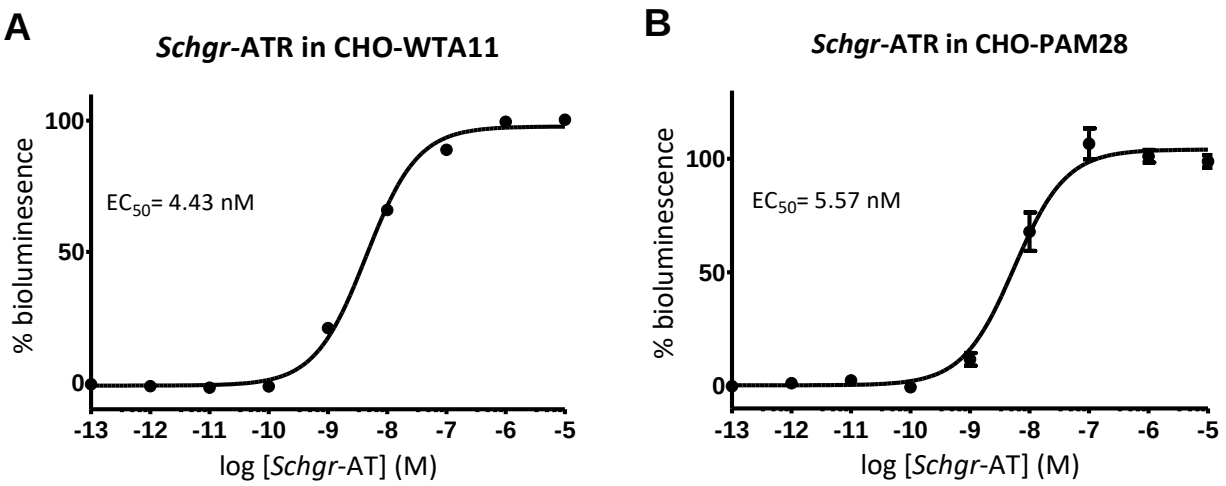

Figure 4.8: Dose-response curve of bioluminescent responses induced in **(A)** CHO-WTA11-*Schgr*-ATR cells and **(B)** CHO-PAM28-*Schgr*-ATR cells. The aequorin bioluminescence assay is executed in two independent transfections. The bioluminescence is measured in triplicate per concentration of *Schgr*-AT and per transfection. Error bars represent the S.E.M. The 100 % level refers to the maximal response level and the zero-response level corresponds to treatment with BSA medium only. In addition, the EC_{50} values are indicated.

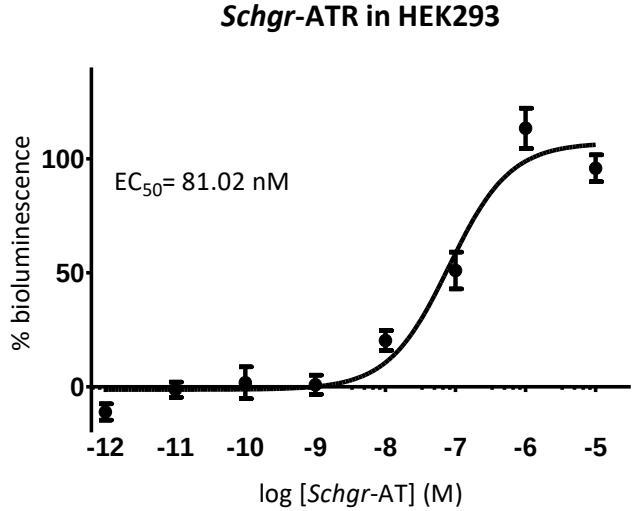

Figure 4.9: Bioluminescent responses induced in HEK293-*Schgr*-ATR cells co-transfected with the $CRE_{(6x)}$-Luc construct. This CRE-dependent luciferase reporter assay is performed in two transfections. The bioluminescence is measured in triplicate per concentration of *Schgr*-AT and per transfection. Error bars represent the S.E.M. The zero level corresponds to treatment with DMEM/F-12/IBMX and the 100 % level refers to the maximal response. In addition, the EC_{50} value is indicated.

4.3.8. The CAMYEL biosensor

In the first experiment (Fig. 3.8, left), no decrease in $BRET^1$ signal is detected when cells are transfected with *Schgr*-ATR and also in the second experiment (Fig. 3.8, right) no increase in $BRET^1$ signal is detected. In both experiment, also the control cells do not respond to *Schgr*-AT stimulation. These results suggest that *Schgr*-ATR signaling might be independent from the AC/cAMP/PKA pathway.

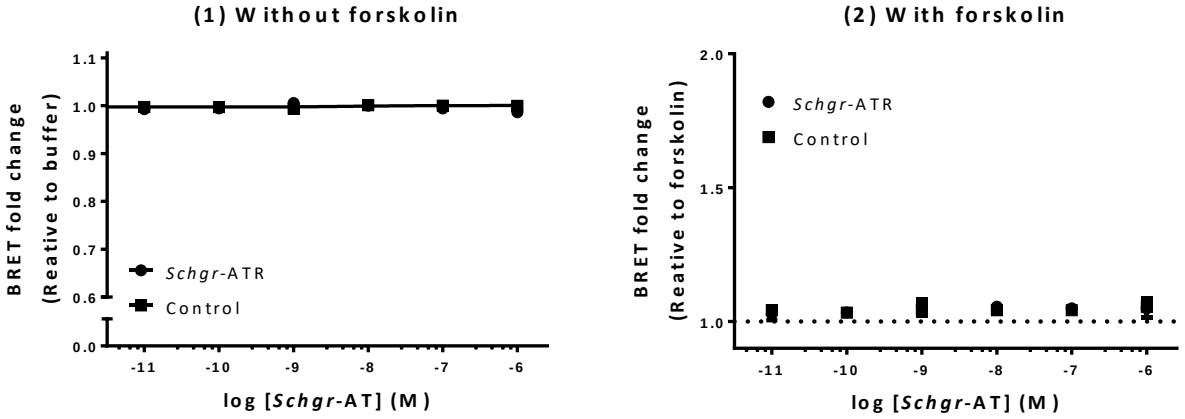

Figure 4.10: Results of CAMYEL biosensor: BRET[1] measured in HEK293T cells transfected with *Schgr*-ATR (●) or without *Schgr*-ATR [control (■)] in two independent transfections. Measurements are taken in duplicate for each concentration of *Schgr*-AT (10 pM - 1 µM). **Left**: measurements are taken in the absence of forskoline. Data (± S.E.M) are presented relative to the baseline (buffer only). **Right**: measurements are taken in the presence of forskolin. Data (± S.E.M) are presented relative to the baseline (buffer with forskolin). The dotted line represents the baseline.

4.3.9. Measuring a direct activation of several G proteins by using BRET[2]-based G protein biosensors

The ΔBRET[2] signal of the HEK293T-*Schgr*-ATR is significantly lower than the control cells upon stimulation with 1 µM *Schgr*-AT for all five biosensors the $G\alpha_{i/o}$ subfamily (Fig. 4.11). Moreover, the ΔBRET[2] signal of $G\alpha_{i2}$, $G\alpha_{i3}$, $G\alpha_{oa}$ and $G\alpha_{ob}$ are dose-dependent with an EC_{50} value in the high nanomolar ranger (Fig. 4.12) suggesting activation of these biosensors. For the $G\alpha_{i1}$ biosensor, a dose-dependent trend is observed although the ΔBRET[2] signal is also low when a concentration of 0.1 nM *Schgr*-AT is applied to the cells. The magnitude of the ΔBRET[2] signals of the $G\alpha_{o}$ biosensors, but not the $G\alpha_{i}$ biosensors, are comparable those detected with the *H. sapiens* chemokine receptor CCR2 (*Homsa*-CCR2; Fig 3.9, right; Corbisier et al., 2015), a receptor known to activate $G\alpha_{i/o}$ proteins.

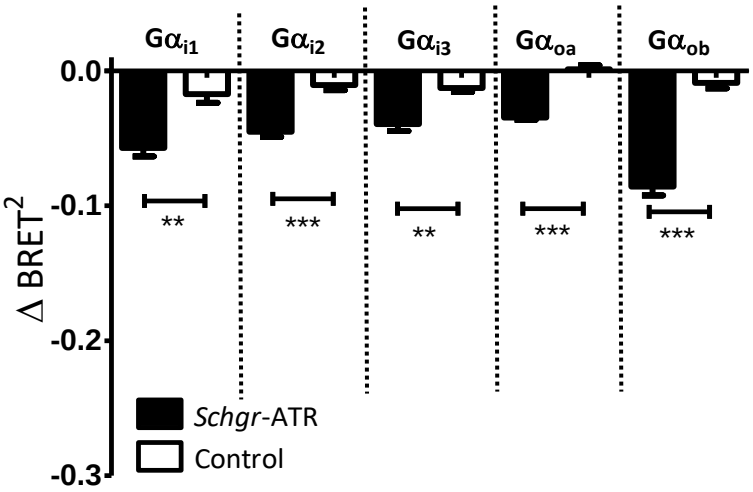

Figure 4.11: Figure 3.9: Summary of the results of the $G\alpha_{i/o}$ subfamily $BRET^2$-based G protein biosensors. The results of HEK293T-*Schgr*-ATR cells (*Schgr*-ATR) and HEK293T cells (control) co-transfected with the $G\alpha_{i1}$, $G\alpha_{i2}$, $G\alpha_{i3}$, $G\alpha_{oa}$ or $G\alpha_{ob}$ biosensor upon stimulation of 1 µM *Schgr*-AT. The data represent the means ± S.E.M of $\Delta BRET^2$ measured in triplicate in two independent transfections. Significant differences ($p < 0.01$ and $p < 0.001$) are indicated by asterisks (** and *** respectively) (student's t-test per $G\alpha_{i/o}$ biosensor). The dotted lines segregate the results per Gαi/o biosensor.

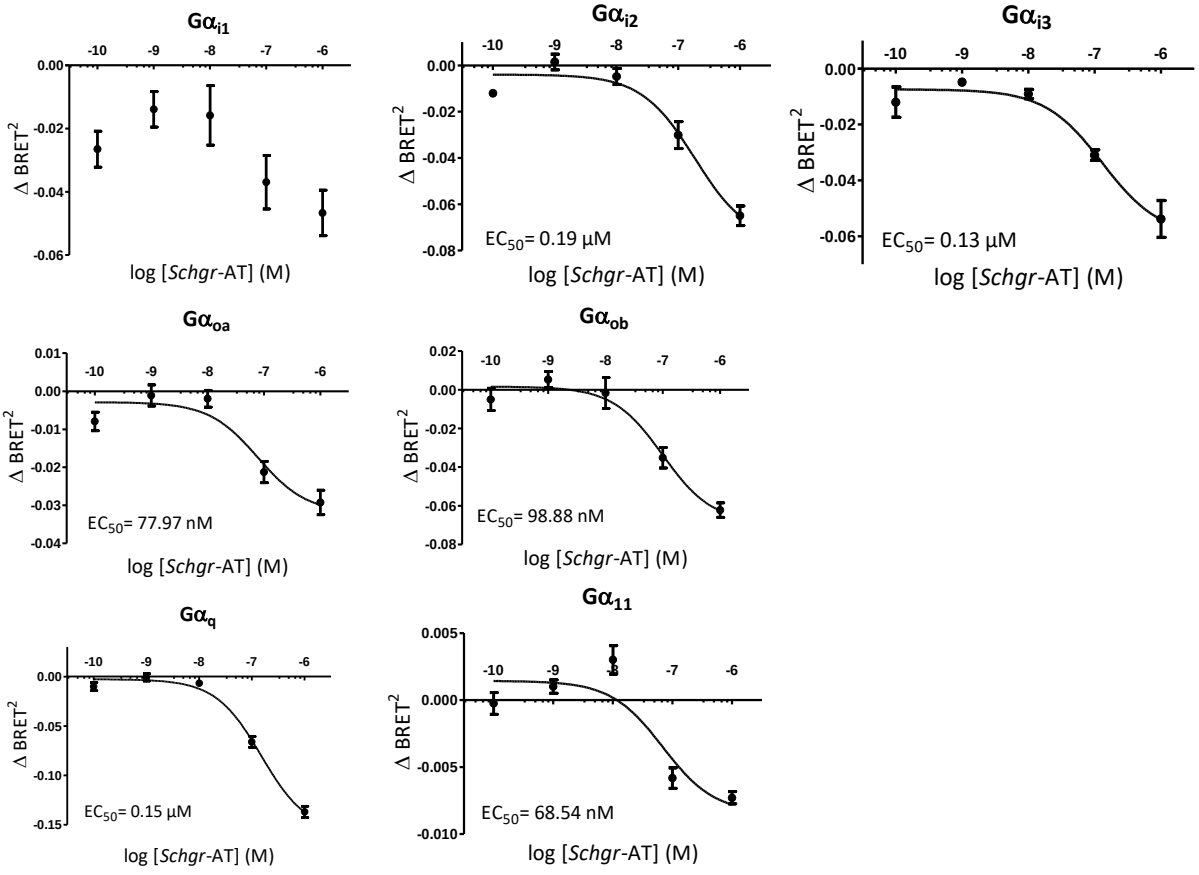

Figure 4.12: Dose-dependent resonse in HEK293T-*Schgr*-ATR cells co-transfected with $BRET^2$-based G protein biosensors consisting of $G\beta_1$, $G\gamma_2$-GFP10 and several Gα subunits upon stimulation of 0.01 nM – 1 µM *Schgr*-AT. The data represent the means ± S.E.M of three independent transfections measured in duplicate per concentration of *Schgr*-AT. The EC_{50} value is indicated in case a dose-dependent reaction is observed.

For the $G\alpha_s$, the only biosensor of the $G\alpha_s$ subfamily that is tested, no activation of the Gα protein is observed (Fig. 4.13). When comparing the magnitude of the $\Delta BRET^2$ signal with the magnitude of the $\Delta BRET^2$ signal detected with the *H. sapiens* β2-adrenergic receptor (*Homsa*-β2-AR; Fig. 3.11, right; Saulière et al., 2012), a receptor know to activate the $G\alpha_s$ proteins, no decrease in $\Delta BRET^2$ signal is detected upon stimulation of HEK293T-*Schgr*-ATR with *Schgr*-AT.

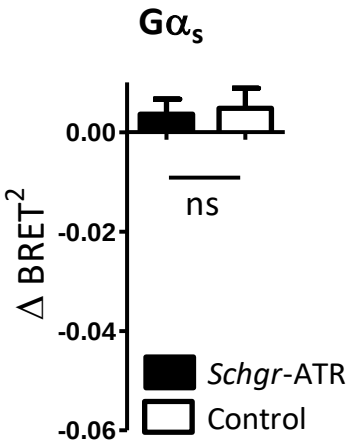

Figure 4.13: Results of the HEK293T-*Schgr*-ATR cells (*Schgr*-ATR) and HEK293T cells (Control) co-transfected with $BRET^2$-based G protein biosensors consisting of $G\beta_1$, $G\gamma_2$-GFP10 and a Gα belonging to the **$G\alpha_s$ subfamily** upon stimulation with 1 µM *Schgr*-AT. The data represent the means ± S.E.M of $\Delta BRET^2$ measured in triplicate in two independent transfections.

Additionally, for both Gα biosensors of the $G\alpha_{q/11}$ subfamily, a significant reduction is detected in the HEK293T-*Schgr*-ATR cells compared to the control cells upon stimulation with *Schgr*-AT (Fig. 4.14). However, the magnitude of the $\Delta BRET^2$ signal is lower than the magnitude of the $\Delta BRET^2$ signal detected with the *H. sapiens* angiotensin II type 1 receptor (*Homsa*-AT1R; Fig. 3.12, B; Saulière et al., 2012), a receptor known to activate $G\alpha_{q/11}$ proteins. The decrease in $\Delta BRET^2$ signal is dose-dependent for both biosensors with an EC_{50} value in the high nanomolar range (Fig. 4.12) suggesting activation of these biosensors.

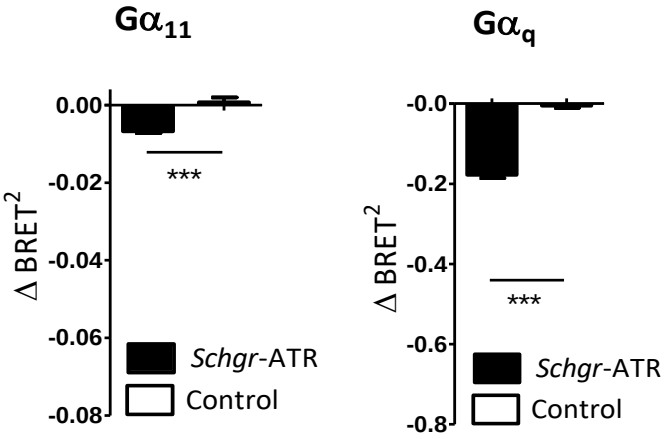

Figure 4.14: Results of the HEK293T-*Schgr*-ATR cells (*Schgr*-ATR) and HEK293T cells (Control) co-transfected with BRET²-based G protein biosensors consisting of $G\beta_1$, $G\gamma_2$-GFP10 and a Gα belonging to the **$G\alpha_{q/11}$ subfamily** upon stimulation of 1 µM *Schgr*-AT: on the **left** the results of the $G\alpha_{11}$ biosensor is depicted and on the **right** the results of the $G\alpha_q$ biosensor is depicted. The data represent the means ± S.E.M of $\Delta BRET^2$ measured in triplicate in two independent transfections. Significant differences ($p < 0.001$) are indicated by asterisks (***).

Finally, neither $G\alpha_{12}$ nor $G\alpha_{13}$ show a significant response in the HEK293T-*Schgr*-ATR cells compared to the control cells upon stimulation with *Schgr*-AT (Fig. 4.15). The $\Delta BRET^2$ signal of the $G\alpha_{12/13}$ biosensors are compared to the $\Delta BRET^2$ signal measured with the *H. sapiens* thromboxane TPα receptor (*Homsa*-TPα-R; Fig 3.13, B; Saulière et al., 2012), a receptor known to activate $G\alpha_{12/13}$ proteins.

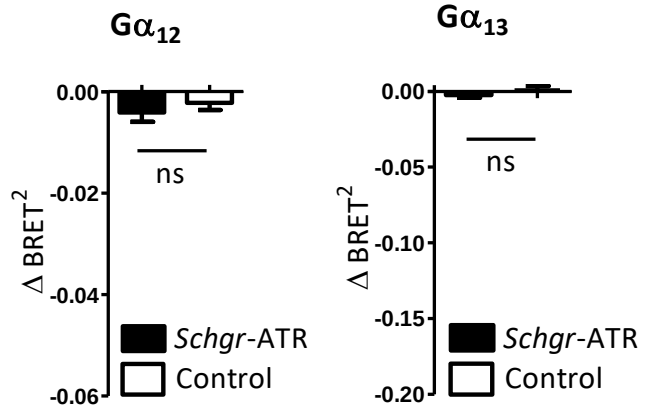

Figure 4.15: Results of the HEK293T-*Schgr*-ATR cells (*Schgr*-ATR) and HEK293T cells (Control) co-transfected with BRET²-based G protein biosensors consisting of $G\beta_1$, $G\gamma_2$-GFP10 and a Gα belonging to the **$G\alpha_{12/13}$ subfamily** upon stimulation of 1 µM *Schgr*-AT. On the **left** the results of the $G\alpha_{12}$ biosensor are depicted and on the **right** the results of the $G\alpha_{13}$ biosensor are depicted. The data represent the means ± S.E.M of $\Delta BRET^2$ measured in triplicate in two independent transfections.

4.4. Discussion

4.4.1. Sequence analysis of the precursor and the receptor and their phylogeny

In the present study, the AT precursor (*Schgr*-AT) and an AT receptor (*Schgr*-ATR) of the desert locust *S. gregaria*, are characterized. Furthermore, the nucleotide sequence of *Schgr*-ATR is completed by RACE and the deduced amino acid sequence has considerable identity with orthologous receptors from other insects. The sequence contains amino acid residues which are highly conserved among Family A GPCRs (Gether, 2000; Hauser and Grimmelikhuijzen, 2014; Venkatakrishnan et al., 2013). However, the sequence contains a DRW motif in the second intracellular loop instead of the typical DRY motif, which is important for protein stabilization and G protein activation (Oldham and Hamm, 2008), and a Y in the sixth TM region instead of the typical W, as it is the case for other AT receptors. AT and its receptor seem to be present in both hemimetabolous and holometabolous insect species, although exceptions exist. *Drosophila* appears to lack both the ligand (Hewes and Taghert, 2001; Vanden Broeck, 2001) and its receptor and a recent study has shown that ecdysis triggering hormone has taken over the role to stimulate JH synthesis (Meiselman et al., 2017). In addition, it was initially thought that the Hymenopteran insects, *A. mellifera* (Hummon et al., 2006) and *N. vitripennis* (Hauser et al., 2010) also lacked an AT-like peptide. However, after a more thorough search, a Hymenopteran AT gene is found (Veenstra et al., 2012) and subsequently, an AT receptor is characterized in the Hymenopteran species *B. terrestris* (Verlinden et al., 2013).

The ATRs show clear sequence identity to the mammalian orexin (ORX) receptors. However, the ORX and AT peptides do not display any obvious sequence identity and ORX does not activate the invertebrate receptors (Vuerinckx et al., 2011). However, Mirabeau and Joly, (2013) found evidence for a common origin of the AT and ORX precursor genes.

A Neighbor-joining tree is constructed using amino acid sequences of insect ATR-like receptors from TM1 to TM7. However, the overall insect phylogeny is not respected in the tree and, since bootstrap values already indicate that the power of some nodes is low as compared to the Lepidopteran and Hymenopteran cluster. Therefore, we conclude that in the future more ATR sequences from novel genome/transcriptome projects from diverse phylogenetic groups may result in an increase of the overall power of such phylogenetic studies. In a more recent study by Zhang and co-workers (2017) a Neighbor-joining tree is constructed with more (recent characterized) insect ATR and ATRL GPCRs, including the *Schgr*-ATR. The human OXR receptors 1 and 2 (*Homsa*-OXR1 and *Homsa*-OXR2) are used as an outgroup. In this phylogenetic analysis, the insect phylogeny seems respected. However, no bootstrap values are indicated.

4.4.2. Tissue distribution and functions of allatotropin

Schgr-AT precursor expression seems to be largely restricted to the central nervous system. This is as expected, since neuropeptides are usually produced in the nervous system and transported towards their target tissues (Caers et al., 2012). Our qRT-PCR data corresponds very well with previous immunological and mass spectrometry data obtained in the locusts *L. migratoria* (Paemen et al., 1992) and *S. gregaria* (Clynen and Schoofs, 2009; Homberg et al., 2004). Moreover, our study confirms the presence of this neuropeptide in extensive areas of the locust brain, including all neuropils in the optic lobe, the antennal lobes, and most areas in the protocerebrum. The first 'AT-related' peptide in locusts is originally purified from male accessory glands of *L. migratoria* (*Lom*-AG-MT1; Paemen et al., 1991) and is identical to *Schgr*-AT. The AT present in the male accessory glands (which show very low relative expression levels) is presumably originating from the (last) abdominal ganglia (which show high relative expression levels) since specific neuroendocrine cells in the abdominal ganglia appear to be the most abundant source of AT in other insect species (Neupert et al., 2009b; Rudwall et al., 2000; Veenstra and Costes, 1999; Veenstra et al., 1994; Veenstra et al., 2012; Zhang et al., 2017).

The *Schgr*-AT precursor shows 100- to 1000- fold higher transcript levels in the central nervous system as compared to the *Schgr*-ATR. This can be explained by the fact that neuropeptides are released in large quantities into the periphery, where they will bind to their receptors, to execute their functions. Moreover, the half-life of a peptide is expected to be shorter than the turnover rate of receptors.

The high transcript levels of ATR in the central nervous system suggest a possible role in sensory processing, learning and memory, and motor control (Elekonich and Horodyski, 2003). In the Madeira cockroach, *Leucophaea maderae*, injections of AT near the accessory medulla, which is identified as the location of the circadian clock in this cockroach and part of the optic lobes, results in changes in circadian locomotor activity (Petri et al., 2002). In *S. gregaria,* high expression levels of ATR are also measured in the optic lobes.

The ATR expression in the CA is probably related to the stimulatory role of AT on the biosynthesis and release of JH. Already in 1977, Tobe and co-workers demonstrate that an allatostimulatory factor released by the CA is responsible for the production of JH. We now also confirm that *Schgr*-AT indeed stimulates the JH production in the CA. Moreover, the AT precursor expression is significantly higher in 10 day old adult females as compared to males. This can be due to the fact that JH (regulated by AT) is demonstrated to be important in females of this age for inducing vitellogenin production and oocyte growth (Glinka and Wyatt, 1996; Pratt and Tobe, 1974; Sevala et al., 1995;

Wyatt et al., 1996). The difference in AT precursor expression was especially pronounced in the abdominal ganglia suggesting that they can be responsible for activation of the CA.

The high expression levels of *Schgr*-ATR in the Malpighian tubules are also observed in *M. sexta* and suggest that AT may have a role in osmoregulation (Horodyski et al., 2011). In *T. infestans* the Malpighian tubules are even found to release an AT-like peptide causing hindgut contractions (Santini and Ronderos, 2007; Sterkel et al., 2010). However, *Schgr*-AT transcript levels appear to be low in the Malpighian tubules of *S. gregaria* suggesting that the Malpighian tubules do not release AT in this insect.

AT seems to play a role in the digestive system since it affects the intestinal motility, as is shown in the bio-assay. In addition, the expression of the *Schgr*-ATR in the salivary glands can be related to a role in the stimulation of saliva secretion as was discovered in *R. prolixus* (Masood and Orchard, 2014). Another link that can be made with the digestive system, is the impact of the nutritional status on the transcript levels of the AT precursor. In larvae of *M. sexta* and the armyworm, *Mythimna separate,* it was shown that starvation leads to higher transcript levels of AT (Lee and Horodyski, 2002; Lee and Horodyski, 2006; Zhang et al., 2008). In larvae, starvation causes an additional molt, indicating that JH levels are elevated. This gives the larvae the opportunity to acquire additional nutrients once they become available in order to successfully complete development to a robust reproductive adult. In contrast, starvation of some insects during the adult stage inhibits oocyte maturation as a consequence of decreasing JH biosynthesis (Tobe and Chapman, 1979; Zhang et al., 2008). The overall regulation of JH titer is complex, since the CA can be influenced by multiple stimulatory and inhibitory factors, and since JH catabolism and binding to JH transport proteins also plays a major role in the control of JH titer (Lee and Horodyski, 2006).

4.4.3. Pharmacological receptor characterization and G protein mediated signaling pathways

The aequorin bioluminescence assay indicates that *Schgr*-AT activates *Schgr*-ATR *in vitro* and causes an increase in intracellular Ca^{2+} levels with an EC_{50} value in the nanomolar range. This result is in line with all pharmacological characterizations of ATRs in other insects. Upon activation by endogenous AT, the AT(L)Rs of *M. sexta*, *T. castaneum* and *B. terrestris* also stimulate intracellular Ca^{2+} levels (Horodyski et al., 2011; Vuerinckx et al., 2011; Verlinden et al., 2013).

The CRE-dependent luciferase assay suggests that stimulation of *Schgr*-ATR by *Schgr*-AT in HEK293 cells causes an increase in intracellular cAMP levels with an EC_{50} value in the nanomolar range. This is in contrast with the results of the CAMYEL biosensor in which *Schgr*-ATR signaling seems to be independent from the AC/cAMP/PKA pathway since no difference in $BRET^1$ signal is measured when

Schgr-ATR is stimulated by *Schgr*-AT in HEK293T cells. All previous studies with pharmacological characterizations of ATRs in *M. sexta*, *T. castaneum* and *B. terrestris* suggested an increase of intracellular cAMP levels upon receptor activation (Horodyski et al., 2011; Vuerinckx et al., 2011; Verlinden et al., 2013). However, all these measurements are performed in our lab with the $CRE_{(6x)}$-Luc construct. Since the measurement of the bioluminescence in the CRE-dependent luciferase reporter assay is dependent on a CRE and thus dependent on the phosphorylation of CREB. However, it has been speculated that a change in bioluminescence may also be caused by Ca^{2+}, since CREB can also be phosphorylated by calcium/calmodulin-dependent protein kinase (Johannessen et al., 2004).

Recently, an additional ATR is pharmacologically characterized in *H. armigera* (Zhang et al., 2017) and, in line with our results and ATRs in other insects, an increase in intracellular Ca^{2+} is detected upon activation of *Helar*-ATR by *Helar*-AT, *Helar*-ATLI, *Helar*-ATLII and *Helar*-ATLIII with EC_{50} values in the micromolar range for *Helar*-AT and *Helar*-ATLIII, and in the nanomolar range for *Helar*-ATLI and *Helar*-ATLII. By using the cAMP-Glo from Promega in HEK293 cells, the conclusion is made that *Helar*-ATR signaling is independent from the cAMP signaling pathway. This result is in line with our results using the CAMYEL biosensor but is not supported by our results using the $CRE_{(6x)}$-Luc construct. Since the CAMYEL interacts directly with cAMP and since it is speculated that CRE-dependent luciferase reporter assay can be influenced by Ca^{2+}, the CAMYEL biosensor seems a more reliable method for verifying receptor coupling to the AC/cAMP/PKA pathway than the CRE-dependent luciferase assay.

Additionally, the downstream G protein mediated signaling pathways are studied in more detail using $BRET^2$-based G protein biosensors which can measure a direct activation of the G protein. To interpret the results obtained in this assay, the (unpublished) *S. gregaria* transcriptome database is screened in order to find G protein subunit sequences by means of a local blast. Five Gα (*Schgr*-$G\alpha_i$, *Schgr*-$G\alpha_o$, *Schgr*-$G\alpha_s$, *Schgr*-$G\alpha_q$ and *Schgr*-$G\alpha_{12/13}$), two Gβ (*Schgr*-$G\beta_1$ and *Schgr*-$G\beta_2$) and two Gγ (*Schgr*-$G\gamma_1$ and *Schgr*–$G\gamma_2$) subunit sequences are identified. The amino acid sequences of the *S. gregaria* Gα subunit are relatively similar to the vertebrate Gα subunit sequences of the $BRET^2$-based G protein biosensors, except for the $G\alpha_{12/13}$ subfamily. *Schgr*-$G\beta_1$ seems to be more related to the *Homsa*-$G\beta_1$ than *Schgr*-$G\beta_2$ while neither *Schgr*-$G\gamma_1$ nor *Schgr*–$G\gamma_2$, respectively, is showing strong sequence identity with the *Homsa*-$G\gamma_2$.

Both $G\alpha_q$ and $G\alpha_{11}$ biosensors are activated since a dose-dependent response is measured upon stimulation of *Schgr*-AT. This result is completely in line with our results in this chapter, using the aequorin bioluminescence assay (without the $G\alpha_{16}$ protein).

Surprisingly, a dose-dependent decrease in $\Delta BRET^2$ signal is observed for four out of five biosensors of the $G\alpha_{i/o}$ subfamily, but not for the $G\alpha_s$ biosensor, suggesting activation of $G\alpha_{i/o}$ proteins. These results are not supported by the CRE-dependent luciferase (which indicates an increase in intracellular cAMP levels upon activation of the receptor) nor the CAMYEL biosensor (which suggest no change in intracellular cAMP levels upon activation of the receptor). However, it should be noted that the $G\alpha_{i/o}$ subfamily may also influence other effectors such as phospholipases (Dorsam and Gutkind, 2007) and thus may influence other secondary messenger molecules such as Ca^{2+}. Therefore, activation of this subfamily does not necessarily result in a decrease in intracellular cAMP levels. Finally, no activation of both Gα biosensors of the $G\alpha_{12/13}$ subfamily is detected.

As mentioned earlier, these $BRET^2$-based G protein biosensors are also used to verify which Gα subunit within a Gα subunit family can be activated. However, since only one $G\alpha_i$ and one $G\alpha_o$ subunit sequence are identified in *S. gregaria*, knowing which $G\alpha_i$ or $G\alpha_o$ biosensor is activated has no added value for understanding the *in vivo* situation. The same goes for the $G\alpha_{q/11}$ biosensors since only one $G\alpha_q$ protein is identified in *S. gregaria.*

Concerning the use of the $BRET^2$-based G protein biosensors to detect signaling of this insect GPCR we make five observations: (1) four out of five biosensors of the $G\alpha_{i/o}$ subfamily and both biosensors of the $G\alpha_{q/11}$ subfamily respond to the insect receptor *Schgr*-ATR, (2) the results of both $G\alpha_q$ and $G\alpha_{11}$ biosensors are in accordance with the aequorin bioluminescence assay, (3) the results of $G\alpha_{i/o}$ biosensors are not supported by the results of both cAMP-dependent reporter assays ($CRE_{(6x)}$-Luc and CAMYEL), and (4) the results obtained with the $G\alpha_s$ biosensor are in accordance with the results obtained with the CAMYEL biosensor. Finally, (5) no activation of both Gα biosensors of the $G\alpha_{12/13}$ subfamily is detected. Notably, the results of the $G\alpha_{12}$ and $G\alpha_{13}$ biosensors are not confirmed by studying more downstream signaling pathways.

Chapter 5:
Characterization of a CRF-related diuretic hormone receptor and its G protein mediated signaling pathways in *Schistocerca gregaria*

The dissections were assisted by Katleen Crabbé, Dr. Darron Cullen, Michiel Holtof, Dr. Cynthia Lenaerts, Dr. Elisabeth Marchal, Dr. Dulce Santos, Dr. Jornt Spit, Dr. Pieter Van Wielendaele and Dr. Heleen Verlinden, and RNA extractions were executed by Toon Wullaert.

5.1. Introduction

Corticotropin-releasing factor (CRF)-related diuretic hormone (DH) is initially isolated in the tobacco hornworm, *Manduca sexta,* (Kataoka et al., 1989) and is named after its first known biological activity, namely the ability to stimulate diuresis. This process is executed by the excretory system (absorption of water and the excretory system in insects, Box 5.1) in which CRF-DH stimulates the primary urine secretion in the Malpighian tubules (Coast et al., 1993; Kay et al., 1991a; Lehmberg et al., 1991; Patel et al., 1995).

Box 5.1: Absorption of water and the excretory system in insects

Transport of water takes place in different parts of the digestive tract in order to enhance both efficiency of digestion and absorption of nutrients, as well as to control water balance in the animal. The excretory system of insects, which removes potential toxic wastes from the body, comprises the Malpighian tubules and the hindgut. In the Malpighian tubules, primary urine is secreted executing the unselective removal of substances from the hemolymph. Water and useful components are reabsorbed in the hindgut while other toxic wastes are added to the lumen (Chapman, 2012; Patel et al., 1995). A schematic representation of the absorptive and excretory cycles in the alimentary canal is presented in Fig. 15.1.

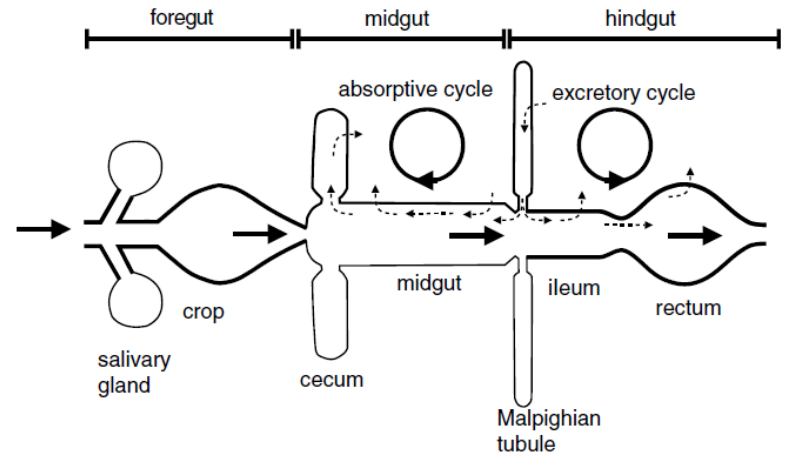

Figure 15.1: Schematic representation of the absorptive and excretory cycles of water in the alimentary canal. Heavy arrows indicate the path of food while the dotted lines show cycles of fluid movements. (Image credits: Chapman, 2012)

Since CRF-DH consists of 44 amino acids in the fruit fly, *Drosophila melanogaster*, an insect in which the physiological role is extensively studied, it's also often referred to as DH44. Over the last three decades, CRF-DH neuropeptides have been isolated or predicted *in silico* in several insect species. CRF-DHs usually consist of 30-54 amino acids and are categorized in long CRF-DHs (more than 40 residues) and short CRF-DHs (less than 40 residues; Blackburn et al., 1991; Coast, 1998). They are

usually amidated neuropeptides, with an exception for the yellow mealworm, *Tenebrio molitor*, in which two non-amidated CRF-DHs are identified (Wiehart et al., 2002). An overview of all predicted and characterized CRF-DH and DH44 peptides in insects can be found in the Database for Insect Neuropeptide Research (DINeR; Yeoh et al., 2017).

The stimulatory effect on fluid secretion in the Malpighian tubules is proven in numerous insects (Audsley et al., 1995; Cabrero et al., 2002; Clottens et al., 1994; Coast et al., 1993; Coast and Kay, 1994; Donini et al., 2008; Holtzhausen and Nicolson, 2007; Iaboni et al., 1998; Kataoka et al., 1989; Kay et al., 1991a; 1991b; 1992; Lehmberg et al., 1991; Patel et al., 1995; Te Brugge et al., 1999; Te Brugge and Orchard, 2002;). The production of primary urine is dependent on cAMP, which increases cationic transport (such as K^+ and Na^+) into the Malpighian tubules (Beyenbach, 1995; O'Donnell et al., 1996). Furthermore, cAMP is identified to act as an intracellular second messenger of CRF-DH in numerous insects (Audsley et al., 1995; Baldwin et al., 2001; Cabrero et al., 2002; Clottens et al., 1994; Coast et al., 1991; 1993; 2010; 2011; Coast and Kay, 1994; Furuya et al., 1998; Kay et al., 1991a; 1991b; 1992; Lehmberg et al., 1991; Morgan et al., 1987; Patel et al., 1995; Te Brugge et al., 1999; Te Brugge and Orchard, 2002; Tobe et al., 2005).

In addition to the stimulatory role in diuresis, CRF-DH appears to play an important role in other physiological functions outside the excretory system as well. For instance, in the desert locust, *Schistocerca gregaria*, physiological studies *in vivo* have shown that CRF-DH has an inhibitory effect on both feeding and reproduction (Van Wielendaele et al., 2012). Injections of this neuropeptide cause a significantly reduced food intake while an RNA interference (RNAi) knockdown shows to have the opposite (*i.e.* stimulatory) effect. These finding suggest that this neuropeptide may induce satiety. Studies in another locust species, the migratory locust, *Locusta migratoria,* reveal that CRF-DH levels increase fivefold (from 0.22 nM in starved locust to 1.5 nM) in fed locusts and also appear to induce satiety, since this neuropeptide is responsible for an increase in the latency of feeding (the period in which the locust starts to eat) and a decrease in the duration of the meals (Audsley et al., 1997; Goldsworthy et al., 2003). Additionally, *S. gregaria* females injected with *Schgr*-CRF-DH show retarded oocyte growth and lower ecdysteroid titers in the hemolymph and ovaries (Van Wielendaele et al., 2012; the female reproductive system, Box 5.2). A subsequent RNAi knockdown results again in the opposite (*i.e*. stimulatory) effect.

Box 5.2: The female reproductive system

The female reproductive system contains the ovaries, lateral oviducts, median oviduct, the accessory glands and the spermatheca. Oogenesis takes place in the panoistic ovaries which consist of ovarioles. Upon ovulation, mature oocytes are directed towards the median oviduct through the lateral oviducts. Fertilization of the eggs occurs when the oocytes pass the opening of the spermatheca in which sperm is stored (Chapman, 2012; Uvarov, 1966).

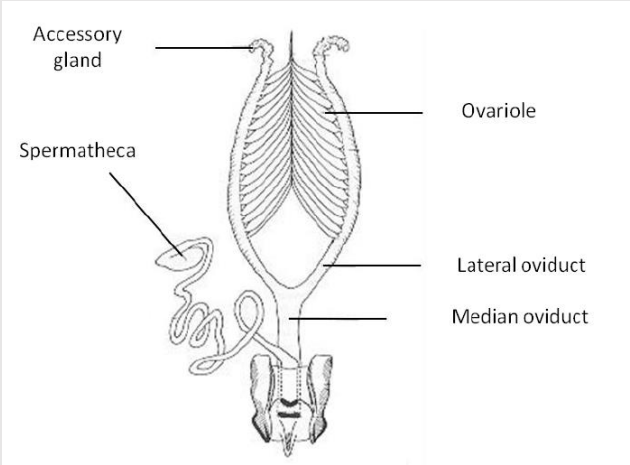

Figure 15.2: The female reproductive system. (Image credits: CIRAD: French Agricultural Research Centre for International Development, 2007; adapted by Van Wielendaele, 2012)

Notably, the two identified *Schgr*-CRF-DH precursor cDNA sequences also encode ovary maturating parsin (OMP), a neurohormone that only appears to be present in the family of the Acrididae, to which *L. migratoria* and *S. gregaria* belong (Richard et al., 1994). This neurohormone stimulates oocyte growth, vitellogenesis and increases hemolymph ecdysteroid levels in adult female *S. gregaria* locusts (Girardie et al., 1998). However, since experiments by Van Wielendaele and co-workers (2012) are not only performed by RNAi assays but also by injection studies with *Schgr*-CRF-DH itself, the physiological effects observed in this study are presumably an action of *Schgr*-CRF-DH and not by *Schgr*-OMP. Notably, OMP is suggested to be a monitoring peptide triggering negative feedback effects.

Additional studies have shown that, also in other insects; CRF-DH is involved in feeding and reproduction. In the kissing bug, *Rhodnius prolixus*, an increase of CRF-DH is measured in the hemolymph in response to a bloodmeal (Lee et al., 2016) and when fifth instars and adults are injected with *Rhopr*-CRF-DH, the intake of a blood meal is smaller (Mollayeva et al., 2018). Furthermore, injected females lay fewer eggs and an *in vitro* assay shows that contractions of the lateral oviducts are inhibited. Additionally, CRF-DH also stimulates the absorption of water in the anterior midgut (Te Brugge et al., 2009) and stimulates contractions of the hindgut (Bhatt et al.,

2014). In another insect, the house cricket, *Acheta domesticus,* CRF-DH stimulates contractions of the foregut and increases cAMP production in this tissue (Blake et al., 1996). When neonates of *M. sexta* are fed with the synthetic diuresin, they show a reduction of food consumption, slower growth, reduced developmental rates, and a high percentage even fails to molt into the second larval phase (Ma et al., 2000). In *D. melanogaster*, CRF-DH (DH44) is involved in the detection and regulation of nutritive sugars (Dus et al., 2015), and DH44 expressing neurons act as a sensor which detects three specific dietary amino acids and promotes food intake (Yang et al., 2018). However, if DH44 signaling is involved in the latter remains unclear (Chen and Dahanukar, 2018).

Other physiological functions of DH44 outside the digestive and reproductive systems have been identified in *D. melanogaster* as well. DH44 appears to regulate rhythmic locomotor activity (Cavanaugh et al., 2014; Cavey et al., 2016), sperm retention and storage in the uterus (Lee et al., 2015) and improves desiccation tolerance (Cannell et al., 2016). Moreover, the increase in resistance to desiccation, starvation and ionic stress, and additionally, a reduced food intake, are also observed when a downregulation of DH44 is only established in a portion of the leucokinin (LK)-expressing neurosecretory cells (ABLKs) in the abdominal ganglia. Surprisingly, the increase in resistance to desiccation and the decrease in food intake are not observed when a DH44 knockdown is establish in all DH44 neurons (Zandawala et al., 2018). Similarly, Dus and co-workers (2015) also do not observe an effect on food intake when DH44 neurons are inactivated or activated. Finally, Zandawala and co-workers (2018) observe an additive effect on fluid secretion in the Malpighian tubules of DH44 and LK. Notably, also in the spotted wing fruit fly *Drosophila suzukii*, DH44 is involved in cold and desiccation tolerance (Terhzaz et al., 2018).

CRF-DHs exert effects on their cellular targets by binding with high affinity to receptors that are members of the secretin receptor-related G protein-coupled receptor (GPCR) family (Family B). The first insect CRF-DH receptor (CRF-DHR) is characterized *in cellulo* in *M. sexta* (Reagan, 1995) and other CRF-DHRs are subsequently characterized *in cellulo* in *A. domesticus* (Reagan, 1996), *R. prolixus.* (Lee et al., 2016) and *D. melanogaster*. In the latter species, two CRF-DHRs are identified (*Drome*-DH44-R1, Johnson et al., 2004; and *Drome*-DH44-R2, Hector et al., 2009). Based on sequence identity, CRF-DHRs are also characterized in the yellow fever mosquito, *Aedes aegypti,* (Jagge and Pietrantonio, 2008) and the silkworm, *Bombyx mori* (Ha et al., 2000). CRF/DHRs are also predicted *in silico* in the red flour beetle, *Tribolium castaneum*, the pea aphid, *Acyrthosiphon pisum*, the African malaria mosquito, *Anopheles gambiae*, the honey bee, *Apis mellifera*, the jewel wasp, *Nasonia vitripennis* and others (Caers et al., 2012).

All *in cellulo* characterized CRF-DHRs evoke an increase in intracellular cAMP levels upon stimulation by their agonist (Hector et al., 2009; Johnson et al. 2004; Lee et al., 2016; Reagan, 1995;1996). When stimulated by four other CRF-DHs, *Manse*-CRF-DHR evokes equal levels of intracellular cAMP, whereas cAMP levels are less high when *Achdo*-CRF-DHR is stimulated by four CRF-DHs other than its endogenous CRF-DH (Reagan, 1996). Additionally, an N-terminally truncated analog (13-41) of *Manse*-DH is able to bind to *Manse*-CRF-DHR but does not stimulate cAMP synthesis. This leads to the conclusion that the N-terminus is required for receptor activation but not for receptor binding (Reagan, 1995). Activation of both *Drome*-DH44-R1 and *Drome*-DH44-R2 induce a translocation of β-arrestin to the plasma membrane and activation of the former also evokes an increase of intracellular Ca^{2+} concentrations, although higher concentrations (EC_{50} = 300 nM) are needed. However, this is not observed with *Drome*-DH44-R2 (Hector et al., 2009). Notably, *Rhopr*-CRF-DHR2B (Lee et al., 2016) also does not influence the PLC/Ca^{2+} pathway.

Similarly as in *D. melanogaster*, two CRF-DHRs are identified in *A. aegypti, A. pisum, R. prolixus and T. castaneum* (Caers et al., 2012; Hector et al., 2009; Jagge and Pietrantonio, 2008; Johnson et al. 2004; Lee et al., 2016). However, since *Rhopr*-CRF-DH-R2A encodes a protein comprising only six TM domains and lacks TM5, only *Rhopr*-CRF-DH-R2B is further characterized (Lee et al., 2016). Hector and co-workers (2009) already point out that having two CRF-DHRs can indicate functional differences between these two receptors. These functional differences are pronounced in both receptor signaling and the physiological roles of the receptor. For instance, *Drome*-DH44-R2 is much more sensitive to *Drome*-DH44 than *Drome*-DH44-R1 and sensitivity of the latter to evoke a translocation of arrestin to the transmembrane is rather low. Furthermore, downregulation of *Drome*-DH44-R2 by RNAi results in a higher sensitivity to osmotic challenges in *D. melanogaster*. This agrees with the fact that expression of *Drome*-DH44-R2 is 200-fold higher in the Malpigian tubules than *Drome*-DH44-R1 (Hector et al., 2009). Over the last years, additional functions of the DH44-Rs have been identified. For instance, *Drome*-DH44-R1 is responsible for sperm retention and storage in the uterus (Lee et al., 2015) and regulation of rhythmic locomotor activity, but is not involved in circadian feeding rhythms (King et al., 2017). A downregulation of *Drome*-DH44-R2 increases desiccation tolerance and impairs starvation tolerance (Cannell et al., 2016).

Relative expression levels of CRF-DHRs are studied in other insects besides *D. melanogaster* as well. In *A. aegypti*, relative transcript levels of one of the two identified CRF-DHRs (GRPDIH1) are high in the Malpighian tubules and increase after a blood meal (Jagge and Pietrantonio, 2008). In addition, in fifth instar *R. prolixus*, relative expression levels of *Rhopr*-CRF-DH-R2B are highest in the immature testes. A closer look into the reproductive system reveals that the expression levels are high in the

male testes of both fifth instars and adults, but not in the adult accessory glands. Relative expression levels are also high in the adult female ovaries. Furthermore, *Rhopr*-CRF-DH-R2B is expressed in many other tissues, including the foregut, the dorsal vessel, the CNS and the fat body.

As indicated by its name, CRF-DH is related to the vertebrate corticotropin-releasing hormone (CRH), also designated as corticotropin-releasing factor (CRF), a neurohormone involved in stress responses, including physiological responses in behavior, food intake and reproduction (Majzoub, 2006). The CRF superfamily includes CRF, urotensin-1/urocortin/sauvagine, urocortin 2, urocortin and CRF-DHs (Lovejoy and Barsyte-Lovejoy, 2010). The latter are also found in molluscs, annelids and in a platyhelminth. The evolutionary link with CRH is supported by evolutionary studies which imply that the deuterostome CRH receptor (CRHR) and the protostome CRF-DHR or DH44R are orthologues and evolved from a single bilaterian ancestral gene. These studies also imply that more recent gene duplication events arose independently in insects, molluscs and vertebrates (Cardoso et al., 2014). Notably, also the peptide itself seems to be inherited by vertebrates as a single peptide instead of in duplicate (Lovejoy and Barsyte-Lovejoy, 2010).

In *S. gregaria*, a member of the Orthoptera well-known for its extreme form of density dependent polyphenism, three putative CRF-DH receptors (*Schgr*-CRF-DHR1, *Schgr*-CRF-DHR2 and *Schgr*-CRF-DHR3) are predicted from an (unpublished, in-house) transcriptome database (Verdonck, 2017). As mentioned earlier, two *Schgr*-CRF-DH precursor cDNA sequences have already been identified by Van Wielendaele and co workers (2012). These CRF-DH precursor sequences are mainly expressed in the central nervous system (CNS) with highest expression levels in the brain. We now complement these data with a quantitative analysis of receptor transcripts of two receptor sequences (*Schgr*-CRF-DHR1 and *Schgr*-CRF-DHR2) in a variety of tissues of immature and mature adult gregarious *S. gregaria* locusts.

Additionally, one of the three predicted CRF-DH receptors (*Schgr*-CRF-DHR1) is cloned and pharmacologically characterized. The G protein mediated downstream signaling pathways are studied by means of the aequorin bioluminescence assay and the bioluminescence resonance energy transfer (BRET)^{1}-based ‘cAMP sensor using YFP-Epac-*R*luc’ (CAMYEL; ATCC MBA-277) biosensor. Finally, a direct activation of the G-proteins is measured using BRET^{2}-based biosensors (Galés et al., 2006).

5.2. Materials and methods

5.2.1. Sequence analysis of *Schgr*-CRF-DHR1, *Schgr*-CRF-DHR2 and *Schgr*-CRF-DHR3

At the start of this project, nucleotide sequences of two putative CRF-DH receptors (*Schgr*-CRF-DHR1 and *Schgr*-CRF-DHR2) are identified by means of a local BLAST scanning the (unpublished) transcriptome database of *S. gregaria* by using amino acid sequences of previously characterized *Drome*-DH44-R1 and *Drome*-DH44-R2 as a query (Johnson et al., 2004; Hector et al., 2009). A local BLAST performed in a filtered, new assembly of the (unpublished, in-house) transcriptome database of *S. gregaria* identified an additional third putative receptor sequence, *Schgr*-CRF-DHR3 (Verdonck, 2017).

The nucleotide sequences of the three putative *Schgr*-DHRs are compared in a multiple sequence alignment and a percent identity matrix [of the full open reading frame (ORF)] is constructed as described in section 2.6. Additionally, amino acid sequences of the three putative *Schgr*-CRF-DHRs are compared with amino acid sequences of other *in cellulo* characterized CRF-DHRs of insects: *D. melanogaster* (*Drome*-DH44-R1; GenBank acc. no. NP_610960.1, and *Drome*-DH44-R2; GenBank acc. no. NP_610789.3), *R. prolixus* (*Rhopr*-CRF-DHR2B; GenBank acc. no. KJ407397), *M. sexta* (*Manse*-CRF-DHR; GenBank acc. no. AAC46469.1) and *A. domesticus* (*Achdo*-CRF-DHR; GenBank acc. no AAC47000.1). Again, a multiple sequence alignment and a percent identity matrix (using sequences from TM1 up to and including TM7) are constructed as described in section 2.6.

5.2.2. Rearing and dissection of the animals

For this study, gregarious male and female tissues from both immature and mature locusts are collected since CRF-DH plays a role in reproduction in this locust species (Van Wielendaele et al., 2012). To do so, *S. gregaria* locusts are reared as described in section 2.1. The locusts are synchronized on the day of ecdysis into the adult stage and placed in separate cages per day. Immature males and females are dissected when they are three days into the adult stage. Brain, optic lobes, salivary glands, ventral nerve cord, gonads, fat body, flight muscle, foregut, caeca, Malpighian tubules, midgut, hindgut, male accessory glands and a piece of the cuticle are dissected under a binary microscope and collected in 2.0 ml tubes containing MagNa Lyser green beads (Roche). Additionally, the corpora cardiaca, corpora allata, the prothoracic gland, the frontal ganglion and the suboesophageal ganglion are collected in RNase-free Screw Cap Micro centrifuge tubes. For the mature samples, the same tissues are collected. However, mature males are dissected when they are 12 – 13 days old and are yellow colored (which is an indication of gregarious male maturity) and mature females are dissected when they are 10 – 13 days old and appear to be into

the vitellogenic stage of ovarian maturation. During this stage the oocyte size strongly increases from 1.7 to 7 mm and oocytes start showing a yellow colour (Tobe and Pratt, 1975). Therefore, tissues are only collected from females with oocyte sizes ranging from 3 to 6 mm. For each tissue in each condition, four pools are dissected consisting of eight animals each. All samples are immediately snap frozen in liquid nitrogen. Until further processing, the samples are stored at -80 °C to protect the tissues from degradation.

5.2.3. RNA extraction and cDNA synthesis

RNA extractions of the tissues collected in the 2.0 ml tubes containing MagNa Lyser green beads are performed utilizing the RNeasy Lipid Tissue Mini Kit (Qiagen, Germantown, MD) as described in section 2.2.1. In contrast, RNA extractions of the tissues collected in the RNase-free Screw Cap Microcentrifuge tubes are executed using the RNAqueous-Micro Kit (Ambion) according to the manufacturer's protocol including the recommended DNase step. Verification of the RNA quantity and quality is performed by using a Nanodrop spectrophotometer (Thermo Fisher Scientific Inc.). cDNA of all samples is synthesized using the PrimeScript RT reagent Kit (Perfect Real Time) from TaKaRa according to the manufacturer's instructions using random hexamers and oligodT primers. Finally, the resulting cDNA is diluted tenfold.

5.2.4. Study of the relative transcript levels using qRT-PCR

By means of qRT-PCR the relative transcript levels of *Schgr*-CRF-DHR1 and *Schgr*-CRF-DHR2 are measured in a variety of tissues. The number of reference genes necessary to calculate the normalization factor (the geometric mean of the stable reference genes) are selected using the qBase+ software v. 2.4 [Biogazelle; based on the proven GeNorm (Vandesompele et al., 2002) and qBase (Hellemans et al., 2007) technology]. This program also indicates which reference genes are the most stable and should be included in the calculation of the normalization factor. The following candidate reference genes are tested: α-tubulin1A, β-actin, CG13220, EF1α, GADPH, ribosomal protein 49 (RP49) and ubiquitin conjugating enzyme 10 (Ubi) (Van Hiel et al., 2009). Primer sequences of these reference genes are enlisted in table 5.1. GADPH, Ubi and CG13220 are selected as the most stable reference genes to calculate NF_3.

Table 5.1: Oligonucleotide primers of candidate reference genes used in qRT-PCR.

Reference genes	Forward primer	Reverse primer
Schgr-α-tubulin1A	5'-TGACAATGAGGCCATCTATG-3'	5'-TGCTTCCATACCCAGGAATGA-3'
Schgr-β-actin	5'-AATTACCATTGGTAACGAGCGATT-3'	5'-TGCTTCCATACCCAGGAATGA-3'
Schgr-CG13220	5'-TGTTCAGTTTTGGCTCTGTTCTGA-3'	5'-ACTGTTCTCCGGCAGAATGC-3'
Schgr-EF1α	5'-GATGCTCCAGGCCACAGAGA-3'	5'-TGCACAGTCGGCCTGTGAT-3'
Schgr-GADPH	5'-GTCTGATGACAACAGTGCAT-3'	5'-GTCCATCACGCCACAACTTTC-3'
Schgr-RP49	5'-CGCTACAAGAAGCTTAAGAGGTCAT-3'	5'-CCTACGGCGCACTCTGTTG-3'
Schgr-Ubi	5'-GACTTTGAGGTGTGGCGTAG-3'	5'-GGATCACAAACACAGAACGA-3'

Abbreviations: *Schgr* = *Schistocerca gregaria*, EF1α = elongation factor 1 α, GADPH = glyceraldehyde-3-phosphate dehydrogenase, RP49 = ribosomal protein 49, Ubi = ubiquitin conjugating enzyme 10

Since most of the previous experiments involving *Schgr*-DH are performed in females (Van Wielendaele et al., 2012) and no significant differences are observed in *Schgr*-DH expression levels between males and females, the tissue distribution analysis is only performed in females. However, two tissue samples derived from the male reproductive system, namely the accessory glands and the male gonads, are also included in the assay. Samples of both stages of maturation are tested since *Schgr*-DH appears to be involved in female reproduction.

Primers for the target genes *Schgr*-CRF-DHR1 and *Schgr*-CRF-DHR1 are designed as described in section 2.3.2. A standard curve is constructed using a serial fivefold dilution of brain cDNA. Primer sequences of target genes are enlisted in table 5.2.

Table 5.2: Oligonucleotide primers of target genes used in qRT-PCR.

Target genes	Forward primer	Reverse primer
Schgr-CRF-DHR1	5'-GCTGCTACTGCACTACTT-3'	5'-AGGCGCTGAGTTGTATATT-3'
Schgr-CRF-DHR2	5'-CCGTCACGATCTTCCTATAC-3'	5'-CAGTCAGAATCCACCAGAA-3'

Abbreviations: *Schgr* = *Schistocerca gregaria* and CRF-DHR = Corticotropin-releasing factor -related diuretic hormone receptor

PCR reactions are performed in a 15 µl reaction volume following the manufacturer's instructions as described in section 2.3.1. Measurements are performed in duplicate with three independent biological pools of adult *S. gregaria* tissues consisting of eight animals each. Additionally, PCR products are analyzed via agarose gel electrophoresis. The resulting single band of the expected size for each transcript is sequenced. No amplification of the fluorescent signal is detected in any negative control sample, proving that the extraction procedure, including the DNase treatment, effectively removed genomic DNA from all the RNA samples and that there is no contamination.

For accurate normalization, the relative transcript levels are calculated using the delta-delta Ct method as described in section 2.3.3 in which a mix of all samples is used as the calibrator sample. Statistical analysis is performed by means of GraphPad Prism 5 (GraphPad Software Inc.), using the

Mann-Whitney U test for comparing two independent groups. A level of $P < 0.05$ is considered significant.

5.2.5. Molecular cloning of *Schgr*-CRF-DHR1 and partial fragments of *Schgr*-CRF-DHR2

The ORF of *Schgr*-CRF-DHR1 is amplified by a PCR reaction on a sample of cDNA of brains by means of a Pwo DNA Polymerase (Roche). The nucleotide sequences of the specific forward primer, containing the CACC Kozak sequence at the 5' side to facilitate translation in mammalian cells (Kozak, 1986), and the specific reverse primer, are enlisted in table 5.3. According to the manufacturer's protocol, the final concentration of the primers is 500 nM. The following PCR program is used: an initial denaturation of 94 °C followed by 30 cycles of 94 °C for 45 s for denaturation, an annealing step of 60 seconds at 61 °C and an elongation at 72 °C for 120 s. After a final elongation at 72 °C for 10 min the program is paused at 10 °C.

Additionally, two partial fragments of *Schgr*-CRF-DHR2 are amplified by a PCR reaction on a sample of cDNA of Malpighian tubules by means of a Q5 High-Fidelity DNA Polymerase (New England BioLabs Inc.). The nucleotide sequences of the primers are also enlisted in table 5.3 (final concentration 500 nM). Notably, the primer sequences include a T7 promoter sequence at the 5' site. The following PCR program is used: an initial denaturation of 98 °C followed by 29 cycles of 98 °C for 20 s for denaturation, an annealing step of 30 seconds at 66 °C and an elongation at 72 °C for 30 s. After a final elongation at 72 °C for 2 min the program is paused at 10 °C.

Table 5.3: Oligonucleotide primers for PCR.

Target genes	Forward primer	Reverse primer
Schgr-CRF-DHR1	5'-CACCATGGAGATGGACGCCGAA-3'	5'-GTCGTCAGAACAGAGTGTCGG-3'
Schgr-CRF-DHR2	5'-TAATACGACTCACTATAGGGTGATGTTCC CGATGCTGGAG-3'	5'-TAATACGACTCACTATAGGGTCGTCGATCACCTCGAC CAC-3'
Schgr-CRF-DHR2	5'-TAATACGACTCACTATAGGGTGCGTCGTC CTGGTGCTACT-3'	5'-TAATACGACTCACTATAGGGGCCCCACGCGGTTATG ATTA-3'

The size of the PCR products are analyzed on a 1 % agarose gel. Fragments of the expected length are cut out of the gel and purified using the GenElute Gel extraction Kit (Sigma-Aldrich). A 3'-A overhang is added using the RedTaq DNA polymerase (Sigma-Aldrich) by heating 15 µl RedTaq mixed with 5 µl gel extract at 72°C during 15 min. Subsequently, the two partial *Schgr*-CRF-DHR2 fragments are cloned into a pCR 4-TOPO vector (Invitrogen) and the ORF of *Schgr*-CRF-DHR1 is cloned into a pcDNA 3.1/V5-His TOPO vector (Invitrogen) following the manufacturer's instructions (described in section 2.5). The vectors are transformed into One Shot TOP10 chemical competent *Escherichia coli* cells (Invitrogen; *Schgr*-CRF-DHR1) or DH5α cells (*Schgr*-CRF-DHR2 fragments) and grown on LB agar plates (35 g/l; Sigma-Aldrich) with ampicillin (10 mg/ml; Invitrogen). Colonies with

an insert are collected and grown in 5 ml LB medium (Sigma-Aldrich) with ampicillin (10 mg/ml). Plasmid purification is performed using the GenElute Plasmid Miniprep Kit (Sigma-Aldrich). The DNA sequence of *Schgr*-CRF-DHR1 is determined using the ABI PRISM 3130 Genetic Analyzer (Applied Biosystems) following the protocol outlined in the BigDye Terminator v1.1 Cycle Sequencing Kit (Applied Biosystems) and the DNA sequences of the two partial *Schgr*-CRF-DHR2 fragments are determined by LGC Genomics (Germany) using the M13 forward and M13 reverse primers. Bacterial cells known to contain the correct ORF of *Schgr*-CRF-DHR1 in the right direction are grown at large scale in 100 ml Luria-Bertani Broth medium. The expression vector is subsequently isolated from these cells using the EndoFree Plasmid Purification Kit (Qiagen) and sequenced once again.

5.2.6. Analysis of the downstream signaling properties of the *Schgr*-CRF-DHR1 using the aequorin bioluminescence assay

Chinese hamster ovary (CHO-WTA11 and CHO-PAM28) are transfected with *Schgr*-CRF-DHR1 in order to test the signaling properties of the receptor after activation with the endogenous peptide *Schgr*-CRF-DH [MGMGPSLSIVNPMDVLRQRLLLEIARRRLRDAEEQIKANKDFLQQI-NH_2; ordered from GL Biochem (Shanghai, China)]. Since the CRE-dependent luciferase assay raises important concerns (as discussed in section 3.4.3 and 4.4.3), this assay is not performed with *Schgr*-CRF-DHR1.

Cell culture and transfections of CHO-WTA11 and CHO-PAM28, and how this assay is performed is described in section 2.7. A dilution series (0.01 fM -10 µM) of *Schgr*-CRF-DH is tested. An additional transfection with empty pcDNA3.1 vector is carried out in each cell line to confirm that the response of the cells is evoked by stimulation of *Schgr*-CRF-DHR1 and not by any other endogenous receptor.

5.2.7. CAMYEL biosensor

Cell culture, transfections and the procedure of this assay are described in section 2.9. Measurements are performed in duplicate per concentration of *Schgr*-CRF-DH (0.1 nM - 1 µM) in two independent transfections for both the experimental condition (with *Schgr*-CRF-DHR1) and the control (without *Schgr*-CRF-DHR1) in both the presence and absence of forskolin.

5.2.8. $BRET^2$-based G protein assay to study the G protein mediated pathways

Cell culture, transfections and the procedure of this assay are described in section 2.10. In the first experiment only one concentration of *Schgr*-CRF-DH (1 µM) is tested whereas in the second experiment multiple concentrations (0.1 nM – 1 µM) of *Schgr*-CRF-DH are applied.

5.3. Results

5.3.1. Cloning and sequence analysis of *Schgr*-CRF-DHR1 and *Schgr*-CRF-DHR2

At the start of this project, two putative CRF-DH receptors (*Schgr*-CRF-DHR1 and *Schgr*-CRF-DHR2) are identified by means of a local BLAST in the (unpublished) transcriptome database. An additional BLAST search in a filtered, new assembly of the (unpublished) transcriptome database revealed the sequence of a third putative receptor, *Schgr*-CRF-DHR3 whereas the sequence of *Schgr*-CRF-DHR2 got lost in this new assembly. Nucleotide sequences of the three putative *S. gregaria* CRF-DHRs (*Schgr*-CRF-DHR1, *Schgr*-CRF-DHR2 and *Schgr*-CRF-DHR3) are compared in a multiple sequence alignment (supplementary Fig. S13) and also a percent identity matrix is constructed using the full ORF of the three receptors (supplementary table S9). *Schgr*-CRF-DHR1 shows a sequence identity of 74 % with *Schgr*-CRF-DHR3 and 67 % with *Schgr*-CRF-DHR2. *Schgr*-CRF-DHR2 and *Schgr*-CRF-DHR3 share a sequence identity of 77%. Surprisingly, the C-terminal sequences of *Schgr*-CRF-DHR2 and *Schgr*-CRF-DHR3 are identical.

The ORF of *Schgr*-CRF-DHR1 and two partial sequences of *Schgr*-CRF-DHR2 are amplified by PCR. *Schgr*-CRF-DHR1 is cloned into an expression vector and the two partial *Schgr*-CRF-DHR2 are cloned into a sequencing vector and subsequently sequenced. The two fragments of *Schgr*-CRF-DHR2 amplified by PCR and confirmed by sequencing are depicted in supplementary Fig. S12. Including the fragment sequenced after amplification by qRT-PCR (also depicted in supplementary Fig. S12), the N-terminal regions of *Schgr*-CRF-DHR2 up till and including TM4 is more or less confirmed by sequencing. Despite multiple attempts, we were never able to amplify the full open reading frame of *Schgr*-CRF-DHR2.

Additionally, a multiple sequence alignment is constructed (Fig. 5.3) with the confirmed amino acid sequence of *Schgr*-CRF-DHR1 and the predicted sequences of *Schgr*-CRF-DHR2 and *Schgr*-CRF-DHR3. The sequences are compared with the amino acid sequences of other insect *in cellulo* characterized insect CRF-DHRs of *D. melanogaster* (*Drome*-DH44-R1 and *Drome*-DH44-R2), *R. prolixus* (*Rhopr*-CRF-DHR2B), *M. sexta* (*Manse*-CRF-DHR) and *A. domesticus (Achdo*-CRF-DHR).

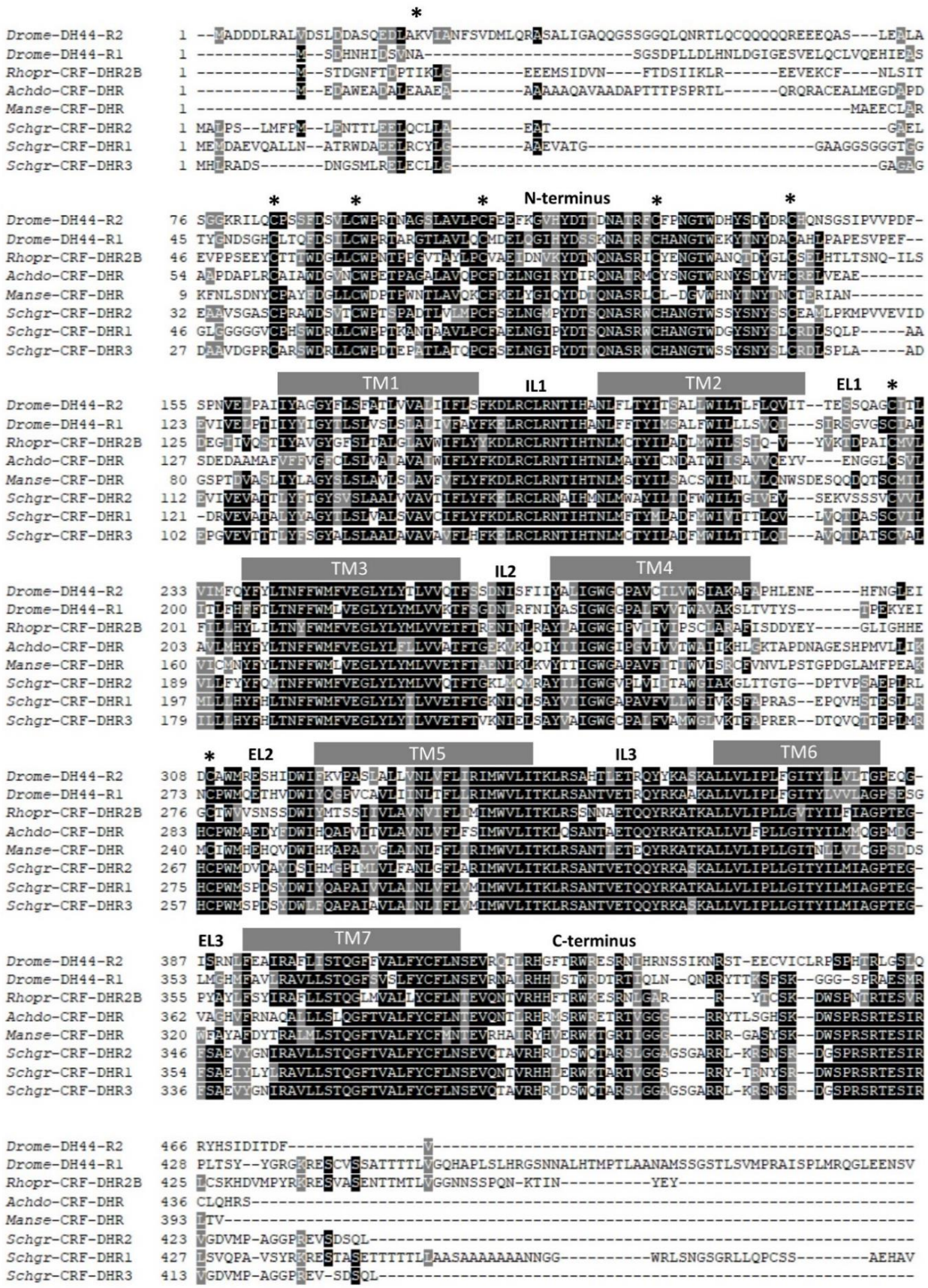
N-terminus
TM1
IL1
TM2
EL1
TM3
IL2
TM4
EL2
TM5
IL3
TM6
EL3
TM7
C-terminus

↑ **Figure 5.3: Multiple sequence alignment** of CRF-DHRs from *D. melanogaster* (*Drome*-DH44-R1; GenBank acc. no. NP_610960.1, and *Drome*-DH44-R2; GenBank acc. no. NP_610789.3), *R. prolixus* (*Rhopr*-CRF-DHR2B; GenBank acc. no. KJ407397), *M. sexta* (*Manse*-CRF-DHR; GenBank acc. no. AAC46469.1), *A. domesticus* (*Achdo*-CRF-DHR; GenBank acc. no AAC47000.1) and *S. gregaria* (*Schgr*-CRF-DHR1, *Schgr*-CRF-DHR2 and *Schgr*-CRF-DHR3). Identical residues between the aligned sequences are highlighted in black, and conservatively substituted residues in grey. Amino acid position is indicated at the left and dashes indicate gaps that are introduced to maximize similarities in the alignment. Putative transmembrane regions of *Schgr*-CRF-DHR1 and *Schgr*-CRF-DHR1 (TM1-TM7) are indicated by grey bars. Conserved cysteine residues that are predicted to form disulfide bridges in the N-terminus, EL1 and EL2 are indicated (*) (Gether, 2000; Venkatakrishnan et al., 2013). The intracellular loops (IL) and the C-terminus of the receptors are shown as well.

The sequences consist of seven transmembrane domains (TM1-TM7), three extracellular loops (EL), three intracellular loops (IL), an extracellular N-terminus and an intracellular C-terminus. All receptors comprise the six conserved cysteine residues known to form disulfide bridges in the N-terminal region of all Family B GPCRs and two conserved cysteine residues in EL1 and EL2 known to form a disulfide bridge between these ELs in all GPCRs (Gether, 2000; Schiöth and Lagerström, 2008). The alignment shows that the sequence is highly conserved, especially in the 7TM regions, IL1 and IL3. From TM1 to TM7 the *Schgr*-CRF-DHR1 shows a sequence similarity of 83 % *Schgr*-CRF-DHR3, 68 % with *Schgr*-CRF-DHR2, 60 % with *Rhopr*-CRF-DHR2B, *Achdo*-CRF-DHR and *Manse*-CRF-DHR, 58 % with *Drome*-DH44-R1, and 53 % with *Drome*-DH44-R2, while *Schgr*-DH44-R2 shows a sequence similarity of 68 % with *Schgr*-CRF-DHR3, 57 % with *Achdo*-CRF-DHR, 55 % with *Rhopr*-CRF-DHR2B, 54 % with *Manse*-CRF-DHR and *Drome*-DH44-R1, and 53 % with *Drome*-DH44-R2. Finally, *Schgr*-CRF-DHR3 shows a sequence similarity of 60 % with *Rhopr*-CRF-DHR2B, 57 % with *Achdo*-CRF-DHR, 56 % with both *Manse*-CRF-DHR and *Drome*-DH44-R1, and 53 % with *Drome*-DH44-R2. The percent identity matrix can be found in supplementary table S10.

5.3.2. RNA extractions

RNA quantity and quality of all samples are enlisted in supplementary tables S11-S14.

5.3.3. Relative transcript levels of *Schgr*-CRF-DHR1 and *Schgr*-CRF-DHR2

Expression of *Schgr*-CRF-DHR1 (Fig. 5.4) is restricted to the central nervous system (CNS). The relative transcript levels are very high in the suboesophageal ganglion, the ventral nerve cord, the frontal ganglion and the brain followed by the optic lobes, corpora cardiaca, corpora allata and prothoracic glands. However, no significant difference is found between mature and immature females and no relative expression can be observed in the examined male tissues. Notably, since an error has occurred in the samples of the salivary glands, the results of these samples are not shown.

Relative transcript levels of *Schgr*-CRF-DHR2 (Fig. 5.4) are highest in the Malpighian tubules and lower transcript levels are found in the fat body. No significant difference in any of the tissues is observed between the mature and immature tissues. Analysis of the dissociation curves of the different amplification products reveals a single melting peak and sequencing of the PCR products ultimately confirms the identity of the amplified DNA with their respective target sequences. The partial fragment of *Schgr*-CRF-DHR2 amplified by qRT-PCR and confirmed by sequencing is depicted in supplementary Fig. S12.

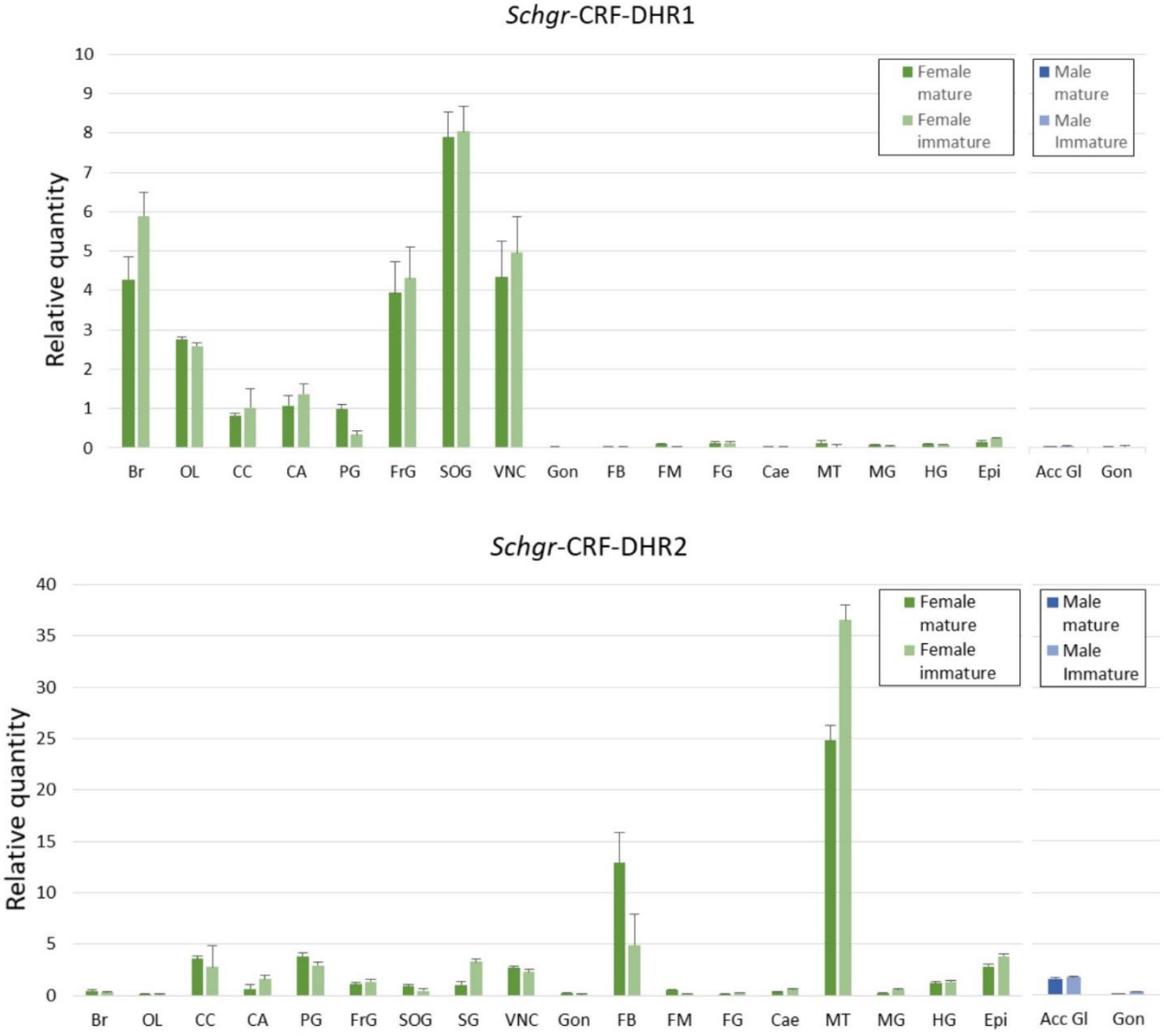

Figure 5.4: Graphic representation of the transcript levels of *Schgr*-CRF-DHR1 and *Schgr*-CRF-DHR2 measured in sexually mature gregarious *S. gregaria*. The data represent mean values ± S.E.M. of three independent tissue samples run in duplicate, normalized relative to CG13220, Ubi and GADPH transcript levels. Abbreviations used: Br = brain, OL = optic lobes, CC = corpora cardiaca, CA = corpora allata; PG = prothoracic glands, FrG = frontal ganglion, SOG = suboesophageal ganglion, SG = salivary gland, VNC = ventral nerve cord, Gon = gonads, FB = fat body, FM = flight muscle, FG = foregut, Cae = caecum, MT = Malpighian tubules, MG = midgut, HG = hindgut, Epi = epidermis, Acc Gl = male accessory glands, GADPH = glyceraldehyde-3-phosphate dehydrogenase, Ubi = ubiquitin conjugating enzyme 10. The results of the females are presented in green while the results of the males are presented in blue.

The partial sequences amplified by qRT-PCR (as depicted in supplementary Fig. S13) show sufficient variation in their nucleotide sequences when compared to the nucleotide sequences of the other *S. gregaria* CRF-DHRs, so we can conclude that the qRT-PCR results of *Schgr*-CRF-DHR1 are indeed the transcript levels of *Schgr*-CRF-DHR1, and not from the predicted *Schgr*-CRF-DHR2 nor *Schgr*-CRF-DHR3, and that the qRT-PCR results of *Schgr*-CRF-DHR2 are indeed the transcript levels of *Schgr*-CRF-DHR2, and not from *Schgr*-CRF-DHR1 nor *Schgr*-CRF-DHR3.

5.3.4. Downstream signaling properties of *Schgr*-CRF-DHR1 using the aequorin bioluminescence assay

Schgr-CRF-DHR1 elicits a sigmoidal dose-dependent response with an EC_{50} value in the high nanomolar range (30.65 nM; Fig.5.5) in CHO-WTA11 cells, containing the promiscuous $G\alpha_{16}$ protein. However, no response was detected in CHO-PAM28 cells (results not shown). The former indicates that *Schgr*-CRF-DH is an agonist of *Schgr*-CRF-DHR1, while the latter indicates that receptor activation does not result in a detectable elevation of intracellular Ca^{2+} levels in absence of the promiscuous $G\alpha_{16}$ subunit.

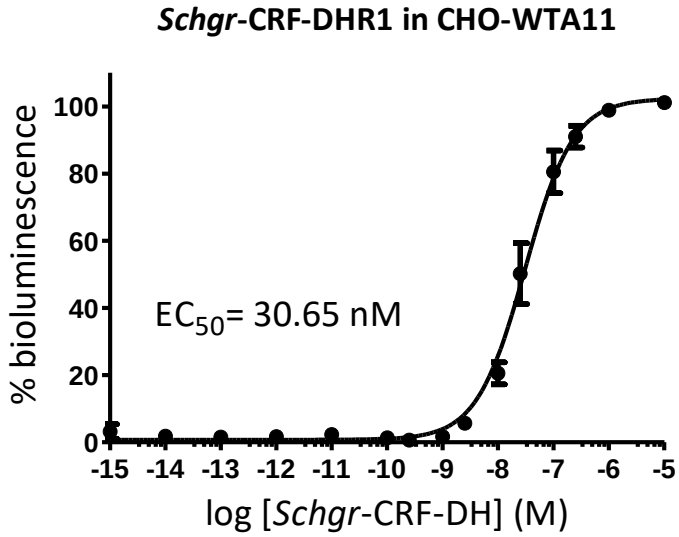

Figure 5.5: Dose-response curve for aequorin-based bioluminescent responses induced in CHO-WTA11-*Schgr*-CRF-DHR1 cells. The aequorin bioluminescence assay is executed in two independent transfections. The bioluminescence is measured in triplicate per concentration of *Schgr*-CRF-DH and per transfection. Error bars represent the S.E.M and the 100 % level refers to the maximal response level. The zero-response level corresponds to treatment with BSA medium only. In addition, the EC_{50} value is indicated.

5.3.5. The CAMYEL biosensor

In the first experiment (Fig. 5.6, left), in which measurements are performed in the absence of forskolin, a dose-dependent decrease in BRET[1] signal is observed with an EC_{50} value in the nanomolar range (4.14 nM) when the cells are transfected with *Schgr*-CRF-DHR1. The control cells

do not respond to *Schgr*-CRF-DH. In the second experiment (Fig. 5.6, right), no decrease in BRET^1 signal is observed in the cells transfected with *Schgr*-CRF-DHR1 and also the control cells do not respond to *Schgr*-CRF-DH. These results suggest that there is an increase in intracellular cAMP levels upon *Schgr*-CRF-DHR1 stimulation with *Schgr*-CRF-DH.

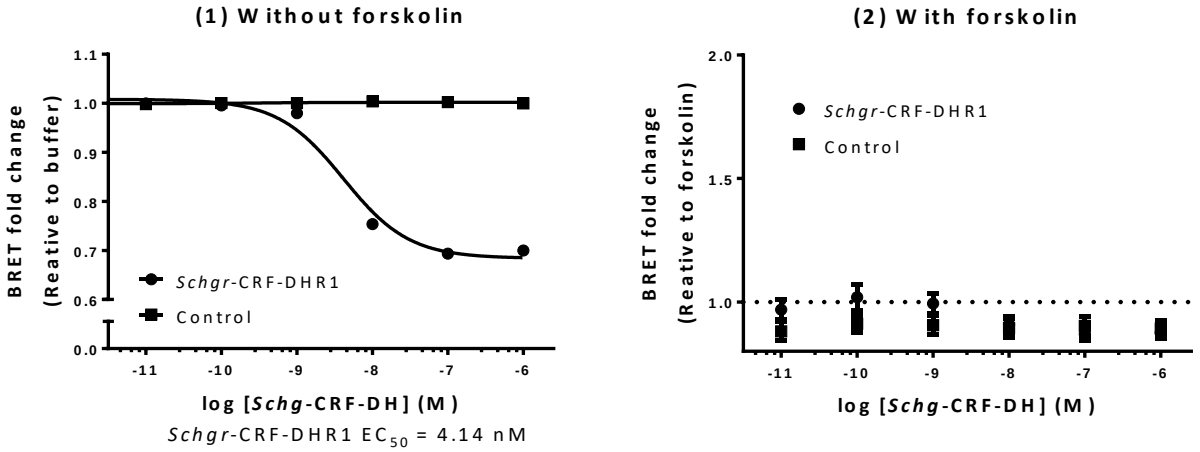

Figure 5.6: Results of CAMYEL biosensor: BRET^1 measured in HEK293T cells transfected with *Schgr*-CRF-DHR1 (●) or without *Schgr*-CRF-DHR1 [control (■)] in two independent transfections. Measurements are taken in duplicate for each concentration of *Schgr*-CRF-DH (10 pM - 1 µM). **Left**: measurements are taken in the absence of forskoline. Data (± S.E.M) are presented relative to the baseline (buffer only). **Right**: measurements are taken in the presence of forskolin. Data (± S.E.M) are presented relative to the baseline (buffer with forskolin). The dotted line represents the baseline.

5.3.6. Measuring a direct activation of the Gα protein by using BRET^2-based G protein biosensors

The ΔBRET^2 signal measured in HEK293T-*Schgr*-CRF-DHR1 cells is significantly lower than the control cells upon addition of 1 µM *Schgr*-CRF-DH for four out of five biosensors ($G\alpha_{i2}$, $G\alpha_{i3}$, $G\alpha_{oa}$ and $G\alpha_{ob}$) of the $G\alpha_{i/o}$ subfamily (Fig. 5.7). Moreover, the ΔBRET^2 signals of $G\alpha_{i2}$, $G\alpha_{i3}$, $G\alpha_{oa}$ and $G\alpha_{ob}$ are dose-dependent with an EC_{50} value in the high nanomolar range (Fig. 5.8) indicating that these biosensors are truly activated. Although the ΔBRET^2 signal is not significantly lower for the $G\alpha_{i1}$ biosensor, a lower trend is observed when only one concentration of *Schgr*-CRF-DH is applied (Fig. 5.7). However, no sigmoidal dose-dependent relationship is observed (Fig. 5.8) since the ΔBRET^2 signal is also lower using a concentration of 0.10 nM *Schgr*-CRF-DH. The magnitude of the ΔBRET^2 signals of the $G\alpha_o$ biosensors, but not the $G\alpha_i$ biosensors, are comparable those detected with the *H. sapiens*

chemokine receptor CCR2 (Fig 3.9, right; Corbisier et al., 2015), a receptor known to activate $G\alpha_{i/o}$ proteins.

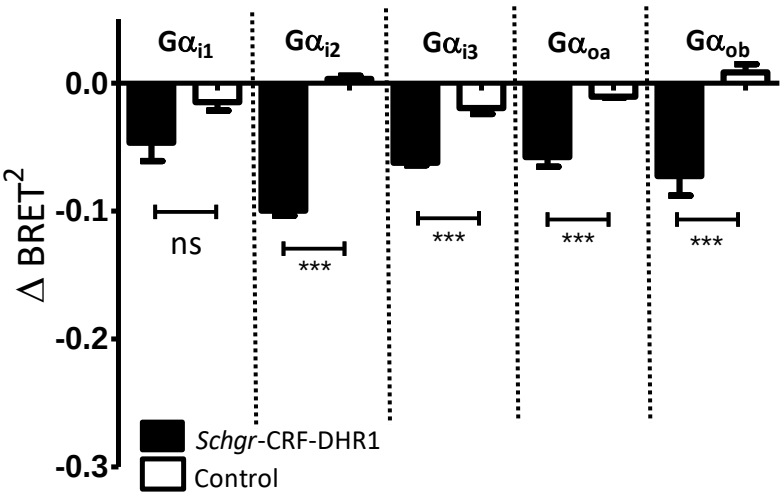

Figure 5.7: Summary of the results of the $G\alpha_{i/o}$ subfamily $BRET^2$-based G protein biosensors. The results of HEK293T-*Schgr*-CRF-DHR1 cells (*Schgr*-CRF-DHR1) and HEK293T cells (control) co-transfected with the $G\alpha_{i1}$, $G\alpha_{i2}$, $G\alpha_{i3}$, $G\alpha_{oa}$ or $G\alpha_{ob}$ biosensor upon stimulation of 1 µM *Schgr*-CRF-DH. The data represent the means ± S.E.M of $\Delta BRET^2$ measured in triplicate in two independent transfections. Significant differences ($p < 0.001$) are indicated by asterisks (***) (student's t-test per $G\alpha_{i/o}$ biosensor). The dotted lines segregate the results per $G\alpha_{i/o}$ biosensor.

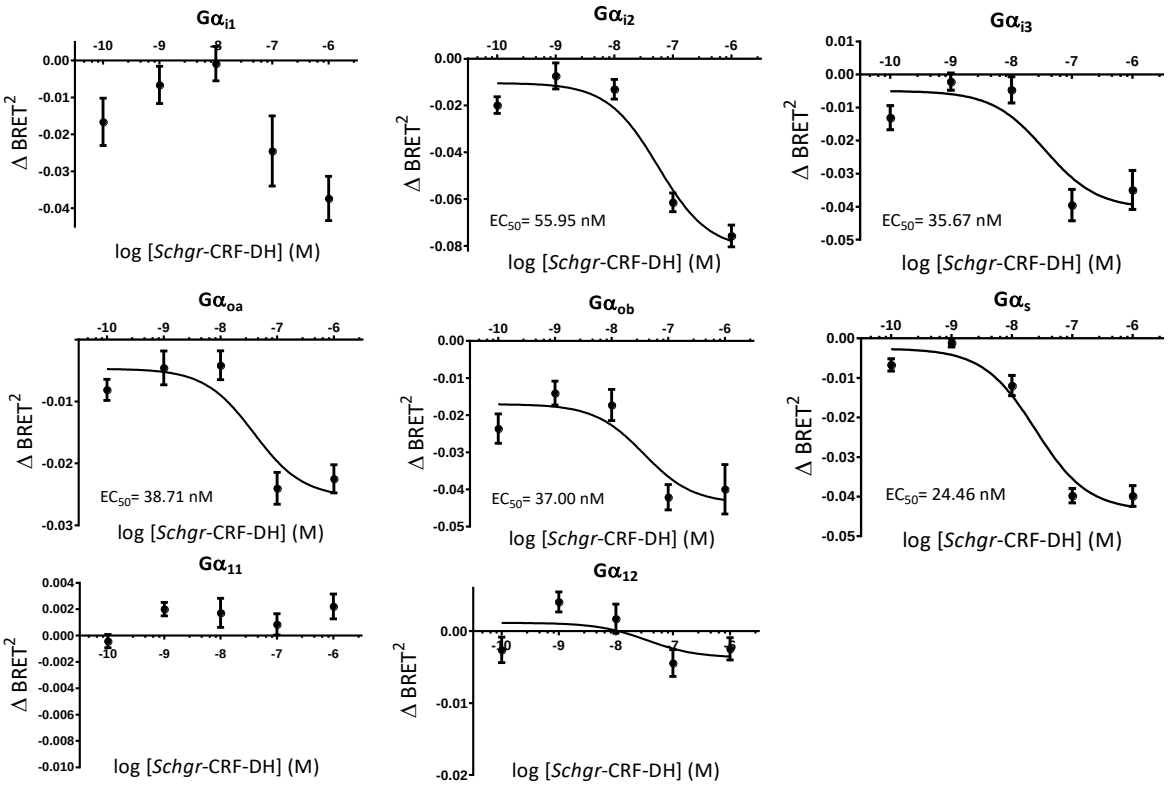

Figure 5.8: Dose-dependent responses in HEK293T-*Schgr*-CRF-DHR1 cells co-transfected with $BRET^2$-based G protein biosensors consisting of $G\beta_1$, $G\gamma_2$-GFP10 and several Gα subunits upon stimulation of 0.01 nM –

1 µM *Schgr*-CRF-DH. The data represent the means ± S.E.M of three independent transfections measured in duplicate per concentration. The EC_{50} value is indicated in case a dose-dependent reaction is observed.

In addition, also for the $G\alpha_s$ biosensor, the only representative of the $G\alpha_s$ subfamily that is tested, a significantly lower $\Delta BRET^2$ signal is measured in the HEK293T-*Schgr*-CRF-DHR1 cells compared to the control cells (Fig. 5.9). Moreover, also this biosensor induces a dose-dependent decrease in $\Delta BRET^2$ signal with an EC_{50} value in the high nanomolar range (Fig. 5.8) indicating that this biosensor is truly activated. The magnitude of the $\Delta BRET^2$ signal is comparable with the magnitude of the $\Delta BRET^2$ signal detected with the *H. sapiens* β2-adrenergic receptor (*Homsa*-β2-AR; Fig. 3.11, right; Saulière et al., 2012), a receptor know to activate the $G\alpha_s$ protein.

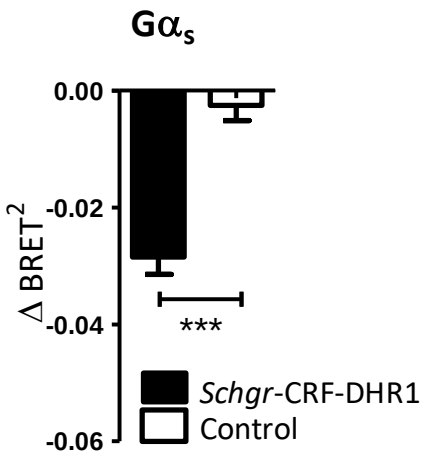

Figure 5.9: Results of the HEK293T-*Schgr*-CRF-DHR1 cells (*Schgr*-CRF-DHR1) and HEK293T cells (Control) co-transfected with $BRET^2$-based G protein biosensors consisting of $G\beta_1$, $G\gamma_2$-GFP10 and a Gα belonging to the **$G\alpha_s$ subfamily** upon stimulation of 1 µM *Schgr*-CRF-DH. The data represent the means ± S.E.M of $\Delta BRET^2$ measured in triplicate in two independent transfections. Significant differences ($p < 0.001$) are indicated by asterisks (***) (student's t-test).

Furthermore, the $G\alpha_{11}$ biosensor nor the $G\alpha_q$ biosensor (Fig. 5.10) are activated when the magnitude of the $\Delta BRET^2$ signal is compared to the magnitude of the $\Delta BRET^2$ signal detected with the *H. sapiens* angiotensin II type 1 receptor (*Homsa*-AT1R; Fig. 3.11, B; Saulière et al., 2012), a receptor known to activate $G\alpha_{q/11}$ proteins.

In addition, the $G\alpha_{12}$ biosensor induces a significantly lower $\Delta BRET^2$ signal in the HEK293T-*Schgr*-CRF-DHR1 cells compared to the control cells (Fig. 5.11) and the magnitude of the $\Delta BRET^2$ signal is comparable to the magnitude of the $BRET^2$ signals detected with the *H. sapiens* thromboxane TPα receptor (*Homsa* TPα-R; Fig. 3.12, B; Saulière et al., 2012), a receptor known to activate $G\alpha_{12/13}$ proteins. However, when multiple concentrations of *Schgr*-CRF-DH are applied, no dose-dependent response is detected (Fig. 5.8). Finally, $G\alpha_{13}$ does not induce a significantly lower $\Delta BRET^2$ signal in the HEK293T-*Schgr*-CRF-DHR1 cells compared to the control cells (Fig. 5.11).

Similarly as with the $G\alpha_{12}$ biosensor, the $\Delta BRET^2$ signal is compared to the $\Delta BRET^2$ signal detected with *Homsa*-TPα-R (Fig. 3.12, B; Saulière et al., 2012).

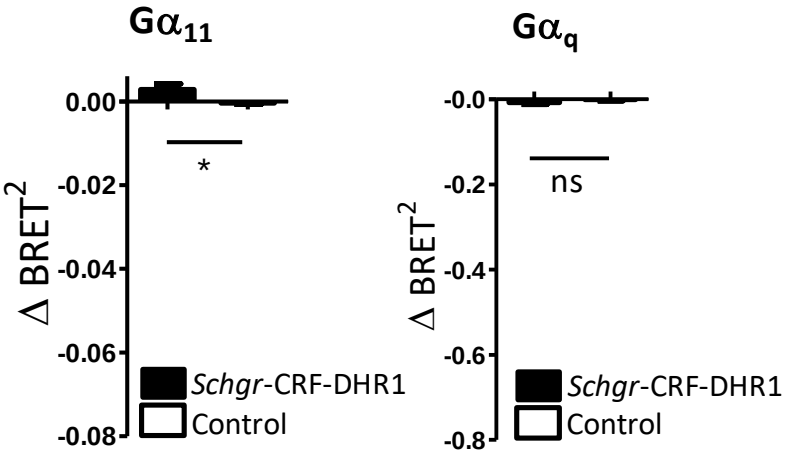

Figure 5.10: Results of the HEK293T-*Schgr*-CRF-DHR1 cells (*Schgr*-CRF-DHR1) and HEK293T cells (Control) co-transfected with $BRET^2$-based G protein biosensors consisting of $G\beta_1$, $G\gamma_2$-GFP10 and a Gα belonging to the **$G\alpha_{q/11}$ subfamily** upon stimulation of 1 µ M *Schgr*-CRF-DH: on the **left** the results of the $G\alpha_{11}$ biosensor is depicted and on the **right** the results of the $G\alpha_q$ biosensor is depicted. The data represent the means ± S.E.M of $\Delta BRET^2$ measured in triplicate in two independent transfections. Significant differences ($p < 0.05$ are indicated by an asterisks (*) (student's t-test).

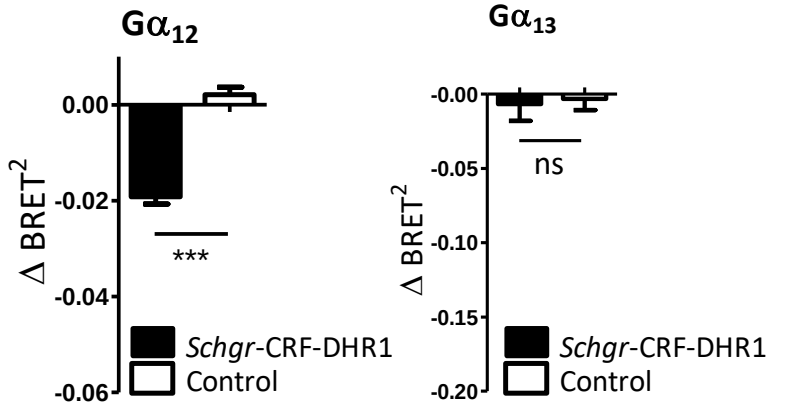

Figure 5.11: Results of the HEK293T-*Schgr*-CRF-DHR1 cells (*Schgr*-CRF-DHR1) and HEK293T cells (Control) co-transfected with $BRET^2$-based G protein biosensors $G\beta_1$, $G\gamma_2$-GFP10 and a Gα belonging to the $G\alpha_{12/13}$ subfamily upon stimulation of 1 µM *Schgr*-CRF-DH: on the **left** the results of the $G\alpha_{12}$ biosensor are depicted and on the **right** the results of the $G\alpha_{13}$ biosensor are depicted. The data represent the means ± S.E.M of $\Delta BRET^2$ measured in triplicate in two independent transfections. Significant difference ($p < 0.001$) is indicated by an asterisks (***) (student's t-test).

5.4. Discussion

5.4.1. Molecular cloning and receptor sequence analysis

In this study, three putative CRF-DHRs are identified and one of them, S*chgr*-CRF-DHR1 is successfully cloned and characterized with cell-based functional receptor assays. The second predicted receptor, S*chgr*-CRF-DHR2, is partially confirmed by sequencing in thee fragments which more or less span the N-terminal part of the receptor up till and including TM4.

As shown in the multiple sequence alignment, the amino acid sequence of all three S*chgr*-CRF-DH receptors are well conserved when compared with the other *in vitro* characterized CRF-DHRs from insects: *D. melanogaster* (*Drome*-DH44-R1 and *Drome*-DH44-R2), *R. prolixus* (*Rhopr*-CRF-DHR2B), *M sexta* (*Manse*-CRF-DHR) and *A. domesticus* (*Achdo*-CRF-DHR), especially in the 7TM regions, IL1 and IL3. The sequence contains amino acid residues which are highly conserved among Family B GPCRs (Gether, 2000).

If the receptors *Schgr*-CRF-DHR2 and *Schgr*-CRF-DHR3 exist *in vivo* remains a question for future studies. The fact that we were able to amplify three partial sequences of *Schgr*-CRF-DHR2 suggests that this receptor does exist *in vivo*. However, the fact that we were never able to fully amplify the ORF together with the fact that the C-terminal sequence of the predicted S*chgr*-CRF-DHR2 is identical to the C-terminal sequence of *Schgr*-CRF-DHR3 suggests that the C-terminal sequence of *Schgr*-CRF-DHR2 might not be correct in the first assembly in of the transcriptome database. This hypothesis is supported by the fact that the predicted sequence of *Schgr*-CRF-DHR2 is not present anymore in the filtered, new assembly of the transcriptome database (Verdonck, 2017). Notably, the predicted *Schgr*-CRF-DHR2 sequence is also not present in the first version of the (unpublished) genomic database of *S. gregaria*. Future versions of the genomic database might give more information about the existence of *Schgr*-CRF-DHR2. In the meantime, the C-terminal region can be sequenced by means of rapid amplification of cDNA ends (RACE) by designing primers in the confirmed fragment.

Since the sequence of the *Schgr*-CRF-DHR3 was only identified in a later phase of this study, no attempts were made to amplify the ORF of this receptor. Notably, this receptor is also present in the first version of the (unpublished) genomic database of *S. gregaria*.

If *Schgr*-CRF-DHR2 and *Schgr*-CRF-DHR3 are receptors for *Schgr*-CRF-DH should also be confirmed by using *in cellulo* assays. However, the fact that the sequence of these receptors are well conserved with the other *in vitro* characterized CRF-DHRs from other insects, including *Schgr*-CRF-DHR1, does suggest that these receptors are receptors for *Schgr*-CRF-DH. Moreover, the fact that

Schgr-CRF-DHR2 is mainly present in the Malpighian tubules, which is expected from CRF-DHRs, also suggests that this receptor might be a receptor for *Schgr*-CRF-DH.

5.4.2. Tissue distribution analysis and functions of CRF-DH

Transcript levels of *Schgr*-CRF-DHR1 and *Schgr*-CRF-DHR2 show a highly dissimilar pattern, which, as pointed out by Hector and co-workers (2009) in a study which compares two CRF-DHRs in *D. melanogaster*, infers functional differences between these two receptors. Relative transcript expression of *Schgr*-CRF-DHR1 is mainly restricted to the CNS with high expression levels in the suboesophageal ganglion, the ventral nerve cord, the frontal ganglion and the brain followed by the optic lobes, corpora cardiaca, corpora allata and prothoracic glands. No significant differences are observed in these tissues when expression levels are compared between mature and immature females.

Expression levels of *Schgr*-CRF-DHR2 are the highest in the Malpighian tubules. This result can undoubtedly be linked to the role of *Schgr*-CRF-DH in osmotic regulation since the effect on primary urine secretion in this organ is proven numerous times in multiple insects. Additionally, expression levels of *Schgr*-CRF-DHR2 are also observed in the fat body.

Although CRF-DH plays a pronounced role in both feeding and reproduction in *S. gregaria*, this is not reflected by the results of the tissue distribution analysis since relative expression of both receptors is low in tissues involved in these processes. This infers that these processes are perhaps regulated by *Schgr*-CRF-DH in an indirect manner or via another receptor type. For instance, expression of *Schgr*-CRF-DHR1 is high in the brain, the optic lobe and the ventral nerve cord, which are part of the central nervous system (CNS, Box 1.1). In addition, expression levels are also high in the suboesophageal ganglion and the frontal ganglion, which are part of the stomatogastric nervous system (SNS, Box 5.3). This part of the nervous system coordinates the processes of feeding and digestion. The suboesophageal ganglion innervates the mouthparts and the salivary glands and thus controls food intake (Audsley and Weaver, 2009; Nation, 2015) whereas the frontal ganglion innervates the foregut enhancing gut motility. Van Wielendaele and co-workers (2012) also point out that the decrease in food intake by *Schgr*-CRF-DH may also result from a decrease in peripheral sensitivity to food stimuli such as gustatory stimuli, olfactory stimuli and chemosensory perception and thus may affect central functions such as appetite and feeding behavior.

Expression of *Schgr*-CRF-DHR2 may also be linked to nutrition-dependent processes, since the fat body plays a role in metabolic regulation. This organ can also be linked to the reproductive system, since it produces vitellogenins, which are yolk precursors that are incorporated in the oocytes during

vitellogenesis (Tobe and Pratt, 1975). However, no significant difference in expression levels is observed between mature and immature females.

Furthermore, as pointed out by Van Wielendaele and co-workers (2012), the negative *in vivo* effect of *Schgr*-CRF-DH on reproduction might also be an indirect effect of the antifeedant activity since feeding provides the energy and proper nutrients to support anabolic processes such as vitellogenesis and ecdysteroidogenesis.

Notably, since the receptor sequence S*chgr*-CRF-DHR3 is only identified in a later stage of this thesis project, levels of this receptor transcript have not been measured in the tissue distribution analysis.

Box 5.3: The stomatogastric nervous system

The stomatogastric nervous system (SNS) comprises the suboesophageal ganglion, the frontal ganglion, the hypocerebral ganglion and the proventricular ganglion (Hartenstein, 1997; Fig. 1.1, Fig. 5.15 and Fig. 5.16). The hypocerebral ganglion is connected to the frontal ganglion, which in turn is connected to the brain (Chapman, 2012). In locusts, the proventricular ganglion is replaced by paired ingluvial ganglia (Fig. 5.16; Rand and Ayali, 2010). The hypocerebral ganglion is in close association with the corpora cardiaca (CNS), in which the neurohormones are stored in the neurohemal part and released at the appropriate moment into the hemolymph (neurohemal site). The suboesophageal ganglion has sensory and motor connections to the mouthparts, salivary glands and neck muscles, and the foregut is innervated by the frontal ganglion regulating motor activity in the gut and thus the passage of food through the gut (Audsley and Weaver, 2009; Rand and Ayali, 2010).

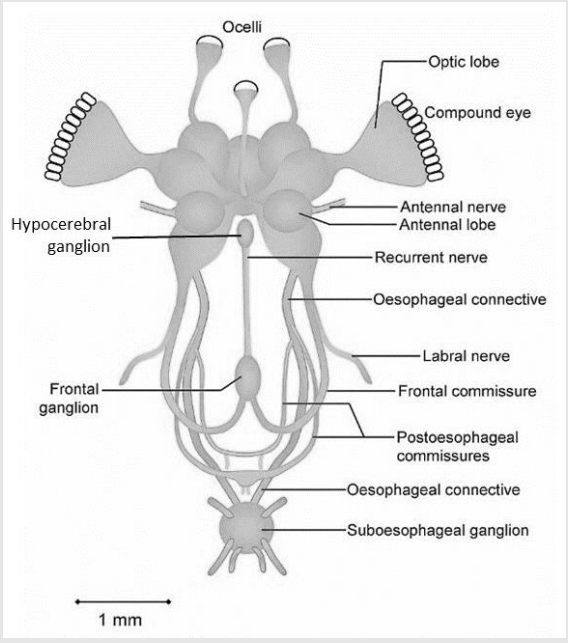

Figure 5.15: Anterior view of a locust brain. (Image credits: Cronodon.com, 2018, based on Bharadwaj and Baneriee, 1971)

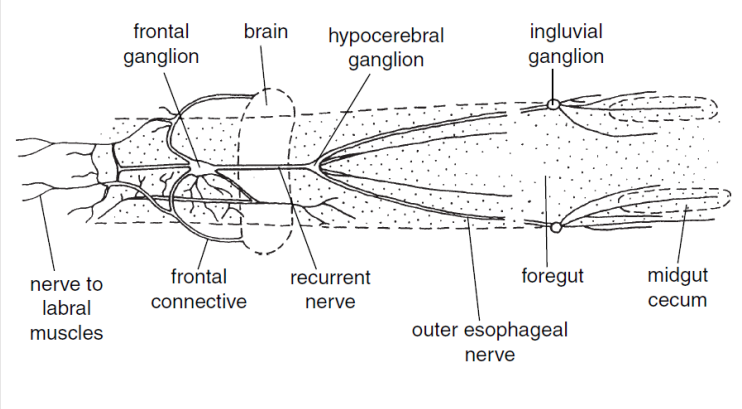

Figure 5.16: Dorsal view of the stomatogastric nervous system of a grasshopper. (Image credits: Chapman, 2012, based on Anderson and Cochrane, 1978)

5.4.3. Pharmacological receptor characterization and G protein mediated signaling pathways

The aequorin bioluminescence assay indicates that *Schgr*-CRF-DH is an agonist of *Schgr*-CRF-DHR1 and that activation of this receptor has no detectable effect on the PLC/Ca^{2+} pathway since no increase in intracellular Ca^{2+} levels is observed in CHO-PAM28 cells. This result is in accordance with the available literature data on other characterized CRF-DHRs in *R. prolixus* (Lee et al., 2016) and *D. melanogaster* (*i.e*. *Drome*-DH44-R2; Hector et al., 2009). However, a stimulatory effect on the PLC/Ca^{2+} pathway has been reported for *Drome*-DH44-R1 (Johnson et al., 2004).

The cAMP reporter assay with the CAMYEL biosensor indicates an increase in cAMP levels upon activation of *Schgr*-CRF-DH1 by *Schgr*-CRF-DH. A stimulatory effect on cAMP levels is in agreement with the data reported for other *in cellulo* characterized CRF-DHRs. Activation of *Achdo*-CRF-DHR, *Manse*-CRF-DHR, *Rhopr*-CRF-DHR2B and both *Drome*-DH44-R1 and *Drome*-DH44-R2 by their endogenous ligand, have a stimulatory effect on the AC/cAMP/PKA pathway (Hector et al., 2009; Johnson et al. 2004; Lee et al., 2016; Reagan, 1995;1996). Different methods have been employed in literature. cAMP levels upon activation of *Manse*-CRF-DHR (Reagan, 1995) and *Achdo*-CRF-DHR (Reagan, 1996) were measured by a radioimmunoassay, cAMP levels upon activation of both *Drome*-DH44-R1 and *Drome*-DH44-R2 (Hector et al., 2009; Johnson et al. 2004) were measured using a $CRE_{(6x)}$-Luc construct and cAMP levels upon activation of *Rhopr*-CRF-DHR2B were measured using the BD ACTOne assay in the HEK293/CNG cell line.

Additionally, the downstream G protein mediated signaling pathways are studied in more detail using $BRET^2$-based G protein biosensors which can measure a direct activation of the G protein. The $G\alpha_s$ biosensors, the only member of the $G\alpha_s$ subfamily that is tested, is activated since a dose-dependent decrease in $\Delta BRET^2$ signal is measured upon stimulation of *Schgr*-CRF-DH. This result is supported by the cAMP reporter assay in this chapter using the CAMYEL biosensor.

In addition, four out of five biosensors ($G\alpha_{i2}$, $G\alpha_{i3}$, $G\alpha_{oa}$ and $G\alpha_{ob}$) of the $G\alpha_{i/o}$ subfamily are activated when *Schgr*-CRF-DHR1 is stimulated by *Schgr*-CRF-DH suggesting activation of $G\alpha_{i/o}$ subunit family. This result is in contrast with the results using the CAMYEL biosensor. However, as discussed in section 4.4.3, activation of the $G\alpha_{i/o}$ subfamily does not necessarily result in a decrease in intracellular cAMP levels. The fact that both $G\alpha_{i/o}$ and $G\alpha_s$ subfamilies are activated may appear contradictory. This aspect is further discussed in section 6.2.1.

Furthermore, neither biosensors of the $G\alpha_{q/11}$ subfamily, namely $G\alpha_q$ and $G\alpha_{11}$, are activated. This result is supported by our results in this chapter using the in the aequorin bioluminescence assay.

In addition, although the $G\alpha_{12}$ induces a significant difference in $\Delta BRET^2$ signal in the HEK293T-*Schgr*-CRF-DHR1 cells compared to the control cells, no clear dose-dependent relationship is observed when multiple concentrations of *Schgr*-CRF-DH are applied. Additional experiments are needed to make any conclusions about activation of the $G\alpha_{12}$ biosensor upon activation of *Schgr*-CRF-DH. Finally, $G\alpha_{13}$ does not induce a significantly lower $BRET^2$ signal in the HEK293T-*Schgr*-CRF-DHR1 cells compared to the control cells.

As mentioned earlier, these $BRET^2$-based G protein biosensors are also used to verify which Gα subunit within a Gα subunit family can be activated. However, since only one $G\alpha_i$ and one $G\alpha_o$ subunit sequence are identified in *S. gregaria*, knowing which $G\alpha_i$ or $G\alpha_o$ biosensor is activated has no added value for understanding the *in vivo* situation.

Taking all this together, we can conclude that *Schgr*-CRF-DH is an agonist of *Schgr*-CRF-DHR1. Agonist-induced activation of the receptor has a stimulatory effect on the AC/cAMP pathway but has no detectable effect on the PLC/Ca^{2+} pathway.

In conclusion, concerning the use of the $BRET^2$-based G protein biosensors to detect signaling of this insect GPCR, we make four major observations: (1) four out of five biosensors of the $G\alpha_{i/o}$ subfamily and the $G\alpha_s$ biosensor respond to the agonist-induced insect receptor *Schgr*-CRF-DHR1, (2) no significant effects are obtained with both biosensors of the $G\alpha_{q/11}$ subfamily, in accordance with the data of the aequorin bioluminescence assay, (3) the results of $G\alpha_s$ but not the $G\alpha_{i/o}$ biosensors are not supported by the results obtained with the CAMYEL biosensor, and (4) no activation of both Gα biosensors of the $G\alpha_{12/13}$ subfamily is detected. Notably, the results of the $G\alpha_{12}$ and $G\alpha_{13}$ biosensors are not confirmed by studying more downstream signaling pathways.

Chapter 6:
General conclusions and perspectives

6.1. Introduction

In this thesis, we have cloned and characterized three insect receptors: the *Bombus terrestris* SIFamide receptor (*Bomte*-SIFR), the *Schistocerca gregaria* allatotropin receptor (*Schgr*-ATR) and one of the three predicted *S. gregaria* corticotropin-releasing factor (CRF)-related diuretic hormone receptors (*Schgr*-CRF-DHR1). We have shown that *Bomte*-SIFa, *Schgr*-AT and *Schgr*-CRF-DH, respectively, can bind to these receptors in the *in cellulo* assays and have investigated which secondary messenger molecules are involved in receptor signaling by using customary *in cellulo* assays. In addition, we have tested the BRET^1-based cAMP sensor using YFP-Epac-*R*luc (CAMYEL) biosensor (ATCC MBA-277; Jiang et al., 2007) as an alternative method to monitor changes in the intracellular cAMP concentrations. Furthermore, we have tested if the BRET^2-based G protein biosensors (Galés et al., 2006) also respond to activation of insect GPCRs and have shown that the biosensors for three out of four Gα protein subfamilies, namely $G\alpha_{i/o}$, $G\alpha_s$ and $G\alpha_{q/11}$, respond to activation of insect GPCRs. Finally, we have looked into the possible functional roles of these receptors by means of a tissue distribution analysis. In this general conclusion, we will discuss these results in a broader context starting with a discussion concerning the methods that are used to study the secondary messenger molecules upon receptor activation. This is followed by a discussion about the G protein subunit sequences identified in both *B. terrestris* and *S. gregaria* and an analysis and a discussion concerning the results of the BRET^2-based G protein biosensors. After we briefly discuss the scientific relevance of the obtained results for the development of new pest control agents, we discuss the future prospects. Finally, we end this chapter with an overall conclusion.

6.2. Methods to study the secondary messenger pathways

6.2.1. Commonly used methods to study the second messenger pathways

We used the aequorin bioluminescence assay and CRE-dependent luciferase reporter assay to detect possible changes in, respectively, intracellular Ca^{2+} and cAMP levels upon receptor stimulation of *Bomte*-SIFR and *Schgr*-ATR. For both receptors, a dose dependent increase in luminescence is measured in both assays, suggesting an increase in both Ca^{2+} and cAMP levels.

However, as discussed in chapters 3 and 4, it is suggested that the measured increase in luminescence in HEK293-cells co-transfected with the $CRE_{(6x)}$-Luc construct could also be triggered by an increase of the Ca^{2+} levels. If this is the case, an increase in luminescence in the CRE-dependent luciferase reporter assay is expected for each receptor that also increases intracellular Ca^{2+} levels. This seems to be the case for other pharmacologically characterized ATRs from *Manduca sexta*

(Horodyski et al., 2011), *B. terrestris* (Verlinden et al., 2013) and *Tribolium castaneum* (Vuerinckx et al., 2011), and other pharmacologically characterized insect GPCRs (Huang et al., 2014; Lenaerts et al., 2017; Zels et al., 2014).

However, the fact that the Ca^{2+} levels can also affect the luminescence measured in the HEK293 cells co-transfected with the $CRE_{(6x)}$-Luc construct, should not always give inconclusive data. If a receptor has no effect on the PLC/Ca^{2+} pathway, this should not interfere with the readout. Furthermore, in some cases, increasing Ca^{2+} levels are demonstrated upon receptor activation in CHO-PAM28 cells, but a reduction in luminescence is observed in HEK293 cells co-transfected with the $CRE_{(6x)}$-Luc construct, suggesting decreasing cAMP levels upon receptor activation (Dillen et al., 2013; Verlinden et al., 2015b).

Additionally, the fact that Ca^{2+} can influence this assay does not necessarily mean that the increasing luminescence is indeed evoked by Ca^{2+} and not by cAMP. For instance, for the *Trica*-SKR, the increasing cAMP levels are also confirmed using the CatchPoint cAMP Fluorescent assay (Molecular Devices) (Zels, 2015). However, since several alternative methods have been developed which directly interact with cAMP, these other methods should be tested to verify which of these are reliable assays for monitoring dynamic changes in the intracellular cAMP levels upon receptor activation, and, if so, it will be useful to know for which concentration range they are reliable.

6.2.2. CAMYEL as an alternative biosensor to monitor cAMP concentrations?

In this study, we have tested the CAMYEL biosensor (ATCC MBA-277; Jiang et al., 2007) as an alternative method to monitor changes in the intracellular cAMP concentrations upon receptor activation. The advantage of this biosensor, compared to the previously used $CRE_{(6x)}$-Luc construct, is the fact that the main core of this biosensor comprises an EPAC protein, also known as exchange factor directly activated by cAMP, which, as the name already suggests, directly interacts with cAMP. However, a disadvantage of the CAMYEL biosensor is the poor dynamic range.

In our study, we tested the CAMYEL biosensor with *Bomte*-SIFR, *Schgr*-ATR and *Schgr*-CRF-DHR1. The results of the *Schgr*-CRF-DHR1 show that this receptor can induce an increase in intracellular cAMP levels upon receptor activation. However, the efficacy of this biosensor could not be proven with the two other receptors, since the results of *Bomte*-SIFR are inconclusive and *Schgr*-ATR seems to act independently from the AC/cAMP/PKA pathway. Therefore, more receptors which influence the AC/cAMP/PKA should be tested to conclude if this is a reliable biosensor to monitor the intracellular cAMP levels upon receptor activation. However, when we look at the results of the

CAMYEL biosensor for our three tested receptors, we expect that this biosensor has a relatively narrow dynamic range.

6.2.3. Alternative methods to study cAMP signaling upon receptor activation

Over the years several other methods have been developed to monitor the cAMP levels upon receptor activation and two of these should, in my opinion, also be tested as alternative methods to monitor intracellular cAMP levels upon receptor activation. The first alternative biosensor is the GloSensor cAMP Assay (Promega) which enables a direct real-time detection of cAMP levels in living cells. The second alternative method is the BD ACT*One* cAMP Assay (BD Biosciences) since this assay can be used to measure both intracellular Ca^{2+} and cAMP levels in the same cell line.

6.3. Identification of G proteins in *B. terrestris* and *S. gregaria*

To interpret the data of the $BRET^2$-based G protein biosensors we also performed a BLAST analysis to identify G protein subunit sequences in the genome database of *B. terrestris* (Sadd et al., 2015) and the transcriptome database of *S. gregaria* (Verdonck, 2017). However, since no overview concerning G proteins in insects exists in literature, we cannot discuss these results in a broader context.

By means of a multiple sequence alignment and a percent identity matrix, we compared these putative insect G protein subunit sequences with the human G protein subunit sequences that were used to construct the $BRET^2$-based G protein biosensors. We compared the G protein subunits per G protein subfamily, with the exception of the $G\alpha_{i/o}$ subfamily in which we analyzed the $G\alpha_i$ and $G\alpha_o$ sequences separately since this subfamily comprises five biosensors. Overall, the insect and human sequences of $G\alpha_i$, $G\alpha_o$, $G\alpha_s$ and $G\alpha_{q/11}$ subunits are very similar. The insect G protein subunits show a sequence identity of ~90 % with each other and ~80 % with the human G protein subunits. These numbers are comparable with these reported by Jacquin-Joly and co-workers (2002), who identified the $G\alpha_q$ subunit sequence in the cabbage moth, *Mamestra brassicae*. They reported a sequence identity of 87 % with the *D. melanogaster* $G\alpha_q$ subunit sequence and a sequence identity of 80 % with the human and mouse $G\alpha_q$ subunit sequence.

However, insect and human members of the $G\alpha_{12/13}$ subfamily show less sequence identity than the other G protein subunit families. Overall, the insect $G\alpha_{12/13}$ subunit sequences only show a sequence identity of 58 % with the human $G\alpha_{12}$ and $G\alpha_{13}$ subunit sequences and of 80 % with each other.

Additionally, we also identified putative Gβ and Gγ subunit sequences in the genome and transcriptome databases of *B. terrestris* and *S. gregaria*, respectively. In contrast to the Gα subunit sequences, we were able to identify two Gβ and two Gγ in each of these species. By looking at the

multiple sequence alignment and the percent identity matrix, we concluded that *Schgr*-Gβ$_1$ and *Bomte*-Gβ$_1$, with a sequence identity of ~86 %, are more related to the *Homsa*-Gβ$_1$ sequence that was used to construct the BRET^2-based G protein biosensor, compared to a sequence identity of ~52 % of *Schgr*-Gβ$_2$ and *Bomte*-Gβ$_2$. The same range of identity is seen when human Gβ sequences are compared (when comparing four *Homsa*-Gβ$_{1-4}$ sequences 78 – 88 % identity is observed). In contrast, *Homsa*-Gβ$_5$ only shares a sequence identity of 51 – 53 % with the four other *Homsa*-Gβ subunit isoforms (Dupré et al., 2009).

The Gγ subunit sequence is much shorter than the Gα and Gβ subunit sequences. Although we did identify two putative Gγ sequences in each insect, none of these is showing a high sequence identity with the human Gγ sequence that was used to construct the Gγ$_2$-GFP10 biosensor. The sequence identity merely ranges from 30 % with *Bomte*-Gγ$_e$ to 42 % with *Bomte*-γ$_1$. Nevertheless, *Schgr*-Gγ$_1$ and *Bomte*-γ$_1$ on one hand and *Schgr*-Gγ$_2$ and *Bomte*-Gγ$_e$ seem to be orthologues showing a sequence identity of 72 % and 92 %, respectively.

Overall, we conclude that the G protein subunit sequences of the two insect species are more similar to each other than to their human counterparts. With exception of the Gα$_{12/13}$ subunit family, the Gα subunit sequences show a high similarity. The Gβ subunits seem to be less conserved, while the Gγ subunit sequences only display a very limited degree of conservation, especially when comparing insects with humans.

6.4. BRET^2-based G protein biosensors

6.4.1. Analysis of the BRET^2-based G protein biosensors

By testing three insect receptors, *Bomte*-SIFR, *Schgr*-ATR and *Schgr*-CRF-DHR1, we have shown that the BRET^2-based G protein biosensors, consisting of the human Gα$_x$Gβ$_1$γ$_2$ combinations, can accurately monitor the activation of insect GPCRs. We have shown that *Bomte*-SIFR activates the Gα$_{i/o}$ and Gα$_q$ biosensors, *Schgr*-ATR activates the Gα$_{i/o}$ and Gα$_{q/11}$ biosensors, and *Schgr*-CRF-DHR1 activates the Gα$_{i/o}$ and Gα$_s$ biosensors. However, we were not able to detect significant activation of any of the biosensors of the Gα$_{12/13}$ subfamily. This may suggest that these receptors do not activate members of this Gα$_{12/13}$ subfamily. Nevertheless, as described above, when we compared the sequences of human and insect (*i.e. B. terrestris* and *S. gregaria*) Gα$_{12/13}$ subfamily members, we found that this subfamily is less conserved than the three other Gα subfamilies.

Furthermore, the insect receptor activation, as monitored with these biosensors, proved to be dose-dependent. Notably, the EC$_{50}$ values of all these activated biosensors were in the high nanomolar range for all three receptors. However, for the Gα$_{i1}$ biosensor, using a concentration of 0.10 nM

Bomte-SIFa, *Schgr*-AT or Schgr-CRF-DH always showed a lot of variation, resulting in a lower BRET^2 signal compared to 1 nM of peptide. Therefore, this biosensor may be considered a less trustworthy biosensor to study G$\alpha_{i/o}$ signaling of insect GPCRs.

It should also be noted that the BRET^2 signal measured upon receptor activation does not result from an amplification of a signal, as is the case for the assays which measure secondary messenger molecules, such as Ca^{2+} and cAMP. In contrast, the BRET^2 signal is generated by a change in conformation of the G proteins (Galés et al., 2006), a signal that is not amplified during G protein signaling.

We have also shown that each receptor is able to activate its own panel of G proteins. However, we also mentioned that the BRET^2-based G protein biosensors do not only show the activation of a G protein subunit family, but can also discriminate which G protein within a given G protein subfamily is activated. Nevertheless, when we look at the numbers of putative G protein subunit sequences identified in *B. terrestris* and *S. gregaria*, we identified only one subunit sequence for each Gα subunit family, with the exception of the G$\alpha_{i/o}$ subfamily, in which we found a Gα_i and a Gα_o sequence. Therefore, showing which specific human Gα protein within a Gα protein subfamily can be activated may have no added value for understanding insect GPCR signaling in natural conditions, since, at least in case of *B. terrestris* and *S. gregaria*, these insects do not possess the same diversity of Gα protein subunits as encountered in humans. Moreover, the data should be interpreted with caution, since using these biosensors also comes with several concerns which are elaborately discussed below (section 6.4.2).

Surprisingly, when the BRET^2-based G-protein biosensors are tested with *Schgr*-CRF-DHR1, both G$\alpha_{i/o}$ and Gα_s biosensors are activated. These results might seem contradictory. However, multiple receptors exist which are able to couple through both G protein subfamilies, such as the human β2-adrenergic receptor (Xiao, 2001) and the human M_2-muscarinic receptor (Griffin et al., 2007). In addition, it should be kept in mind that receptor signaling is very complicated and depends on the specific cellular conditions, such as the cell type and the presence of accessory proteins. The *Schgr*-CRF-DHR1 might have the intrinsic capacity to couple to both G-protein subfamilies, and overexpression of the Gα proteins in this *in cellulo* assay might reveal this intrinsic capacity.

In addition, several receptors exist that are known to couple through several Gα proteins, depending on the cell type. For instance, stimulation of the chemokine receptor CXCR4 by CXCL12 induces chemotaxis in lymphocytes through coupling through Gα_{i2}, whereas chemotaxis in dendritic cells is induced by coupling through both Gα_{i1} and Gα_q (Rubin, 2009).

Activation of both subfamilies ($G\alpha_{i/o}$ and $G\alpha_s$) does not only have an effect on AC but these $G\alpha$ subunits can also interact with other effector proteins (Dorsam and Gutkind, 2007). This might also explain why the results of the cAMP reporter assays do not support the results of the $BRET^2$-based G-protein biosensors, which is the case for all three receptors. It should also be noted that both cAMP reporter assays also show contradictory results. For instance, the CRE-dependent luciferase assay shows an increase in bioluminescent reporter activity when *Schgr*-ATR is activated, while the CAMYEL biosensor shows no detectable response. However, as discussed in section 6.2, both assays have some disadvantages, and alternative methods should be tested to detect intracellular cAMP levels upon receptor activation.

Finally, the magnitude of the $\Delta BRET^2$ signals obtained with insect receptors is compared to the magnitude of the $\Delta BRET^2$ signals of human GPCR receptors which are known to activate certain biosensors. For all three receptors, the $\Delta BRET^2$ signals of the $G\alpha_o$ biosensors ($G\alpha_{oa}$ and $G\alpha_{ob}$) are comparable to the $\Delta BRET^2$ signals measured with the *H. sapiens* chemokine receptor CCR2 (Corbisier et al., 2015). However, the $\Delta BRET^2$ signals of the $G\alpha_i$ ($G\alpha_{i1}$, $G\alpha_{i2}$, $G\alpha_{i3}$) biosensors are only in the same range as *Homsa*-CCR2 for *Bomte*-SIFR (except for $G\alpha_{i1}$), but not for *Schgr*-ATR, nor *Schgr*-CRF-DHR1. In addition, also the $\Delta BRET^2$ signal of the $G\alpha_s$ biosensor for *Schgr*-CRF-DHR1 is lower when compared to the *H. sapiens* β2-adrenergic receptor (*Homsa*-β2-AR; Saulière et al., 2012), and the $\Delta BRET^2$ signal of the $G\alpha_{q/11}$ biosensors for *Bomte*-SIFR (only $G\alpha_q$) and *Schgr*-ATR are lower when compared to the *H. sapiens* angiotensin II type 1 receptor (*Homsa*-AT1R; Saulière et al., 2012).

The fact that, in general, these $BRET^2$-based G protein biosensors have a lower magnitude in $\Delta BRET^2$ signal is no surprise, since receptor signaling is very complicated and depends on the specific cellular conditions. Moreover, these tests are performed with human-based biosensors in HEK cells. This concern is, amongst other concerns, elaborately discussed below.

6.4.2. Concerns using the $BRET^2$-based G protein biosensors

Using vertebrate $BRET^2$-based G protein biosensors to study insect G protein mediated signaling entails several concerns. In this section we enlist most important concerns.

6.4.2.1. Using human HEK cells and human-based biosensors

The first concern regarding the $BRET^2$-based G protein assay is the fact that this assay is performed in vertebrate HEK cells and that the biosensors are constructed with vertebrate proteins. As elaborated in the general introduction, GPCR signaling is dependent on the intracellular milieu and is highly context specific. However, the physiological conditions in this vertebrate cell line can differ from the physiological conditions of insect cells. This may impact posttranslational modifications,

such as glycosylation, palmitoylation and phosphorylation, and thus may affect, amongst others, receptor maturation, protein folding and receptor signaling (Hanyaloglu and Zastrow, 2008; Moore et al., 2006).

Additionally, the endocytic pathway may be regulated differently influencing receptor desensitization, internalization or degradation, and essential interacting partners may not be present. We have discussed that receptor signaling may take place at the plasma membrane, in endosomes or in the secretory compartments, such as the endoplasmic reticulum and the Golgi apparatus (Irannejad et al., 2017; Wootten et al., 2018). We now also know that receptor trafficking also depends on GPCR partners and thus the signalosome composition. (Hanyaloglu and Zastrow, 2008; Oakley et al., 2000; Pierce et al., 2002; Thomsen et al., 2016). However, receptor trafficking might be differentially regulated in vertebrate cell lines compared to insect cells. Moreover, since this mechanism is highly dependent on the environmental context, the use of cell lines in general, even if they would be insect cell lines, may give a distorted interpretation of receptor signaling compared to the *in vivo* situation since both the receptor and the effector are overexpressed. However, a recent study Ehrlich and co-workers (2019) shows that the results of the $G\alpha_i$ $BRET^2$-based G protein biosensors in the *in cellulo* assay are in agreement with the results of an *in vivo* study in native neurons when the mu opioid receptor (MOR) is tested with both experimental systems.

6.4.2.2. Gβγ dimer combination

Another concern using these $BRET^2$-based G protein biosensors is the fact that these biosensors are composed of one Gβγ dimer combination, namely the $G\beta_1\gamma_2$ dimer. In humans, 16 different Gα subunit encoding genes, 5 Gβ subunit genes and 13 Gγ subunit genes are identified (Wootten et al., 2018). Knowing that additional variants exist due to alternative splicing and post-translational processing, leading to up to one thousand theoretically possible heterotrimeric combinations (Denis et al., 2012), using one Gβγ dimer combination to study the G protein mediated signaling might not be sufficient to study G protein mediated signaling for all GPCRs, even though this $G\beta_1\gamma_2$ dimer combination has proven its value in several studies with vertebrate receptors (Audet et al., 2008: Bellot et al., 2015; Bruzzone et al., 2014; Busnelli et al., 2012; Capra et al., 2013; Corbisier et al., 2015; Damian et al., 2015; De Henau et al., 2016; Galandrin et al., 2008; 2016; Galés et al., 2006; Garcia et al., 2018; Hansen et al., 2013; Leduc et al., 2009; Maurice et al., 2010; M'Kadmi et al., 2015; Peverelli et al., 2013; Rives et al., 2012 Onfroy et al., 2017; Saulière et al., 2012; Schmitz et al., 2014; Schrage et al., 2015). Moreover, this Gβγ dimer combination might not be the right combination to

study G protein mediated signaling of insect GPCRs. As discussed above, we identified two putative Gβ subunit and two putative Gγ subunit sequences in both *B. terrestris* and *S. gregaria*. For each of these species, one Gβ subunit is identified that is more related to the *Homsa*-$G\beta_1$ sequence that was used to construct the BRET biosensor, namely *Schgr*-$G\beta_1$ and *Bomte*-$G\beta_1$. However, none of the identified Gγ subunit sequences is clearly similar to *Homsa*-$G\gamma_2$. Therefore, since the quality and efficiency of effector activation by G proteins is not only determined by the structure of the Gα subunit, but also by the structure and the composition of the Gβγ dimer, this can have important implications for receptor signaling of insect GPCRs (Cabrera-Vera et al., 2003; Oldham and Hamm, 2008).

In addition to the impact of the Gβγ dimer combinations, Gβ and Gγ separately also impact receptor signaling. Since all identified Gγ subunit sequences of *B. terrestris* and *S. gregaria* do not seem to show a very clear similarity with the human $G\gamma_2$ subunit, this could have major consequences for receptor signaling. Furthermore, although we did identify two Gβ subunit sequences which are similar to *Homsa*-$G\beta_1$, the sequence variation is sufficient to alter signaling properties of the receptor. Moreover, the sequence variation is in the same range as the sequence variation between *Homsa*-$G\beta_{1\text{-}4}$ (Dupré et al., 2009). Since the same degree of variation has an impact on receptor signaling within humans, this degree of variation may also impact G protein mediated signaling of insect GPCRs.

Taken all this together, we should be aware that the human dimer combination $G\beta_1\gamma_2$ in the $BRET^2$-based G protein assay has its limitations and might bias G protein mediated signaling of insect GPCRs.

6.4.2.3. G protein stoichiometry

The biased activity of GPCR ligands also seems to be dependent on the stoichiometry of the G protein Gα subunit. The degree of Gα subunit expression appears to have an impact on receptor signaling. Since the $BRET^2$-based G protein biosensors evoke an overexpression of the Gα subunit this might also influence receptor signaling. Therefore, results obtained with these *in vitro* cellular assays should be further confirmed in *in vivo* systems (Onfroy et al., 2017).

6.5. Scientific relevance of the obtained results for the development of new pest control agents

There is a continuing search for new pest control agents that are selective in their mechanisms of action, environmentally friendly and discriminative only against the target species. Neuropeptides and their receptors (usually GPCRs) are an excellent target for pest management strategies (Altstein and Nässel, 2010; Gäde and Goldsworthy, 2003). To date, only one insecticide targeting an insect GPCR is commercially available, namely Amitraz, which targets the octapamine receptor (Casida and Durkin, 2013).

Under the denominator "integrated pest management", it is important that multiple, suppressive tactics are approached to avoid resistance to pesticides and minimize the impact on human health and other organisms (Ehler, 2006). This emphasizes the necessity of this continuous search for new targets and new strategies with alternated modes of action.

A first potential strategy to target neuropeptide receptor systems is the RNA interference (RNAi) technology. Via the delivery of gene-specific double-stranded RNA molecules, a species-specific endogenous gene silencing of the neuropeptide, its receptor, or both can be triggered. This post transcriptional gene silencing mechanism is currently seen as a promising strategy, as exemplified by the elevated number of reports on this topic, as reviewed by Santos and co-workers (2014) and Vogel and co-workers (2019).

The second strategy is the identification of stable compounds with an enhanced half-life that bind to the GPCRs evoking the desired cellular and subsequent physiological responses. These compounds can be selected in high-throughput *in cellulo* screening assays. The signaling properties of the selected compound can be further investigated with BRET^2-based G protein biosensors since biased agonism has important implications for drug design (Denis et al., 2012). This is demonstrated by a study of Galandrin and co-workers (2016) in which they use these BRET^2-based biosensors and showed that the peptide Angiotensin-(1-7) has biased activity at *Homsa*-AT1-R. Moreover, this compound acts as an antagonist for the G protein mediated signaling pathways, which is known to induce cardiodeleterious effects, but acts as an agonist for the β-arrestin signaling pathway, which induces a cardioprotective effect. In contrast, the octapeptide angiotensin II (AngII), which also acts on *Homsa*-AT1-R, signals through both the G protein, more specifically $G\alpha_q$ and $G\alpha_{i3}$, and the β-arrestin signaling pathway. This example also emphasizes important applications of reliable BRET^2-based biosensors to detect β-arrestin and G protein activation in the process of developing pesticides.

6.6. Future prospects

6.6.1. Localization of the neuropeptide precursors and GPCRs

In this study, we investigate the relative transcript levels of several neuropeptide precursors and receptors by means of qRT-PCR. Now that we know in which tissues these genes are expressed, it might be interesting to localize the transcripts and proteins in more detail. For instance, RNA probes can be designed for *in situ* hybridization on cryosections of the brain or full Malpighian tubules to detect transcripts in specific regions of the brain or specific cells in the Malpighian tubules. The proteins can be localized in more detail by means of immunocytochemistry (Cabrero et al., 2002).

6.6.2. Functional studies

The tissue distribution analysis of the receptors can already be used to infer possible functional roles of the neuropeptides and their corresponding receptors. However, to truly investigate the physiological functions, additional studies are in order. By means of injection studies, functional responses can be provoked. In addition, knockout studies or knockdown studies of neuropeptides and their receptors can give a clearer understanding of the physiological roles. The RNAi technology, which was already mentioned as a potential strategy to target components of neuropeptide signaling pathways for pest control, is an important molecular tool to establish a post-transcriptional knockdown triggered by long double (ds)RNA molecules and has proven its value in insects (Santos et al., 2014; Vogel et al., 2019).

Injection and RNAi studies have already been performed for *Schgr*-CRF-DH by Van Wielendaele and co-workers (2012), but not for *Bomte*-SIFa, *Schgr*-AT or their receptors. I did, however, induce an RNAi knockdown for *Schgr*-CRF-DHR1 and *Schgr*-CRF-DHR2, using two RNAi constructs for each receptor transcript. Sadly, I did not observe any statistically significant effects in this pilot study (results not shown).

6.6.3. Pharmacological studies of the secondary messenger pathways

In this study, we monitor the fluctuations of the secondary molecules Ca^{2+} and cAMP upon receptor activation and use $BRET^2$-based G protein biosensors to detect the direct activation of several G proteins. However, these are not the only downstream signaling pathways activated by GPCRs. Therefore, it would also be interesting to investigate other signaling pathways as well, including the G protein independent signaling pathways, such as the β-arrestin signaling pathways.

6.6.3.1. β-arrestin signaling pathways

As discussed in the general introduction, β-arrestins play a crucial role in GPCR desensitization, resensitization, receptor sequestration and G protein independent signaling. Due to their importance in receptor signaling, it would be interesting to also study arrestin activation and recruitment at insect GPCRs. To date, multiple biosensors are developed to monitor effects of arrestins upon receptor activation.

For instance, by fusing the β-arrestin to an energy donor and fusing the receptor to an energy acceptor, BRET can also be used to detect β-arrestin recruitment to the plasma membrane. In this case, an increase in BRET signal is expected (Corbisier et al., 2015).

Domain Therapeutics, the company that also commercialized the BRET^2-based G protein biosensors also developed BRET^2-based biosensors to study arrestin activation. These biosensors are also commercialized under the name BioSens-All biosensors. In order to measure arrestin activation and recruitment to the plasma membrane, a GFP is fused to the N-terminus of β-arrestin while *R*luc is linked to its C-terminus. Receptor activation and β-arrestin recruitment to the plasma membrane triggers a conformational change of β-arrestin which results in the separation of the donor molecule *R*luc and the acceptor GFP and thus results in a decrease in BRET^2 signal. These biosensors have been developed with the human β-arrestin1 and β-arrestin2 molecules (Domain Therapeutics, 2019b). These biosensors could be tested with the insect GPCRs or similar biosensors could also be developed with insect β-arrestin proteins. However, it is important to take into account legal considerations since these biosensors are patented in the United States (University of Montreal, Bouvier and Charest, 2004a), Canada (University of Montreal, Bouvier and Charest, 2005) and under the International Patent Cooperation Union (University of Montreal Bouvier and Charest, 2004b). Notwithstanding, the former biosensor, in which β-arrestin is fused to an energy donor and the receptor to an energy acceptor, is not patented.

6.6.3.2. Other signaling pathways

GPCRs do not only transduce their signal through G protein signaling pathways or β-arrestin signaling pathways, but also other effectors are involved in receptor signaling, such as GPCR kinases (GRKs). In addition, also other secondary molecules, besides Ca^{2+} and cAMP, are involved in GPCR downstream signaling pathways. It would be interesting to look at these other signaling pathways as well. For instance, Promega has designed a GloSensor cGMP Assay to monitor cGMP concentrations upon receptor activation, similarly to the GloSensor cAMP Assay (Promega). Furthermore, multiple assays to monitor other transducers and secondary messenger molecules

exist, besides the ones mentioned in this thesis. However, discussing all these assays is beyond the scope of this thesis and these will not be discussed any further.

6.6.4. Design of insect BRET^2-based G protein biosensors

Since several concerns are addressed using the human BRET^2-based G protein biosensors with insect GPCRs, it might be useful to design similar BRET^2-based biosensors with insect G proteins. We have shown that the sequences of the G protein subunits are more similar between *B. terrestris* and *S. gregaria,* when compared to the human G protein subunits, and this is probably also a fact for insect G protein subunits in general. By designing BRET^2-based G protein constructs with insect G protein subunits, G protein activation would occur with G protein subunits which more closely resemble the structures of endogenous G protein subunits. By performing this assay in insect cells, the native structure and mode of action of the GPCR and the G proteins are respected.

Notwithstanding the potential of developing this BRET assay with insect G proteins, also in this case it is important to take into account legal considerations since these BRET^2-based G protein biosensors are patented in the United States (University of Montreal; Bouvier et al., 2006a) and under the International Patent Cooperation Treaty (University of Montreal; Bouvier et al., 2006b). However, these legal concerns could be mitigated by requesting for authorization or establishing a collaboration.

6.6.5. Receptor oligomerization

To date, no reports exist on receptor dimerization or higher order oligomerization in insects. Furthermore, finding two receptors that form dimers or oligomers in insects is like finding a needle in a haystack, since, in theory, every GPCR can bind any other GPCR expressed in the same cells. It should also be considered that dimerization measured in an *in vitro* cellular assay does not prove *in vivo* dimerization. Therefore, the identification of receptor di- or oligomerization should also include proof that these receptors are indeed expressed in the same cells, preferably in the same subcellular compartment.

Several methods have been developed to detect receptor di- or oligomerization. One of these methods also uses the BRET technology to show homo- and heterodimer formation. Additionally, sequential resonance energy transfer (SRET), a combination of FRET and BRET, has allowed detection of GPCR trimers, and a combination of BRET with molecular complementation, using GPCRs fused to complementary hemiproteins of donor/acceptor BRET pairs, permits detection of tetramers (Franco et al., 2016).

In addition to the use of BRET-based assays to prove that certain receptors can form dimers or higher order oligomers, $BRET^2$-based G protein biosensors and BRET-based β-arrestin biosensors can be used to study the impact of homodimer, heterodimer or oligomer formation on receptor signaling. Therefore, it would be worthwhile to study these $BRET^2$-based G protein biosensors in more detail or consider constructing $BRET^2$-based biosensors with insect specific proteins.

6.6.6. BRET biosensors for studying intracellular trafficking and endocytosis

As mentioned earlier, GPCR signaling is a complex process and G protein mediated signaling can also take place in endosomes or in secretory compartments, such as the endoplasmic reticulum and the Golgi apparatus (Irannejad et al., 2017; Vilardaga et al., 2014; Wootten et al., 2018). The use of BRET biosensors to detect the direct activation of G proteins or β-arrestin translocation has already been discussed. In addition, enhanced bystander BRET biosensors have been developed to quantitatively monitor GPCRs and β-arrestin trafficking in live cells. Knowing more about the intracellular trafficking and endocytosis of the receptors might give useful information for drug action, since receptor trafficking can be differentially regulated by ligands, potentially affecting cell responsiveness and drug efficacies. In enhanced bystander BRET, the donor luciferase (*R*luc) and the fluorescent acceptor (rGFP) are both from *Renilla reniformis*. This is in contrast with the conventional BRET assays, in which the non-naturally interacting chromophores, luciferase from *R. reniformis* (*R*luc) and a GFP variant from *Aeqorea victoria,* are used. By choosing for naturally interacting chromophores, the BRET signal is improved, which makes it possible to detect a BRET signal in live cells in real-time (Namkung et al., 2016).

6.6.7. Blocking or stimulating Gα subunits

In the future, it would also be possible to study G protein mediated signaling in more detail by blocking or stimulating Gα-protein subfamilies with Gα-protein inhibitors or stimulators. For instance, pertussis toxin (PTX) is used to inhibit $G\alpha_{i/o}$ signaling and the plant-derived depsipeptide FR900359 (Schrage et al., 2015) is reported to be a selective, cell-permeable inhibitor of the $G\alpha_{q/11}$ subfamily. This compound is commercially available under the name UBO-QIC. Notably, an earlier study reported that the bacterial derived depsipeptide YM-254890 blocks $G\alpha_{q/11}$ signaling as well (Nishimura et al., 2010). However, this compound has been withdrawn and is no longer available to researchers (Schrage et al., 2015). Additionally, a cholera toxin appears to stimulate the $G\alpha_s$-protein (Lencer, 2001; Holdfeldt et al., 2017). In insects, the pertussis toxin has already been used in *L. migratoria* in order to characterize the tyramine receptor (Vanden Broeck et al., 1995).

6.7. Overall conclusion

In this thesis we have provided evidence that BRET^2-based G protein biosensors for three out of four G protein subfamilies, namely G$\alpha_{i/o}$, Gα_s and G$\alpha_{q/11}$, respond to activation of insect GPCRs. These results pave the way to use this BRET^2-based G protein assay to unravel the G protein mediated pathways of insect receptors. However, to fully understand insect G protein signaling, more receptors should be tested with these biosensors. However, since G protein subunits seem to be less diverse in insects than in humans, and since knowing which specific G protein biosensor within a G protein subunit family is activated might not give any added value if this subunit family has only one member in insects, it might be useful to test which of the biosensors of a certain G protein subunit family is the most reliable biosensor to test G protein activation by a given insect GPCR. Finally, it might also be useful to develop new biosensors based on G proteins from insects.

References

Abdel-Latief, M., Hoffmann, K.H., 2014. Functional activity of allatotropin and allatostatin in the pupal stage of a holometablous insect, *Tribolium castaneum* (Coleoptera, Tenebrionidae). Peptides 53, 172–184. https://doi.org/10.1016/j.peptides.2013.10.007

Adami, M.L., Damborenea, C., Ronderos, J.R., 2011. Expression of a neuropeptide similar to allatotropin in free living turbellaria (platyhelminthes). Tissue Cell 43, 377–83. https://doi.org/10.1016/j.tice.2011.07.005

Agrawal, T., Sadaf, S., Hasan, G., 2013. A genetic RNAi screen for IP_3/Ca^{2+} coupled GPCRs in *Drosophila* identifies the PdfR as a regulator of insect flight. PLoS Genet. 9, e1003849. https://doi.org/10.1371/journal.pgen.1003849

Ahn, S.-J., Martin, R., Rao, S., Choi, M.-Y., 2017. Neuropeptides predicted from the transcriptome analysis of the gray garden slug *Deroceras reticulatum*. Peptides 93, 51–65. https://doi.org/10.1016/j.peptides.2017.05.005

Alonso, V., Friedman, P.A., 2013. Minireview: Ubiquitination-regulated G protein-coupled receptor signaling and trafficking. Mol. Endocrinol. 27, 558–572. https://doi.org/10.1210/me.2012-1404

Altstein, M., Nässel, D.R., 2010. Neuropeptide signaling in insects. Springer, Boston, MA, pp. 155–165. https://doi.org/10.1007/978-1-4419-6902-6_8

Anderson, M., Cochrane, D.G., 1978. Studies on the mid-gut of the desert locust *Schistocerca gregaria*. Ultrastructure of the muscle coat and its innervation. J. Morphol. 156, 257–278. https://doi.org/10.1002/jmor.1051560208

Areiza, M., Nouzova, M., Rivera-Perez, C., Noriega, F.G., 2014. Ecdysis triggering hormone ensures proper timing of juvenile hormone biosynthesis in pharate adult mosquitoes. Insect Biochem. Mol. Biol. 54, 98–105. https://doi.org/10.1016/j.ibmb.2014.09.006

Arendt, A., Neupert, S., Schendzielorz, J., Predel, R., Stengl, M., 2016. The neuropeptide SIFamide in the brain of three cockroach species. J. Comp. Neurol. 524, 1337–1360. https://doi.org/10.1002/cne.23910

Arey, B.J., 2012. The role of glycosylation in receptor signaling. IntechOpen 273–286. https://doi.org/10.5772/32009

Audet, N., Galés, C., Archer-Lahlou, E., Vallières, M., Schiller, P.W., Bouvier, M., Pineyro, G., 2008. Bioluminescence resonance energy transfer assays reveal ligand-specific conformational changes within preformed signaling complexes containing delta-opioid receptors and heterotrimeric G proteins. J. Biol. Chem. 283, 15078–88. https://doi.org/10.1074/jbc.M707941200

Audsley, N., Down, R.E., Isaac, R.E., 2015. Genomic and peptidomic analyses of the neuropeptides from the emerging pest, *Drosophila suzukii*. Peptides 68, 33–42. https://doi.org/10.1016/j.peptides.2014.08.006

Audsley, N., Goldsworthy, G.J., Coast, G.M., 1997. Circulating levels of *Locusta* diuretic hormone: The effect of feeding. Peptides 18, 59–65. https://doi.org/10.1016/S0196-9781(96)00234-3

Audsley, N., Kay, I., Hayes, T.K., Coast, G.M., 1995. Cross reactivity studies of CRF-related peptides on insect Malpighian tubules. Comp. Biochem. Physiol. Part A Physiol. 110, 87–93. https://doi.org/10.1016/0300-9629(94)00132-D

Audsley, N., Weaver, R.J., 2009. Neuropeptides associated with the regulation of feeding in insects. Gen.

Comp. Endocrinol. 162, 93–104. https://doi.org/10.1016/j.ygcen.2008.08.003

Audsley, N., Weaver, R.J., 2006. Analysis of peptides in the brain and corpora cardiaca-corpora allata of the honey bee, *Apis mellifera* using MALDI-TOF mass spectrometry. Peptides 27, 512–520. https://doi.org/10.1016/j.peptides.2005.08.022

Badisco, L., Huybrechts, J., Simonet, G., Verlinden, H., Marchal, E., Huybrechts, R., Schoofs, L., De Loof, A., Vanden Broeck, J., 2011a. Transcriptome analysis of the desert locust central nervous system: production and annotation of a *Schistocerca gregaria* EST database. PLoS One 6, e17274. https://doi.org/10.1371/journal.pone.0017274

Badisco, L., Marchal, E., Van Wielendaele, P., Verlinden, H., Vleugels, R., Vanden Broeck, J., 2011b. RNA interference of insulin-related peptide and neuroparsins affects vitellogenesis in the desert locust *Schistocerca gregaria*. Peptides 32, 573–580. https://doi.org/10.1016/j.peptides.2010.11.008

Baggerman, G., Boonen, K., Verleyen, P., De Loof, A., Schoofs, L., 2005. Peptidomic analysis of the larval *Drosophila melanogaster* central nervous system by two-dimensional capillary liquid chromatography quadrupole time-of-flight mass spectrometry. J. Mass Spectrom. 40, 250–60. https://doi.org/10.1002/jms.744

Bai, H., Palli, S.R., 2016. Identification of G protein-coupled receptors required for vitellogenin uptake into the oocytes of the red flour beetle, *Tribolium castaneum*. Sci. Rep. 6, 27648. https://doi.org/10.1038/srep27648

Baldwin, D.C., Schegg, K.M., Furuya, K., Lehmberg, E., Schooley, D.A., 2001. Isolation and identification of a diuretic hormone from *Zootermopsis nevadensis*. Peptides 22, 147–152. https://doi.org/10.1016/S0196-9781(00)00371-5

Bao, C., Yang, Y., Huang, H., Ye, H., Girardie, A., 2015. Neuropeptides in the cerebral ganglia of the mud crab *Scylla paramamosain*: transcriptomic analysis and expression profiles during vitellogenesis. Sci. Rep. 5, 17055. https://doi.org/10.1038/srep17055

Bellot, M., Galandrin, S., Boularan, C., Matthies, H.J., Despas, F., Denis, C., Javitch, J., Mazères, S., Sanni, S.J., Pons, V., Seguelas, M.-H., Hansen, J.L., Pathak, A., Galli, A., Sénard, J.-M., Galés, C., 2015. Dual agonist occupancy of AT1-R–α2C-AR heterodimers results in atypical Gs-PKA signaling. Nat. Chem. Biol. 11, 271–279. https://doi.org/10.1038/nchembio.1766

Bendena, W.G., 2010. Neuropeptide physiology in insects. Springer, Boston, MA, pp. 166–191. https://doi.org/10.1007/978-1-4419-6902-6_9

Beyenbach, K.W., 1995. Mechanism and regulation of electrolyte transport in Malpighian tubules. J. Insect Physiol. 41, 197–207. https://doi.org/10.1016/0022-1910(94)00087-W

Bharadwaj, R.K., Banerjee, S.K., 1971. The nervous system of the desert locust, *Schistocerca gregaria* (Orthoptera: Acrididae) with a discussion on muscle innervation. J. Nat. Hist. 5, 183–208. https://doi.org/10.1080/00222937100770111

Bhatt, G., da Silva, R., Orchard, I., 2014. The molecular characterization of the kinin transcript and the physiological effects of kinins in the blood-gorging insect, *Rhodnius prolixus*. Peptides 53, 148–158. https://doi.org/10.1016/J.PEPTIDES.2013.04.009

Bil, M., Timmermans, I., Verlinden, H., Huybrechts, R., 2016. Characterization of the adipokinetic hormone receptor of the anautogenous flesh fly, *Sarcophaga crassipalpis*. J. Insect Physiol. 89, 52–59. https://doi.org/10.1016/j.jinsphys.2016.04.001

Blackburn, M.B., Kingan, T.G., Bodnar, W., Shabanowitz, J., Hunt, D.F., Kempe, T., Wagner, R.M., Raina, A.K., Schnee, M.E., Ma, M.C., 1991. Isolation and identification of a new diuretic peptide from the tobacco hornworm, *Manduca sexta*. Biochem. Biophys. Res. Commun. 181, 927–932. https://doi.org/10.1016/0006-291X(91)92025-F

Blake, P.D., Kay, I., Coast, G.M., 1996. Myotropic activity of *Acheta* diuretic peptide on the foregut of the house cricket, *Acheta domesticus* (L.). J. Insect Physiol. 42, 1053–1059. https://doi.org/10.1016/S0022-1910(96)00063-7

Blanpain, C., Lee, B., Vakili, J., Doranz, B.J., Govaerts, C., Migeotte, I., Sharron, M., Dupriez, V., Vassart, G., Doms, R.W., Parmentier, M., 1999. Extracellular cysteines of CCR5 are required for chemokine binding, but dispensable for HIV-1 coreceptor activity. J. Biol. Chem. 274, 18902–8. https://doi.org/10.1074/JBC.274.27.18902

Bockaert, J., Pin, J.P., Zuker, C., 1999. Molecular tinkering of G protein-coupled receptors: an evolutionary success. EMBO J. 18, 1723–9. https://doi.org/10.1093/emboj/18.7.1723

Boerjan, B., Cardoen, D., Bogaerts, A., Landuyt, B., Schoofs, L., Verleyen, P., 2010. Mass spectrometric profiling of (neuro)-peptides in the worker honeybee, *Apis mellifera*. Neuropharmacology 58, 248–258. https://doi.org/10.1016/j.neuropharm.2009.06.026

Bourne, H.R., Sanders, D.A., McCormick, F., 1991. The GTPase superfamily: conserved structure and molecular mechanism. Nature 349, 117–127. https://doi.org/10.1038/349117a0

Bouvier, M., Charest, P., 2005. Double brilliance beta-arrestin: a biosensor for monitoring the activity of receptors and signalling molecules, and method of using same. CA2607015C.

Bouvier, M., Charest, P., 2004a. Double brilliance beta-arrestin: a biosensor for monitoring the activity of receptors and signalling molecules, and method of using same. US7932080B2.

Bouvier, M., Charest, P., 2004b. Double brilliance beta-arrestin: a biosensor for monitoring the activity of receptors and signalling molecules, and method of using same. WO2005105850A1.

Bouvier, M., Galés, C., Breton, B., 2006a. Biosensors for monitoring receptor-mediated G-protein activation. US9029097B2.

Bouvier, M., Galés, C., Breton, B., 2006b. Biosensors for monitoring receptor-mediated G-protein activation. WO2006086883A1.

Brough, S.J., Shah, P., 2009. Use of aequorin for G protein-coupled receptor hit identification and compound profiling. Methods Mol. Biol. 552, 181–98. https://doi.org/10.1007/978-1-60327-317-6_13

Bruzzone, A., Saulière, A., Finana, F., Sénard, J.-M., Lüthy, I., Galés, C., 2014. Dosage-dependent regulation of cell proliferation and adhesion through dual β_2 -adrenergic receptor/cAMP signals. FASEB J. 28, 1342–1354. https://doi.org/10.1096/fj.13-239285

Burrows, M., 1996. The neurobiology of an insect brain. Oxford University Press, Oxford. https://doi.org/10.1093/acprof:oso/9780198523444.001.0001

Busnelli, M., Saulière, A., Manning, M., Bouvier, M., Galés, C., Chini, B., 2012. Functional selective oxytocin-derived agonists discriminate between individual G protein family subtypes. J. Biol. Chem. 287, 3617–3629. https://doi.org/10.1074/jbc.M111.277178

Butcher, A.J., Kong, K.C., Prihandoko, R., Tobin, A.B., 2012. Physiological role of G-protein coupled receptor phosphorylation. Springer, Berlin, Heidelberg, pp. 79–94. https://doi.org/10.1007/978-3-642-23274-9_5

Cabrera-Vera, T.M., Vanhauwe, J., Thomas, T.O., Medkova, M., Preininger, A., Mazzoni, M.R., Hamm, H.E., 2003. Insights into G-protein structure, function, and regulation. Endocr. Rev. 24, 765–781. https://doi.org/10.1210/er.2000-0026

Cabrero, P., Radford, J.C., Broderick, K.E., Costes, L., Veenstra, J. a, Spana, E.P., Davies, S. a, Dow, J. a T., 2002. The *Dh* gene of *Drosophila melanogaster* encodes a diuretic peptide that acts through cyclic AMP. J. Exp. Biol. 205, 3799–3807.

Caers, J., Boonen, K., Van Den Abbeele, J., Van Rompay, L., Schoofs, L., Van Hiel, M.B., 2015. Peptidomics of neuropeptidergic tissues of the tsetse fly *Glossina morsitans morsitans*. J. Am. Soc. Mass Spectrom. 26, 2024–2038. https://doi.org/10.1007/s13361-015-1248-1

Caers, J., Janssen, T., Van Rompay, L., Broeckx, V., Van Den Abbeele, J., Gäde, G., Schoofs, L., Beets, I., 2016a. Characterization and pharmacological analysis of two adipokinetic hormone receptor variants of the tsetse fly, *Glossina morsitans morsitans*. Insect Biochem. Mol. Biol. 70, 73–84. https://doi.org/10.1016/j.ibmb.2015.11.010

Caers, J., Van Hiel, M.B., Peymen, K., Zels, S., Van Rompay, L., Van Den Abbeele, J., Schoofs, L., Beets, I., 2016b. Characterization of a neuropeptide F receptor in the tsetse fly, *Glossina morsitans morsitans*. J. Insect Physiol. 93–94, 105–111. https://doi.org/10.1016/j.jinsphys.2016.09.013

Caers, J., Verlinden, H., Zels, S., Vandersmissen, H.P., Vuerinckx, K., Schoofs, L., 2012. More than two decades of research on insect neuropeptide GPCRs: An overview. Front. Endocrinol. (Lausanne). 3, 1–30. https://doi.org/10.3389/fendo.2012.00151

Cahill III, T.J., Thomsen, A.R.B., Tarrasch, J.T., Plouffe, B., Nguyen, A.H., Yang, F., Huang, L.-Y., Kahsai, A.W., Bassoni, D.L., Gavino, B.J., Lamerdin, J.E., Triest, S., Shukla, A.K., Berger, B., Little, J., Antar, A., Blanc, A., Qu, C.-X., Chen, X., Kawakami, K., Inoue, A., Aoki, J., Steyaert, J., Sun, J.-P., Bouvier, M., Skiniotis, G., Lefkowitz, R.J., Performed, G.S., 2017. Distinct conformations of GPCR-β-arrestin complexes mediate desensitization, signaling, and endocytosis 114, 2562–2567. https://doi.org/10.1073/pnas.1701529114

Cannell, E., Dornan, A.J., Halberg, K.A., Terhzaz, S., Dow, J.A.T., Davies, S.A., 2016. The corticotropin-releasing factor-like diuretic hormone 44 (DH44) and kinin neuropeptides modulate desiccation and starvation tolerance in *Drosophila melanogaster*. Peptides 80, 96–107. https://doi.org/10.1016/j.peptides.2016.02.004

Capra, V., Busnelli, M., Perenna, A., Ambrosio, M., Accomazzo, M.R., Galés, C., Chini, B., Rovati, G.E., 2013. Full and partial agonists of thromboxane prostanoid receptor unveil fine tuning of receptor superactive conformation and G protein activation. PLoS One 8, e60475. https://doi.org/10.1371/journal.pone.0060475

Cardoso, J.C.R., Félix, R.C., Bergqvist, C.A., Larhammar, D., 2014. New insights into the evolution of vertebrate CRH (corticotropin-releasing hormone) and invertebrate DH44 (diuretic hormone 44) receptors in metazoans. Gen. Comp. Endocrinol. 209, 162–70. https://doi.org/10.1016/j.ygcen.2014.09.004

Carlsson, M.A., Diesner, M., Schachtner, J., Nässel, D.R., 2010. Multiple neuropeptides in the *Drosophila* antennal lobe suggest complex modulatory circuits. J. Comp. Neurol. 518, 3359–3380. https://doi.org/10.1002/cne.22405

Casida, J.E., Durkin, K.A., 2013. Neuroactive insecticides: targets, selectivity, resistance, and secondary effects. Annu. Rev. Entomol. 58, 99–117. https://doi.org/10.1146/annurev-ento-120811-153645

Cavanaugh, D.J., Geratowski, J.D., Wooltorton, J.R.A., Spaethling, J.M., Hector, C.E., Zheng, X., Johnson, E.C., Eberwine, J.H., Sehgal, A., 2014. Identification of a circadian output circuit for rest: Activity rhythms in

drosophila. Cell 157, 689–701. https://doi.org/10.1016/j.cell.2014.02.024

Cavey, M., Collins, B., Bertet, C., Blau, J., 2016. Circadian rhythms in neuronal activity propagate through output circuits. Nat. Neurosci. 19, 587–595. https://doi.org/10.1038/nn.4263

Chapman, R.F., 2012. The insects: Structure and function. Cambridge University Press, Cambridge. https://doi.org/10.1017/CBO9781139035460

Chen, C., Shahabi, V., Xu, W., Liu-Chen, L.Y., 1998. Palmitoylation of the rat mu opioid receptor. FEBS Lett. 441, 148–52.

Chen, Y.C.D., Dahanukar, A., 2018. DH44 neurons: gut-brain amino acid sensors. Cell Res. 28, 1048–1049. https://doi.org/10.1038/s41422-018-0101-z

Chini, B., Parenti, M., 2009. G-protein-coupled receptors, cholesterol and palmitoylation: facts about fats. J. Mol. Endocrinol. 42, 371–379. https://doi.org/10.1677/jme-08-0114

Christie, A.E., 2017. Neuropeptide discovery in *Proasellus cavaticus*: Prediction of the first large-scale peptidome for a member of the Isopoda using a publicly accessible transcriptome. Peptides 97, 29–45. https://doi.org/10.1016/j.peptides.2017.09.003

Christie, A.E., 2016. Prediction of *Scylla olivacea* (Crustacea; Brachyura) peptide hormones using publicly accessible transcriptome shotgun assembly (TSA) sequences. Gen. Comp. Endocrinol. 230–231, 1–16. https://doi.org/10.1016/j.ygcen.2016.03.008

Christie, A.E., 2015a. Neuropeptide discovery in *Symphylella vulgaris* (Myriapoda, Symphyla): *In silico* prediction of the first myriapod peptidome. Gen. Comp. Endocrinol. 223, 73–86. https://doi.org/10.1016/j.ygcen.2015.09.021

Christie, A.E., 2015b. *In silico* prediction of a neuropeptidome for the eusocial insect *Mastotermes darwiniensis*. Gen. Comp. Endocrinol. 224, 69–83. https://doi.org/10.1016/j.ygcen.2015.06.006

Christie, A.E., 2015c. *In silico* characterization of the neuropeptidome of the Western black widow spider *Latrodectus hesperus*. Gen. Comp. Endocrinol. 210, 63–80. https://doi.org/10.1016/j.ygcen.2014.10.005

Christie, A.E., 2014a. Expansion of the *Litopenaeus vannamei* and *Penaeus monodon* peptidomes using transcriptome shotgun assembly sequence data. Gen. Comp. Endocrinol. 206, 235–254. https://doi.org/10.1016/j.ygcen.2014.04.015

Christie, A.E., 2014b. Identification of the first neuropeptides from the Amphipoda (Arthropoda, Crustacea). Gen. Comp. Endocrinol. 206, 96–110. https://doi.org/10.1016/j.ygcen.2014.07.010

Christie, A.E., 2014c. Prediction of the first neuropeptides from a member of the Remipedia (Arthropoda, Crustacea). Gen. Comp. Endocrinol. 201, 74–86. https://doi.org/10.1016/j.ygcen.2014.01.017

Christie, A.E., 2014d. Peptide discovery in the ectoparasitic crustacean *Argulus siamensis*: Identification of the first neuropeptides from a member of the Branchiura. Gen. Comp. Endocrinol. 204, 114–125. https://doi.org/10.1016/j.ygcen.2014.05.004

Christie, A.E., 2008. *In silico* analyses of peptide paracrines/hormones in Aphidoidea. Gen. Comp. Endocrinol. 159, 67–79. https://doi.org/10.1016/j.ygcen.2008.07.022

Christie, A.E., Chi, M., 2015a. Identification of the first neuropeptides from the enigmatic hexapod order Protura. Gen. Comp. Endocrinol. 224, 18–37. https://doi.org/10.1016/j.ygcen.2015.05.015

Christie, A.E., Chi, M., 2015b. Neuropeptide discovery in the Araneae (Arthropoda, Chelicerata, Arachnida):

elucidation of true spider peptidomes using that of the Western black widow as a reference. Gen. Comp. Endocrinol. 213, 90–109. https://doi.org/10.1016/j.ygcen.2015.02.003

Christie, A.E., Cieslak, M.C., Roncalli, V., Lenz, P.H., Major, K.M., Poynton, H.C., 2018a. Prediction of a peptidome for the ecotoxicological model *Hyalella azteca* (Crustacea; Amphipoda) using a *de novo* assembled transcriptome. Mar. Genomics 38, 67–88. https://doi.org/10.1016/j.margen.2017.12.003

Christie, A.E., Hull, J.J., Richer, J.A., Geib, S.M., Tassone, E.E., 2017. Prediction of a peptidome for the western tarnished plant bug *Lygus hesperus*. Gen. Comp. Endocrinol. 243, 22–38. https://doi.org/10.1016/j.ygcen.2016.10.008

Christie, A.E., Kutz-Naber, K.K., Stemmler, E.A., Klein, A., Messinger, D.I., Goiney, C.C., Conterato, A.J., Bruns, E.A., Hsu, Y.-W.A., Li, L., Dickinson, P.S., 2007. Midgut epithelial endocrine cells are a rich source of the neuropeptides APSGFLGMRamide (*Cancer borealis* tachykinin-related peptide Ia) and GYRKPPFNGSIFamide (Gly1-SIFamide) in the crabs *Cancer borealis*, *Cancer magister* and *Cancer productus*. J. Exp. Biol. 210, 699–714. https://doi.org/10.1242/jeb.02696

Christie, A.E., Pascual, M.G., Yu, A., 2018b. Peptidergic signaling in the tadpole shrimp *Triops newberryi*: A potential model for investigating the roles played by peptide paracrines/hormones in adaptation to environmental change. Mar. Genomics 39, 45–63. https://doi.org/10.1016/j.margen.2018.01.005

Christie, A.E., Stemmler, E.A., Peguero, B., Messinger, D.I., Provencher, H.L., Scheerlinck, P., Hsu, Y.-W.A., Guiney, M.E., de la Iglesia, H.O., Dickinson, P.S., 2006. Identification, physiological actions, and distribution of VYRKPPFNGSIFamide (Val1-SIFamide) in the stomatogastric nervous system of the American lobster *Homarus americanus*. J. Comp. Neurol. 496, 406–421. https://doi.org/10.1002/cne.20932

CIRAD (French Agricultural Research Centre for International Development), 2007. Les criquets ravageurs [WWW Document]. URL http://locust.cirad.fr/tout_savoir/anatomie/anatomie_10.html (accessed 1.16.19).

Clottens, F.L., Holman, G.M., Coast, G.M., Totty, N.F., Hayes, T.K., Kay, I., Mallet, A.I., Wright, M.S., Chung, J.S., Truong, O., Bull, D.L., 1994. Isolation and characterization of a diuretic peptide common to the house fly and stable fly. Peptides 15, 971–979. https://doi.org/10.1016/0196-9781(94)90059-0

Clynen, E., Schoofs, L., 2009. Peptidomic survey of the locust neuroendocrine system. Insect Biochem. Mol. Biol. 39, 491–507. https://doi.org/10.1016/j.ibmb.2009.06.001

Coast, G.M., 1998. Insect diuretic peptides: Structures, evolution and actions. Am. Zool. 38, 442–449. https://doi.org/10.1093/icb/38.3.442

Coast, G.M., Cusinato, O., Kay, I., Goldsworthy, G.J., 1991. An evaluation of the role of cyclic AMP as an intracellular second messenger in Malpighian tubules of the house cricket, *Acheta domesticus*. J. Insect Physiol. 37, 563–573. https://doi.org/10.1016/0022-1910(91)90033-V

Coast, G.M., Kay, I., 1994. The effects of *Acheta* diuretic peptide on isolated malpighian tubules from the house cricket *Acheta domesticus*. J. Exp. Biol. 187, 225–243.

Coast, G.M., Nachman, R.J., Lopez, J., 2011. The control of Malpighian tubule secretion in a predacious hemipteran insect, the spined soldier bug *Podisus maculiventris* (Heteroptera, Pentatomidae). Peptides 32, 493–499. https://doi.org/10.1016/j.peptides.2010.11.009

Coast, G.M., Rayne, R.C., Hayes, T.K., Mallet, a I., Thompson, K.S., Bacon, J.P., 1993. A comparison of the effects of two putative diuretic hormones from *Locusta migratoria* on isolated locust Malpighian tubules. J. Exp. Biol. 175, 1–14. https://doi.org/10.1145/2207676.2208734

Coast, G.M., Te Brugge, V.A., Nachman, R.J., Lopez, J., Aldrich, J.R., Lange, A., Orchard, I., 2010. Neurohormones implicated in the control of Malpighian tubule secretion in plant sucking heteropterans: The stink bugs *Acrosternum hilare* and *Nezara viridula*. Peptides 31, 468–473. https://doi.org/10.1016/j.peptides.2009.09.017

Corbisier, J., Galès, C., Huszagh, A., Parmentier, M., Springael, J.-Y., 2015. Biased signaling at chemokine receptors. J. Biol. Chem. 290, jbc.M114.596098. https://doi.org/10.1074/jbc.M114.596098

Cronodon.com, 2018. The Insect Nervous System [WWW Document]. URL http://cronodon.com/BioTech/insect_nervous_systems.html (accessed 1.17.19).

Crooks, G.E., Hon, G., Chandonia, J.-M., Brenner, S.E., 2004. WebLogo: a sequence logo generator. Genome Res. 14, 1188–90. https://doi.org/10.1101/gr.849004

Cullen, D.A., Cease, A.J., Latchininsky, A. V., Ayali, A., Berry, K., Buhl, J., De Keyser, R., Foquet, B., Hadrich, J.C., Matheson, T., Ott, S.R., Poot-Pech, M.A., Robinson, B.E., Smith, J.M., Song, H., Sword, G.A., Vanden Broeck, J., Verdonck, R., Rogers, S.M., 2017. From molecules to management: Mechanisms and consequences of locust phase polyphenism. Adv. In Insect Phys. 53, 167–285. https://doi.org/10.1016/BS.AIIP.2017.06.002

Damian, M., Mary, S., Maingot, M., M'Kadmi, C., Gagne, D., Leyris, J.-P., Denoyelle, S., Gaibelet, G., Gavara, L., Garcia de Souza Costa, M., Perahia, D., Trinquet, E., Mouillac, B., Galandrin, S., Galès, C., Fehrentz, J.-A., Floquet, N., Martinez, J., Marie, J., Banères, J.-L., 2015. Ghrelin receptor conformational dynamics regulate the transition from a preassembled to an active receptor:G_q complex. Proc. Natl. Acad. Sci. 112, 1601–1606. https://doi.org/10.1073/pnas.1414618112

De, A., Arora, R., Jasani, A., 2014. Engineering aspects of bioluminescence resonance energy transfer systems, in: Engineering in Translational Medicine. Springer London, London, pp. 257–300. https://doi.org/10.1007/978-1-4471-4372-7_10

De, A., Ray, P., Loening, A.M., Gambhir, S.S., 2009. $BRET^3$: A red-shifted bioluminescence resonance energy transfer (BRET)-based integrated platform for imaging protein-protein interactions from single live cells and living animals. FASEB J. 23, 2702–2709. https://doi.org/10.1096/fj.08-118919

De Henau, O., Degroot, G.-N., Imbault, V., Robert, V., De Poorter, C., Mcheik, S., Galés, C., Parmentier, M., Springael, J.-Y., 2016. Signaling properties of Chemerin receptors CMKLR1, GPR1 and CCRL2. PLoS One 11, e0164179. https://doi.org/10.1371/journal.pone.0164179

de Wet, J.R., Wood, K. V, DeLuca, M., Helinski, D.R., Subramani, S., 1987. Firefly luciferase gene: structure and expression in mammalian cells. Mol. Cell. Biol. 7, 725–37. https://doi.org/10.1128/MCB.7.2.725

Deng, X. le, Kai, Z.P., Chamberlin, M.E., Horodyski, F.M., Yang, X.L., 2016. The discovery of a novel antagonist - *Manduca sexta* allatotropin analogue - as an insect midgut active ion transport inhibitor. Pest Manag. Sci. 72, 2176–2180. https://doi.org/10.1002/ps.4251

Denis, C., Sauliere, A., Galandrin, S., Senard, J.-M., Gales, C., 2012. Probing heterotrimeric G-protein activation: Applications to biased ligands. Curr. Pharm. Des. 18, 128–144. https://doi.org/10.2174/138161212799040466

DeWire, S.M., Ahn, S., Lefkowitz, R.J., Shenoy, S.K., 2007. β-arrestins and cell signaling. Annu. Rev. Physiol. 69, 483–510. https://doi.org/10.1146/annurev.physiol.69.022405.154749

Dickinson, P.S., Stemmler, E.A., Cashman, C.R., Brennan, H.R., Dennison, B., Huber, K.E., Peguero, B., Rabacal, W., Goiney, C.C., Smith, C.M., Towle, D.W., Christie, A.E., 2008. SIFamide peptides in clawed lobsters and freshwater crayfish (Crustacea, Decapoda, Astacidea): a combined molecular, mass spectrometric

and electrophysiological investigation. Gen. Comp. Endocrinol. 156, 347–60. https://doi.org/10.1016/j.ygcen.2008.01.011

Dickson, B.J., 2008. Wired for sex: the neurobiology of *Drosophila* mating decisions. Science (80-.). 322, 904–909. https://doi.org/10.1126/science.1159276

Dillen, S., Zels, S., Verlinden, H., Spit, J., Van Wielendaele, P., Vanden Broeck, J., 2013. Functional characterization of the short neuropeptide F receptor in the desert locust, *Schistocerca gregaria*. PLoS One 8, e53604. https://doi.org/10.1371/journal.pone.0053604

Dircksen, H., Neupert, S., Predel, R., Verleyen, P., Huybrechts, J., Strauss, J., Hauser, F., Stafflinger, E., Schneider, M., Pauwels, K., Schoofs, L., Grimmelikhuijzen, C.J.P., 2011. Genomics, transcriptomics, and peptidomics of Daphnia pulex neuropeptides and protein hormones. J. Proteome Res. 10, 4478–4504. https://doi.org/10.1021/pr200284e

Dirsh, V.M., 1953. Morphometrical studies on phases of the desert locust. Anti Locust Bul. 16, 1–34.

Diviani, D., Osman, H., Reggi, E., 2018. A-kinase anchoring protein-Lbc: A molecular scaffold involved in cardiac protection. J. Cardiovasc. Dev. Dis. 5, 12. https://doi.org/10.3390/jcdd5010012

Domain Therapeutics, 2019a. Domain Therapeutics - BioSens-All ™ [WWW Document]. URL http://www.domaintherapeutics.com/research-and-technology/biosens-all.html (accessed 2.28.19).

Domain Therapeutics, 2019b. BioSens-All: β-arrestin biosensor.

Donini, A., O'Donnell, M.J., Orchard, I., 2008. Differential actions of diuretic factors on the Malpighian tubules of *Rhodnius prolixus*. J. Exp. Biol. 211, 42–48. https://doi.org/10.1242/jeb.011882

Dorsam, R.T., Gutkind, J.S., 2007. G-protein-coupled receptors and cancer. Nat. Rev. Cancer 7, 79–94. https://doi.org/10.1038/nrc2069

Dragan, A.I., Pavlovic, R., Mcgivney, J.B., Casas-Finet, J.R., Bishop, E.S., Strouse, R.J., Schenerman, M.A., Geddes, C.D., 2012. SYBR Green I: Fluorescence properties and interaction with DNA. J Fluoresc 22, 1189–1199. https://doi.org/10.1007/s10895-012-1059-8

Dragulescu-Andrasi, A., Chan, C.T., De, A., Massoud, T.F., Gambhir, S.S., 2011. Bioluminescence resonance energy transfer (BRET) imaging of protein-protein interactions within deep tissues of living subjects. Proc. Natl. Acad. Sci. U. S. A. 108, 12060–5. https://doi.org/10.1073/pnas.1100923108

Dupré, D.J., Robitaille, M., Rebois, R.V., Hébert, T.E., 2009. The role of Gβγ subunits in the organization, assembly, and function of GPCR signaling complexes. Annu. Rev. Pharmacol. Toxicol. 49, 31–56. https://doi.org/10.1146/annurev-pharmtox-061008-103038

Dus, M., Lai, J.S.Y., Gunapala, K.M., Min, S., Tayler, T.D., Hergarden, A.C., Geraud, E., Joseph, C.M., Suh, G.S.B., 2015. Nutrient sensor in the brain directs the action of the brain-gut axis in *Drosophila*. Neuron 87, 139–151. https://doi.org/10.1016/j.neuron.2015.05.032

Duve, H., Audsley, N., Weaver, R.J., Thorpe, A., 2000. Triple co-localisation of two types of allatostatin and an allatotropin in the frontal ganglion of the lepidopteran *Lacanobia oleracea* (Noctuidae): Innervation and action on the foregut. Cell Tissue Res. 300, 153–63.

Duve, H., East, P.D., Thorpe, A., 1999. Regulation of lepidopteran foregut movement by allatostatins and allatotropin from the frontal ganglion. J. Comp. Neurol. 413, 405–416.

Ehler, L.E., 2006. Perspective Integrated pest management (IPM): definition, historical development and implementation, and the other IPM. Pest Manag. Sci. Pest Manag Sci 62, 787–789. https://doi.org/10.1002/ps.1247

Ehrlich, A.T., Semache, M., Gross, F., Da Fonte, D.F., Runtz, L., Colley, C., Mezni, A., LeGouill, C., Lukashova, V., Hogue, M., Darcq, E., Bouvier, M., Kieffer, B.L., 2019. Biased signaling of the mu opioid receptor revealed in native neurons. iScience 14, 47–57. https://doi.org/10.1016/j.isci.2019.03.011

Eichel, K., Jullié, D., Von Zastrow, M., 2016. β-Arrestin drives MAP kinase signalling from clathrin-coated structures after GPCR dissociation. Nat. Cell Biol. 18, 303–310. https://doi.org/10.1038/ncb3307

Elekonich, M.M., Horodyski, F.M., 2003. Insect allatotropins belong to a family of structurally-related myoactive peptides present in several invertebrate phyla. Peptides 24, 1623–1632. https://doi.org/10.1016/j.peptides.2003.08.011

Elphick, M.R., Mirabeau, O., 2014. The evolution and variety of RFamide-type neuropeptides: Insights from deuterostomian invertebrates. Front. Endocrinol. (Lausanne). 5, 1–11. https://doi.org/10.3389/fendo.2014.00093

Enserink, M., 2004. Entomology: Can the war on locusts be won? Science (80-.). 306, 1880–1882. https://doi.org/10.1126/science.306.5703.1880

Escribá, P. V., Wedegaertner, P.B., Goñi, F.M., Vögler, O., 2007. Lipid-protein interactions in GPCR-associated signaling. Biochim. Biophys. Acta - Biomembr. 1768, 836–852. https://doi.org/10.1016/j.bbamem.2006.09.001

Farran, B., 2017. An update on the physiological and therapeutic relevance of GPCR oligomers. Pharmacol. Res. 117, 303–327. https://doi.org/10.1016/j.phrs.2017.01.008

Feyereisen, R., Tobe, S.S., 1981. A rapid partition assay for routine analysis of juvenile hormone release by insect corpora allata. Anal. Biochem. 111, 372–375. https://doi.org/10.1016/0003-2697(81)90575-3

Food and Agricultural Organization of the United Nations: Locust watch, 2009. Frequently Asked Questions (FAQs) about locusts [WWW Document]. URL http://www.fao.org/ag/locusts/en/info/info/faq/index.html (accessed 2.20.19).

Food and Agricultural Organization of the United Nations, 2015. FAO desert locust information service [WWW Document]. URL http://www.fao.org/emergencies/resources/documents/resources-detail/en/c/278608/ (accessed 2.19.19).

Food and Agriculture Organization of the United Nations, 2019. Locust watch [WWW Document]. 2019. URL http://www.fao.org/ag/locusts/en/info/info/index.html (accessed 2.22.19).

Franco, R., Martínez-Pinilla, E., Lanciego, J.L., Navarro, G., 2016. Basic pharmacological and structural evidence for class A G-protein-coupled receptor heteromerization. Front. Pharmacol. 7, 1–10. https://doi.org/10.3389/fphar.2016.00076

Fredriksson, R., Lagerström, M.C., Lundin, L.-G., Schiöth, H.B., 2003. The G-protein-coupled receptors in the human genome form five main families. Phylogenetic analysis, paralogon groups, and fingerprints. Mol. Pharmacol. 63, 1256–72. https://doi.org/10.1124/mol.63.6.1256

Furuya, K., Schegg, K.M., Schooley, D.A., 1998. Isolation and identification of a second diuretic hormone from *Tenebrio molitor*. Peptides 19, 619–626. https://doi.org/10.1016/S0196-9781(97)00475-0

Gäde, G., Goldsworthy, G.J., 2003. Insect peptide hormones: A selective review of their physiology and potential application for pest control. Pest Manag. Sci. 59, 1063–1075. https://doi.org/10.1002/ps.755

Galandrin, S., Denis, C., Boularan, C., Marie, J., M'Kadmi, C., Pilette, C., Dubroca, C., Nicaise, Y., Seguelas, M.H., N'Guyen, D., Banères, J.L., Pathak, A., Sénard, J.M., Galés, C., 2016. Cardioprotective angiotensin-(1-7) peptide acts as a natural-biased ligand at the angiotensin II type 1 receptor. Hypertension 68,

1365–1374. https://doi.org/10.1161/HYPERTENSIONAHA.116.08118

Galandrin, S., Oligny-Longpré, G., Bonin, H., Ogawa, K., Galés, C., Bouvier, M., 2008. Conformational rearrangements and signaling cascades involved in ligand-biased mitogen-activated protein kinase signaling through the beta1-adrenergic receptor. Mol. Pharmacol. 74, 162–72. https://doi.org/10.1124/mol.107.043893

Galés, C., Van Durm, J.J.J., Schaak, S., Pontier, S., Percherancier, Y., Audet, M., Paris, H., Bouvier, M., 2006. Probing the activation-promoted structural rearrangements in preassembled receptor–G protein complexes. Nat. Struct. Mol. Biol. 13, 778–786. https://doi.org/10.1038/nsmb1134

Galizia, C.G., Eisenhardt, D., Martin, G., 2012. Honeybee neurobiology and behavior. Springer Netherlands, Dordrecht. https://doi.org/10.1007/978-94-007-2099-2

Garcia, C., Maurel-Ribes, A., Nauze, M., N'Guyen, D., Martinez, L.O., Payrastre, B., Sénard, J.-M., Galés, C., Pons, V., 2018. Deciphering biased inverse agonism of cangrelor and ticagrelor at $P2Y_{12}$ receptor. Cell. Mol. Life Sci. https://doi.org/10.1007/s00018-018-2960-3

Gellerer, A., Franke, A., Neupert, S., Predel, R., Zhou, X., Liu, S., Reiher, W., Wegener, C., Homberg, U., 2015. Identification and distribution of SIFamide in the nervous system of the desert locust *Schistocerca gregaria*. J. Comp. Neurol. 523, 108–25. https://doi.org/10.1002/cne.23671

Gether, U., 2000. Uncovering molecular mechanisms involved in activation of G protein-coupled receptors. Endocr. Rev. 21, 90–113. https://doi.org/10.1210/er.21.1.90

Gilman, A.G., 1984. G proteins and dual control of adenylate cyclase. Cell 36, 577–9. https://doi.org/10.1016/0092-8674(84)90336-2

Girardie, J., Huet, J.-C., Atay-Kadiri, Z., Saghir Ettaouil, Delbecque, J.-P., Fournier, B., Jean-Claude Pernollet, Girardie, A., 1998. Isolation, sequence determination, physical and physiological characterization of the neuroparsins and ovary maturing parsins of *Schistocerca gregaria*. Insect Biochem. Mol. Biol. 28, 641–650. https://doi.org/10.1016/S0965-1748(98)00053-8

Glinka, a. V., Wyatt, G.R., 1996. Juvenile hormone activation of gene transcription in locust fat body. Insect Biochem. Mol. Biol. 26, 13–18. https://doi.org/10.1016/0965-1748(95)00045-3

Goldsworthy, G.J., Chung, J.S., Simmonds, M.S.J., Tatari, M., Varouni, S., Poulos, C.P., 2003. The synthesis of an analogue of the locust CRF-like diuretic peptide, and the biological activities of this and some C-terminal fragments. Peptides 24, 1607–1613. https://doi.org/10.1016/j.peptides.2003.09.010

Goulson, D., 2010. Bumblebees: behaviour, ecology, and conservation, Second. ed, Florida Entomologist. Oxford University Press, New York,.

Griffin, M.T., Figueroa, K.W., Liller, S., Ehlert, F.J., 2007. Estimation of agonist activity at G protein-coupled receptors: analysis of M_2 muscarinic receptor signaling through $G_{i/o}$,G_s, and G_{15}. J. Pharmacol. Exp. Ther. 321, 1193–207. https://doi.org/10.1124/jpet.107.120857

György, B., Tóth, E., Tarcsa, E., Falus, A., Buzás, E.I., 2006. Citrullination: A posttranslational modification in health and disease. Int. J. Biochem. Cell Biol. 38, 1662–1677. https://doi.org/10.1016/J.BIOCEL.2006.03.008

Ha, S.D., Kataoka, H., Suzuki, A., Kim, B.J., Kim, H.J., Hwang, S.H., Kong, J.Y., 2000. Cloning and sequence analysis of cDNA for diuretic hormone receptor from the *Bombyx mori*. Mol Cells 10, 13–17.

Hansen, J.T., Lyngsø, C., Speerschneider, T., Hansen, P.B.L., Galés, C., Weiner, D.M., Sheikh, S.P., Burstein, E.S., Hansen, J.L., 2013. Functional enhancement of AT1R potency in the presence of the TPαR is

revealed by a comprehensive 7TM receptor co-expression screen. PLoS One 8, e58890. https://doi.org/10.1371/journal.pone.0058890

Hanyaloglu, A.C., Zastrow, M. von, 2008. Regulation of GPCRs by endocytic membrane trafficking and its potential implications. Annu. Rev. Pharmacol. Toxicol. 48, 537–568. https://doi.org/10.1146/annurev.pharmtox.48.113006.094830

Harada, A., Yoshida, M., Minakata, H., Nomoto, K., Muneoka, Y., Kobayashi, M., 1993. Structure and function of the molluscan myoactive tetradecapeptides. Zoolog. Sci. 10, 257–65.

Hartenstein, V., 1997. Development of the insect stomatogastric nervous system. Trends Neurosci. 20, 421–427. https://doi.org/10.1016/S0166-2236(97)01066-7

Hauser, F., Cazzamali, G., Williamson, M., Blenau, W., Grimmelikhuijzen, C.J.P., 2006. A review of neurohormone GPCRs present in the fruitfly *Drosophila melanogaster* and the honey bee *Apis mellifera*. 80, 1–19. https://doi.org/10.1016/j.pneurobio.2006.07.005

Hauser, F., Grimmelikhuijzen, C.J.P., 2014. Evolution of the AKH/corazonin/ACP/GnRH receptor superfamily and their ligands in the Protostomia. Gen. Comp. Endocrinol. 209, 35–49. https://doi.org/10.1016/j.ygcen.2014.07.009

Hauser, F., Neupert, S., Williamson, M., Predel, R., Tanaka, Y., Grimmelikhuijzen, C.J.P., 2010. Genomics and peptidomics of neuropeptides and protein hormones present in the parasitic wasp *Nasonia vitripennis*. J. Proteome Res. 9, 5296–5310. https://doi.org/10.1021/pr100570j

Hawtin, S.R., Tobin, A.B., Patel, S., Wheatley, M., 2001. Palmitoylation of the vasopressin V1a receptor reveals different conformational requirements for signaling, agonist-induced receptor phosphorylation, and sequestration. J. Biol. Chem. 276, 38139–46. https://doi.org/10.1074/jbc.M106142200

Hector, C.E., Bretz, C. a, Zhao, Y., Johnson, E.C., 2009. Functional differences between two CRF-related diuretic hormone receptors in *Drosophila*. J. Exp. Biol. 212, 3142–3147. https://doi.org/10.1242/jeb.033175

Hernaândez-Martõânez, S., Saânchez-Zavaleta, M., Brito, K., Herrera-Ortiz, A., Ons, S., Noriega, F.G., 2017. Allatotropin: A pleiotropic neuropeptide that elicits mosquito immune responses. PLoS One 12, 1–21. https://doi.org/10.1371/journal.pone.0175759

Heuer, C.M., Binzer, M., Schachtner, J., 2012. SIFamide in the brain of the sphinx moth, *Manduca sexta*. Acta Biol. Hung. 63 Suppl 2, 48–57. https://doi.org/10.1556/ABiol.63.2012.Suppl.2.4

Hewes, R.S., Taghert, P.H., 2001. Neuropeptides and neuropeptide receptors in the *Drosophila melanogaster* genome. Genome Res. 11, 1126–1142. https://doi.org/10.1101/gr.169901

Hildebrandt, J.D., 1997. Role of subunit diversity in signaling by heterotrimeric G proteins. Biochem. Pharmacol. 54, 325–339. https://doi.org/10.1016/S0006-2952(97)00269-4

Holdfeldt, A., Dahlstrand Rudin, A., Gabl, M., Rajabkhani, Z., König, G.M., Kortenis, E., Dahlgren, C., Forsman, H., 2017. Reactivation of $G\alpha_i$-coupled formyl peptide receptors is inhibited by $G\alpha_q$-selective inhibitors when induced by signals generated by the platelet-activating factor receptor. J. Leukoc. Biol. 102, 871–880. https://doi.org/10.1189/jlb.2a0317-086rr

Holtzhausen, W.D., Nicolson, S.W., 2007. Beetle diuretic peptides: The response of mealworm (*Tenebrio molitor*) Malpighian tubules to synthetic peptides, and cross-reactivity studies with a dung beetle (*Onthophagus gazella*). J. Insect Physiol. 53, 361–369. https://doi.org/10.1016/j.jinsphys.2006.12.010

Homberg, U., Brandl, C., Clynen, E., Schoofs, L., Veenstra, J. a, 2004. *Mas*-allatotropin/*Lom*-AG-myotropin I

immunostaining in the brain of the locust, *Schistocerca gregaria*. Cell Tissue Res. 318, 439–57. https://doi.org/10.1007/s00441-004-0913-7

Hopkins, A.L., Groom, C.R., 2002. The druggable genome. Nat. Rev. Drug Discov. 1, 727–730. https://doi.org/10.1038/nrd892

Horn, F., Bettler, E., Oliveira, L., Campagne, F., Cohen, F.E., Vriend, G., 2003. GPCRDB information system for G protein-coupled receptors. Nucleic Acids Res. 31, 294–297. https://doi.org/10.1093/nar/gkg103

Horodyski, F.M., Verlinden, H., Filkin, N., Vandersmissen, H.P., Fleury, C., Reynolds, S.E., Kai, Z., Vanden Broeck, J., 2011. Isolation and functional characterization of an allatotropin receptor from *Manduca sexta*. Insect Biochem. Mol. Biol. 41, 804–814. https://doi.org/10.1016/j.ibmb.2011.06.002

Hoste, B., Luyten, L., Claeys, I., Clynen, E., Rahman, M.M., Loof, A., Breuer, M., 2002. An improved breeding method for solitarious locusts. Entomol. Exp. Appl. 104, 281–288. https://doi.org/10.1046/j.1570-7458.2002.01014.x

Hou, Y., Azpiazu, I., Smrcka, A., Gautam, N., 2000. Selective role of G protein γ subunits in receptor interaction. J. Biol. Chem. 275, 38961–38964. https://doi.org/10.1074/jbc.C000604200

Huang, J., Marchal, E., Hult, E.F., Zels, S., Vanden Broeck, J., Tobe, S.S., 2014. Mode of action of allatostatins in the regulation of juvenile hormone biosynthesis in the cockroach, *Diploptera punctata*. Insect Biochem. Mol. Biol. 54, 61–68. https://doi.org/10.1016/j.ibmb.2014.09.001

Hummon, A.B., Richmond, T.A., Verleyen, P., Baggerman, G., Huybrechts, J., Ewing, M.A., Vierstraete, E., Rodriguez-Zas, S.L., Schoofs, L., Robinson, G.E., Sweedler, J. V., 2006. From the genome to the proteome: uncovering peptides in the *Apis* Brain. Science (80-.). 314, 647–649. https://doi.org/10.1126/science.1124128

Huybrechts, J., Nusbaum, M.P., Bosch, L. Vanden, Baggerman, G., De Loof, A., Schoofs, L., 2003. Neuropeptidomic analysis of the brain and thoracic ganglion from the Jonah crab, *Cancer borealis*. Biochem. Biophys. Res. Commun. 308, 535–44.

Iaboni, A., Holman, G.M., Nachman, R.J., Orchard, I., Coast, G.M., 1998. Immunocytochemical localisation and biological activity of diuretic peptides in the housefly, *Musca domestica*. Cell Tissue Res. 294, 549–560. https://doi.org/10.1007/s004410051205

Inosaki, A., Yasuda, A., Shinada, T., Ohfune, Y., Numata, H., Shiga, S., 2010. Mass spectrometric analysis of peptides in brain neurosecretory cells and neurohemal organs in the adult blowfly, *Protophormia terraenovae*. Comp. Biochem. Physiol. - A Mol. Integr. Physiol. 155, 190–199. https://doi.org/10.1016/j.cbpa.2009.10.036

Inoue, M.N., Yokoyama, J., Washitani, I., 2008. Displacement of Japanese native bumblebees by the recently introduced *Bombus terrestris* (L.) (Hymenoptera: Apidae). J. Insect Conserv. 12, 135–146. https://doi.org/10.1007/s10841-007-9071-z

Inouye, S., Noguchi, M., Sakaki, Y., Takagi, Y., Miyata, T., Iwanaga, S., Miyata, T., Tsuji, F.I., 1985. Cloning and sequence analysis of cDNA for the luminescent protein aequorin. Proc. Natl. Acad. Sci. U. S. A. 82, 3154–8. https://doi.org/10.1073/PNAS.82.10.3154

Irannejad, R., Pessino, V., Mika, D., Huang, B., Wedegaertner, P.B., Conti, M., Von Zastrow, M., 2017. Functional selectivity of GPCR-directed drug action through location bias. Nat. Chem. Biol. 13, 799–806. https://doi.org/10.1038/nchembio.2389

Irannejad, R., von Zastrow, M., 2014. GPCR signaling along the endocytic pathway. Curr. Opin. Cell Biol. 27,

109–116. https://doi.org/10.1016/j.ceb.2013.10.003

Jacquin-Joly, E., François, M.C., Burnet, M., Lucas, P., Bourrat, F., Maida, R., 2002. Expression pattern in the antennae of a newly isolated lepidopteran Gq protein α subunit cDNA. Eur. J. Biochem. 269, 2133–2142. https://doi.org/10.1046/j.1432-1033.2002.02863.x

Jagge, C.L., Pietrantonio, P. V., 2008. Diuretic hormone 44 receptor in Malpighian tubules of the mosquito *Aedes aegypti*: evidence for transcriptional regulation paralleling urination. Insect Mol. Biol. 17, 413–426. https://doi.org/10.1111/j.1365-2583.2008.00817.x

Janssen, I., Schoofs, L., Spittaels, K., Neven, H., Vanden Broeck, J., Devreese, B., Van Beeumen, J., Shabanowitz, J., Hunt, D.F., De Loof, A., 1996. Isolation of *NEB*-LFamide, a novel myotropic neuropeptide from the grey fleshfly. Mol. Cell. Endocrinol. 117, 157–165. https://doi.org/10.1016/0303-7207(95)03746-2

Jiang, L.I., Collins, J., Davis, R., Lin, K.M., DeCamp, D., Roach, T., Hsueh, R., Rebres, R.A., Ross, E.M., Taussig, R., Fraser, I., Sternweis, P.C., 2007. Use of a cAMP BRET sensor to characterize a novel regulation of cAMP by the sphingosine 1-phosphate/G13 pathway. J. Biol. Chem. 282, 10576–10584. https://doi.org/10.1074/jbc.M609695200

Johannessen, M., Delghandi, M.P., Moens, U., 2004. What turns CREB on? Cell. Signal. 16, 1211–27. https://doi.org/10.1016/j.cellsig.2004.05.001

Johnson, E.C., Bohn, L.M., Taghert, P.H., 2004. *Drosophila* CG8422 encodes a functional diuretic hormone receptor. J. Exp. Biol. 207, 743–748. https://doi.org/10.1242/jeb.00818

Jørgensen, L.M., Hauser, F., Cazzamali, G., Williamson, M., Grimmelikhuijzen, C.J.P., 2006. Molecular identification of the first SIFamide receptor. Biochem. Biophys. Res. Commun. 340, 696–701. https://doi.org/10.1016/j.bbrc.2005.12.062

Kahsai, A.W.K., Pani, B., Lefkowitz, R.J., 2018. GPCR signaling: conformational activation of arrestins. Cell Res. 3–4. https://doi.org/10.1038/s41422-018-0067-x

Kai, Z.P., Zhu, J.J., Deng, X. Le, Yang, X.L., Chen, S.S., 2018. Discovery of a *manduca sexta* allatotropin antagonist from a *manduca sexta* allatotropin receptor homology model. Molecules 23. https://doi.org/10.3390/molecules23040817

Kang, D.S., Denlinger, D.L., Sim, C., 2014. Suppression of allatotropin simulates reproductive diapause in the mosquito *Culex pipiens*. J. Insect Physiol. 64, 48–53. https://doi.org/10.1016/j.jinsphys.2014.03.005

Kataoka, H, Toschi, A., Li, J.P., Carney, R.L., Schooley, D.A., Kramer, S.J., 1989. Identification of an allatotropin from adult *manduca sexta*. Science 243, 1481–3. https://doi.org/10.1126/science.243.4897.1481

Kataoka, Hiroshi, Troetschler, R.G., Li, J.P., Kramer, S.J., Carney, R.L., Schooley, D. a., 1989. Isolation and identification of a diuretic hormone from the tobacco hornworm, *Manduca sexta*. Proc. Natl. Acad. Sci. U. S. A. 86, 2976–2980.

Kay, I., Coast, G.M., Cusinato, O., WHEELER, C.H., Totty, N.F., Goldsworthy, G.J., 1991a. Isolation and characterization of a diuretic peptide from *Acheta domesticus.* Evidence for a family of insect diuretic peptides. Biol. Chem. Hoppe. Seyler. 372, 505–512. https://doi.org/10.1515/bchm3.1991.372.2.505

Kay, I., Patel, M., Coast, G.M., Totty, N.F., Mallet, A.I., Goldsworthy, G.J., 1992. Isolation, characterization and biological activity of a CRF-related diuretic peptide from *Periplaneta americana L*. Regul. Pept. 42, 111–22.

Kay, I., Wheeler, C.H., Coast, G.M., Totty, N.F., Cusinato, O., Patel, M., Goldsworthy, G.J., 1991b.

Characterization of a diuretic peptide from *Locusta migratoria*. Biol. Chem. Hoppe. Seyler. 372, 929–934. https://doi.org/10.1515/bchm3.1991.372.2.929

Kenakin, T., Miller, L.J., 2010. Seven transmembrane receptors as shapeshifting proteins: The impact of allosteric modulation and functional selectivity on new drug discovery. Pharmacol. Rev. 62, 265–304. https://doi.org/10.1124/pr.108.000992

Kerbl, A., Conzelmann, M., Jékely, G., Worsaae, K., 2017. High diversity in neuropeptide immunoreactivity patterns among three closely related species of *Dinophilidae* (Annelida). J. Comp. Neurol. 525, 3596–3635. https://doi.org/10.1002/cne.24289

Kim, D., Šimo, L., Park, Y., 2018a. Molecular characterization of neuropeptide elevenin and two elevenin receptors, *Is*ElevR1 and *Is*ElevR2, from the blacklegged tick, *Ixodes scapularis*. Insect Biochem. Mol. Biol. 101, 66–75. https://doi.org/10.1016/j.ibmb.2018.07.005

Kim, D., Šimo, L., Vancová, M., Urban, J., Park, Y., 2018b. Neural and endocrine regulation of osmoregulatory organs in tick: Recent discoveries and implications. Gen. Comp. Endocrinol. https://doi.org/10.1016/J.YGCEN.2018.08.004

Kim, Y.F., Sandeman, D.C., Benton, J.L., Beltz, B.S., 2014. Birth, survival and differentiation of neurons in an adult crustacean brain. Dev. Neurobiol. 74, 602–615. https://doi.org/10.1002/dneu.22156

Knight, M., Campbell, A., Smith, S., Trewavas, A., 1991. Recombinant aequorin as a probe for cytosolic free Ca^{2+} in *Escherichia coli*. FEBS Lett. 282, 405–408.

Knight, P.J.K., Pfeifer, T.A., Grigliatti, T.A., 2003. A functional assay for G-protein-coupled receptors using stably transformed insect tissue culture cell lines. Anal. Biochem. 320, 88–103. https://doi.org/10.1016/S0003-2697(03)00354-3

Kobilka, B., 1992. Adrenergic receptors as models for G protein-coupled receptors. Annu. Rev. Neurosci. 15, 87–114. https://doi.org/10.1146/annurev.ne.15.030192.000511

Koladich, P.M., Cusson, M., Bendena, W.G., Tobe, S.S., McNeil, J.N., 2002. Cardioacceleratory effects of *Manduca sexta* allatotropin in the true armyworm moth, *Pseudaletia unipuncta*. Peptides 23, 645–651. https://doi.org/10.1016/S0196-9781(01)00658-1

Kolakowski, L.F., 1994. GCRDb: a G-protein-coupled receptor database. Receptors Channels 2, 1–7.

Kostiou, V.D., Theodoropoulou, M.C., Hamodrakas, S.J., 2016. GprotPRED: Annotation of Gα, Gβ and Gγ subunits of G-proteins using profile Hidden Markov Models (pHMMs) and application to proteomes. Biochim. Biophys. Acta - Proteins Proteomics 1864, 435–440. https://doi.org/10.1016/J.BBAPAP.2016.02.005

Kozak, M., 1986. Point mutations define a sequence flanking the AUG initiator codon that modulates translation by eukaryotic ribosomes. Cell 44, 283–92.

Koziol, U., 2018. Precursors of neuropeptides and peptide hormones in the genomes of tardigrades. Gen. Comp. Endocrinol. 267, 116–127. https://doi.org/10.1016/j.ygcen.2018.06.012

Koziol, U., Koziol, M., Preza, M., Costábile, A., Brehm, K., Castillo, E., 2016. *De novo* discovery of neuropeptides in the genomes of parasitic flatworms using a novel comparative approach. Int. J. Parasitol. 46, 709–721. https://doi.org/10.1016/j.ijpara.2016.05.007

Kristiansen, K., 2004. Molecular mechanisms of ligand binding, signaling, and regulation within the superfamily of G-protein-coupled receptors: Molecular modeling and mutagenesis approaches to receptor structure and function. Pharmacol. Ther. 103, 21–80.

https://doi.org/10.1016/j.pharmthera.2004.05.002

Lecoq, M., 2004. Vers une solution durable au problème du criquet pèlerin? Sécheresse 15, 217–224.

Leduc, M., Breton, B., Galés, C., Le Gouill, C., Bouvier, M., Chemtob, S., Heveker, N., 2009. Functional selectivity of natural and synthetic prostaglandin EP4 receptor ligands. J. Pharmacol. Exp. Ther. 331, 297–307. https://doi.org/10.1124/jpet.109.156398

Lee, H.R., Zandawala, M., Lange, A.B., Orchard, I., 2016. Isolation and characterization of the corticotropin-releasing factor-related diuretic hormone receptor in *Rhodnius prolixus*. Cell. Signal. 28, 1152–1162. https://doi.org/10.1016/j.cellsig.2016.05.020

Lee, K.-M., Daubnerová, I., Isaac, R.E., Zhang, C., Choi, S., Chung, J., Kim, Y.-J., 2015. A neuronal pathway that controls sperm ejection and storage in female *Drosophila*., Current Biology. https://doi.org/10.1016/j.cub.2015.01.050

Lee, K.Y., Chamberlin, M.E., Horodyski, F.M., 2002. Biological activity of *Manduca sexta* allatotropin-like peptides, predicted products of tissue-specific and developmentally regulated alternatively spliced mRNAs. Peptides 23, 1933–1941. https://doi.org/10.1016/S0196-9781(02)00181-X

Lee, K.Y., Horodyski, F.M., 2006. Effects of starvation and mating on corpora allata activity and allatotropin (*Manse*-AT) gene expression in *Manduca sexta*. Peptides 27, 567–574. https://doi.org/10.1016/j.peptides.2005.08.024

Lee, K.Y., Horodyski, F.M., 2002. Restriction of nutrient intake results in the increase of a specific *Manduca sexta* allatotropin (*Manse*-AT) mRNA in the larval nerve cord. Peptides 23, 653–661. https://doi.org/10.1016/S0196-9781(01)00659-3

Lee, K.Y., Horodyski, F.M., Chamberlin, M.E., 1998. Inhibition of midgut ion transport by allatotropin (*Mas*-AT) and *Manduca* FLRFamides in the tobacco hornworm *Manduca sexta*. J. Exp. Biol. 201, 3067–74.

Lefkowitz, R.J., Shenoy, S.K., 2005. Transduction of receptor signals by beta-arrestins. Science 308, 512–517. https://doi.org/10.1126/science.1109237

Lehmberg, E., Ota, R.B., Furuya, K., King, D.S., Applebaum, S.W., Ferenz, H.-J., Schooley, D.A., 1991. Identification of a diuretic hormone of *Locusta migratoria*. Biochem. Biophys. Res. Commun. 179, 1036–1041. https://doi.org/10.1016/0006-291X(91)91923-Z

Lenaerts, C., Cools, D., Verdonck, R., Verbakel, L., Vanden Broeck, J., Marchal, E., 2017. The ecdysis triggering hormone system is essential for successful moulting of a major hemimetabolous pest insect, *Schistocerca gregaria*. Sci. Rep. 7, 46502. https://doi.org/10.1038/srep46502

Lencer, W.I., 2001. Microbes and microbial toxins: Paradigms for microbial-mucosal Interactions V. Cholera: invasion of the intestinal epithelial barrier by a stably folded protein toxin. Am. J. Physiol. Liver Physiol. 280, G781–G786. https://doi.org/10.1152/ajpgi.2001.280.5.g781

Li, B., Predel, R., Neupert, S., Hauser, F., Tanaka, Y., Cazzamali, G., Williamson, M., Arakane, Y., Verleyen, P., Schoofs, L., Schachtner, J., Grimmelikhuijzen, C.J.P., Park, Y., 2007. Genomics, transcriptomics, and peptidomics of neuropeptides and protein hormones in the red flour beetle *Tribolium castaneum*. Genome Res. 18, 113–122. https://doi.org/10.1101/gr.6714008

Li, C., Yun, X., Hu, X., Zhang, Y., Sang, M., Liu, X., Wu, W., Li, B., 2013. Identification of G protein-coupled receptors in the pea aphid, *Acyrthosiphon pisum*. Genomics 102, 345–354. https://doi.org/10.1016/j.ygeno.2013.06.003

Li, K.W., Holling, T., de With, N.D., Geraerts, W.P., 1993. Purification and characterization of a novel

tetradecapeptide that modulates oesophagus motility in *Lymnaea stagnalis*. Biochem. Biophys. Res. Commun. 197, 1056–61.

Life Technologies Corporation, 2012. Real-time PCR handbook. Appl. Biosyst. 1–70.

Linder, M.E., Deschenes, R.J., 2007. Palmitoylation: Policing protein stability and traffic. Nat. Rev. Mol. Cell Biol. 8, 74–84. https://doi.org/10.1038/nrm2084

Lismont, E., Mortelmans, N., Verlinden, H., Vanden Broeck, J., 2018. Molecular cloning and characterization of the SIFamide precursor and receptor in a hymenopteran insect, *Bombus terrestris*. Gen. Comp. Endocrinol. 258. https://doi.org/10.1016/j.ygcen.2017.10.014

Lismont, E., Vleugels, R., Marchal, E., Badisco, L., Van Wielendaele, P., Lenaerts, C., Zels, S., Tobe, S.S., Vanden Broeck, J., Verlinden, H., 2015. Molecular cloning and characterization of the allatotropin precursor and receptor in the desert locust, *Schistocerca gregaria*. Front. Neurosci. 9, 84. https://doi.org/10.3389/fnins.2015.00084

Lohse, M.J., Nuber, S., Hoffmann, C., 2012. Fluorescence/bioluminescence resonance energy transfer techniques to study G-protein-coupled receptor activation and signaling. Pharmacol. Rev. 64, 299–336. https://doi.org/10.1124/pr.110.004309

Lovejoy, D.A., Barsyte-Lovejoy, D., 2010. Characterization of a corticotropin-releasing factor (CRF)/diuretic hormone-like peptide from tunicates: Insight into the origins of the vertebrate CRF family. Gen. Comp. Endocrinol. 165, 330–336. https://doi.org/10.1016/j.ygcen.2009.07.013

Luttrell, L.M., Maudsley, S., Bohn, L.M., 2015. Fulfilling the promise of "biased" G protein-coupled receptor agonism. Mol. Pharmacol. 88, 579–588. https://doi.org/10.1124/mol.115.099630

Lwalaba, D., Hoffmann, K.H., Woodring, J., 2010. Control of the release of digestive enzymes in the larvae of the fall armyworm, *Spodoptera frugiperda*. Arch. Insect Biochem. Physiol. 73, 14–29. https://doi.org/10.1002/arch.20332

M'Kadmi, C., Leyris, J.-P., Onfroy, L., Galés, C., Saulière, A., Gagne, D., Damian, M., Mary, S., Maingot, M., Denoyelle, S., Verdié, P., Fehrentz, J.-A., Martinez, J., Banères, J.-L., Marie, J., 2015. Agonism, antagonism, and inverse agonism bias at the Ghrelin receptor signaling. J. Biol. Chem. 290, 27021–39. https://doi.org/10.1074/jbc.M115.659250

Ma, M., Bors, E.K., Dickinson, E.S., Kwiatkowski, M.A., Sousa, G.L., Henry, R.P., Smith, C.M., Towle, D.W., Christie, A.E., Li, L., 2009. Characterization of the *Carcinus maenas* neuropeptidome by mass spectrometry and functional genomics. Gen. Comp. Endocrinol. 161, 320–334. https://doi.org/10.1016/j.ygcen.2009.01.015

Ma, M., Chen, R., Sousa, G.L., Bors, E.K., Kwiatkowski, M.A., Goiney, C.C., Goy, M.F., Christie, A.E., Li, L., 2008. Mass spectral characterization of peptide transmitters/hormones in the nervous system and neuroendocrine organs of the American lobster *Homarus americanus*. Gen. Comp. Endocrinol. 156, 395–409. https://doi.org/10.1016/j.ygcen.2008.01.009

Ma, M., Emery, S.B., Wong, W.K.R., De Loof, A., 2000. Effects of *Manduca* diuresin on neonates of the tobacco hornworm, *Manduca sexta*. Gen. Comp. Endocrinol. 118, 1–7. https://doi.org/10.1006/gcen.1999.7435

Majzoub, J.A., 2006. Corticotropin-releasing hormone physiology. Eur. J. Endocrinol. 155, S71–S76. https://doi.org/10.1530/eje.1.02247

Marchal, E., Badisco, L., Verlinden, H., Vandersmissen, T., Van Soest, S., Van Wielendaele, P., Vanden Broeck, J., 2011. Role of the Halloween genes, Spook and Phantom in ecdysteroidogenesis in the desert locust,

Schistocerca gregaria. J. Insect Physiol. 57, 1240–8. https://doi.org/10.1016/j.jinsphys.2011.05.009

Marchal, E., Schellens, S., Monjon, E., Bruyninckx, E., Marco, H., Gäde, G., Vanden Broeck, J., Verlinden, H., 2018. Analysis of peptide ligand specificity of different insect adipokinetic hormone receptors. Int. J. Mol. Sci. 19, 542. https://doi.org/10.3390/ijms19020542

Martelli, C., Pech, U., Kobbenbring, S., Pauls, D., Bahl, B., Sommer, M.V., Pooryasin, A., Barth, J., Arias, C.W.P., Vassiliou, C., Luna, A.J.F., Poppinga, H., Richter, F.G., Wegener, C., Fiala, A., Riemensperger, T., 2017. SIFamide translates hunger signals into appetitive and feeding behavior in *Drosophila*. Cell Rep. 20, 464–478. https://doi.org/10.1016/j.celrep.2017.06.043

Masood, M., Orchard, I., 2014. Molecular characterization and possible biological roles of allatotropin in *Rhodnius prolixus*. Peptides 53, 159–171. https://doi.org/10.1016/j.peptides.2013.10.017

Matthiesen, K., Nielsen, J., 2011. Cyclic AMP control measured in two compartments in HEK293 cells: Phosphodiesterase K_M is more important than phosphodiesterase localization. PLoS One 6, e24392. https://doi.org/10.1371/journal.pone.0024392

Maurice, P., Daulat, A.M., Turecek, R., Ivankova-Susankova, K., Zamponi, F., Kamal, M., Clement, N., Guillaume, J.-L., Bettler, B., Galès, C., Delagrange, P., Jockers, R., 2010. Molecular organization and dynamics of the melatonin MT_1 receptor/RGS20/G_i protein complex reveal asymmetry of receptor dimers for RGS and G_i coupling. EMBO J. 29, 3646–59. https://doi.org/10.1038/emboj.2010.236

McIntire, W.E., MacCleery, G., Garrison, J.C., 2001. The G protein β subunit is a determinant in the coupling of G_s to the β_1-adrenergic and A2a adenosine receptors. J. Biol. Chem. 276, 15801–9. https://doi.org/10.1074/jbc.M011233200

Meeusen, T., Mertens, I., Clynen, E., Baggerman, G., Nichols, R., Nachman, R.J., Huybrechts, R., De Loof, A., Schoofs, L., 2002. Identification in *Drosophila melanogaster* of the invertebrate G protein-coupled FMRFamide receptor. Proc. Natl. Acad. Sci. U. S. A. 99, 15363–8. https://doi.org/10.1073/pnas.252339599

Meiselman, M., Lee, S.S., Tran, R.-T., Dai, H., Ding, Y., Rivera-Perez, C., Wijesekera, T.P., Dauwalder, B., Noriega, F.G., Adams, M.E., 2017. Endocrine network essential for reproductive success in *Drosophila melanogaster*. Proc. Natl. Acad. Sci. 114, E3849–E3858. https://doi.org/10.1073/pnas.1620760114

Mertens, I., Meeusen, T., Huybrechts, R., De Loof, A., Schoofs, L., 2002. Characterization of the short neuropeptide F receptor from *Drosophila melanogaster*. Biochem. Biophys. Res. Commun. 297, 1140–8.

Messinger, D.I., Kutz, K.K., Le, T., Verley, D.R., Hsu, Y.-W. a, Ngo, C.T., Cain, S.D., Birmingham, J.T., Li, L., Christie, A.E., 2005. Identification and characterization of a tachykinin-containing neuroendocrine organ in the commissural ganglion of the crab *Cancer productus*. J. Exp. Biol. 208, 3303–3319. https://doi.org/10.1242/jeb.01787

Milligan, G., Marshall, F., Rees, S., 1996. G16 as a universal G protein adapter: implications for agonist screening strategies. Trends Pharmacol. Sci. 17, 235–7.

Mirabeau, O., Joly, J.-S., 2013. Molecular evolution of peptidergic signaling systems in bilaterians. Proc. Natl. Acad. Sci. U. S. A. 110, E2028-37. https://doi.org/10.1073/pnas.1219956110

Moench, S.J., Moreland, J., Stewart, D.H., Dewey, T.G., 1994. Fluorescence studies of the location and membrane accessibility of the palmitoylation sites of rhodopsin. Biochemistry 33, 5791–5796. https://doi.org/10.1021/bi00185a017

Mollayeva, S., Orchard, I., Lange, A.B., 2018. The involvement of *Rhopr*-CRF/DH in feeding and reproduction in the blood-gorging insect *Rhodnius prolixus*. Gen. Comp. Endocrinol. 258, 79–90. https://doi.org/10.1016/j.ygcen.2017.07.005

Møller, T.C., Moreno-Delgado, D., Pin, J.-P., Kniazeff, J., 2017. Class C G protein-coupled receptors: reviving old couples with new partners. Biophys. Reports 3, 57–63. https://doi.org/10.1007/s41048-017-0036-9

Moore, C.A.C., Milano, S.K., Benovic, J.L., 2006. Regulation of receptor trafficking by GRKs and arrestins. Annu. Rev. Physiol. 69, 451–482. https://doi.org/10.1146/annurev.physiol.69.022405.154712

Morgan, P.J., Siegert, K.J., Mordue, W., 1987. Preliminary characterisation of locust diuretic peptide (DP-1) and another corpus cardiacum peptide (LCCP). Insect Biochem. 17, 383–388. https://doi.org/10.1016/0020-1790(87)90082-5

Mortier, A., Gouwy, M., Van Damme, J., Proost, P., 2011. Effect of posttranslational processing on the *in vitro* and *in vivo* activity of chemokines. Exp. Cell Res. 317, 642–654. https://doi.org/10.1016/j.yexcr.2010.11.016

Myung, C.-S., Lim, W.K., DeFilippo, J.M., Yasuda, H., Neubig, R.R., Garrison, J.C., 2006. Regions in the G protein gamma subunit important for interaction with receptors and effectors. Mol. Pharmacol. 69, 877–87. https://doi.org/10.1124/mol.105.018994

Nagata, S., Matsumoto, S., Mizoguchi, A., Nagasawa, H., 2012. Identification of cDNAs encoding allatotropin and allatotropin-like peptides from the silkworm, *Bombyx mori*. Peptides 34, 98–105. https://doi.org/10.1016/j.peptides.2012.01.002

Namkung, Y., Le Gouill, C., Lukashova, V., Kobayashi, H., Hogue, M., Khoury, E., Song, M., Bouvier, M., Laporte, S.A., 2016. Monitoring G protein-coupled receptor and β-arrestin trafficking in live cells using enhanced bystander BRET. Nat. Commun. 7. https://doi.org/10.1038/ncomms12178

Nation, J.L., 2015. Insect physiology and biochemistry, third. ed. CRC Press, Boca Raton.

Neupert, S., Fusca, D., Schachtner, J., Kloppenburg, P., Predel, R., 2012. Toward a single-cell-based analysis of neuropeptide expression in *Periplaneta americana* antennal lobe neurons. J. Comp. Neurol. 520, 694–716. https://doi.org/10.1002/cne.22745

Neupert, S., Russell, W.K., Predel, R., Russell, D.H., Strey, O.F., Teel, P.D., Nachman, R.J., 2009a. The neuropeptidomics of *Ixodes scapularis* synganglion. J. Proteomics 72, 1040–1045. https://doi.org/10.1016/j.jprot.2009.06.007

Neupert, S., Schattschneider, S., Predel, R., 2009b. Allatotropin-related peptide in cockroaches: Identification via mass spectrometric analysis of single identified neurons. Peptides 30, 489–494. https://doi.org/10.1016/j.peptides.2008.10.023

Nishimura, A., Kitano, K., Takasaki, J., Taniguchi, M., Mizuno, N., Tago, K., Hakoshima, T., Itoh, H., 2010. Structural basis for the specific inhibition of heterotrimeric G_q protein by a small molecule. Proc. Natl. Acad. Sci. 107, 13666–71. https://doi.org/10.1073/pnas.1003553107

Nouzova, M., Brockhoff, A., Mayoral, J.G., Goodwin, M., Meyerhof, W., Noriega, F.G., 2012. Functional characterization of an allatotropin receptor expressed in the corpora allata of mosquitoes. Peptides 34, 201–208. https://doi.org/10.1016/j.peptides.2011.07.025

O'Donnell, M.J., Dow, J.A., Huesmann, G.R., Tublitz, N.J., Maddrell, S.H., 1996. Separate control of anion and cation transport in Malpighian tubules of *Drosophila melanogaster*. J. Exp. Biol. 199.

Oakley, R.H., Laporte, S.A., Holt, J.A., Caron, M.G., Barak, L.S., 2000. Differential affinities of visual arrestin, βarrestin1, and βarrestin2 for G protein-coupled receptors delineate two major classes of receptors. J. Biol. Chem. 275, 17201–17210. https://doi.org/10.1074/jbc.M910348199

Oeh, U., Dyker, H., Lösel, P., Hoffmann, K.H., 2001. In vivo effects of *Manduca sexta* allatotropin and allatostatin on development and reproduction in the fall armyworm, *Spodoptera frugiperda* (Lepidoptera, Noctuidae). Invertebr. Reprod. Dev. 39, 239–247. https://doi.org/10.1080/07924259.2001.9652488

Offermanns, S., Simon, M.I., 1995. G alpha 15 and G alpha 16 couple a wide variety of receptors to phospholipase C. J. Biol. Chem. 270, 15175–80.

Oka, Y., Korsching, S.I., 2009. The fifth element in animal Gα protein evolution. Commun. Integr. Biol. 2, 227–229. https://doi.org/10.4161/cib.2.3.8080

Oka, Y., Saraiva, L.R., Kwan, Y.Y., Korsching, S.I., 2009. The fifth class of Galpha proteins. Proc Natl Acad Sci USA 106, 1484–1489. https://doi.org/10.1073/pnas.0809420106

Oldham, W.M., Hamm, H.E., 2008. Heterotrimeric G protein activation by G-protein-coupled receptors. Nat. Rev. Mol. Cell Biol. 9, 60–71. https://doi.org/10.1038/nrm2299

Onfroy, L., Galandrin, S., Pontier, S.M., Seguelas, M.-H., N'Guyen, D., Sénard, J.-M., Galés, C., 2017. G protein stoichiometry dictates biased agonism through distinct receptor-G protein partitioning. Sci. Rep. 7, 7885. https://doi.org/10.1038/s41598-017-07392-5

Ons, S., Richter, F., Urlaub, H., Pomar, R.R., 2009. The neuropeptidome of *Rhodnius prolixus* brain. Proteomics 9, 788–792. https://doi.org/10.1002/pmic.200800499

Paemen, L., Schoofs, L., De Loof, A., 1992. Localization of *Lom*-AG-myotropin I-like substances in the male reproductive and nervous tissue of the locust, *Locusta migratoria*. Cell Tissue Res. 268, 91–7.

Paemen, L., Tips, A., Schoofs, L., Proost, P., Van Damme, J., De Loof, A., 1991. *Lom*-AG-myotropin: A novel myotropic peptide from the male accessory glands of *Locusta migratoria*. Peptides 12, 7–10. https://doi.org/10.1016/0196-9781(91)90158-L

Pagano, A., Rovelli, G., Mosbacher, J., Lohmann, T., Duthey, B., Stauffer, D., Ristig, D., Schuler, V., Meigel, I., Lampert, C., Stein, T., Prezeau, L., Blahos, J., Pin, J., Froestl, W., Kuhn, R., Heid, J., Kaupmann, K., Bettler, B., 2001. C-terminal interaction is essential for surface trafficking but not for heteromeric assembly of $GABA_B$ receptors. J. Neurosci. 21, 1189–202. https://doi.org/10.1523/JNEUROSCI.21-04-01189.2001

Park, S., Sonn, J.Y., Oh, Y., Lim, C., Choe, J., 2014. SIFamide and SIFamide receptor defines a novel neuropeptide signaling to promote sleep in *Drosophila*. Mol. Cells 37, 295–301. https://doi.org/10.14348/molcells.2014.2371

Patel, M., Hayes, T.K., Coast, G.M., 1995. Evidence for the hormonal function of a CRF-related diuretic peptide (*Locusta*-Dp) in *Locusta migratoria*. J Exp Biol 198, 793–804.

Pener, M.P., 1991. Locust phase polymorphism and its endocrine relations. Adv. In Insect Phys. 23, 1–79. https://doi.org/10.1016/S0065-2806(08)60091-0

Pener, M.P., Yerushalmi, Y., 1998. The physiology of locust phase polymorphism: An update. J. Insect Physiol. 44, 365–377. https://doi.org/10.1016/S0022-1910(97)00169-8

Petersen, T.N., Brunak, S., von Heijne, G., Nielsen, H., 2011. SignalP 4.0: discriminating signal peptides from transmembrane regions. Nat. Methods 8, 785–786. https://doi.org/10.1038/nmeth.1701

Petri, B., Homberg, U., Loesel, R., Stengl, M., 2002. Evidence for a role of GABA and *Mas*-allatotropin in photic

entrainment of the circadian clock of the cockroach *Leucophaea maderae*. J. Exp. Biol. 205, 1459–1469.

Peverelli, E., Busnelli, M., Vitali, E., Giardino, E., Galés, C., Lania, A.G., Beck-Peccoz, P., Chini, B., Mantovani, G., Spada, A., 2013. Specific roles of G_i protein family members revealed by dissecting SST5 coupling in human pituitary cells. J. Cell Sci. 126, 638–44. https://doi.org/10.1242/jcs.116434

Pfleger, K.D.G., Eidne, K.A., 2006. Illuminating insights into protein-protein interactions using bioluminescence resonance energy transfer (BRET). Nat. Methods 3, 165–174. https://doi.org/10.1038/nmeth841

Pierce, K.L., Premont, R.T., Lefkowitz, R.J., 2002. Seven-transmembrane receptors. Nat. Rev. Mol. Cell Biol. 3, 639–650. https://doi.org/10.1038/nrm908

Poels, J., Birse, R.T., Nachman, R.J., Fichna, J., Janecka, A., Vanden Broeck, J., Nässel, D.R., 2009. Characterization and distribution of NKD, a receptor for *Drosophila* tachykinin-related peptide 6. Peptides 30, 545–556. https://doi.org/10.1016/j.peptides.2008.10.012

Poels, J., Van Loy, T., Vandersmissen, H.P., Van Hiel, B., Van Soest, S., Nachman, R.J., Vanden Broeck, J., 2010. Myoinhibiting peptides are the ancestral ligands of the promiscuous *Drosophila* sex peptide receptor. Cell. Mol. Life Sci. 67, 3511–3522. https://doi.org/10.1007/s00018-010-0393-8

Poels, J., Verlinden, H., Fichna, J., Van Loy, T., Franssens, V., Studzian, K., Janecka, A., Nachman, R.J., Vanden Broeck, J., 2007. Functional comparison of two evolutionary conserved insect neurokinin-like receptors. Peptides 28, 103–108. https://doi.org/10.1016/j.peptides.2006.06.014

Polanska, M.A., Yasuda, A., Harzsch, S., 2007. Immunolocalisation of crustacean-SIFamide in the median brain and eyestalk neuropils of the marbled crayfish. Cell Tissue Res. 330, 331–344. https://doi.org/10.1007/s00441-007-0473-8

Pratt, G.E., Tobe, S.S., 1974. Juvenile hormones radiobiosynthesised by corpora allata of adult female locusts *in vitro*. Life Sci. 14, 575–586. https://doi.org/10.1016/0024-3205(74)90372-5

Predel, R., Wegener, C., Russell, W.K., Tichy, S.E., Russell, D.H., Nachman, R.J., 2004. Peptidomics of CNS-associated neurohemal systems of adult *Drosophila melanogaster*: A mass spectrometric survey of peptides from individual flies. J. Comp. Neurol. 474, 379–392. https://doi.org/10.1002/cne.20145

Priyam, A., Woodcroft, B.J., Rai, V., Munagala, A., Moghul, I., Ter, F., Gibbins, M.A., Moon, H., Leonard, G., Rumpf, W., Wurm, Y., 2015. Sequenceserver: a modern graphical user interface for custom BLAST databases. bioRxiv.

Promega, n.d. GloSensor™ Technology [WWW Document]. 2019. URL https://be.promega.com/products/cell-signaling/gpcr-signaling/glosensor-camp-cgmp-protease-biosensors/?catNum=E1290&tabset0=1 (accessed 3.5.19).

Qanbar, R., Bouvier, M., 2003. Role of palmitoylation/depalmitoylation reactions in G-protein-coupled receptor function. Pharmacol. Ther. 97, 1–33. https://doi.org/10.1016/S0163-7258(02)00300-5

Rahman, M.M., Neupert, S., Predel, R., 2013. Neuropeptidomics of the Australian sheep blowfly *Lucilia cuprina* (Wiedemann) and related Diptera. Peptides 41, 31–37. https://doi.org/10.1016/j.peptides.2012.12.021

Rajagopal, S., Rajagopal, K., Lefkowitz, R.J., 2010. Teaching old receptors new tricks: biasing seven-transmembrane receptors. Nat. Rev. Drug Discov. 9, 373–386. https://doi.org/10.1038/nrd3024

Rand, D., Ayali, A., 2010. Neuroanatomy and neurophysiology of the locust hypocerebral ganglion. J. Insect Physiol. 56, 884–892. https://doi.org/10.1016/J.JINSPHYS.2010.04.001

Reagan, J.D., 1996. Molecular cloning and function expression of a diuretic hormone receptor from the house cricket, *Acheta domesticus*. Insect Biochem. Mol. Biol. 26, 1–6. https://doi.org/10.1016/0965-1748(95)00074-7

Reagan, J.D., 1995. Functional expression of a diuretic hormone receptor in baculovirus-infected insect cells: evidence suggesting that the N-terminal region of diuretic hormone is associated with receptor activation. Insect Biochem. Mol. Biol. 25, 535–9. https://doi.org/0965174895000214

Reiter, E., Ahn, S., Shukla, A.K., Lefkowitz, R.J., 2011. Molecular mechanism of β-arrestin-biased agonism at seven-transmembrane receptors. Annu. Rev. Pharmacol. Toxicol. 52, 179–197. https://doi.org/10.1146/annurev.pharmtox.010909.105800

Richard, O., Tamarelle, M., Girardie, J., Geoffre, S., 1994. Restricted occurrence of *Locusta migratoria* ovary maturing parsin in the brain-corpora cardiaca complex of various insect species. Histochemistry 102, 233–239. https://doi.org/10.1007/BF00268900

Riehle, M.A., Garczynski, S.F., Crim, J.W., Hill, C.A., Brown, M.R., 2002. Neuropeptides and peptide hormones in *Anopheles gambiae*. Science 298, 172–5. https://doi.org/10.1126/science.1076827

Rives, M.-L., Rossillo, M., Liu-Chen, L.-Y., Javitch, J.A., 2012. 6'-Guanidinonaltrindole (6'-GNTI) is a G protein-biased κ-opioid receptor agonist that inhibits arrestin recruitment. J. Biol. Chem. 287, 27050–4. https://doi.org/10.1074/jbc.C112.387332

Roller, L., Yamanaka, N., Watanabe, K., Daubnerová, I., Žitňan, D., Kataoka, H., Tanaka, Y., 2008. The unique evolution of neuropeptide genes in the silkworm *Bombyx mori*. Insect Biochem. Mol. Biol. 38, 1147–1157. https://doi.org/10.1016/j.ibmb.2008.04.009

Rouillé, Y., Duguay, S.J., Lund, K., Furuta, M., Gong, Q., Lipkind, G., Oliva, A.A., Chan, S.J., Steiner, D.F., 1995. Proteolytic processing mechanisms in the biosynthesis of neuroendocrine peptides: The subtilisin-like proprotein convertases. Front. Neuroendocrinol. https://doi.org/10.1006/frne.1995.1012

Rubin, J.B., 2009. Chemokine signaling in cancer: One hump or two? Semin. Cancer Biol. 19, 116–122. https://doi.org/10.1016/j.semcancer.2008.10.001

Rudwall, A.J., Sliwowska, J., Nässel, D.R., 2000. Allatotropin-like neuropeptide in the cockroach abdominal nervous system: Myotropic actions, sexually dimorphic distribution and colocalization with serotonin. J. Comp. Neurol. 428, 159–173. https://doi.org/10.1002/1096-9861(20001204)428:1

Sadd, B.M., Barribeau, S.M., Bloch, G., de Graaf, D.C., Dearden, P., Elsik, C.G., Gadau, J., Grimmelikhuijzen, C.J.P., Hasselmann, M., Lozier, J.D., Robertson, H.M., Smagghe, G., Stolle, E., Van Vaerenbergh, M., Waterhouse, R.M., Bornberg-Bauer, E., Klasberg, S., Bennett, A.K., Câmara, F., Guigó, R., Hoff, K., Mariotti, M., Munoz-Torres, M., Murphy, T., Santesmasses, D., Amdam, G. V, Beckers, M., Beye, M., Biewer, M., Bitondi, M.M.G., Blaxter, M.L., Bourke, A.F.G., Brown, M.J.F., Buechel, S.D., Cameron, R., Cappelle, K., Carolan, J.C., Christiaens, O., Ciborowski, K.L., Clarke, D.F., Colgan, T.J., Collins, D.H., Cridge, A.G., Dalmay, T., Dreier, S., du Plessis, L., Duncan, E., Erler, S., Evans, J., Falcon, T., Flores, K., Freitas, F.C.P., Fuchikawa, T., Gempe, T., Hartfelder, K., Hauser, F., Helbing, S., Humann, F.C., Irvine, F., Jermiin, L.S., Johnson, C.E., Johnson, R.M., Jones, A.K., Kadowaki, T., Kidner, J.H., Koch, V., Köhler, A., Kraus, F.B., Lattorff, H.M.G., Leask, M., Lockett, G.A., Mallon, E.B., Antonio, D.S.M., Marxer, M., Meeus, I., Moritz, R.F.A., Nair, A., Näpflin, K., Nissen, I., Niu, J., Nunes, F.M.F., Oakeshott, J.G., Osborne, A., Otte, M., Pinheiro, D.G., Rossié, N., Rueppell, O., Santos, C.G., Schmid-Hempel, R., Schmitt, B.D., Schulte, C., Simões, Z.L.P., Soares, M.P.M., Swevers, L., Winnebeck, E.C., Wolschin, F., Yu, N., Zdobnov, E.M., *et al.*, 2015. The genomes of two key bumblebee species with primitive eusocial organization. Genome Biol. 16, 76. https://doi.org/10.1186/s13059-015-0623-3

Santini, M.S., Ronderos, J.R., 2007. Allatotropin-like peptide released by Malpighian tubules induces hindgut activity associated with diuresis in the Chagas disease vector *Triatoma infestans* (Klug). J. Exp. Biol. 210, 1986–1991. https://doi.org/10.1242/jeb.004291

Santos, D., Vanden Broeck, J., Wynant, N., 2014. Systemic RNA interference in locusts: Reverse genetics and possibilities for locust pest control. Curr. Opin. Insect Sci. 6, 9–14. https://doi.org/10.1016/j.cois.2014.09.013

Saulière, A., Bellot, M., Paris, H., Denis, C., Finana, F., Hansen, J.T., Altié, M.-F., Seguelas, M.-H., Pathak, A., Hansen, J.L., Sénard, J.-M., Galés, C., 2012. Deciphering biased-agonism complexity reveals a new active AT1 receptor entity. Nat. Chem. Biol. 8, 622–630. https://doi.org/10.1038/nchembio.961

Schiöth, H.B., Lagerström, M.C., 2008. Structural diversity of g proteincoupled receptors and significance for drug discovery. Nat. Rev. Drug Discov. 7, 339–357. https://doi.org/10.1038/nrd2518

Schmitz, A.-L., Schrage, R., Gaffal, E., Charpentier, T.H., Wiest, J., Hiltensperger, G., Morschel, J., Hennen, S., Häußler, D., Horn, V., Wenzel, D., Grundmann, M., Büllesbach, K.M., Schröder, R., Brewitz, H.H., Schmidt, J., Gomeza, J., Galés, C., Fleischmann, B.K., Tüting, T., Imhof, D., Tietze, D., Gütschow, M., Holzgrabe, U., Sondek, J., Harden, T.K., Mohr, K., Kostenis, E., 2014. A cell-permeable inhibitor to trap $G\alpha_q$ proteins in the empty pocket conformation. Chem. Biol. 21, 890–902. https://doi.org/10.1016/J.CHEMBIOL.2014.06.003

Schoofs, L., Mark Holman, G., Hayes, T.K., Nachman, R.J., De Loof, A., 1990. Isolation, identification and synthesis of locustamyotropin II, an additional neuropeptide of *Locusta migratoria*: Member of the cephalomyotropic peptide family. Insect Biochem. 20, 479–484. https://doi.org/10.1016/0020-1790(90)90029-T

Schrage, R., Schmitz, A.L., Gaffal, E., Annala, S., Kehraus, S., Wenzel, D., Büllesbach, K.M., Bald, T., Inoue, A., Shinjo, Y., Galandrin, S., Shridhar, N., Hesse, M., Grundmann, M., Merten, N., Charpentier, T.H., Martz, M., Butcher, A.J., Slodczyk, T., Armando, S., Effern, M., Namkung, Y., Jenkins, L., Horn, V., Stößel, A., Dargatz, H., Tietze, D., Imhof, D., Gales, C., Drewke, C., Müller, C.E., Hölzel, M., Milligan, G., Tobin, A.B., Gomeza, J., Dohlman, H.G., Sondek, J., Harden, T.K., Bouvier, M., Laporte, S.A., Aoki, J., Fleischmann, B.K., Mohr, K., König, G.M., Tüting, T., Kostenis, E., 2015. The experimental power of FR900359 to study G_q-regulated biological processes. Nat. Commun. 6, 1–7. https://doi.org/10.1038/ncomms10156

Sellami, A., Veenstra, J.A., 2015. SIFamide acts on fruitless neurons to modulate sexual behavior in *Drosophila melanogaster*. Peptides 74, 50–56. https://doi.org/10.1016/j.peptides.2015.10.003

Sevala, V.L., Davey, K.G., Prestwich, G.D., 1995. Photoaffinity labeling and characterization of a juvenile hormone binding protein in the membranes of follicle cells of *Locusta migratoria*. Insect Biochem. Mol. Biol. 25, 267–273. https://doi.org/10.1016/0965-1748(94)00065-P

Shenoy, S.K., Lefkowitz, R.J., 2005. Seven-transmembrane receptor signaling through β--arrestin. Sci. Signal. 2005, cm10–cm10. https://doi.org/10.1126/stke.2005/308/cm10

Shental-Bechor, D., Levy, Y., 2009. Folding of glycoproteins: toward understanding the biophysics of the glycosylation code. Curr. Opin. Struct. Biol. 19, 524–533. https://doi.org/10.1016/j.sbi.2009.07.002

Sheu, Y.A., Kricka, L.J., Pritchett, D.B., 1993. Measurement of intracellular calcium using bioluminescent aequorin expressed in human cells. Anal. Biochem. 209, 343–347. https://doi.org/10.1006/ABIO.1993.1132

Shimomura, O., 1995. Luminescence of aequorin is triggered by the binding of two Calcium ions. Biochem. Biophys. Res. Commun. 211, 359–363. https://doi.org/10.1006/BBRC.1995.1821

Shimomura, O., Teranishi, K., 2000. Light-emitters involved in the luminescence of coelenterazine. Luminescence 15, 51–58. https://doi.org/10.1002/(SICI)1522-7243

Shukla, A.K., Xiao, K., Lefkowitz, R.J., 2011. Emerging paradigms of β-arrestin-dependent seven transmembrane receptor signaling. Trends Biochem. Sci. 36, 457–69. https://doi.org/10.1016/j.tibs.2011.06.003

Shuman, S., 1994. Novel approach to molecular cloning and polynucleotide synthesis using vaccinia DNA topoisomerase. J. Biol. Chem. 269, 32678–84.

Siehler, S., 2009. Regulation of RhoGEF proteins by $G_{12/13}$ -coupled receptors. Br. J. Pharmacol. 158, 41–49. https://doi.org/10.1111/j.1476-5381.2009.00121.x

Siju, K.P., Reifenrath, A., Scheiblich, H., Neupert, S., Predel, R., Hansson, B.S., Schachtner, J., Ignell, R., 2014. Neuropeptides in the antennal lobe of the yellow fever mosquito, *Aedes aegypti*. J. Comp. Neurol. 522, 592–608. https://doi.org/10.1002/cne.23434

Šimo, L., Koči, J., Park, Y., 2013. Receptors for the neuropeptides, myoinhibitory peptide and SIFamide, in control of the salivary glands of the blacklegged tick *Ixodes scapularis*. Insect Biochem. Mol. Biol. 43, 376–87. https://doi.org/10.1016/j.ibmb.2013.01.002

Šimo, L., Park, Y., 2014. Neuropeptidergic control of the hindgut in the black-legged tick *Ixodes scapularis*. Int. J. Parasitol. 44, 819–826. https://doi.org/10.1016/j.ijpara.2014.06.007

Šimo, L., Žitňan, D., Park, Y., 2009. Two novel neuropeptides in innervation of the salivary glands of the black-legged tick, *Ixodes scapularis*: Myoinhibitory peptide and sifamide. J. Comp. Neurol. 517, 551–563. https://doi.org/10.1002/cne.22182

Sithigorngul, P., Pupuem, J., Krungkasem, C., Longyant, S., Chaivisuthangkura, P., Sithigorngul, W., Petsom, A., 2002. Seven novel FMRFamide-like neuropeptide sequences from the eyestalk of the giant tiger prawn *Penaeus monodon*. Comp. Biochem. Physiol. B. Biochem. Mol. Biol. 131, 325–37.

Sladen, F.W.L., 1912. The humble-bee : its life-history and how to domesticate it : with descriptions of all the British species of *Bombus* and *Psithyrus*: including The humble bee, 1892. Logaston Press.

Smith, J.S., Lefkowitz, R.J., Rajagopal, S., 2018. Biased signalling: From simple switches to allosteric microprocessors. Nat. Rev. Drug Discov. 17, 243–260. https://doi.org/10.1038/nrd.2017.229

Stemmler, Elizabeth A., Cashman, C.R., Messinger, D.I., Gardner, N.P., Dickinson, P.S., Christie, A.E., 2007. High-mass-resolution direct-tissue MALDI-FTMS reveals broad conservation of three neuropeptides (APSGFLGMRamide, GYRKPPFNGSIFamide and pQDLDHVFLRFamide) across members of seven decapod crustaean infraorders. Peptides 28, 2104–2115. https://doi.org/10.1016/J.PEPTIDES.2007.08.019

Stemmler, Elizabeth A, Cashman, C.R., Messinger, D.I., Gardner, N.P., Dickinson, P.S., Christie, A.E., 2007. High-mass-resolution direct-tissue MALDI-FTMS reveals broad conservation of three neuropeptides (APSGFLGMRamide, GYRKPPFNGSIFamide and pQDLDHVFLRFamide) across members of seven decapod crustaean infraorders. Peptides 28, 2104–15. https://doi.org/10.1016/j.peptides.2007.08.019

Sterkel, M., Riccillo, F.L., Ronderos, J.R., 2010. Cardioacceleratory and myostimulatory activity of allatotropin in *Triatoma infestans*. Comp. Biochem. Physiol. - A Mol. Integr. Physiol. 155, 371–377. https://doi.org/10.1016/j.cbpa.2009.12.002

Symmons, P.., Cressman, K., 2001. Desert locust guidelines: biology and behaviour. Food and Agriculture Organization of the United Nations, Rome.

Symmons, P.M., Cressman, K., Fresco, L.O., 2001. Desert Locust Guidelines 5. Campaign organization and

execution.

Tamura, K., Stecher, G., Peterson, D., Filipski, A., Kumar, S., 2013. MEGA6: Molecular evolutionary genetics analysis version 6.0. Mol. Biol. Evol. 30, 2725–2729. https://doi.org/10.1093/molbev/mst197

Tanaka, Y., Suetsugu, Y., Yamamoto, K., Noda, H., Shinoda, T., 2014. Transcriptome analysis of neuropeptides and G-protein coupled receptors (GPCRs) for neuropeptides in the brown planthopper *Nilaparvata lugens*. Peptides 53, 125–33. https://doi.org/10.1016/j.peptides.2013.07.027

Tateyama, M., Kubo, Y., 2011. The intra-molecular activation mechanisms of the dimeric metabotropic glutamate receptor 1 differ depending on the type of G proteins. Neuropharmacology 61, 832–841. https://doi.org/10.1016/J.NEUROPHARM.2011.05.031

Te Brugge, V. a, Miksys, S.M., Coast, G.M., Schooley, D. a, Orchard, I., 1999. The distribution of a CRF-like diuretic peptide in the blood-feeding bug *Rhodnius prolixus*. J. Exp. Biol. 202, 2017–2027.

Te Brugge, V., Ianowski, J.P., Orchard, I., 2009. Biological activity of diuretic factors on the anterior midgut of the blood-feeding bug, *Rhodnius prolixus*. Gen. Comp. Endocrinol. 162, 105–112. https://doi.org/10.1016/j.ygcen.2009.01.025

Te Brugge, V., Paluzzi, J.-P., Schooley, D. a, Orchard, I., 2011. Identification of the elusive peptidergic diuretic hormone in the blood-feeding bug *Rhodnius prolixus*: a CRF-related peptide. J. Exp. Biol. 214, 371–81. https://doi.org/10.1242/jeb.046292

Te Brugge, V.A., Orchard, I., 2002. Evidence for CRF-like and kinin-like peptides as neurohormones in the blood-feeding bug, *Rhodnius prolixus*. Peptides 23, 1967–1979. https://doi.org/10.1016/S0196-9781(02)00184-5

Terhzaz, S., Alford, L., Yeoh, J.G.C., Marley, R., Dornan, A.J., Dow, J.A.T., Davies, S.A., 2018. Renal neuroendocrine control of desiccation and cold tolerance by *Drosophila suzukii*. Pest Manag. Sci. 74, 800–810. https://doi.org/10.1002/ps.4663

Terhzaz, S., Rosay, P., Goodwin, S.F., Veenstra, J.A., 2007. The neuropeptide SIFamide modulates sexual behavior in *Drosophila*. Biochem. Biophys. Res. Commun. 352, 305–310. https://doi.org/10.1016/j.bbrc.2006.11.030

Thomsen, A.R.B., Plouffe, B., Cahill, T.J., Shukla, A.K., Tarrasch, J.T., Dosey, A.M., Kahsai, A.W., Strachan, R.T., Pani, B., Mahoney, J.P., Huang, L., Breton, B., Heydenreich, F.M., Sunahara, R.K., Skiniotis, G., Bouvier, M., Lefkowitz, R.J., 2016. GPCR G-protein-β-arrestin super-complex mediates sustained G-protein signaling. Cell 166, 907–919. https://doi.org/10.1016/j.cell.2016.07.004

Tobe, S., Pratt, G., 1975. Corpus allatum activity *in vitro* during ovarian maturation in the desert locust, *Schistocerca gregaria*. J. Exp. Biol. 62, 611–627.

Tobe, S.S., Chapman, C.S., 1979. The effects of starvation and subsequent feeding on juvenile hormone synthesis and oocyte growth in *Schistocerca americana gregaria*. J. Insect Physiol. 25, 701–708.

Tobe, S.S., Chapman, C.S., Pratt, G.E., 1977. Decay in juvenile hormone biosynthesis by insect corpus allatum after nerve transection. Nature 268, 728–730. https://doi.org/10.1038/268728a0

Tobe, S.S., Pratt, G.E., 1974. The influence of substrate concentrations on the rate of insect juvenile hormone biosynthesis by corpora allata of the desert locust *in vitro*. Biochem. J. 144, 107–13.

Tobe, S.S., Zhang, J.R., Schooley, D.A., Coast, G.M., 2005. A study of signal transduction for the two diuretic peptides of *Diploptera punctata*. Peptides 26, 89–98. https://doi.org/10.1016/j.peptides.2004.07.013

Tobin, A.B., 2008. G-protein-coupled receptor phosphorylation: Where, when and by whom. Br. J. Pharmacol.

153, 167–176. https://doi.org/10.1038/sj.bjp.0707662

Ubuka, T., Tsutsui, K., 2014. Evolution of gonadotropin-inhibitory hormone receptor and its ligand. Gen. Comp. Endocrinol. 209, 148–161. https://doi.org/10.1016/j.ygcen.2014.09.002

Ukena, K., Oumi, T., Matsushima, O., Ikeda, T., Fujita, T., Minakata, H., Nomoto, K., 1995. A novel gut tetradecapeptide isolated from the earthworm, *Eisenia foetida*. Peptides 16, 995–9.

United Nations, 2017. World population prospects: The 2017 revision. New York.

Uvarov, B., 1977. Grasshoppers and locusts. A Handb. Gen. acridology Vol. 2. Behav. Ecol. Biogeogr. Popul. Dyn.

Uvarov, B., 1966. Grasshoppers and locusts: Anatomy, physiology, development, phase polymorphism, introduction to taxonomy, Vol. 1. ed. Camebridge UP, Cambridge.

van der Valk, H., 2007. Review of the efficacy of *Metarhizium anisopliae* var. *acridum* against the desert locust, FAO - U.N. Publications. Rome.

Van Hiel, M.B., Van Loy, T., Poels, J., Vandersmissen, H.P., Verlinden, H., Badisco, L., Vanden Broeck, J., 2010. Neuropeptide receptors as possible targets for development of insect pest control agents. Adv. Exp. Med. Biol. 692, 211–26.

Van Hiel, M.B., Van Wielendaele, P., Temmerman, L., Van Soest, S., Vuerinckx, K., Huybrechts, R., Vanden Broeck, J., Simonet, G., 2009. Identification and validation of housekeeping genes in brains of the desert locust *Schistocerca gregaria* under different developmental conditions. BMC Mol. Biol. 10, 56. https://doi.org/10.1186/1471-2199-10-56

Van Wielendaele, P., 2012. Neuropeptides controlling food uptake and reproduction in the desert locust *Schistocerca gregaria*. KU Leuven.

Van Wielendaele, P., Dillen, S., Marchal, E., Badisco, L., Vanden Broeck, J., 2012. CRF-like diuretic hormone negatively affects both feeding and reproduction in the desert locust, *Schistocerca gregaria*. PLoS One 7, e31425. https://doi.org/10.1371/journal.pone.0031425

Vanden Broeck, J., 2001a. Insect G protein-coupled receptors and signal transduction. Arch. Insect Biochem. Physiol. 48, 1–12. https://doi.org/10.1002/arch.1054

Vanden Broeck, J., 2001b. Neuropeptides and their precursors in the fruitfly, *Drosophila melanogaster*. Peptides 22, 241–254. https://doi.org/10.1016/S0196-9781(00)00376-4

Vanden Broeck, J., Vulsteke, V., Huybrechts, R., De Loof, A., 1995. Characterization of a cloned locust tyramine receptor cDNA by functional expression in permanently transformed *Drosophila* S2 cells. J. Neurochem. 64, 2387–2395. https://doi.org/10.1046/j.1471-4159.1995.64062387.x

Vanden Broeck, J.J.M., 1996. G-protein-coupled receptors in Insect cells. Int. Rev. Cytol. 164, 189–268. https://doi.org/10.1016/S0074-7696(08)62387-6

Vandersmissen, H.P., Nachman, R.J., Vanden Broeck, J., 2013. Sex peptides and MIPs can activate the same G protein-coupled receptor. Gen. Comp. Endocrinol. 188, 137–143. https://doi.org/10.1016/j.ygcen.2013.02.014

Vandesompele, J., De Preter, K., Pattyn, F., Poppe, B., Van Roy, N., De Paepe, A., Speleman, F., 2002. Accurate normalization of real-time quantitative RT-PCR data by geometric averaging of multiple internal control genes. Genome Biol. 3.

Vázquez-Acevedo, N., Rivera, N.M., Torres-González, A.M., Rullan-Matheu, Y., Ruíz-Rodríguez, E.A., Sosa,

M.A., 2009. GYRKPPFNGSIFamide (Gly-SIFamide) modulates aggression in the freshwater prawn *Macrobrachium rosenbergii*. Biol. Bull. 217, 313–326. https://doi.org/10.1086/BBLv217n3p313

Veenstra, J. a., Rodriguez, L., Weaver, R.J., 2012. Allatotropin, leucokinin and AKH in honey bees and other Hymenoptera. Peptides 35, 122–130. https://doi.org/10.1016/j.peptides.2012.02.019

Veenstra, J. a, Lehman, H.K., Davis, N.T., 1994. Allatotropin is a cardioacceleratory peptide in *Manduca sexta*. J. Exp. Biol. 188, 347–354.

Veenstra, J.A., 2016. Similarities between decapod and insect neuropeptidomes. PeerJ 4, e2043. https://doi.org/10.7717/peerj.2043

Veenstra, J.A., 2011. Neuropeptide evolution: Neurohormones and neuropeptides predicted from the genomes of *Capitella teleta* and *Helobdella robusta*. Gen. Comp. Endocrinol. 171, 160–75. https://doi.org/10.1016/j.ygcen.2011.01.005

Veenstra, J.A., 2010. Neurohormones and neuropeptides encoded by the genome of *Lottia gigantea*, with reference to other mollusks and insects. Gen. Comp. Endocrinol. 167, 86–103. https://doi.org/10.1016/j.ygcen.2010.02.010

Veenstra, J.A., 2000. Mono- and dibasic proteolytic cleavage sites in insect neuroendocrine peptide precursors. Arch. Insect Biochem. Physiol. 43, 49–63.

Veenstra, J.A., Costes, L., 1999. Isolation and identification of a peptide and its cDNA from the mosquito *Aedes aegypti* related to *Manduca sexta* allatotropin. Peptides 20, 1145–1151. https://doi.org/10.1016/S0196-9781(99)00117-5

Veenstra, J.A., Rombauts, S., Grbić, M., 2012. *In silico* cloning of genes encoding neuropeptides, neurohormones and their putative G-protein coupled receptors in a spider mite. Insect Biochem. Mol. Biol. 42, 277–295. https://doi.org/10.1016/j.ibmb.2011.12.009

Velthuis, H.H.W., Doorn, A., 2006. A century of advances in bumblebee domestication and the economic and environmental aspects of its commercialization for pollination. Apidologie 37, 421–451. https://doi.org/10.1051/apido:2006019

Venkatakrishnan, A.J., Deupi, X., Lebon, G., Tate, C.G., Schertler, G.F., Babu, M.M., 2013. Molecular signatures of G-protein-coupled receptors. Nature 494, 185–194. https://doi.org/10.1038/nature11896

Verdonck, R., 2017. Phase transition in the desert locust *Schistocerca gregaria*: a transcriptomic approach. KU Leuven.

Verger, P.J.P., Boobis, A.R., 2013. Reevaluate pesticides for food security and safety. Science 341, 717–718. https://doi.org/10.1126/science.1241572

Verleyen, P., Huybrechts, J., Baggerman, G., Van Lommel, A., De Loof, A., Schoofs, L., 2004a. SIFamide is a highly conserved neuropeptide: A comparative study in different insect species. Biochem. Biophys. Res. Commun. 320, 334–341. https://doi.org/10.1016/j.bbrc.2004.05.173

Verleyen, P., Huybrechts, J., Sas, F., Clynen, E., Baggerman, G., De Loof, A., Schoofs, L., 2004b. Neuropeptidomics of the grey flesh fly, *Neobellieria bullata*. Biochem. Biophys. Res. Commun. 316, 763–770. https://doi.org/10.1016/j.bbrc.2004.02.115

Verleyen, P., Huybrechts, J., Schoofs, L., 2009. SIFamide illustrates the rapid evolution in Arthropod neuropeptide research. Gen. Comp. Endocrinol. 162, 27–35. https://doi.org/10.1016/j.ygcen.2008.10.020

Verlinden, H., Badisco, L., Marchal, E., Van Wielendaele, P., Vanden Broeck, J., 2009. Endocrinology of

reproduction and phase transition in locusts. Gen. Comp. Endocrinol. 162, 79–92. https://doi.org/10.1016/j.ygcen.2008.11.016

Verlinden, H., Gijbels, M., Lismont, E., Lenaerts, C., Vanden Broeck, J., Marchal, E., 2015a. The pleiotropic allatoregulatory neuropeptides and their receptors: A mini-review. J. Insect Physiol. 80, 2–14. https://doi.org/10.1016/j.jinsphys.2015.04.004

Verlinden, H., Lismont, E., Bil, M., Urlacher, E., Mercer, A., Vanden Broeck, J., Huybrechts, R., 2013. Characterisation of a functional allatotropin receptor in the bumblebee, *Bombus terrestris* (Hymenoptera, Apidae). Gen. Comp. Endocrinol. 193, 193–200.

Verlinden, H., Vleugels, R., Marchal, E., Badisco, L., Tobback, J., Pflüger, H.-J., Blenau, W., Vanden Broeck, J., 2010. The cloning, phylogenetic relationship and distribution pattern of two new putative GPCR-type octopamine receptors in the desert locust (*Schistocerca gregaria*). J. Insect Physiol. 56, 868–75. https://doi.org/10.1016/j.jinsphys.2010.03.003

Verlinden, H., Vleugels, R., Verdonck, R., Urlacher, E., Vanden Broeck, J., Mercer, A., 2015b. Pharmacological and signalling properties of a D2-like dopamine receptor (Dop3) in *Tribolium castaneum*. Insect Biochem. Mol. Biol. 56, 9–20. https://doi.org/10.1016/j.ibmb.2014.11.002

Verlinden, H., Vleugels, R., Zels, S., Dillen, S., Lenaerts, C., Crabbé, K., Spit, J., Vanden Broeck, J., 2014. Receptors for neuronal or endocrine signalling molecules as potential targets for the control of insect pests. Adv. In Insect Phys. 46, 167–303. https://doi.org/10.1016/B978-0-12-417010-0.00003-3

Vilardaga, J.P., Jean-Alphonse, F.G., Gardella, T.J., 2014. Endosomal generation of cAMP in GPCR signaling. Nat. Chem. Biol. 10, 700–706. https://doi.org/10.1038/nchembio.1611

Villalobos-Sambucaro, M.J., Diambra, L.A., Noriega, F.G., Ronderos, J.R., 2016. Allatostatin-C antagonizes the synergistic myostimulatory effect of allatotropin and serotonin in *Rhodnius prolixus* (Stal). Gen. Comp. Endocrinol. 233, 1–7. https://doi.org/10.1016/j.ygcen.2016.05.009

Villalobos-Sambucaro, M.J., Lorenzo-Figueiras, A.N., Riccillo, F.L., Diambra, L.A., Noriega, F.G., Ronderos, J.R., 2015. Allatotropin modulates myostimulatory and cardioacceleratory activities in *Rhodnius prolixus* (Stal). PLoS One 10, e0124131. https://doi.org/10.1371/journal.pone.0124131

Violin, J.D., Lefkowitz, R.J., 2007. β-Arrestin-biased ligands at seven-transmembrane receptors. Trends Pharmacol. Sci. 28, 416–422. https://doi.org/10.1016/j.tips.2007.06.006

Vleugels, R., Lenaerts, C., Baumann, A., Vanden Broeck, J., Verlinden, H., 2013. Pharmacological characterization of a 5-HT1-type serotonin receptor in the red flour beetle, *Tribolium castaneum*. PLoS One 8, e65052. https://doi.org/10.1371/journal.pone.0065052

Vogel, E., Santos, D., Mingels, L., Verdonckt, T.-W., Broeck, J. Vanden, 2019. RNA interference in insects: Protecting beneficials and controlling pests. Front. Physiol. 9, 1912. https://doi.org/10.3389/fphys.2018.01912

Vroling, B., Sanders, M., Baakman, C., Borrmann, A., Verhoeven, S., Klomp, J., Oliveira, L., de Vlieg, J., Vriend, G., 2011. GPCRDB: information system for G protein-coupled receptors. Nucleic Acids Res. 39, D309–D319. https://doi.org/10.1093/nar/gkq1009

Vuerinckx, K., Verlinden, H., Lindemans, M., Vanden Broeck, J., Huybrechts, R., 2011. Characterization of an allatotropin-like peptide receptor in the red flour beetle, *Tribolium castaneum*. Insect Biochem. Mol. Biol. 41, 815–822. https://doi.org/10.1016/j.ibmb.2011.06.003

Weaver, R.J., Audsley, N., 2009. Neuropeptide regulators of juvenile hormone synthesis: Structures,

functions, distribution, and unanswered questions. Ann. N. Y. Acad. Sci. 1163, 316–329. https://doi.org/10.1111/j.1749-6632.2009.04459.x

Weaver, R.J., Audsley, N., 2008. Neuropeptides of the beetle, *Tenebrio molitor* identified using MALDI-TOF mass spectrometry and deduced sequences from the *Tribolium castaneum* genome. Peptides 29, 168–178. https://doi.org/10.1016/j.peptides.2007.09.020

Wiehart, U., Torfs, P., Van Lommel, A., Nicolson, S., Schoofs, L., 2002. Immunocytochemical localization of a diuretic hormone of the beetle *Tenebrio molitor Tenmo*-DH37, in nervous system and midgut. Cell Tissue Res. 308, 421–429. https://doi.org/10.1007/s00441-002-0552-9

Wikipedia, 2019. Aardhommel-groep [WWW Document]. URL https://nl.wikipedia.org/wiki/Aardhommel-groep (accessed 1.16.19).

Wisler, J.W., Xiao, K., Thomsen, A.R., Lefkowitz, R.J., 2014. Recent developments in biased agonism. Curr. Opin. Cell Biol. 27, 18–24. https://doi.org/10.1016/j.ceb.2013.10.008

Wootten, D., Christopoulos, A., Marti-Solano, M., Babu, M.M., Sexton, P.M., 2018. Mechanisms of signalling and biased agonism in G protein-coupled receptors. Nat. Rev. Mol. Cell Biol. https://doi.org/10.1038/s41580-018-0049-3

World Health Organization, 2018. Malaria [WWW Document]. URL https://www.who.int/en/news-room/fact-sheets/detail/malaria (accessed 2.18.19).

World Health Organization, 2017. Vector-borne diseases [WWW Document]. URL https://www.who.int/news-room/fact-sheets/detail/vector-borne-diseases (accessed 1.15.19).

Wyatt, G.R., Braun, R.P., Zhang, J., 1996. Priming effect in gene activation by juvenile hormone in locust fat body. 640, 633–640.

Xiao, R.P., 2001. β-adrenergic signaling in the heart: dual coupling of the β_2-adrenergic receptor to G_s and G_i proteins. Sci. STKE 2001, re15. https://doi.org/10.1126/stke.2001.104.re15

Xu, Y., Piston, D.W., Johnson, C.H., 1999. A bioluminescence resonance energy transfer (BRET) system: application to interacting circadian clock proteins. Proc. Natl. Acad. Sci. U. S. A. 96, 151–6.

Yagi, K.J., Tobe, S.S., 2001. The radiochemical assay for juvenile hormone biosynthesis in insects: Problems and solutions. J. Insect Physiol. 47, 1227–1234. https://doi.org/10.1016/S0022-1910(01)00124-X

Yamanaka, N., Yamamoto, S., Žitňan, D., Watanabe, K., Kawada, T., Satake, H., Kaneko, Y., Hiruma, K., Tanaka, Y., Shinoda, T., Kataoka, H., 2008. Neuropeptide receptor transcriptome reveals unidentified neuroendocrine pathways. PLoS One 3, e3048. https://doi.org/10.1371/journal.pone.0003048

Yan, X.-C., Chen, Z.-F., Sun, J., Matsumura, K., Wu, R.S.S., Qian, P.-Y., 2012. Transcriptomic analysis of neuropeptidesepti and peptide hormones in the barnacle *Balanus amphitrite*: Evidence of roles in larval settlement. PLoS One 7, e46513. https://doi.org/10.1371/journal.pone.0046513

Yang, Z., Huang, R., Fu, X., Wang, G., Qi, W., Mao, D., Shi, Z., Shen, W.L., Wang, L., 2018. A post-ingestive amino acid sensor promotes food consumption in *Drosophila*. Cell Res. 28, 1013–1025. https://doi.org/10.1038/s41422-018-0084-9

Yasuda-Kamatani, Y., Yasuda, A., 2006. Characteristic expression patterns of allatostatin-like peptide, FMRFamide-related peptide, orcokinin, tachykinin-related peptide, and SIFamide in the olfactory system of crayfish *Procambarus clarkii*. J. Comp. Neurol. 496, 135–147. https://doi.org/10.1002/cne.20903

Yasuda, A., Yasuda-Kamatani, Y., Nozaki, M., Nakajima, T., 2004. Identification of GYRKPPFNGSIFamide

(crustacean-SIFamide) in the crayfish *Procambarus clarkii* by topological mass spectrometry analysis. Gen. Comp. Endocrinol. 135, 391–400. https://doi.org/10.1016/j.ygcen.2003.10.001

Yeoh, J.G.C., Pandit, A.A., Zandawala, M., Nässel, D.R., Davies, S.-A., Dow, J.A.T., 2017. DINeR: Database for insect neuropeptide research. Insect Biochem. Mol. Biol. 86, 9–19. https://doi.org/10.1016/j.ibmb.2017.05.001

Zandawala, M., Marley, R., Davies, S.A., Nässel, D.R., 2018. Characterization of a set of abdominal neuroendocrine cells that regulate stress physiology using colocalized diuretic peptides in *Drosophila*. Cell. Mol. Life Sci. 75, 1099–1115. https://doi.org/10.1007/s00018-017-2682-y

Zels, S., 2015. Pharmacological and functional characterization of the sulfakininsignaling system in *Locusta migratoria* and *Tribolium castaneum*. KU Leuven.

Zels, S., Verlinden, H., Dillen, S., Vleugels, R., Nachman, R.J., Vanden Broeck, J., 2014. Signaling properties and pharmacological analysis of two sulfakinin receptors from the red flour beetle, *Tribolium castaneum*. PLoS One 9, e94502. https://doi.org/10.1371/journal.pone.0094502

Zhang, F., Wang, J., Thakur, K., Hu, F., Zhang, J.G., Jiang, X.F., An, S.H., Jiang, H., Jiang, L., Wei, Z.J., 2017. Isolation functional characterization of allatotropin receptor from the cotton bollworm, *Helicoverpa armigera*. Peptides 1–12. https://doi.org/10.1016/j.peptides.2017.11.019

Zhang, L., Luo, L., Jiang, X., 2008. Starvation influences allatotropin gene expression and juvenile hormone titer in the female adult oriental armyworm, *Mythimna separata*. Arch. Insect Biochem. Physiol. 68, 63–70. https://doi.org/10.1002/arch.20255

Zoephel, J., Reiher, W., Rexer, K.-H., Kahnt, J., Wegener, C., 2012. Peptidomics of the agriculturally damaging larval stage of the cabbage root fly *Delia radicum* (Diptera: Anthomyiidae). PLoS One 7, e41543. https://doi.org/10.1371/journal.pone.0041543

Appendices

A.1. Supplementary figures

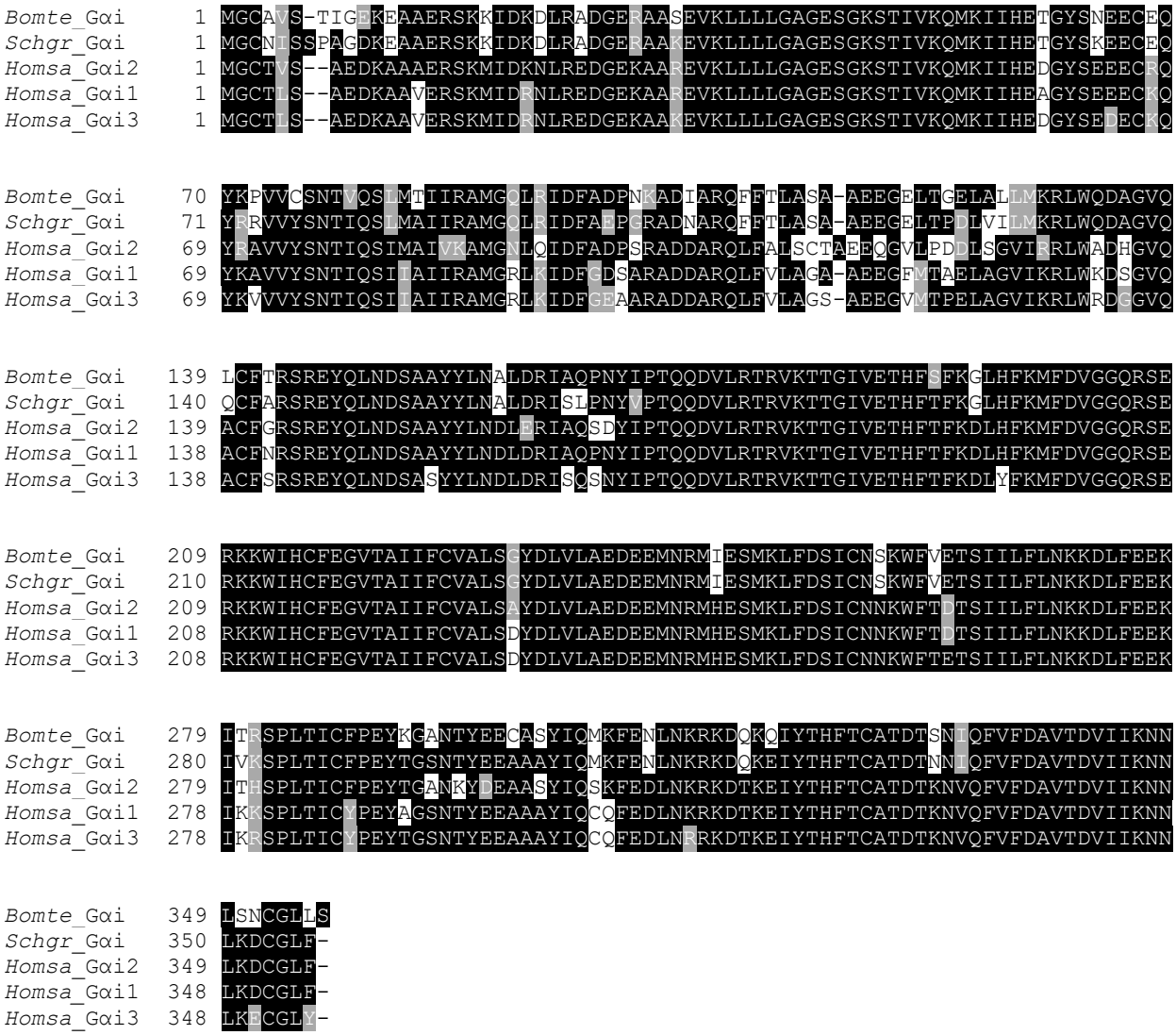

Supplementary Fig. S1: Multiple sequence alignment of $G\alpha_i$ subunits of *Homo sapiens* (*Homsa*) $G\alpha_{i1}$ (GenBank accession number P63096), $G\alpha_{i2}$ (GenBank accession number P04899) and $G\alpha_{i3}$ (GenBank accession number P08754), *Bombus terrestris* (*Bomte*) $G\alpha_i$ (GenBank accession number XP_003393073.1) and *Schistocerca gregaria* (*Schgr*) $G\alpha_i$ (unpublished sequence). The amino acid position is indicated at the left. Identical residues between the aligned sequences are highlighted in black, and conservatively substituted residues in grey. Dashes indicate gaps that are introduced to maximize similarities in the alignment.

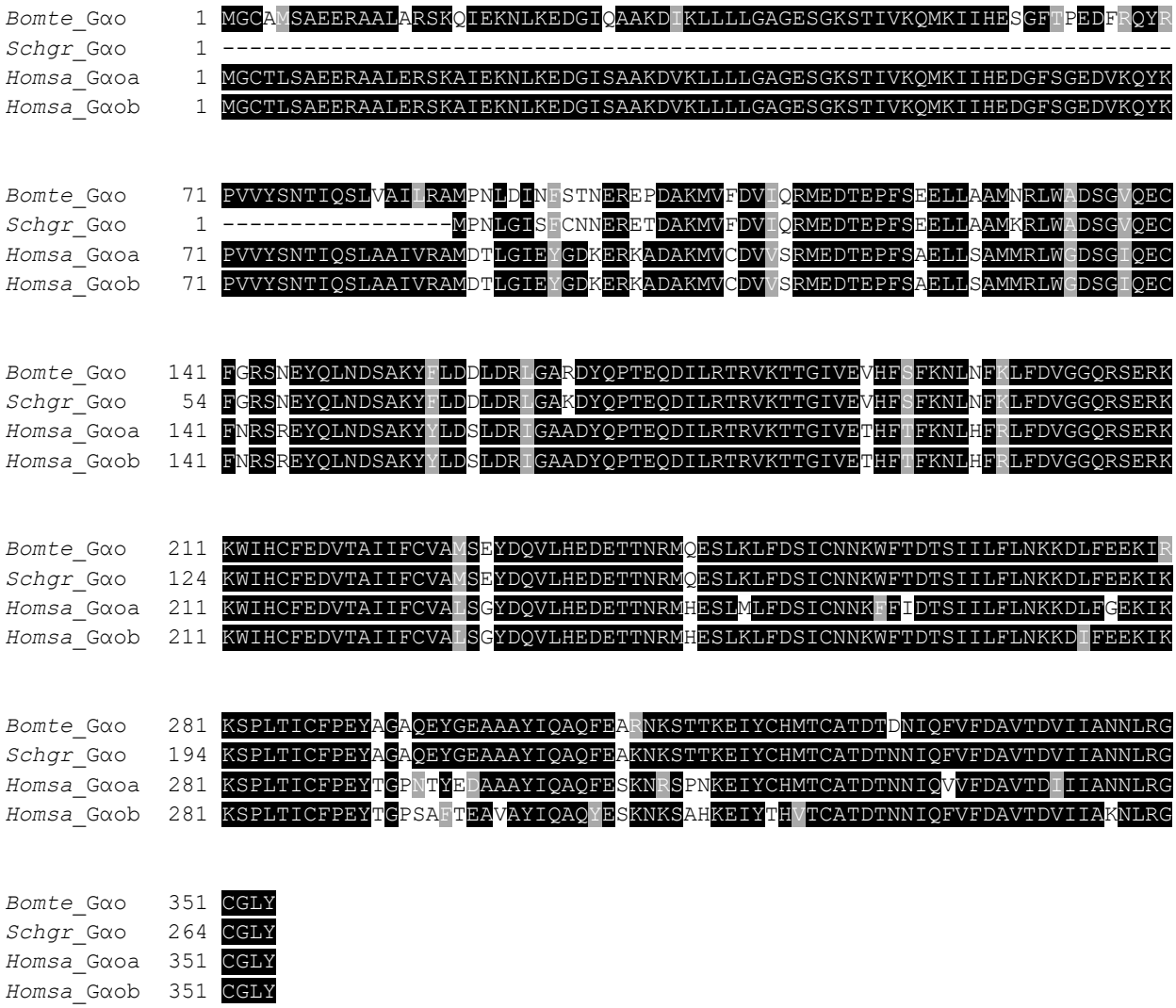

Supplementary Fig. S2: Multiple sequence alignment of $G\alpha_o$ subunits of *Homo sapiens* (*Homsa*) $G\alpha_{oa}$ (GenBank accession number NP_066268.1) and $G\alpha_{ob}$ (GenBank accession number NP_620073.2), *Bombus terrestris* (*Bomte*) $G\alpha_o$ (GenBank accession number XP_003401632.1), and *Schistocerca gregaria* (*Schgr*) $G\alpha_o$ (unpublished sequence). The amino acid position is indicated at the left. Identical residues between the aligned sequences are highlighted in black, and conservatively substituted residues in grey. Dashes indicate gaps that are introduced to maximize similarities in the alignment.

Supplementary Fig. S3: Multiple sequence alignment of $G\alpha_s$ subunits of *Homo sapiens* (*Homsa*) $G\alpha_s$ (GenBank accession number P63092), *Bombus terrestris* (*Bomte*) $G\alpha_s$ (GenBank accession number XP_003402502.1), and *Schistocerca gregaria* (*Schgr*) $G\alpha_s$ (unpublished data). The amino acid position is indicated at the left. Identical residues between the aligned sequences are highlighted in black, and conservatively substituted residues in grey. Dashes indicate gaps that are introduced to maximize similarities in the alignment.

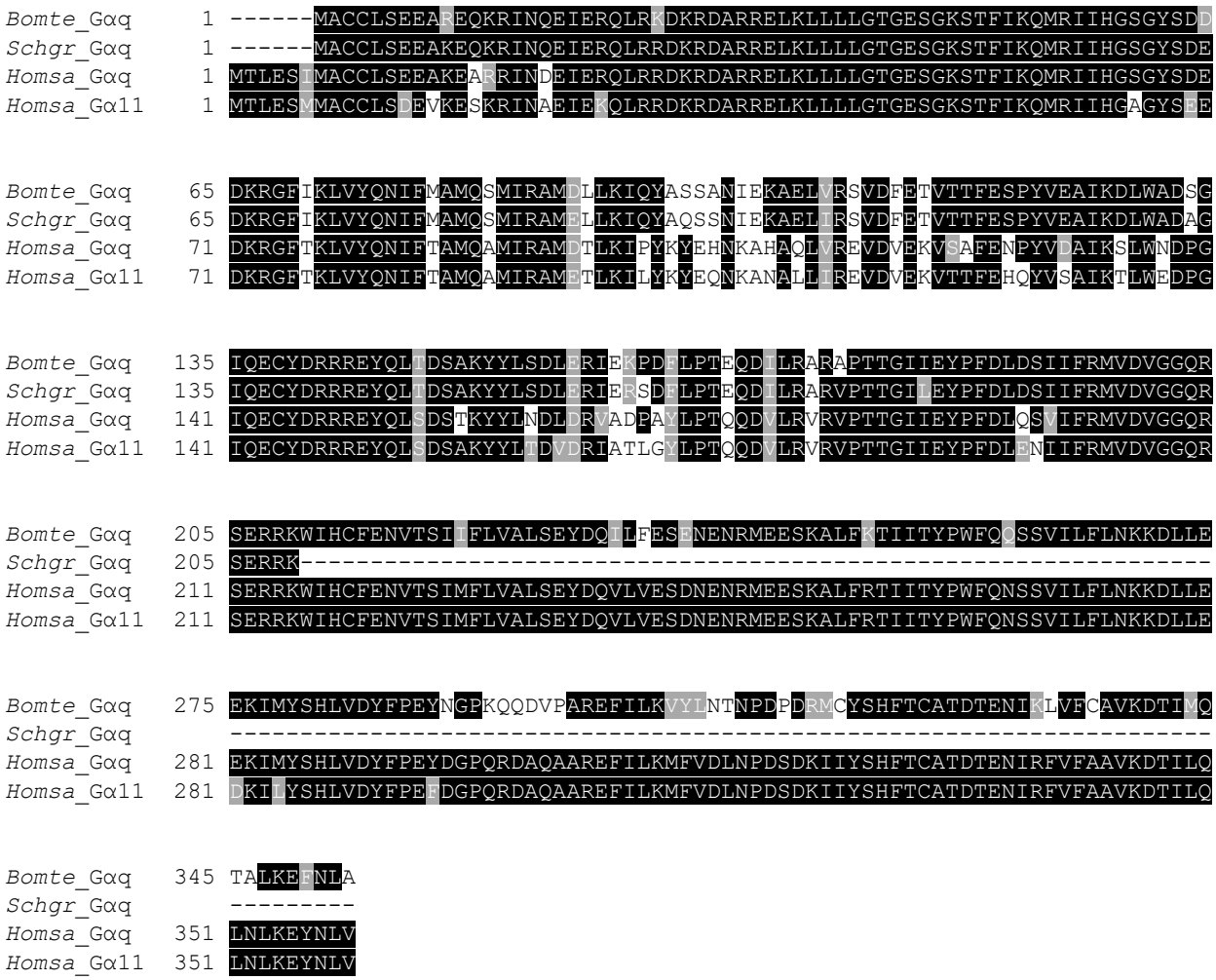

Supplementary Fig. S4: Multiple sequence alignment of $G\alpha_q$ subunits of *Homo sapiens* (*Homsa*) $G\alpha_q$ (GenBank accession number P50148) and $G\alpha_{11}$ (GenBank accession number P29992), *Bombus terrestris* (*Bomte*) $G\alpha_q$ (GenBank accession number XP_012174289.1), and *Schistocerca gregaria* (*Schgr*) $G\alpha_q$ (unpublished data). The amino acid position is indicated at the left. Identical residues between the aligned sequences are highlighted in black, and conservatively substituted residues in grey. Dashes indicate gaps that are introduced to maximize similarities in the alignment.

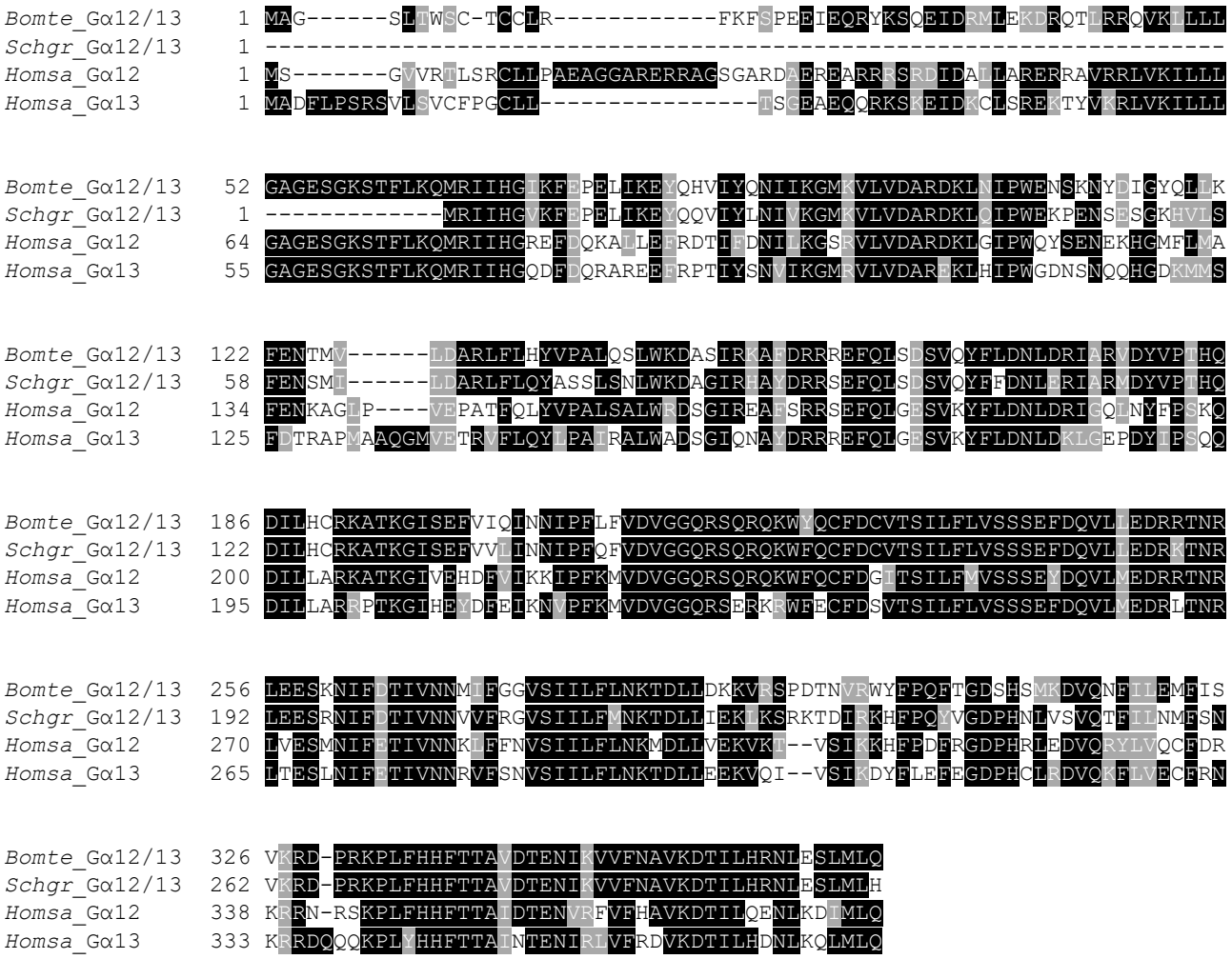

Supplementary Fig. S5: Multiple sequence alignment of $G\alpha_{12/13}$ subunits of *Homo sapiens* (*Homsa*) $G\alpha_{12}$ (GenBank accession number Q03113) and $G\alpha_{13}$ (GenBank accession number Q14344), *Bombus terrestris* (*Bomte*) $G\alpha_{12/13}$ (GenBank accession number XP_012174580.1), and *Schistocerca gregaria* (*Schgr*) $G\alpha_{12/13}$ (unpublished data). The amino acid position is indicated at the left. Identical residues between the aligned sequences are highlighted in black, and conservatively substituted residues in grey. Dashes indicate gaps that are introduced to maximize similarities in the alignment.

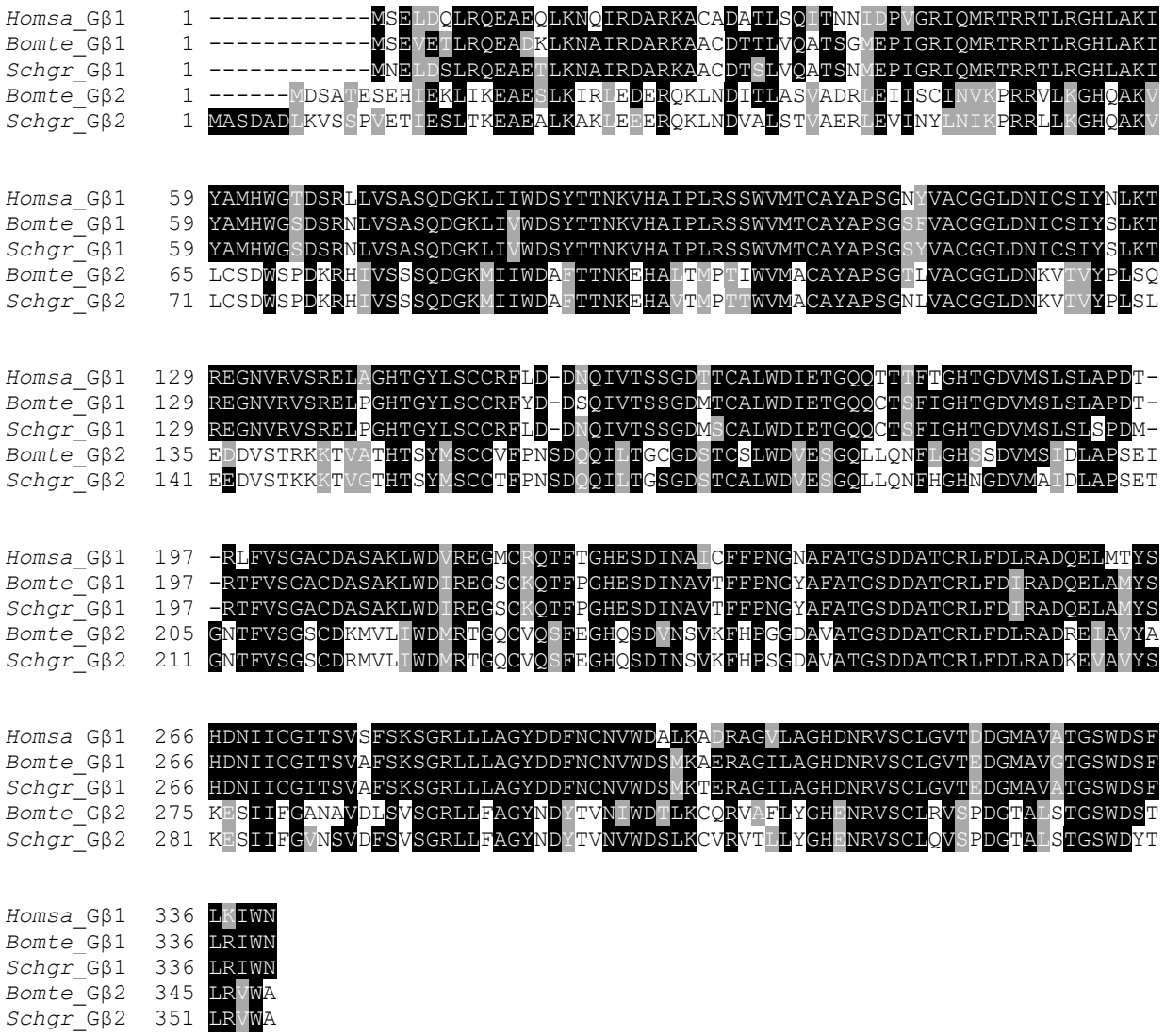

Supplementary Fig. S6: Multiple sequence alignment of Gβ subunits of *Homo sapiens* (*Homsa*) $G\beta_1$ (GenBank accession number P62873), *Bombus terrestris* (*Bomte*) $G\beta_1$ (GenBank accession number XP_003400659.1) and $G\beta_2$ (GenBank accession number XP_012165841.1), and *Schistocerca gregaria* (*Schgr*) $G\beta_1$ and $G\beta_2$ (unpublished data). The amino acid position is indicated at the left. Identical residues between the aligned sequences are highlighted in black, and conservatively substituted residues in grey. Dashes indicate gaps that are introduced to maximize similarities in the alignment.

Supplementary Fig. S7: Multiple sequence alignment of Gγ subunits of *Homo sapiens* (*Homsa*) Gγ1 (GenBank accession number P59768), *Bombus terrestris* (*Bomte*) Gγ1 (GenBank accession number XP_003402137.1) and $G\gamma_e$ (GenBank accession number XP_003400491.1), and *Schistocerca gregaria* (*Schgr*) $G\gamma_1$ and $G\gamma_2$ (unpublished data). Identical residues between the aligned sequences are highlighted in black, and conservatively substituted residues in grey. Dashes indicate gaps that are introduced to maximize similarities in the alignment.

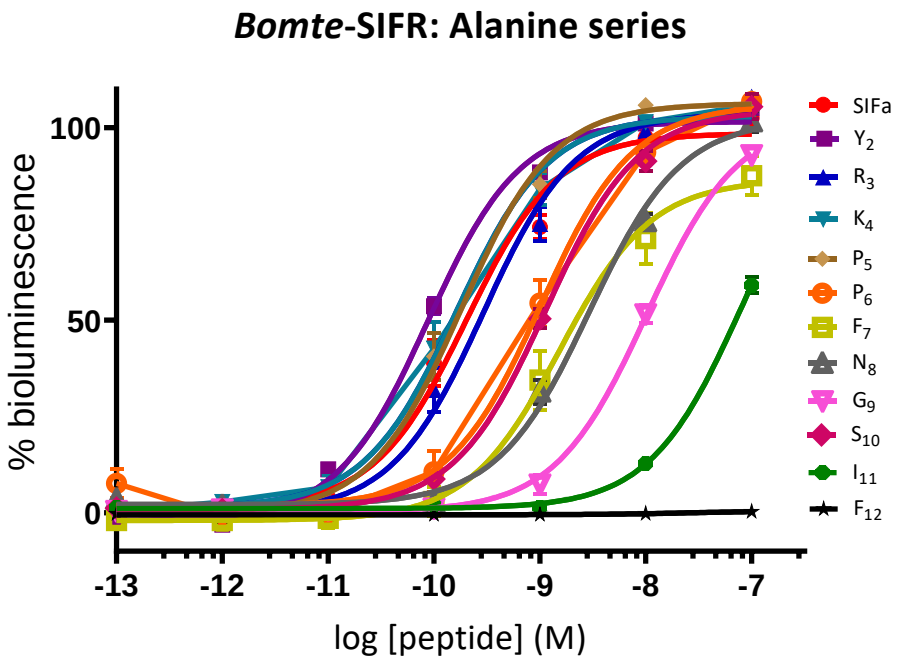

Supplementary Fig. S8: Bioluminescent responses induced in CHO-WTA11-*Bomte*-SIFR cells by several peptides (alanine series). This calcium reporter assay is executed in two independent transfections. The bioluminescence is measured in duplicate per concentration of peptide and per transfection. Error bars represent the S.E.M. The 100 % level refers to the maximal response level at 100 nM after stimulation of the endogenous *Bomte*-SIFa. The zero-response level corresponds to treatment with BSA medium only. The amino acid sequences of the peptides are enlisted in table 3.3 in section 3.3.10 on page 82.

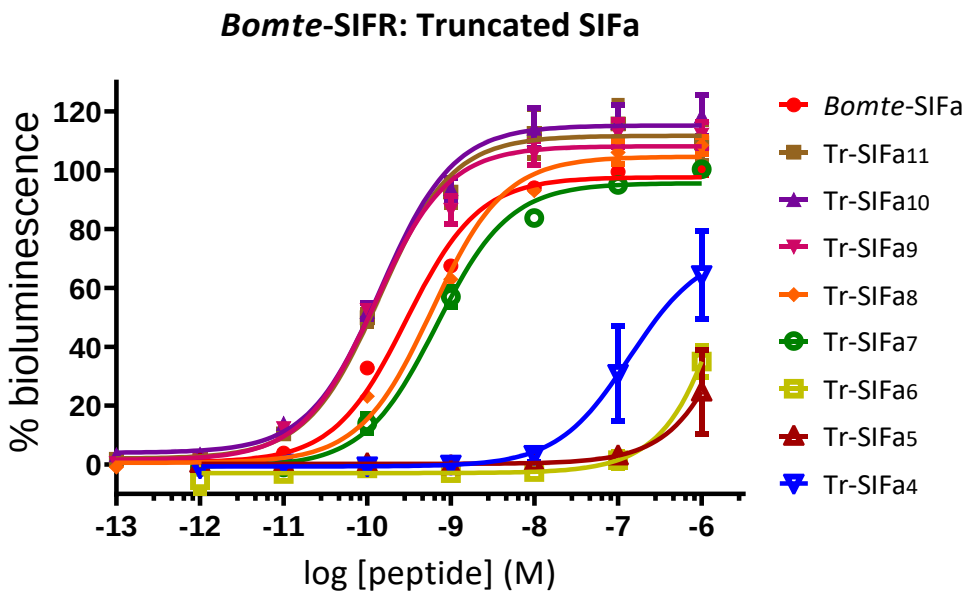

Supplementary Fig. S9: Bioluminescent responses induced in CHO-WTA11-*Bomte*-SIFR cells by several truncated SIFamide peptides. This calcium reporter assay is executed in two independent transfections. The bioluminescence is measured in duplicate per concentration of peptide and per transfection. Error bars represent the S.E.M. The 100 % level refers to the maximal response level at 1 µM after stimulation of the endogenous *Bomte*-SIFa. The zero-response level corresponds to treatment with BSA medium only. The amino acid sequences of the peptides are enlisted in table 3.3 in section 3.3.10 on page 82.

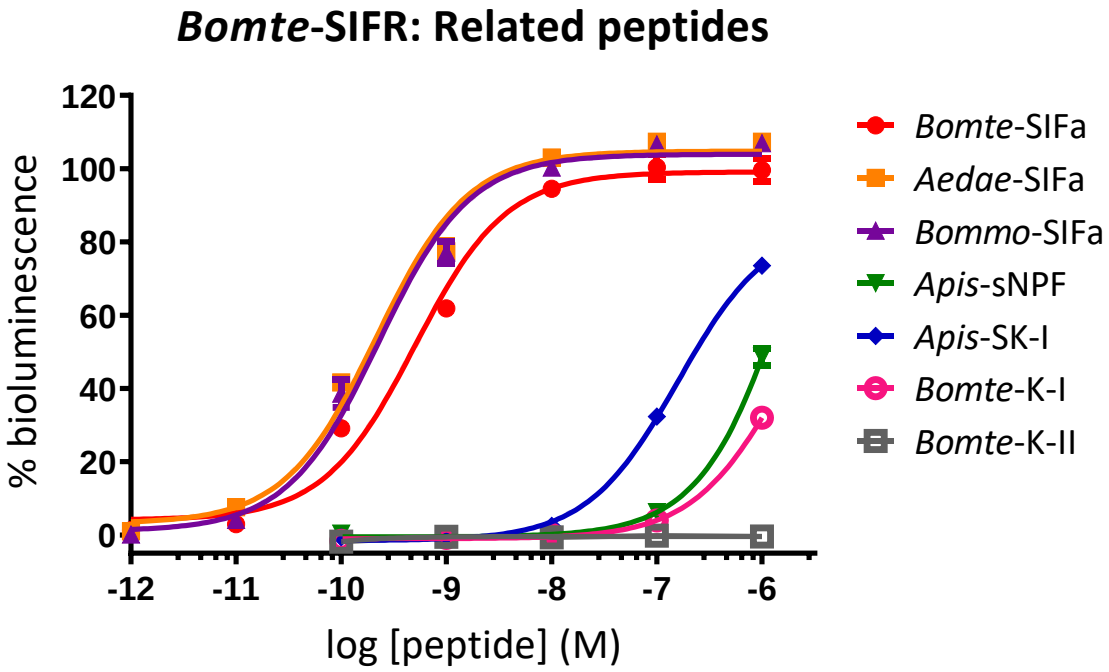

Supplementary Fig. S10: Bioluminescent responses induced in CHO-WTA11-*Bomte*-SIFR cells by SIFamide from other insects and related Hymenopteran peptides. This calcium reporter assay is executed in two independent transfections. The bioluminescence is measured in duplicate per concentration of peptide and per transfection. Error bars represent the S.E.M. The 100 % level refers to the maximal response level at 1 µM after stimulation of the endogenous *Bomte*-SIFa. The zero-response level corresponds to treatment with BSA medium only. The amino acid sequences of the peptides are enlisted in table 3.3 in section 3.3.10 on page 82.

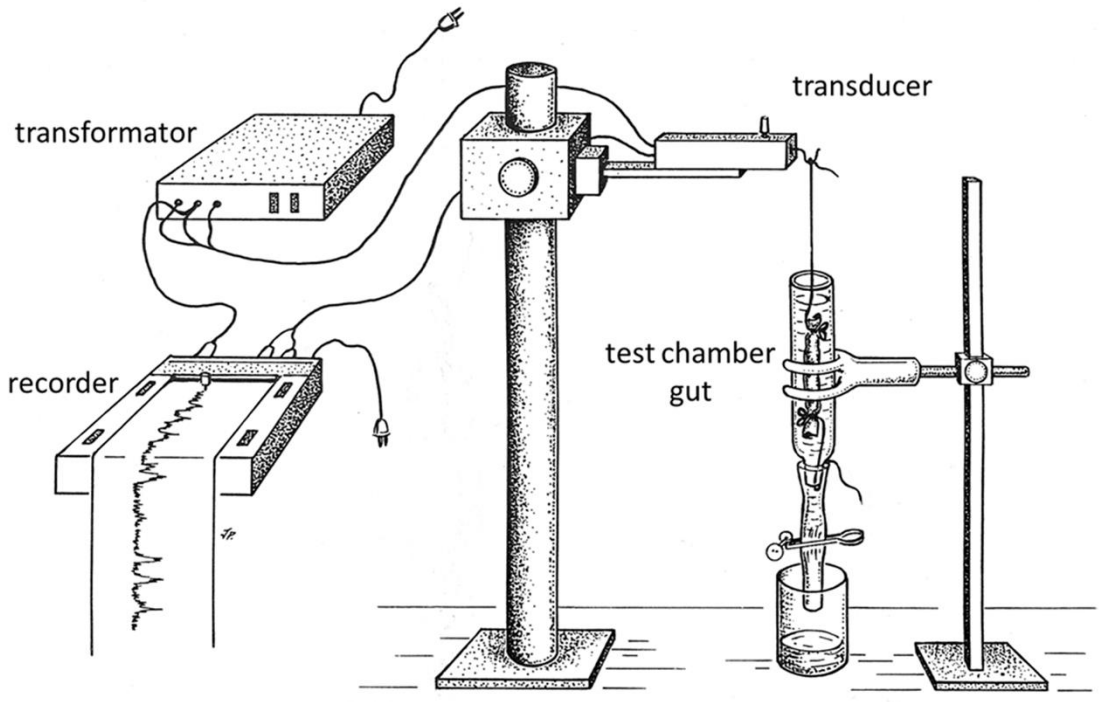

Supplementary Fig. S11: Schematic diagram of the *in vitro* locust gut motility bioassay. (Image credits: created by Julie Puttemans).

ATGGCGCTGCCATCGCTGATGTTCCCGATGCTGGAGAACACTACTCTGGAGGAGCTGCAGTGCCTGCTGGCGGAA
GCCACGGGGGCGGAGCTGGAAGCGGCGGTGTCGGGGGCCAGCTGCCCCCGAGCCTGGGACAGCGTCACCTGCTGG
CCAACCTCGCCGGCCGACACTCTCGTGCTGATGCCCTGCTTCTCGGAGCTCAACGGCATGCCGTATGACACCAGC
CAAAATGCGAGCCGGTGGTGCCACGCGAACGGCACGTGGTCGAGCTACAGCAACTACTCGTCGTGCGAGGCGATG
CTGCCCAAGATGCCGGTGGTCGAGGTGATCGACGAGGTGATCGTCGAGGTGGCCACGACGCTCTACTTCACCGGC
TACTCCGTCTCGCTCGCCGCCCTCGTCGTCGCCGTCACGATCTTCCTATACTTCAAAGAATTGCGATGCCTCCGA
AATGCCATCCACATGAATCTCATGTGGGCGTATATCCTCACCGACTTCTGGTGGATTCTGACTGGTATTGTAGAG
GTATCAGAGAAAGTGAGTAGCTCTGTATGCGTCGTCCTGGTGCTACTTTTCTACTATTTTCAGATGACTAACTTC
TTCTGGATGTTTGTAGAAGGACTTTATTTGTATATGCTGGTGGTGCAAACGTTTACGGGGAAGCTTATGCAGATG
CGTGCTTACATCCTCATTGGATGGGGGGTGCCACTAGTAATCATAACCGCGTGGGGCATCGCGAAAGGTCTCACT
ACGGGGACGGGAGACCCCACGGTGCCGAGCGCCGAACCGCTGCGCCTGCACTGCCCGTGGATGGACGTTGACGCG
TACGACTCGATCCACATGGGCCCCATCATGCTCGTGCTGTTCGCTAACCTCGGCTTCCTCGCCAGGATTATGTGG
GTGCTGATCACGAAGCTGCGGTCGGCGAACACGGTGGAGACGCAGCAGTACCGGAAGGCCAGCAAGGCGCTGCTG
GTGCTGATCCCGCTGCTCGGCATCACCTACATCCTCATGATCGCAGGGCCCACGGAGGGCTTCTCCGCTGAGGTC
TACGGCAACATCCGCGCCGTACTCCTGTCTACACAGGGCTTCACGGTGGCGCTGTTCTACTGCTTCCTCAACTCG
GAGGTGCAGACGGCGGTGCGGCACCGGCTGGACAGCTGGCAGACGGCTCGCAGTCTCGGCGGCGCGGGCTCCGGC
GCCCGCAGGCTCAAGAGGTCCAACAGCCGCGACGGCTCGCCCAGGTCCCGCACCGAGAGCATACGGGTAGGCGAC
GTGATGCCGGCTGGAGGCCCCCGGGAGGTGTCGGACAGTCAGCTCTGA

Supplementary Fig. S12: Nucleotide sequence of predicted *Schgr*-CRF-DHR2. The two partial sequences highlighted in light grey are confirmed sequences after amplification by PCR while the sequence highlighted in dark grey is sequenced upon amplification by qRT-PCR.


Schgr-CRF-DHR2
Schgr-CRF-DHR1
Schgr-CRF-DHR3

↑ Supplementary Fig. S13: Multiple sequence alignment of nucleotide sequences of *Schgr*-CRF-DHR1, *Schgr*-CRF-DHR2 and *Schgr*-CRF-DHR3.The amino acid position is indicated at the right. Identical residues between the aligned sequences are highlighted in black, and conservatively substituted residues in grey. The light grey bar indicates the sequence of *Schgr*-CRF-DHR1 amplified by qRT-PCR and confirmed by sequencing while the dark grey bar indicates the sequence of *Schgr*-CRF-DHR2 amplified by qRT-PCR and confirmed by sequencing.

A.2. Supplementary tables

Supplementary table S1: **Percent identity matrix of $G\alpha_i$ subunits** of *Homo sapiens* (*Homsa*) $G\alpha_{i1}$ (GenBank accession number P63096), $G\alpha_{i2}$ (GenBank accession number P04899) and $G\alpha_{i3}$ (GenBank accession number P08754), *Bombus terrestris* (*Bomte*) $G\alpha_i$ (GenBank accession number XP_003393073.1) and *Schistocerca gregaria* (*Schgr*) $G\alpha_i$ (unpublished sequence) constructed by the EBI Clustal Omega Multiple Sequence alignment software. Identities are expressed as a percentage of similarity.

	***Bomte*-$G\alpha_i$**	***Schgr*-$G\alpha_i$**	***Homsa*-$G\alpha_{i1}$**	***Homsa*-$G\alpha_{i2}$**	***Homsa*-$G\alpha_{i3}$**
***Bomte*-$G\alpha_i$**	100.00	59.58	79.94	81.07	79.38
***Schgr*-$G\alpha_i$**	59.58	100.00	81.98	83.33	82.49
***Homsa*-$G\alpha_{i1}$**	79.94	81.98	100.00	87.57	85.59
***Homsa*-$G\alpha_{i2}$**	81.07	83.33	87.57	100.00	93.79
***Homsa*-$G\alpha_{i3}$**	79.38	82.49	85.59	93.79	100.00

Supplementary table S2: **Percent identity matrix of $G\alpha_o$ subunits** of *Homo sapiens* (*Homsa*) $G\alpha_{oa}$ (GenBank accession number NP_066268.1) and $G\alpha_{ob}$ (GenBank accession number NP_620073.2), *Bombus terrestris* (*Bomte*) $G\alpha_o$ (GenBank accession number XP_003401632.1), and *Schistocerca gregaria* (*Schgr*) $G\alpha_o$ (unpublished sequence) constructed by the EBI Clustal Omega Multiple Sequence alignment software. Identities are expressed as a percentage of similarity.

	***Bomte*-$G\alpha_o$**	***Schgr*-$G\alpha_o$**	***Homsa*-$G\alpha_{oa}$**	***Homsa*-$G\alpha_{ob}$**
***Bomte*-$G\alpha_o$**	100.00	96.25	81.92	82.20
***Schgr*-$G\alpha_o$**	96.25	100.00	82.77	83.15
***Homsa*-$G\alpha_{oa}$**	81.92	82.77	100.00	94.35
***Homsa*-$G\alpha_{ob}$**	82.20	83.15	94.35	100.00

Supplementary table S3: **Percent identity matrix of $G\alpha_s$ subunits** of *Homo sapiens* (*Homsa*) $G\alpha_s$ (GenBank accession number P63092), *Bombus terrestris* (*Bomte*) $G\alpha_s$ (GenBank accession number XP_003402502.1), and *Schistocerca gregaria* (*Schgr*) $G\alpha_s$ (unpublished data) constructed by the EBI Clustal Omega Multiple Sequence alignment software. Identities are expressed as a percentage of similarity.

	***Homsa*-$G\alpha_s$**	***Bomte*-$G\alpha_s$**	***Schgr*-$G\alpha_s$**
***Homsa*-$G\alpha_s$**	100.00	73.68	77.31
***Bomte*-$G\alpha_s$**	73.68	100.00	83.38
***Schgr*-$G\alpha_s$**	77.31	83.38	100.00

Supplementary table S4: Percent identity matrix of $G\alpha_{q/11}$ subunits of *Homo sapiens* (*Homsa*) $G\alpha_q$ (GenBank accession number P50148) and $G\alpha_{11}$ (GenBank accession number P29992), *Bombus terrestris* (*Bomte*) $G\alpha_q$ (GenBank accession number XP_012174289.1), and *Schistocerca gregaria* (*Schgr*) $G\alpha_q$ (unpublished data) constructed by the EBI Clustal Omega Multiple Sequence alignment software. Identities are expressed as a percentage of similarity.

	***Bomte*-$G\alpha_q$**	***Schgr*-$G\alpha_q$**	***Homsa*-$G\alpha_q$**	***Homsa*-$G\alpha_{11}$**
***Bomte*-$G\alpha_q$**	100.00	94.26	79.04	76.77
***Schgr*-$G\alpha_q$**	94.26	100.00	78.95	78.95
***Homsa*-$G\alpha_q$**	79.04	78.95	100.00	90.25
***Homsa*-$G\alpha_{11}$**	76.77	78.95	90.25	100.00

Supplementary table S5: **Percent identity matrix of $G\alpha_{12/13}$ subunits** of *Homo sapiens* (*Homsa*) $G\alpha_{12}$ (GenBank accession number Q03113) and $G\alpha_{13}$ (GenBank accession number Q14344), *Bombus terrestris* (*Bomte*) $G\alpha_{12/13}$ (GenBank accession number XP_012174580.1), and *Schistocerca gregaria* (*Schgr*) $G\alpha_{12/13}$ (unpublished data) constructed by the EBI Clustal Omega Multiple Sequence alignment software. Identities are expressed as a percentage of similarity.

	***Bomte*-$G\alpha_{12/13}$**	***Schgr*-$G\alpha_{12/13}$**	***Homsa*-$G\alpha_{12}$**	***Homsa*-$G\alpha_{13}$**
***Bomte*-$G\alpha_{12/13}$**	100.00	79.67	58.47	58.40
***Schgr*-$G\alpha_{12/13}$**	79.67	100.00	59.74	58.42
***Homsa*-$G\alpha_{12}$**	58.47	59.74	100.00	65.75
***Homsa*-$G\alpha_{13}$**	58.40	58.42	65.75	100.00

Supplementary table S6: **Percent identity matrix of Gβ subunits** of *Homo sapiens* (*Homsa*) $G\beta_1$ (GenBank accession number P62873), *Bombus terrestris* (*Bomte*) $G\beta_1$ (GenBank accession number XP_003400659.1) and $G\beta_2$ (GenBank accession number XP_012165841.1), and *Schistocerca gregaria* (*Schgr*) $G\beta_1$ and $G\beta_2$ (unpublished data) constructed by the EBI Clustal Omega Multiple Sequence alignment software. Identities are expressed as a percentage of similarity.

	***Homsa*-$G\beta_1$**	***Bomte*-$G\beta_1$**	***Schgr*-$G\beta_1$**	***Bomte*-$G\beta_2$**	***Schgr*-$G\beta_2$**
***Homsa*-$G\beta_1$**	100.00	85.88	86.47	50.88	52.35
***Bomte*-$G\beta_1$**	85.88	100.00	95.29	51.47	52.94
***Schgr*-$G\beta_1$**	86.47	95.29	100.00	50.59	52.65
***Bomte*-$G\beta_2$**	50.88	51.47	50.59	100.00	83.95
***Schgr*-$G\beta_2$**	52.35	52.94	52.65	83.95	100.00

Supplementary table S7: **Percent identity matrix of Gγ subunits** of *Homo sapiens* (*Homsa*) Gγ1 (GenBank accession number P59768), *Bombus terrestris* (*Bomte*) Gγ1 (GenBank accession number XP_003402137.1) and Gγe (GenBank accession number XP_003400491.1), and *Schistocerca gregaria* (*Schgr*) $G\gamma_1$ and $G\gamma_2$ (unpublished data) constructed by the EBI Clustal Omega Multiple Sequence alignment software. Identities are expressed as a percentage of similarity.

	***Bomte*-$G\gamma_e$**	***Schgr*-$G\gamma_2$**	***Homsa*-$G\gamma_2$**	***Bomte*-$G\gamma_1$**	***Schgr*-$G\gamma_1$**
***Bomte*-$G\gamma_e$**	100.00	92.19	30.43	27.54	18.84
***Schgr*-$G\gamma_2$**	92.19	100.00	34.43	25.81	20.97
***Homsa*-$G\gamma_2$**	30.43	34.43	100.00	42.03	39.13
***Bomte*-$G\gamma_1$**	27.54	25.81	42.03	100.00	72.86
***Schgr*-$G\gamma_1$**	18.84	20.97	39.13	72.86	100.00

Supplementary table S8: **Gene specific oligonucleotide primers** used for RACE of *Schgr*-ATR in this study

Target gene	5' RACE	3' RACE
cDNA synthesis	5'-GTACACCATGTTCCAGTAGT-3'	5'-CATGTTCGCCATCTGCTAC-3'
PCR 1	5'-CCAGAGAGAAGTCTGGAGTG-3'	5'-TCCACCTGCTCAACATACTG-3'
PCR 2	5'-ACATTGGAGGACGGTGACA-3'	5'-CCGTCAACCCAGTCATCTAC-3'

Supplementary table S9: **Percent identity matrix of open reading frame *S. gregaria* DH receptors**

	***Schgr*-CRF-DHR1**	***Schgr*-CRF-DHR3**	***Schgr*-CRF-DHR2**
***Schgr*-CRF-DHR1**	100.00	73.89	66.98
***Schgr*-CRF-DHR3**	73.89	100.00	76.18
***Schgr*-CRF-DHR2**	66.98	76.18	100.00

Supplementary table S10: **Percent identity matrix of insect DH receptors TM1 - TM7:** *R. prolixus* (*Rhopr*-CRF-DHR2B; GenBank acc. no. KJ407397), CRF-DHRs from *D. melanogaster* (*Drome*-DH44-R1; GenBank acc. no. NP_610960.1, and *Drome*-DH44-R2; GenBank acc. no. NP_610789.3), *M. sexta* (*Manse*-CRF-DHR; GenBank acc. no. AAC46469.1), *A. domesticus* (*Achdo*-CRF-DHR; GenBank acc. no AAC47000.1) and *S. gregaria* (*Schgr*-CRF-DHR1, *Schgr*-CRF-DHR2 and *Schgr*-CRF-DHR3).

	***Rhopr*-CRF-DHR2B**	***Drome*-DH44-R1**	***Drome*-DH44-R2**	***Manse*-CRF-DHR**	***Achdo*-CRF-DHR**	***Schgr*-CRF-DHR2**	***Schgr*-CRF-DHR1**	***Schgr*-CRF-DHR3**
***Rhopr*-CRF-DHR2B**	100.00	50.00	52.21	55.20	54.88	54.92	60.25	59.43
***Drome*-DH44-R1**	50.00	100.00	60.24	57.20	54.47	53.69	57.76	55.75
***Drome*-DH44-R2**	52.21	60.24	100.00	59.92	50.81	53.25	52.85	53.25
***Manse*-CRF-DHR**	55.20	57.20	59.92	100.00	54.12	53.97	59.45	56.30
***Achdo*-CRF-DHR**	54.88	54.47	50.81	54.12	100.00	56.92	59.68	57.31
***Schgr*-CRF-DHR2**	54.92	53.69	53.25	53.97	56.92	100.00	67.72	68.11
***Schgr*-CRF-DHR1**	60.25	57.76	52.85	59.45	59.68	67.72	100.00	83.07
***Schgr*-CRF-DHR3**	59.43	55.75	53.25	56.30	57.31	68.11	83.07	100.00

Supplementary table S11: Results of the RNA quantity and quality of all four pooled tissue samples of immature *Schistocerca gregaria* females. The concentration of the samples is determined by the absorbance at 260 nm whereas the ratio of the sample absorbance measured at 260 nm and 280 nm is used to assess RNA purity. A ratio of ~2 is considered pure RNA.

Immature Females		POOL 1	POOL 1	POOL 2	POOL 2	POOL 3	POOL 3	POOL 4	POOL 4
		concentration (ng/µl)	260/280	**concentration (ng/µl)**	260/280	**concentration (ng/µl)**	260/280	**concentration (ng/µl)**	260/280
Br	Brain	**342**	1.90	**257**	2.14	**327**	2.14	**426**	1.95
OL	Optic Lobes	**133**	2.10	**185**	2.17	**152**	2.14	**188**	2.19
CC	Corpora cardiaca	**89**	2.13	**94**	2.02	**108**	2.03	**102**	1.95
CA	Corpora allata	**47**	1.90	**43**	1.81	**46**	1.82	**39**	1.87
PG	Prothoracic gland	**246**	1.89	**155**	2.00	**192**	1.97	**93**	2.48
FG	Frontal ganglion	**33**	2.33	**46**	2.05	**37**	2.37	**42**	1.96
SOG	Suboesophageal ganglion	**167**	1.85	**121**	1.89	**90**	1.95	**105**	1.96
SG	Salivary glands	**625**	2.11	**691**	2.17	**516**	2.08	**431**	2.08
VNC	Ventral nerve cord	**1130**	2.12	**903**	2.14	**936**	2.13	**951**	2.16
GON	Gonads	**892**	2.13	**820**	2.16	**885**	2.15	**943**	2.13
FB	Fat body	**1189**	2.15	**758**	2.14	**1021**	2.13	**1008**	2.15
FM	Flight muscle	**1225**	2.15	**967**	2.13	**1078**	2.14	**1076**	2.15
FG	Foregut	**1127**	2.12	**1152**	2.12	**920**	2.12	**1000**	2.12
CAE	Caeca	**1440**	2.14	**993**	2.15	**1757**	2.15	**1143**	2.16
MT	Malpighian tubules	**1083**	2.20	**890**	2.20	**833**	2.14	**1251**	2.23
MG	Midgut	**1382**	2.16	**1146**	2.15	**1320**	2.16	**1340**	2.15
HG	Hindgut	**878**	2.18	**1024**	2.13	**894**	2.16	**1076**	2.16
ACC GL	Male accessory glands	**/**	/	**/**	/	**/**	/	**/**	/
CU	Cuticle	**1105**	2.14	**1168**	2.15	**1041**	2.15	**789**	2.14

Supplementary table S12: Results of the RNA quantity and quality in all four pooled tissue samples of immature *Schistocerca gregaria* males. The concentration of the samples is determined by the absorbance at 260 nm whereas the ratio of the sample absorbance measured at 260 nm and 280 nm is used to assess RNA purity. A ratio of ~2 is considered pure RNA.

Immature Males		POOL 1	POOL 1	POOL 2	POOL 2	POOL 3	POOL 3	POOL 4	POOL 4
		concentration (ng/µl)	260/280	**concentration (ng/µl)**	260/280	**concentration (ng/µl)**	260/280	**concentration (ng/µl)**	260/280
Br	Brain	**462**	2.04	**207**	2.15	**323**	2.15	**237**	2.15
OL	Optic Lobes	**185**	2.15	**158.**	2.16	**201**	2.17	**139**	2.14
CC	Corpora cardiaca	**105**	1.87	**123**	1.95	**108**	1.96	**103**	1.88
CA	Corpora allata	**38**	1.78	**42**	1.75	**44**	1.82	**48**	1.84
PG	Prothoracic gland	**237**	1.92	**221**	1.86	**184**	1.89	**179**	1.84
FG	Frontal ganglion	**33**	1.88	**35**	1.80	**29**	1.76	**27**	1.88
SOG	Suboesophageal ganglion	**123**	1.84	**162**	1.67	**85**	1.88	**103**	1.86
SG	Salivary glands	**460**	2.09	**561**	2.07	**447**	2.11	**498**	2.09
VNC	Ventral nerve cord	**778**	2.16	**853**	2.14	**1177**	2.15	**673**	2.12
GON	Gonads	**1138**	2.14	**1152**	2.12	**1026**	2.15	**1115**	2.12
FB	Fat body	**769**	2.13	**639**	2.16	**1102**	2.15	**593**	2.17
FM	Flight muscle	**1056**	2.13	**930**	2.14	**928**	2.15	**1042**	2.13
FG	Foregut	**1001**	2.14	**792**	2.13	**924**	2.15	**851**	2.10
CAE	Caeca	**1496**	2.15	**1157**	2.15	**1255**	2.14	**1051**	2.15
MT	Malpighian tubules	**860**	2.27	**419**	2.19	**1289**	2.27	**836**	2.25
MG	Midgut	**977**	2.16	**1418**	2.15	**1862**	2.14	**1203**	2.15
HG	Hindgut	**659**	2.17	**906**	2.16	**1038**	2.17	**1009**	2.15
ACC GL	Male accessory glands	**576**	2.09	**610**	2.09	**688**	2.10	**675**	2.13
CU	Cuticle	**613**	2.16	**705.4**	2.15	**853**	2.14	**952**	2.15

Supplementary table S13: Results of the RNA quantity and quality in all four pooled tissue samples of mature *Schistocerca gregaria* females. The concentration of the samples is determined by the absorbance at 260 nm whereas the ratio of the sample absorbance measured at 260 nm and 280 nm is used to assess RNA purity. A ratio of ~2 is considered pure RNA.

		POOL 1	POOL 1	POOL 2	POOL 2	POOL 3	POOL 3	POOL 4	POOL 4
Mature Females		**concentration (ng/µl)**	260/280	**concentration (ng/µl)**	260/280	**concentration (ng/µl)**	260/280	**concentration (ng/µl)**	260/280
Br	Brain	**485**	2.13	**436**	2.08	**588**	2.14	**508**	2.10
OL	Optic Lobes	**219**	2.12	**224**	1.97	**186**	2.01	**174**	2.16
CC	Corpora cardiaca	**301**	2.04	**253**	2.02	**293**	2.04	**369**	2.03
CA	Corpora allata	**118**	2.00	**78**	1.99	**81**	2.00	**86**	1.97
PG	Prothoracic gland	**275**	2.03	**291**	2.01	**321**	1.99	**292**	2.02
FG	Frontal ganglion	**101**	2.01	**68**	2.34	**73**	2.24	**21**	1.55
SOG	Suboesophageal ganglion	**138**	2.09	**263**	1.89	**161**	1.97	**306**	1.86
SG	Salivary glands	**565**	2.11	**1010**	2.09	**896**	2.13	**764**	2.08
VNC	Ventral nerve cord	**906**	2.13	**1118**	2.10	**962**	2.10	**1070**	2.12
GON	Gonads	**994**	2.15	**774**	2.15	**929**	2.13	**1158**	2.16
FB	Fat body	**1038**	2.09	**1052**	2.13	**848**	2.14	**1059**	2.12
FM	Flight muscle	**968**	2.13	**796**	2.12	**934**	2.14	**950**	2.14
FG	Foregut	**630**	2.12	**505**	2.08	**523**	2.06	**526**	2.09
CAE	Caeca	**794**	2.16	**856**	2.16	**994**	2.16	**1258**	2.16
MT	Malpighian tubules	**595**	2.16	**1006**	2.16	**525**	2.14	**711**	2.29
MG	Midgut	**1197**	2.14	**1246**	2.14	**1102**	2.15	**1017**	2.13
HG	Hindgut	**542**	2.09	**840**	2.14	**626**	2.11	**755**	2.15
ACC GL	Male accessory glands	**/**	/	**/**	/	**/**	/	**/**	/
CU	Cuticle	**1129**	2.12	**1085**	2.12	**1017**	2.11	**1003**	2.11

Supplementary table S14: Results of the RNA quantity and quality in all four pooled tissue samples of mature *Schistocerca gregaria* males. The concentration of the samples is determined by the absorbance at 260 nm whereas the ratio of the sample absorbance measured at 260 nm and 280 nm is used to assess RNA purity. A ratio of ~2 is considered pure RNA.

Mature Males		POOL 1	POOL 1	POOL 2	POOL 2	POOL 3	POOL 3	POOL 4	POOL 4
		concentration (ng/µl)	260/280	**concentration (ng/µl)**	260/280	**concentration (ng/µl)**	260/280	**concentration (ng/µl)**	260/280
Br	Brain	**300**	2.16	**292**	2.02	**330.25**	2.13	**240**	2.15
OL	Optic Lobes	**167**	2.17	**206**	2.19	**207**	2.16	**108**	2.21
CC	Corpora cardiaca	**112**	1.74	**86**	1.98	**116**	1.98	**102**	2.05
CA	Corpora allata	**36**	1.93	**66**	1.97	**42**	2.47	**31**	1.95
PG	Prothoracic gland	**93**	1.97	**108**	1.88	**86**	2.03	**139**	1.91
FG	Frontal ganglion	**21**	2.19	**35**	2.15	**33**	2.27	**42**	1.81
SOG	Suboesophageal ganglion	**73**	1.92	**179**	1.68	**70.66**	1.99	**150**	1.75
SG	Salivary glands	**246**	2.11	**403**	2.09	**351**	1.97	**317**	2.09
VNC	Ventral nerve cord	**638**	2.12	**364**	2.12	**529**	2.07	**192**	2.01
GON	Gonads	**999**	2.17	**928**	2.16	**1149**	2.15	**1008**	2.14
FB	Fat body	**63**	2.17	**59**	2.04	**199**	2.17	**84**	2.07
FM	Flight muscle	**914**	2.13	**883**	2.13	**1049**	2.16	**885**	2.15
FG	Foregut	**925**	2.11	**491**	2.07	**529**	2.16	**794**	2.12
CAE	Caeca	**676**	2.10	**825**	2.10	**803**	2.12	**630**	2.15
MT	Malpighian tubules	**1085**	2.26	**781**	2.18	**380**	2.06	**885**	2.17
MG	Midgut	**1178**	2.26	**1214**	2.15	**1171**	2.12	**1043**	2.14
HG	Hindgut	**1104**	2.14	**706**	2.04	**637**	2.07	**657**	2.06
ACC GL	Male accessory glands	**444**	2.04	**412**	2.14	**1034**	2.15	**1062**	2.14
CU	Cuticle	**1100**	2.12	**848**	2.12	**1079**	2.14	**1133**	2.13

List of publications

Publications in international peer-reviewed journals

Verlinden, H., **Lismont, E.**, Bil, M., Urlacher, E., Mercer, A., Vanden Broeck, J., Huybrechts, R. (2013). Characterization of a functional allatotropin receptor in the bumblebee, *Bombus terrestris* (Hymenoptera, Apidae). General and Comparative Endocrinology, 193, 193-200.

Lismont, E., Vleugels, R., Marchal, E., Badisco, L., Van Wielendaele, P., Lenaerts, C., Zels, S., Tobe, S., Vanden Broeck, J., Verlinden, H. (2015). Molecular Cloning and characterization of the allatotropin precursor and receptor in the desert locust, *Schistocerca gregaria*. Frontiers in Neuroscience, 84, 1-14.

Verlinden, H., Gijbels, M., **Lismont, E**., Lenaerts, C., Vanden Broeck, J., Marchal, E. (2015). The pleiotropic allatoregulatory neuropeptides and their receptors: A mini-review. Journal of Insect Physiology, S0022-1910(15)00082-7.

Lismont, E., Mortelmans, N., Verlinden, H., Vanden Broeck, J. Molecular cloning and characterization of the SIFamide precursor and receptor in a Hymenopteran insect, *Bombus terrestris* (2018). General and Comparative Endocrinology, 258, 39-52.

Meeting abstracts, presented at scientific conferences and symposia

Oral presentations

Lismont E., Corbisier J., Mortelmans N., Galés C., Verlinden H., Parmentier M., Springael J., Vanden Broeck J. (2016). Using BRET biosensors to detect direct G protein activation. Conference of European Comparative Endocrinologists. Leuven, Belgium, 21- 25 August 2016.

Verlinden H., Marchal E., **Lismont E**., Vanden Broeck J. (2016). The pleiotropic allatoregulatory neuropeptides and their receptors. Conference of European Comparative Endocrinologists. Leuven, Belgium, 21 - 25 August 2016.

Vanden Broeck J., Marchal E., **Lismont E**., Lenaerts C., Van Wielendaele P., Dillen S., Zels S., Cullen D., Verlinden H. (2016). Study of neuropeptides and peptide receptors in locust physiology. Invertebrate Neuropeptide Conference 2016 (INC2016). Ouro Preto (Brazil), 14-18 February 2016.

Verlinden H., **Lismont E**., Marchal E., Tobe S., Vanden Broeck J. (2016). Molecular cloning and characterization of the allatotropin precursor and receptor in the desert locust. Invertebrate Neuropeptide Conference. Ouro Preto, Brazil, 14-18 February 2016.

Lismont, E., Verlinden, H., Bil, M., Huybrechts R, Vanden Broeck, J. (2014). Characterization of a functional allatotropin receptor in the bumblebee, *Bombus terrestris*. Conference of European Comparative Endocrinologists (CECE). Rennes, France, 25-29 August, 2014.

Poster

Bil, M., Verlinden, H., **Lismont, E**., Huybrechts, R. (2013). Characterization of the allatotropin receptor in the bumblebee, *Bombus terrestris*. International Congress of Comparative Endocrinology (ICCE). Barcelona, Spain, 15-19 July 2013.

Meeting abstracts, presented at other scientific conferences and symposia

Oral presentation

Lismont E., Vanden Broeck J. (2016). BRET biosensors to detect direct G protein activation at insect G protein-coupled receptors. PAI/IUAP. Leuven, Belgium, 12 December 2016.

Lismont, E., Zels, S., Van Wielendaele, P., Verlinden, H., Vanden Broeck, J. (2015). Identification of novel receptors and their ligands: pharmacological and functional characterization of peptide GPCRs in insects. PAI/IUAP 7/40 meeting. Leuven, Belgium, 1 July 2015.

Poster

Lismont, E., Verlinden, H., Bil, M., Huybrechts R, Vanden Broeck, J. (2015). Characterization of a functional allatotropin receptor in the bumblebee, *Bombus terrestris*. PAI/IUAP 7/40 meeting. Leuven, Belgium, 1 July 2017.

Lismont E., Verlinden H., Bil M., Huybrechts R., Vanden Broeck J. (2016). Characterization of a functional allatotropin receptor in the bumblebee, *Bombus terrestris*. PAI/IUAP 7/40 meeting. Leuven, Belgium 12 December 2016.

Lismont, E., Verlinden, H., Bil, M., Huybrechts R, Vanden Broeck, J. (2014). Characterization of a functional allatotropin receptor in the bumblebee, *Bombus terrestris*. PAI/IUAP 7/40 meeting. Brussels, Belgium, 19 June 2014.